THE UNIVERSITY
of LIVERPOOL

A Study of the Mechanical Properties and Scaling Effects in a Thermoplastic Fibre-Metal Laminate

Thesis submitted in accordance with the requirements of
The University of Liverpool for the degree of Doctor in Philosophy by

J. Gonzalo Carrillo

Department of Engineering

July 2007

ACKNOWLEDGEMENTS

I would like to thank the University of Liverpool for allowing me to develop this research project and the Mexican funding CONACYT for providing the grant for my studies.

I would also like to thank to all the technical staff at the Engineering Department that gave me assistance in the sample preparation and testing, and also for their valuable guidance to achieve my work.

Especial thanks to my supervisor Professor Wesley Cantwell for his very professional guidance and support, patience and friendship throughout this research project.

Thanks to my family and friends to offer me support and attention throughout this period of my life here in Liverpool.

PUBLICATIONS

J.G. Carrillo and W.J. Cantwell. ***Mechanical Properties of a Novel Fiber-Metal Laminate Based on a Polypropylene Composite.*** Mechanics of Materials. In Press.

J.G. Carrillo and W.J. Cantwell. ***Comparative Study of Two Scaling Techniques using a Novel Fiber-Metal Laminate.*** Advanced Composite Letters. In Press.

J.G. Carrillo and W.J. Cantwell. ***Scaling Effects in the Low Velocity Impact Response of Fiber Metal Laminates.*** Journal of Reinforced Plastics and Composites. In Press.

J.G. Carrillo and W.J. Cantwell. ***Scaling Effects in the tensile behavior of Fiber-metal Laminates.*** Journal of Composite Science and Technology, Vol. 67, No. 7-8, pp. 1684-1693, 2007.

J.G. Carrillo and W.J. Cantwell, ***Study of High Performance Hybrid Laminates Based on a Thermoplastic Matrix***. SAMPE, Long Beach California, Vol. 51, 2006.

W.J. Cantwell, P. Cortes, R. Abdullah, G. Carrillo-Baeza, L. Mosse, M. Cardew-Compston and S. Kalyanasundaram. ***Novel Fibre-Metal Laminates Based on Thermoplastic Matrices***. ICCST-5, Sharjah, United Arab Emirates, 2005.

W.J. Cantwell, P. Cortes, R. Abdullah, G. Carrillo-Baeza, L. Mosse, M. Cardew-Compston and S. Kalyanasundaram. ***A Novel Lightweight Hybrid for Impact-Resistant Applications.*** SAMPE Europe, Paris, 2005.

ABSTRACT

This study investigates scaling effects in a novel fibre-metal laminate (FML) system based on a thermoplastic matrix. The material is based on an aluminium alloy, a self-reinforced polypropylene composite and a polypropylene film acting as an interlayer adhesive. Initially, the mechanical characterisation of the FMLs and their constituents are characterised in tension, flexure and under impact loading. Additionally, the level of adhesion between the composite and aluminium constituents is characterised using fracture mechanics procedures. The performance of the FML is investigated and compared to that offered by its constituents, enabling the advantages of these novel hybrid systems to be highlighted. Two different laminate constructions are employed here, these being an $[Al, 0°/90°]_s$ FML and an $[Al, +/- 45°]_s$ FML. Pronounced differences were observed between the two laminates, with the strain to failure of the latter being approximately 50% greater than the former. Interestingly, flexural tests revealed that the fibre orientation did not affect either the maximum stress or the strain at failure of the FML.

The second part of the study focuses on investigating scaling effects in this FML system. Here, scale model tests are used to predict the full-scale behaviour of fibre-metal laminates. Two laminates are investigated in this part of the research programme, these being $[Al_n, 0°/90°_n]_s$ and $[Al_n, +/- 45°_n]_s$ with n = ¼, ½, ¾ and 1. Tensile tests are undertaken on laminates prepared using three different scaling approaches, these being 1D (scaling the thickness dimension), 2D (scaling the in-plane dimensions) and 3D scaling, where all of the dimensions are scaled appropriately. Here, a small decrease in the value of these parameters was observed with increasing specimen size, suggesting that modest scaling effects do exist. Additionally, flexural tests are carried out using a 3D scaling approach, giving a direct comparison with the results generated in tension. The final part of this section investigates scaling effects in the low velocity impact response of the FMLs. Here, it is shown that the impact energy to initiate fracture in the FMLs does not exhibit any size dependency. Other test parameters, such as the impact duration are shown to obey the scaling law, with less than ten percent deviation from the normalised data being observed.

TABLE OF CONTENT

CHAPTER I. INTRODUCTION

This chapter presents an overview of the development of advanced composite materials and their use in the different areas such as aerospace, automotive and construction sectors. The objective of this chapter is to highlight current uses of composites and to discuss the potential offered by the next generation of laminated materials, including fibre-metal laminates. The chapter will also give a brief overview of scaling, highlighting the importance of using a scaling approach to study the behaviour of advanced composite materials. The objectives and the motivation of this study, the general procedure and the structure of the thesis are also included here.

1.1. Overview of Composite Materials and Hybrids

By the broadest definition, a composite material is one in which two or more different materials are combined to form a single structure with an identifiable interface. A composite is therefore a heterogeneous material that offers a wide range of outstanding mechanical and physical properties [**1-4**]. The properties of that new structure are dependant upon the properties of the constituent materials as well as the properties of the interface. In the more familiar world of metals, the mixing of different materials typically forms bonds at the atomic level (alloys), composites typically form molecular bonds in which the original materials retain their identity and mechanical properties.

One of the earliest known composite materials created by our ancestors, involved the mixing of straw and mud to construct homes and other dwellings. Here, the straw was used as the fibre reinforcement and the clay was the matrix. Today, the Maya people continue to construct their homes using such materials, using straw and vegetable fibre as the reinforcement in those rather primitive structures.

One of the most efficient and complex structures known is the human body (see Figure 1.1), which is an example of the efficient use of fibrous composites. The muscles are present in a layered system consisting of fibres at different angles and in different concentrations. This system results in a very strong, efficient, versatile and adaptable structure which is capable of performing amazing feats.

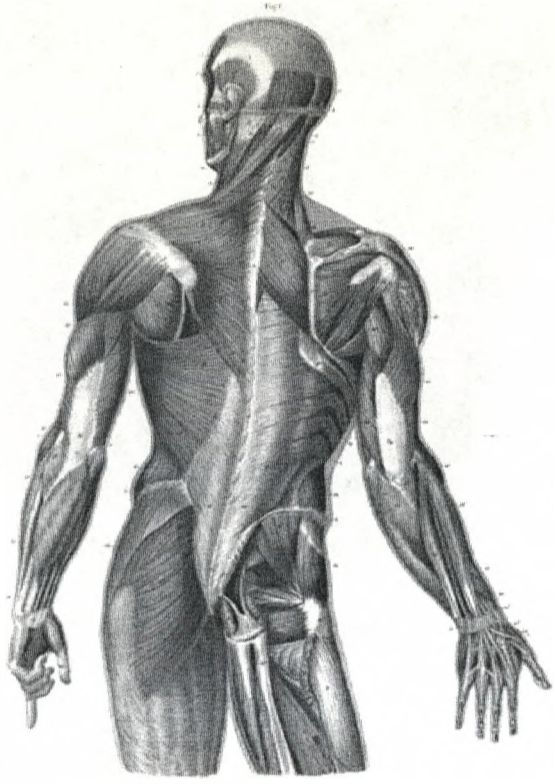

Figure 1.1. Human anatomy [5].

Nowadays, advanced composite materials are the ultimate designer material. By using various configurations of highly packed long slender fibres, one can obtain an enormous range of material properties. Furthermore, by changing the fibres and/or the matrix, interchanging the components, and designing the interface, the material options can become even wider, almost uncountable. The real limits to all of these opportunities are usually determined by the cost of the manufacturing process.

1.2. Advanced Composite Materials

The field of composite materials has been studied since the beginning of time, from the most natural objects including the human body, plants and animals, to the most recent developments for specialised materials for lightweight vehicles such as cars, planes, rockets and ships. The development of new composites and new applications is now accelerating. There can be no question that in the competitive worldwide markets of the 21st century, engineers and scientists will meet the challenges that they face through the use of engineered composites.

Today, when one speaks of composite materials, or just "composites", one is referring to the highly engineered combinations of polymer resins and reinforcing materials such as glass fibre-reinforced plastic (GFRP). Fibre-reinforced plastic (FRP) is a very general term for many different combinations of reinforcement materials and bonding resins. Thus, the term "composites" is used extremely broadly to describe many materials with many different properties targeted at an even larger number of applications. To show how composites have changed the world, it is worth looking around one's surroundings and realising that much of what one can see are components made of composite materials.

An example of the increasing use of advanced composite materials is in the Airbus fleet of aircraft (see Figure 1.2), where the use of composite materials has rocketed. This is likely to continue thanks to the availability of new technologies and the improved mechanical properties of advanced composite materials [**6**].

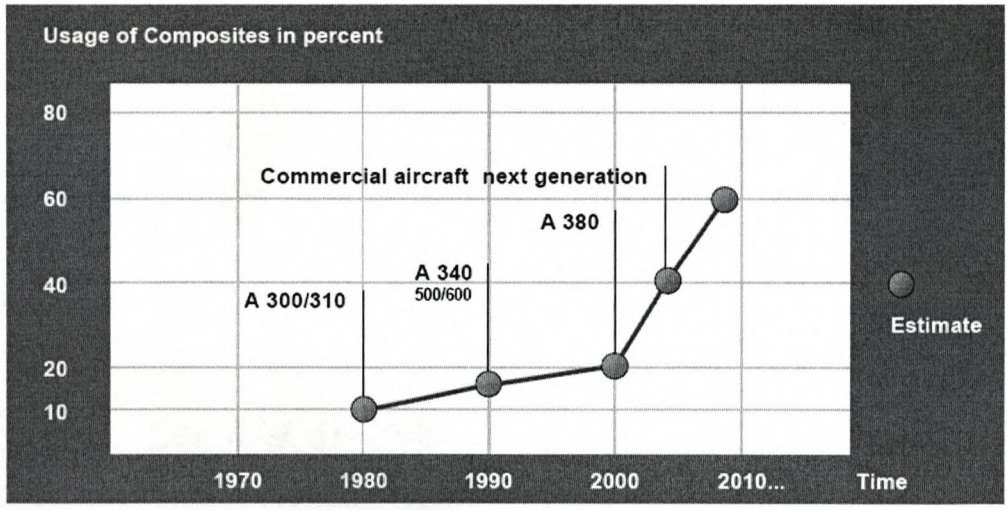

Figure 1.2. Increasing use of composite materials in the Airbus fleet of aircraft [7].

In this rapidly changing time for composites, thermoplastics (such as PP and PEEK) are relatively new materials that are replacing thermosets as the matrix material in these high performance systems. Thermoplastics hold much promise for use in aviation applications and industry in general. One of their primary advantages is that they are easy to produce. They are also more durable and tougher than thermosets, particularly for light impacts, as such the case of a tool dropped accidentally on an

aircraft wing. Whereas the tool could easily damage a thermoset material, it is unlikely to introduce significant damage in the thermoplastic composite.

1.2.1. Aerospace Applications

Fibrous composites have found applications in aircraft dating from the first flight of the Wright Brothers' Flyer 1, in North Carolina, 1903, to the latest military and civil aircraft. In addition they are being used in more demanding applications such as unmanned aerial vehicles (UAVs), space launchers and satellites. Aircraft and spacecraft are typical weight-sensitive structures in which composite materials are cost-effective [**8,9**].

The increased use of composites has been a result of their high specific strength and stiffness, when compared to the more conventional materials, and the ability to shape and tailor their structure to produce more aerodynamically efficient structural configurations. However, affordability is the key to survival in aerospace manufacturing, whether civil or military, and therefore, every effort should be devoted to the analysis and computational simulation of the manufacturing and assembly process, as well as the simulation of the subsequent performance of the structure, since all are intimately connected [**10,11**]. The development of new technologies and materials takes many years before they become mature enough to find a real application, especially in the civil aviation where more rigorous analyses are required.

Nowadays, composites offer significant weight savings, a key requirement for aircraft in terms of fuel consumption. By replacing aluminium structures with composite materials, reductions in weight of thirty percent can be readily achieved. In some components, other requirements such as impact toughness, fatigue toughness, corrosion resistance and fire resistance are important criteria, depending on their end use [**9**].

Carbon fibre-reinforced epoxy resin is currently the main composite used in aerospace applications such as the Airbus fleet of aircraft. GFRP was the first composite by Airbus, when it was introduced in the A300 fairing. Subsequently, CFRP was used in the fin box, the rudder, the keel beam and the horizontal stabiliser. The A310 was the

first aircraft with a CFRP fin box. Today, all of the tails of the A310 aircraft and thirteen percent of the A340 wings are made from CFRP [**6**].

Fibre metal laminates (FMLs) represents a new generation of advanced composite material. In its basic configuration it consist of two layers of metal (usually aluminium), and a core material (typically a FRP), in a sandwich configuration. The introduction of FMLs has yielded not only a reduction in operating costs (through a reduced weight) and better maintainability, but also a reduction in production costs. Currently FMLs are being used in the entire upper fuselage of the A380, the world's largest commercial aircraft (see Figure 1.3). In this aircraft, composites will represent the main materials for the wing boxes, the fin boxes, the keel beams, tails, flaps, leading edges, ribs, fairings, spoilers, ailerons, etc. [**12**].

Figure 1.3. The Airbus A380 [12]

1.2.2. Automotive Applications

Significant effort has been made in order to introduce composite materials into the automotive industry over recent decades, initially in an attempt to reduce weight. Nowadays, attention is again growing due to the need to combat environmental

pollution. Many industries are turning to advanced composite material when creating new and innovative products. Fibre reinforced plastic materials are widely recognized for their light weight and high strength. These materials are already being used with success in automotive applications and their use is expected to increase in the near future [**13**].

Short fibre-based composites are used in many non-structural automotive applications. Bulk moulding compound (BMC) is a thermosetting-based composite consisting of short glass fibres and fillers embedded in a polyester resin. BMCs are used to produce distributor caps and housings, headlamp bodies and reflectors. Short fibre-reinforced thermoplastics are found in door mirror housings, radiator end caps, intake manifolds, clutch and accelerator pedals. One of the most successful applications of short fibre composites is in air intake manifolds made from glass fibre-reinforced nylon. Polypropylene-based composites, reinforced by rubber and organic fillers, are currently used to manufacture car bumpers [**14**]. Glass mat thermoplastics (GMT) consisting of a combination of several layers of glass fibre mat in polypropylene matrix are used in many automotive components including seat structures, noise shields, instrument panels, load floors, battery trays and front ends. Sheet moulding compounds (SMC) are one of the most widely used composites for producing large exterior body panels such as wings, side extension panels, rear quarter panels, hoods and tailgates. SMC is similar to BMC, being a thermosetting-based composite, but contains longer fibre reinforcements.

Racing cars are a good example of the highly-efficient use of composites, where the three basic requirements are; high stiffness, strength and a minimum weight. At present, carbon fibre-reinforced epoxies are the main composite used in motor racing applications [**15**]. Aramid fibre and high molecular weight polyethylene fibre-reinforced composites are being developed to meet all of the major design requirements. The use of composites in Formula 1 racing cars includes survival cells, engine covers, side pods, flaps, main planes and nose boxes.

An example of the use of composites in commercial cars is the development of the Chrysler ME 412 concept car which was conceived as a lightweight car, made with hi-

tech materials. For example, the main structure consists of a carbon fibre-reinforced plastic, aluminium and other light alloys (see Figure 1.4).

Figure 1.4. A Chrysler ME 412 concept car made largely with fibre-reinforced plastic and light-weight alloy metals [16].

1.2.3. Marine Applications

One of the earliest and most widespread uses for composites was in the manufacture of pleasure boats. For many years, nearly all boats were wood, and much work was needed to maintain them. By the 1950's, boat builders began the transition to fibreglass hulls. Such designs were easier to build and significantly lower in cost, because complex shapes were more easily formed in fibreglass than in wood or metal. Boat buyers acquired attractive new styles that were cheaper, easier to transport, extremely durable and easy to maintain. For example, fibreglass does not rust as does steel nor does it rot like wood. Despite the nostalgia associated with the beauty of wood in ship hulls, such construction has been left to the few purists of ship ownership.

Glass fibre-based composites are the preferred choice for marine applications due to their competitive cost and their ease of fabrication [**17,18**]. Thermosetting-based polymers are the most commonly used matrices in the marine industry. Unsaturated polyester resins are widely used resins since they offer satisfactory mechanical properties, environmental resistance in marine environments, low cost and they can be fabricated easily. Vinyl ester resins are the second choice, since they offer superior

mechanical properties to polyester resins although at a higher cost. Epoxy resins are used in high performance components such as vessels where high strength and toughness are required. Composite applications in the marine industry can be found in hulls, decks, masts, engine shrouds and interior panels (see Figure 1.5).

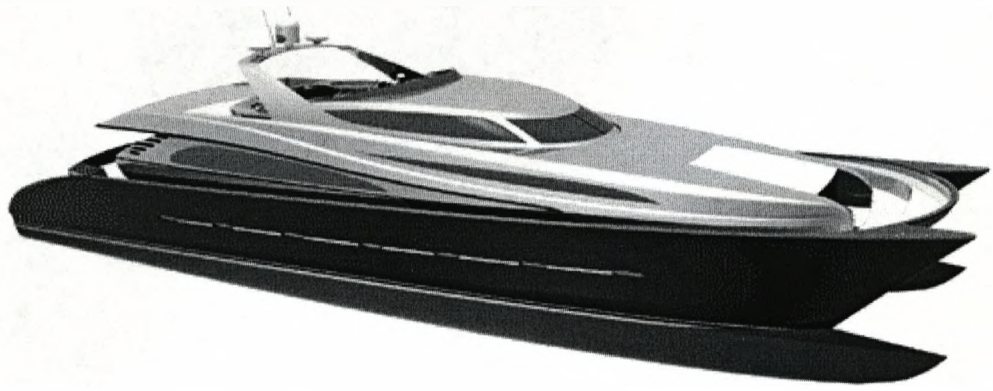

*Figure 1.5. All composite luxury yacht [**19**].*

In the area of marine defence, composites offer similar advantages. Military ships have traditionally been made of steel, an ideal material for ship construction, being both durable and cost-effective. However, steel ships rust, requiring constant maintenance. The heavy weight of steel ships also places limits on their speed and increases fuel consumption. Given that warships often encounter mine fields, the magnetic signature of ships is of great concern. Composites are non-magnetic and make an ideal material for any ship expected to encounter mine warfare conditions. It is likely that composites will be used in future for military ships, such as the new Littoral Combat Ship (LCS), (see Figure 1.6) an important new concept for a war vessel.

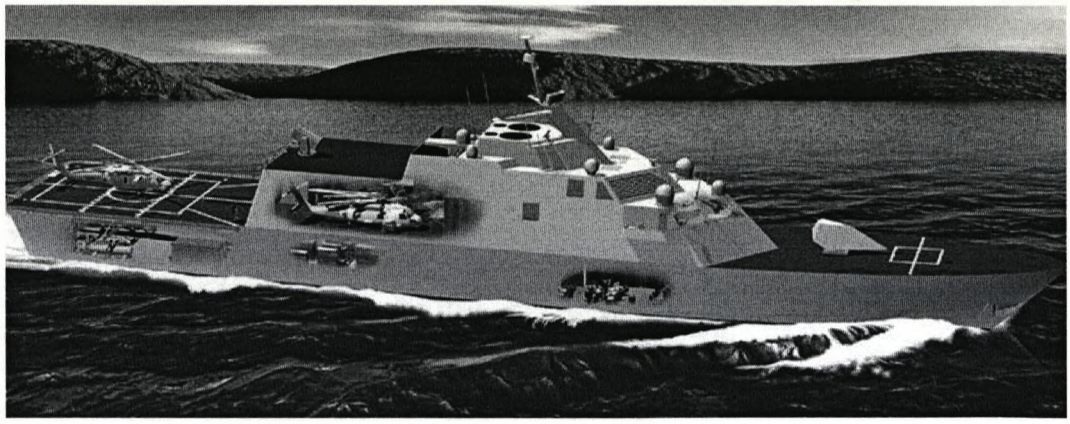

*Figure 1.6. The Littoral Combat Ship (LCS), a composite material design [**20**].*

1.2.4. Rail Applications

In rail vehicle applications, composites are found in cabin ends, lightweight fittings in passenger vehicles, floors and ceiling panels as shown in Figure 1.7. The principal composite for railway applications is a glass fibre-reinforced thermosetting composite due to its relatively low cost [**21**]. Carbon and aramid fibres are sometimes used, particularly in load-bearing designs. Thermoplastic and thermosetting resins are commonly used matrices here, although phenolic resins are sometimes used in applications where fire retardance is required.

*Figure 1.7. Train cabin constructed largely with fibre-reinforced plastic [**22**].*

1.2.5. Construction Industry

Due to their lightweight, high stiffness-to-weight and strength-to-weight ratios, and potentially high resistance to environmental degradation, resulting in lower life-cycle costs, polymer composites are increasingly being considered for use in civil infrastructure applications. Examples include the retrofitting and rehabilitation of buildings and bridges as well as the construction of new structural systems [**23,24**].

Fibre-reinforced plastic (FRP) materials are used increasingly in a large range of applications, in both new builds and repair, as well as in conjunction with adhesives and laminating resins. The growth in the use of composite in applications involving concrete, metallic and timber structures has highlighted the need for more guidance in the design, application and approval processes.

FRP products were first used to reinforce concrete structures in the 1950s. Over the next two decades, the quality of the FRP materials improved considerably, manufacturing methods became more automated and material costs decreased. The use of these materials for the external reinforcement of concrete bridge structures started in the 1980s, first as a substitute for steel plate bonding and then as a substitute for steel confinement shells for bridge columns [**25,26**].

The technology for external retrofitting was developed primarily in Japan (sheet wrapping) and Europe (laminate bonding). Today there are more than 1000 concrete slab/steel girder bridges in Japan that have been strengthened with sheet bonding to the columns (see Figure 1.8). Also, many thousands of bridge columns have been seismically upgraded with the same materials. The on going development of cost-effective production techniques for FRP composites has progressed to the level that they are ready for use in the construction industry. Reduced material costs, coupled with labour savings associated with its low weight and comparably simpler installation, relatively unlimited material length availability, and immunity to corrosion, make FRP materials an attractive solution for post-strengthening, repair, seismic retrofit, and infrastructure security [**27**].

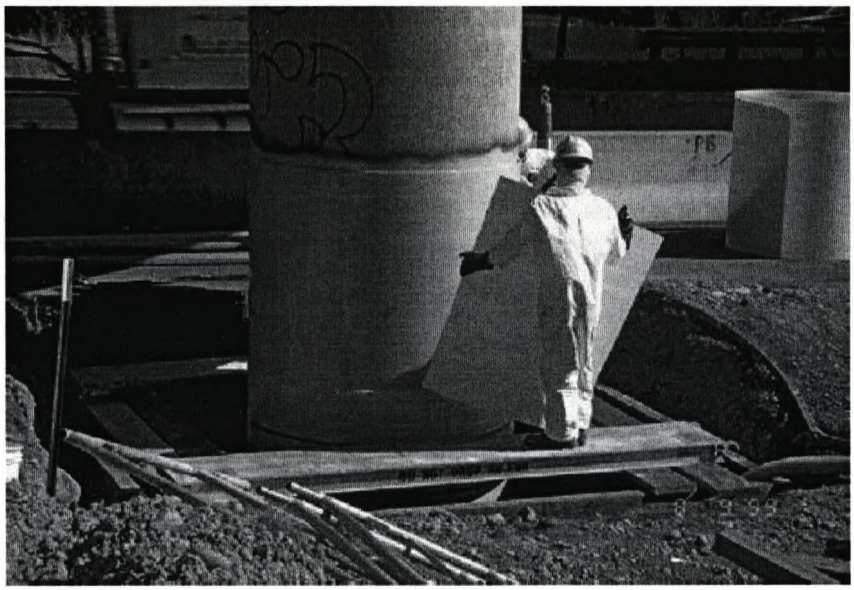

Figure 1.8. Reinforcement of concrete column with FRP composites to improve strength and seismic resistance [28].

Examples of new bridges include the Smart Composite Bridge (see Figure 1.9), that was constructed of lightweight durable composite materials. These materials ranged from glass fibre and soybean resin to recycled composite parts from Ranger trucks. These materials were fashioned into square tubes in combination with I beams made of glass and carbon materials. The bridge is stronger than it looks, containing sensors to monitor stress and fatigue during operation. Although it is used for pedestrian traffic and light vehicle traffic in the University of Missouri-Rolla campus, USA, it is rated for highway truck traffic. Because it is so lightweight, the bridge was built off-site, then transported and set into place, a task that was completed in about half a day. This represented a major change in construction practices, because most bridges are constructed on site.

This type of technology could be used in the decking of conventional bridges, to the section that usually needs to be replaced. A composite deck could be placed on an existing concrete and steel bridge rather than replacing the entire bridge. Sections of the composite decking could be kept on hand, thereby cutting down on repair time.

Another feature of the Smart Composite Bridge is the fibre optic sensors that are embedded in the bridge. They are connected to an optic fibre line that allows

researchers to access data from their desktop computers. The sensors can monitor the bridge for signs of fatigue and strain.

Figure 1.9. Smart composite bridge [29].

1.2.6. Sport and Leisure

Over the last thirty years, composite materials, plastics and ceramics have become dominant emerging materials. The volume and number of applications of composite materials have grown steadily, relentlessly penetrating and conquering new markets.

Modern composite materials constitute a significant proportion of the engineering materials market, ranging from everyday products to sophisticated niche applications [**30**]. Fibre-reinforced composites offer a wide range of properties which can be applied to suit the property requirements for a designed product. The use of composite materials yields lighter, stiffer and stronger sporting goods compared to wood or conventional metals. High strength carbon fibre-based composites are used to produce lightweight tennis rackets which are sixty-five percent lighter and three times stronger than titanium. Other applications can be found in trainer shoes, golf balls, fishing rods, etc. A good example is the all-composite bike frame, produced not only for the top cyclists, but also commercially (see Figure 1.10).

*Figure 1.10. Lightweight bike with its all-composite frame [**31**].*

An example of an advanced composite leisure gadget, is the lightweight Pentax K100D digital camera, with its housing made of fibre-reinforced plastic and stainless steel as shown in Figure 1.11. Examples such as this are in abundance these days, going from FRP laptop cases to carbon fibre pens.

*Figure 1.11. The K100D Pentax hi-tech digital camera constructed with FRP [**32**].*

1.3. FMLs, Hybrid Materials

Fibre Metal Laminates (FMLs) represent a family of hybrid materials, consisting of alternating layers of thin metal sheets and fibre reinforced plastic. The concept, invented in the late 1970s, has resulted in materials such as the aramid/aluminium laminate (ARALL), the carbon/aluminium laminate (CARE) and glass/aluminium laminate (GLARE). The first large scale application of GLARE is in the fuselage of the Airbus A-380 aircraft. Large sections of the fuselage, both in the front and aft section will have a GLARE skin. Took more than 20 years of research and development before this material could be introduced to the A-380 [**33**].

Nowadays, high performance fibre-metal laminates (FMLs) are attracting great interest from the aerospace sector since they combine the best attributes of their constituents. Currently, hybrid laminates are based on epoxy resins, which require a long processing cycle to ensure complete cure. In principle, the use of laminates based on thermoplastic materials will result in a shorter processing time, a lower cost and the possibility of re-shaping the final structure.

Future developments in aviation are likely to include supersonic civil transportation and therefore, aerospace structures capable of withstanding relatively high temperatures for long periods of time will be required. In principle, FMLs should be one of the most promising candidates to fulfil such requirements.

1.4. Overview of Scaling Effects in Engineering Structures

When the strength of a material decreases with increasing specimen size under the same test conditions, it is said to exhibit a size effect. The history of size effects stretches back to Leonardo da Vinci, in 1500s where he described tests on different lengths of iron wire to measure how its tensile strength reduced with increasing length [**34**]. Galileo (1638) rejected the size effect law proposed by Leonardo, which identified an inverse proportionality between the strength of a rope and its length, and speculated on the size effect in the bones of large animals, calling their bulkiness the 'weakness of the giants', (Figure 1.12).

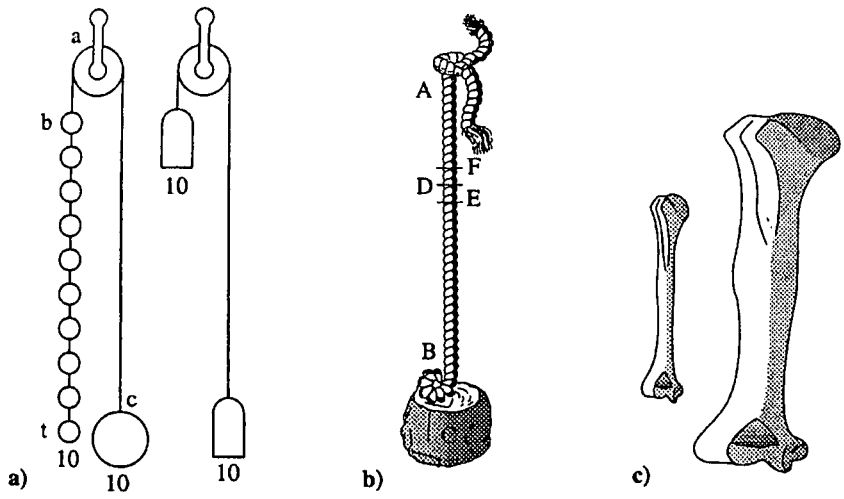

*Figure 1.12. Figures illustrating initial studies on size effects by a) Leonardo da Vinci in the early 1500's and b, c) Galileo Galilei in 1638 [**34**].*

Given the increased probability of finding a flaw with increasing material volume, large brittle bodies tend to fail at lower stress levels than smaller ones when both are subjected to the same kind of uniform stress field, such as pure tension. This is known as the 'size effect' [**35,36**].

The comprehensive data base of design information which exists for metals is not yet available for composite materials. This lack of information makes accurate analysis using conventional finite element techniques difficult. Consequently, composite prototypes must be fabricated and tested as part of design evaluation. Such testing, especially if it involves destruction of the design article, is expensive and time consuming.

One of the problems in designing large structures from composite materials is extrapolating strength data obtained from small coupon data to values appropriate to the large structure. For homogeneous, isotropic materials this can often be successfully accomplished by means of the Weibull statistical function. Although partial success has been achieved through the use of this technique on CFRP, there appear to be problems that render its use less than straightforward [**37**].

An alternate method for understanding and predicting the response of structures under a variety of loading conditions is through the use of scale model testing. While the application of scale model testing is well know in fluid mechanics; for example, wind tunnel tests on models to determine flight loads, the method has not yet received as much attention as an experimental technique in solid mechanics. However, interest in scale model testing of fibre-composites is growing as the size and complexity of test articles increases.

The problem of designing, building and testing a scale model structure constructed of advanced, fibre-reinforced composite materials is challenging. Due to the complexity of the material itself, the problem of scaling a composite component may be examined at several levels. The most elemental approach is to scale the constituent materials, the fibre and the matrix. Scaling the microstructure at this level would involve scaling the fibre diameters and fibre shapes, and ensuring uniformity of the fibre spacing. Fibre volume fractions should be the same for both model and prototype systems. However, for many structural problems, this degree of scaling becomes impractical and unnecessary.

The composite laminate represents the next level of complexity to examine. Scaling considerations for the laminate can be simplified if the individual lamina properties are smeared, i.e., the heterogeneous nature of the material is ignored at the microscopic level and the laminate is treated as a homogeneous, orthotropic sheet. This assumption is made when macroscopic structural aspects of the problem are more significant than material considerations for achieving a scaled response. However, it is necessary to understand how changes in the material microstructure, including the initiation and growth of damage, accumulate in the material and affect the overall structural response at various dimensional scales.

Test data obtained in the laboratory on small coupon specimens are routinely assumed to be valid for full-scale structures with no regard for possible distortions due to size or scale. This assumption is made even though size effects in the failure behaviour of metallic structures is well documented **[38-40]**. The limitations of scale modelling must be identified, so that tests on sub-scale composite structures will generate valid data for predicting prototype behaviour. Once the problems involved in testing scale

models are identified and understood, the technique can be utilised as a valuable, cost-effective design tool.

1.5. Objective of this Study

Size effects are important from a fundamental point of view in understanding failure. They are also important in a practical sense since tests to establish values of material strength are normally performed on relatively small specimens. If the strength decreases significantly with increasing specimen size, then potentially disastrous failures could occur if proper account were not taken of size effects. An understanding of size effects is also required in order to be able to correctly interpret the results of scaled model tests on structures [**41**].

Testing scale models can provide a cost-effective alternative to destructive testing of expensive composites prototypes and can be used to verify predictions obtained from finite element analyses. It is necessary, however, to understand the limitations involved in testing scale model structures before the technique can be fully utilised.
The objectives of this work are:

- To characterise the mechanical properties of a novel fibre-metal laminate based on an advanced thermoplastic composite material and its constituent materials,
- To predict the mechanical properties under quasi-static and low velocity impact conditions,
- To characterise the interfacial fracture properties of the bi-material constituents,
- To understand the tensile, flexure and impact properties at different scale sizes with different fibre configurations,
- To develop a set of dimensionless parameters which form the scaling law governing the correlation between the model and the prototype.

1.6. Motivation of the study

Due to the intricacy of their internal microstructure, fibre reinforced composite materials belong to a special category of materials presenting some complex and hence challenging scaling problems. Complications may arise from factors upon

which standard similitude laws cannot be satisfied. Such factors are; fabrication, fibre diameter, fibre/matrix interface, ply interface, and the test method.

As a result of the complexity of the problem resulting from the large number of variables involved (geometry, material system, lay-up, stacking sequence, environment, and loading mode), research studies to date, have failed to establish the exact causes of strength degradation in scaled composite laminates. Consequently, various researchers have different views on what is causing the observed scale effect. Some have associated the problem with edge effects, [**42-44**], while others have attacked the problem from a statistical point of view, [**45-47**], or a combination of the two.

Many engineering structures evolve from small scale models, which can be manufactured and tested under controlled laboratory conditions. Consequently, it is important that any effects associated with scaling be identified, well understood, and correlated to model size. It is important to determine whether such measurements are representative of the behaviour of large scale components.

The motivation for the study of scaling effects in a novel thermoplastic FML and its constituents was twofold; firstly, this will be the first scaling study undertaken on these type of hybrid composites, and secondly, the need to increase the understanding of scaling effects in the wide variety of composite configurations.

1.7. General Procedure

A brief explanation of the procedure adopted in this work is given below. First, the optimum conditions (pressure, temperature and time) to manufacture the FML are identified before a full consolidation process is undertaken. Here, the plates are fabricated using a self-reinforced polypropylene composite (SRPP), a high strength woven polymer fibre composite. The FML consolidation process involved a single shot process, bonding the aluminium and the SRPP with the aid of an adhesive film.

The first part of this study involves characterising the FML and its constituents, using tensile and flexural test techniques following ASTM D3039 and ASTM D790-80 testing standards respectively. Here, the strain at break, the yield stress, the strength and the Young's modulus are obtained and predictions are made using a rule of mixtures approach to obtain values for scaled specimens. Also, FMLs were impacted under low velocity impact conditions to determine their perforation energies and characterise their fracture mechanisms. Additionally, indentation tests and interfacial fracture analysis were carried out to complement this study.

The second part of this work consisted of a scaling study of the FML and its constituent materials, using tensile and flexural tests. Here, different aspects of the scaling study was covered such as, scaling techniques (ply-level and sublaminate-level), stacking sequences (0°/90° and +/-45°), and scaling configurations (1D, 2D and 3D scaling). The FMLs were; $[Al_n, 0°/90°_n]_s$ and $[Al_n, +/-45°_n]_s$ with n = ¼, ½, ¾, and 1. Similarly, scaling effects were studied for scaled plates to determine different factors of impact tests, such as impact duration, deflection and fracture, this, using proportional impact energies for a direct comparison.

1.8. Structure of the Thesis

This study is divided in five chapters including the present one, described as follows;

- Chapter I presents an overview of the current situation and the importance of this work, highlighting the purpose of this study and its associated benefits.
- Chapter II presents a literature review, which is divided in five main sections: 1) Polymeric resins, 2) Composite materials, 3) Metal alloys, 4) Fibre metal laminates, and 5) A review of previous scaling studies.
- Chapter III Describes the experimental work performed in this research, and is divided into six sections: 1) Materials investigated, 2) Manufacturing processes, 3) Mechanical properties of the materials, 4) A scaling study on the tensile properties, 5) A scaling study of flexural properties, and 6) A scaling study of the low velocity impact response of the FMLs.
- Chapter IV presents and discusses the results obtained in Chapter III.
- Chapter V presents the conclusions and recommendations for future work.

1.9. References

1. K Ashbee. *Fundamental Principles of Fiber Reinforced Composites*, Lancaster, USA; Technomic Publishing, 1989.

2. R M Jones. *Mechanics of Composite Materials*, London; Taylor and Francis Ltd., 1999.

3. R W Hertzberg. *Deformation and Fracture Mechanics of Engineering Materials*, Wiley and Sons, 1996.

4. D Hull and T W Clyne. *An Introduction of Composite Materials*, Cambridge University Press, 2005.

5. Human Anatomy, http://www.anatomyatlases.org, 2007.

6. R Abbott. *Composites in General Aviation.* In: Comprehensive Composite Materials, edited by A Kelly and C Zweben, Elsevier, p. 165-180. 2000.

7. Ticona, *Ticona Composites.* http://www.ticona-media.com, 2007.

8. D Gay, V Suong, H Stephen, and W Tsai. *Composite Materials; Design and Applications*, CRC Press, 2005.

9. M C-Y Niu. *Composite; Airframe Structures*, Hong Kong Conmilit Press, 2005.

10. C Soutis. *Fibre Reinforced Composites in Aircraft Construction.* Progress in Aerospace Sciences, 41; 143-151, 2005.

11. L B Ilcewicz, D J Hoffman, and A J Fawcett. *Composite Applications in Commercial Airframe Structures.* In: Comprehensive Composite Materials, edited by A Kelly and C Zweben, Elsevier, p. 87-119. 2000.

12. Airbus, *Airbus A380.* http://www.airbus.com, 2007.

13. Automotive Supplement. *New Developments Help Composites Compete.* Reinforced Plastics, 47; 27-31, 2003.

14. R Brooks. *Composites in Automotive Applications: Design.* In: Comprehensive Composite Materials, edited by A Kelly and C Zweben, Elsevier, p. 341-363. 2000.

15. S McBeath. *Competition Car Composites; A Practical Handbook*, Haynes Publishing, 2000.

16. Chrysler, *Chrysler ME 412.* http://www.chrysler.co.uk, 2007.

17. I D Ulzurrun, F Lopez, M A Herreros, and J C Suarez. *Tests of Deck-to-Hull Adhesive Joints in GFRP Boats.* Engineering Failure Analysis, 14; 310-320, 2007.

18. R A Shenoi and A R Dodkins. *Design of Ships and Marine Structures Made from FRP Composite Materials.* In: Comprehensive Composite Materials, edited by A Kelly and C Zweben, Elsevier, p. 429-449. 2000.

19. Composite Boats, http://www.compositeboats.com, 2007.

20. Littoral Combat Ship, http://www.globalsecurity.org, 2007.

21. M Robinson. *Applications in Trains and Railways.* In: Comprehensive Composite Materials, edited by A Kelly and C Zweben, Elsevier, p. 395-428. 2000.

22. Railway Technology, http://www.railway-technology.com, 2007.

23. L Cheng and V M Karbhari. *New Bridge Systems Using FRP Composites and Concrete: A State-of-the-Art Review.* Progress in Structural Engineering and Materials, 8; 143-154, 2006.

24. A Biddah. *Structural Reinforcement of Bridge Decks using Pulruded GFRP Grating.* Composite Structures, 74; 80-88, 2006.

25. V M Karbhari and L Zhao. *Use of Composites for 21st Century Civil Infrastructure.* Computer Methods in Applied Mechanics and Engineering, 185; 433-454, 2000.

26. A C Berg, L C Bank, M G Oliva, and J S Russell. *Construction and Cost Analysis of an FRP Reinforced Concrete Bridge Deck.* Construction and Building Materials, 20; 515-526, 2006.

27. M Uemura. *Reinforcement of Concrete Columns with CFRP.* In: Comprehensive Composite Materials, edited by A Kelly and C Zweben, Elsevier, p. 529-539. 2000.

28. V M Karbhari. *Fiber Reinforced Composite Bridge Systems - Transition from the Laboratory to the Field.* Composite Structures, 66; 5-16, 2004.

29. American Composites Manufacturers Association, http://www.mdacomposites.org, 2007.

30. V P McConnell. *Application of Composites in Sporting Goods.* In: Comprehensive Composite Materials, edited by A Kelly and C Zweben, Elsevier, p. 787-809. 2000.

31. Giant, http://www.giant-bicycles.com, 2007.

32. Pentax, *Pentax K100D.* http://www.pentax.co.uk, 2007.

33. J Sinke. *Development of Fibre Metal Laminates: Concurrent Multi-Scale Modelling and Testing.* Journal of Materials Science, 41; 6777-6788, 2006.

34. Z P Bazant. *Scaling of Structural Strength,* Hermes Penton Science, 2005.

35. C Zweben. *Is There a Size Effect in Composites?* Composites, 25; 451-454, 1994.

36. E S Taylor. *Dimensional Analysis for Engineers,* Oxford University Press, 1974.

37. J W Hitchon and D C Phillips. *The Effect of Specimen Size on the Strength of CFRP.* Composites, 9; 119-124, 1978.

38. E Booth, D Collier, and J Miles. *Impact Scalability of Plated Steel Structures.* In: Structural Crashworthiness, edited by N Jones and T Wierzbicki, Butterworths, p. 136-174. 1983.

39. T A Duffey, M C Cheresh, and S H Sutherland. *Experimental Verification of Scaling Laws for Punch-Impact-Loaded Structures.* International Journal of Impact Engineering, 2; 103-117, 1984.

40. N Jones. *Scaling of Inelastic Structures Loaded Dynamically.* In: Structural Impact and Crashworthiness, edited by G A Davies, Elsevier, p. 45-74. 1984.

41. M R Wisnom. *Size Effects in the Testing of Fibre-Composite Materials.* Composites Science and Technology, 59; 1937-1957, 1999.

42. M R Wisnom and M I Jones. *Size Effects in Interlaminar Tensile and Shear Strength of Unidirectional Glass Fibre/Epoxy.* Journal of Reinforced Plastics and Composites, 15; 2-15, 1996.

43. M R Wisnom, M I Jones, and G F J Hill. *Interlaminar Tensile Strength of Carbon Fibre-Epoxy-Specimen Size, Layup and Manufacturing Effects.* Advanced Composites Letters, 10; 171-177, 2001.

44. P Lagace, J Brewer, and C Kassapoglou. *The Effect of Thickness on Interlaminar Stresses and Delamination in Straigth-Edged Laminates*. Journal of Composites Technology and Research, 9; 81-87, 1987.

45. A G Atkins. *Scaling in Combined Plastic Flow and Fracture*. International Journal of Mechanical Sciences, 30; 173-191, 1988.

46. A Tabiei and J Sun. *Analytical Simulation of Strength Size Effect in Composites Materials*. Composites: Part B, 31; 133-139, 2000.

47. B V Sankar. *Scaling of Low-Velocity Impact for Symetric Composite Laminates*. Journal of Reinforced Plastics and Composites, 2; 296-309, 1992.

CHAPTER II. LITERATURE REVIEW

This chapter presents a review of the published information currently available on composites and fibre-metal laminates, including the different kinds of polymeric resins that are commonly used to consolidate these materials. Included in this chapter is a review of the scaling studies undertaken in composite.

2.1 Polymeric Resins

Polymers can be defined as high molecular weight organic compounds, natural or synthetic, with a structure that can be represented by a repeated small unit, the mer. Examples include polyethylene, rubber and cellulose. Synthetic polymers are formed by addition or condensation polymerisation of monomers. Some polymers are elastomers, some are plastics, and some are fibres. When two or more dissimilar monomers are involved, the product is called copolymer. The chain lengths of commercial thermoplastics vary form ~1000 to >100,000 repeating units. Thermosetting polymers approach infinity after curing, but their resin precursors, often called prepolymers, may be relatively short, within ~6 to ~100 repeating units before curing. The length of the polymer chains, usually measured by molecular weight, has a very significant effect on the performance properties of plastics and profound effects on their processability [**1,2**].

Polymer resins are used frequently as a composite matrix. The purpose of the matrix is to bind the reinforcements together by virtue of its cohesive and adhesive characteristics, to transfer load to and between reinforcements, and to protect the reinforcements from environments and handling. The matrix also provides a solid form to the composite, which aids handling during manufacture and is typically required in a finished part. This is particularly necessary in discontinuously reinforced composites, because the reinforcements are not of sufficient length to be of a handleable form [**3,4**]. Because the reinforcements are typically stronger and stiffer, the matrix is often the "weak link" in the composite from a structural perspective. As a continuous phase, the matrix therefore controls the transverse properties, interlaminar strength, and elevated-temperature strength of the composite. However, the matrix allows the strength of the reinforcement to be used to their full potential by providing effective load transfer from external forces. The matrix holds reinforcing fibres in the proper orientation and position so that they can carry the intended loads and distributes the loads more or less evenly among the reinforcements. Further, the matrix provides a vital inelastic response so that stress concentrations are reduced dramatically and internal stresses are redistributed from broken reinforcements [**5**].

In general, polymer-matrices can be divided into two types, thermosettings and thermoplastics, where thermosetting matrices are polymerised in a non-reversible chemical reaction.

2.1.1 Thermosetting Polymers

Thermosetting polymers are formed by the reaction between two monomers, through a cross-linking process. Once formed by heat, they cannot be reshaped [4]. Although epoxies are sensitive to moisture in both their cured and uncured states, they are generally superior to polyesters in resisting moisture and other environmental influences and offer lower cure shrinkage and excellent mechanical properties. Even though the elongation-to-failure of most cured epoxies is relatively low, for many applications, epoxies provide an almost unbeatable combination of handling characteristics, processing flexibility, composite mechanical properties, and acceptable cost. Modified toughened epoxy resin formulations (typically via the addition of thermoplastic or rubber additives) have improved elongation capabilities.

The categories of thermosetting polymers include [6,7]:

- ***Unsaturated polyesters:*** They offer good mechanical, electrical and chemical resistance properties. Their major applications are in large components, such as boats and large volume productions. However, their relatively high shrinkage on cure, their sensitivity to some aggressive solvents and their appreciable moisture absorption, preclude their utilisation in high performance applications.
- ***Vinyl esters:*** These polymers are a subfamily of the polyester resins. However, vinyl esters offer a higher tensile elongation, resilience, toughness, heat and chemical resistance than the conventional unsaturated polyester resins. They are commonly used for chemical resistance purposes.
- ***Epoxides:*** They offer a good balance of physical, mechanical and electrical properties. However, epoxies have a tendency to absorb moisture, which can lead to a decrease in their mechanical properties. These resins can be made from a wide range of starting components and their final properties may therefore vary.
- ***Phenolics:*** These kinds of resins offer excellent thermal stability (up to 300 °C), good resistance to moisture, solvents and acids (except to strong alkalis), and on burning do not produce toxic smoke. They are used in military and high-

performance aerospace applications, where dimensional stability at high loads and temperatures is required.

- ***Polyimides:*** These materials offer a high level of thermal and environmental resistance and retain their mechanical properties at temperatures up to 320 °C. Their applications have been limited to the aerospace and electronics sectors where high quality, performance and temperature are required and the high cost can be justified.
- ***Bismaleimides:*** These polymers are less expensive than polyimide resins. They are relatively easy to process, offer good mechanical strength and stiffness, but are generally brittle and may exhibit cure-shrinkage.

Epoxy resins are a class of thermoset materials used extensively in structural and specialty composite applications because they offer a unique combination of properties that are unattainable with other thermoset resins. Available in a wide variety of physical forms from low-viscosity liquid to high-melting solids, they are amenable to a wide range of processes and applications. Epoxies offer high strength, low shrinkage, excellent adhesion to various substrates, effective electrical insulation, chemical and solvent resistance, low cost, and low toxicity. They are easily cured without evolution of volatiles or by products by a broad range of chemical species. Epoxy resins are also chemically compatible with most substrates and tend to wet surfaces easily, making them especially well suited to composites applications.

Epoxy resins are routinely used as adhesives, coatings, encapsulates, casting materials, potting compounds, and binders. Some of their most interesting applications are found in the aerospace and recreational industries where resins and fibres are combined to produce complex composite structures. Epoxy technologies satisfy a variety of nonmetallic composite designs in commercial and military aerospace applications, including flooring panels, ducting, vertical and horizontal stabilizers, wings, and even the fuselage. This same chemistry, developed for aerospace applications, is now being used to produce lightweight bicycle frames, golf clubs, snowboards, racing cars, and musical instruments [**5**].

Moisture absorption decreases the glass transition temperature (T_g) of an epoxy resin. Because a significant loss of epoxy properties occurs at the T_g, the glass transition in most cases describes the upper-use temperature limit of the composite. To avoid subjecting the resins to temperatures equal to or higher than this so-called wet T_g (the wet T_g is the T_g measured after the polymer matrix has been exposed to a specified humid environment and allowed to absorb moisture until it reaches equilibrium), epoxy resins are presently limited to a maximum service temperature of about 120 °C for highly loaded, long-term applications and even lower temperatures (80 to 105 °C) for toughened epoxy resins. Although this limit is conservative for some applications, its imposition has generally avoided serious thermal-performance difficulties. Considerable effort continues to be expended to develop epoxy resins that will perform satisfactorily at higher temperatures when wet. However, progress in increasing the 120 °C limit has been slow [**8**].

2.1.2 Thermoplastic Polymers

Thermoplastic materials are divided into categories based on fundamental differences in morphology. These morphologies are described as crystalline, semi-crystalline, and amorphous [**4**]. Semi-crystalline materials have domains of highly ordered molecular structure (crystallites) having well-defined melting points. Crystalline development is a thermodynamic and transport phenomena controlled by balance in mobility and free energy of molecules. Cooling rate can influence crystalline content and distribution [**3**]. Thermoplastic polymers include [**2,6,9**]:

- ***Polyolefins:*** They are made by repeated units of carbon and hydrogen atoms exclusively without ring structures. Due to their flexibility, strength, lightness, stability, permeability, and easy processability, these sorts of polymers are world widely used, such as polyethylene and polypropylene.
- ***Styrenics:*** These are amorphous polymers formed by repeating an aromatic ring molecule as a side group along its structure. In general, they are more expensive than polyolefins, and their strength and modulus also exceed those of the polyolefins, i.e., polystyrene and acrylonitrile-butadiene-styrene.
- ***Vinyls:*** The principal resin in the vinyl's group is the polyvinyl chloride (PVC). It is inexpensive and has good chemical and insulation resistance. Its flexural and tensile properties are similar to most polymers in the styrene family.

- ***Acrylics:*** Polymethyl-methacrylate (PMMA) is a polymer that belongs to this group. It is amorphous and even though its processing is easier than vinyls, it is sensitive to many solvents and is attacked by strong acids.
- ***Fluoropolymers:*** They offer a notable chemical and environmental resistance, good impact properties and absorb very little moisture. However, they have a low modulus, a high density and are considered expensive resins, i.e., PTFE (Teflon).
- ***Polyesters:*** There are many types of polyester offering a wide range of properties. Many of the commercially well-established polyesters are semi-crystalline with high melting temperatures that absorb moderate amounts of moisture, i.e., polyethylene-terephthalate and polybutylene-terephthalate.
- ***Polyamides:*** Most polyamides are semi-crystalline and have relatively low melt viscosities. They offer excellent strength, stiffness, toughness and a good chemical resistance. However, they are sensitive to strong acids and absorb significant quantities of moisture, i.e., nylons.
- ***Polyimides:*** These polymers offer excellent electrical properties and are solvent, flame, and heat resistance. Polyetherimide (PEI) is an amorphous polymer that belongs to this family and is characterised for having high service temperature, high fracture toughness, good interfacial adhesion and a non-flammable behaviour.
- ***Polyethers:*** These polymers contain an ether group that imparts flexibility to the molecule and makes them easy to process. There are a wide variety of chemical types in the polyether family, such as polyether-ether-ketone (PEEK) that is a semi-crystalline polymer, which offers a high temperature service, high strength, modulus and impact strength, excellent chemical resistance, and is non-flammable; unfortunately, they are relatively expensive.
- ***Sulphur-Containing Polymers:*** This sort of polymer involves the presence of a sulphur or sulphone group. This group contributes to the rigidity, thermal, oxidative and hydrolysis resistance of the structure, i.e., polyphenylene-sulphide.

The effects of crystallinity are similar to cross-linking in that resin stiffness and solvent resistance increase with increasing crystalline content **[10,11]**. Above the T_g softening occurs more gradually in crystalline materials than in amorphous materials and progresses toward a melting point that is characterised by a sudden change to an

apparent liquid state. In this respect, crystallinity is quite different from cross-linking, where the material thermally degrades without entering a liquid state. Semi-crystalline materials typically exhibit very good chemical resistance. Unlike thermoset composites, a great degree of useful strength and stiffness may remain well above the T_g of these thermoplastic composites. Amorphous resins are glassy solids at low temperatures since molecular motion is severely restricted, while above their T_g, amorphous materials lose their strength quickly even when reinforced with continuous fibres. Physical aging effects, creep behaviour, and sensitivity to fatigue also are more pronounced **[2,12]**. Their lack of a defined melting temperature (T_m), keep them in the rubbery state up to the degradation point.

Special amorphous, high-temperature resins have randomly ordered molecular structures and do not exhibit a sharp melting point. Instead, they soften gradually with rising temperature. At the beginning of the year 2000, only a few thermoplastic polymers have emerged to dominate the aerospace field. These high-temperature polymers are PEEK, PEI, polyphenylene-sulphide (PPS), and polyether-ketone-ketone (PEKK). Although PEKK exhibits excellent properties, its applications have progressed at a slower rate [**6**]. Table 2.1 shows some properties of these polymers.

Material	Glass Transition Temp. (°C)	Melting Temp. Range (°C)	Max. Operating Temp. (°C)
PP	-20	160-190	110
PA	50	220-270	170
PES	230	-	180
PEI	220	-	170
PAI	275	-	230
PPS	90	290-340	240
PEEK	145	350-390	250

Table 2.1. Thermal data for some important engineering thermoplastics [6].

The dual goal of improving both hot/wet properties and impact resistance of composite matrices has led to the development, and limited use, of high-temperature thermoplastic resin matrices. These materials are very different from the commodity thermoplastics (such as polyethylene, polyvinyl chloride, and polystyrene) that are commonly used as plastic bags, plastic piping, and plastic tableware. The commodity

thermoplastics exhibit very little resistance to elevated temperatures, while the high-performance thermoplastics exhibit a resistance that can be superior to that of epoxy. Thermoplastic-matrix materials are tougher and offer the potential of improved hot/wet resistance and long-term room-temperature storage. Because of their high strains-to-failure, they also are the only matrices currently available that allow, at least theoretically, the new intermediate-modulus, high-strength (and strain) carbon fibres to use their full strain potential in the composite.

These materials include such resins as polyether-ether-ketone, polyphenylene-sulphide, polyether-imide (all of which are intended to maintain their thermoplastic character in the final composite), and others, such as polyamideimide, which is originally moulded as a thermoplastic but is then postcured in the final composite to produce partial thermosetting characteristics (and thus improved subsequent temperature resistance). Thermoplastic matrices do not absorb any significant amount of water, but organic solvent resistance is an area of concern for the noncrystalline thermoplastics [**5**].

2.1.3 Polypropylene

Polypropylene (PP) is a tough lightweight thermoplastic made by the polymerisation of high-purity propylene gas in the presence of an organometallic catalyst at relatively low pressures and temperatures (see Figure 2.1). This polyolefin has a T_g = -20 °C and a T_m = 165 °C. PP is used as matrix in numerous composite products. Its appeal is both low density and low cost. Because polypropylene is semi-crystalline, its heat distortion temperature increases significantly from 55 °C to 130 °C. Since polypropylene is nonpolar, it absorbs very little water. Due its T_g below room temperature, it exhibits a high impact strength. Because of these properties, polypropylene is used 90% of the time in glass mat thermoplastic (GMT) sheet material for compression moulding. Short and long fibre-reinforced polypropylene made by melt impregnation is available from many sources for injection moulding applications [**8,13**].

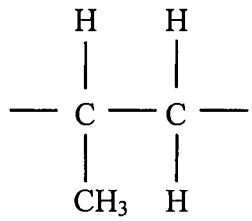

Figure 2.1. The chemical structure of polypropylene.

Polypropylene has had a remarkable growth in production over the past 45 years. The reasons for this growth have been the versatility of the polymer; the ability of the polymer to be modified and tailored for specific applications; its overall balance of physical, mechanical, electrical, chemical, and thermal properties; and a competitive price. Additionally, PP-based materials have a very good stability over a wide temperature range and have outstanding retention of mechanical properties after recycling and also in many cases an incineration ability. The competitive price comes from wide availability of the basic monomer and the simplicity of the polymerisation systems available today. The polymer can be processed on a wide variety of equipment, thus allowing it to be transformed easily, simply, and safely into a wide variety of usable articles.

Traditionally, the primary driving force to change to PP-based materials for applications using engineering resins has been cost. Applications include a wide variety of automotive parts such as fan blades, instrumented panels, headlamp support frames consisting of thermoset composite have been replaced by glass fibre-reinforced PP. In these types of applications, new tooling is often used to improve the strength in the weaker sections of the part. In a sense, existing tool design and part geometry may not be directly applied to parts converted to PP. Increased wall thickness and consideration for the creep characteristic differences may need to be studied; however, PP can be applied. In most cases, the cost per unit volume frequently weighs in favour of PP-based materials [**3,13**].

2.1.4 Advantages and Disadvantages of Polymeric Resins

Polymeric resins are gaining attractive mechanical properties that suit many supersonic aircraft requirements as well as for most commercial aircraft requirements. They also offer dimensional stability and attractive dielectric characteristics. Good flame-retardant and wear-resistant characteristics are also common. One of the most remarkable characteristics of thermoplastic materials is that they can be processed as a finished product in a very short period of time, also they can be re-shaped and the row material can be store for a longer period of time when are compared with thermosetting polymers. On the other hand, thermosettings are excellent candidates for prepregs due to their ease of wetting fibres and superb mechanical properties, creating excellent composites. Thermosetting resins have disadvantages, including limited period of shelf life with longer processing time than thermoplastics.

2.2 Composite Materials

A composite material is a macroscopic combination of two or more distinct materials (heterogeneous), having a recognisable interface between them, the matrix and the reinforcement. Composites are used not only for their structural properties, but also for electrical, thermal, and environmental applications. Modern composite materials are usually optimised to achieve a particular balance of properties for a given range of applications [**14-16**]. Given the vast range of materials that may be considered as composites and the broad range of uses for which composite materials may be designed, it is difficult to agree upon a single, simple, and useful definition. However, as a common practical definition, composite materials may be restricted to emphasise those materials that contain a continuous matrix constituent that binds together and provides form to an array of a stronger, stiffer reinforcement constituent. The resulting composite material has a balance of structural properties that is superior to either constituent material alone.

Composite materials have attracted interest since the beginning of life, from the most natural objects, including straw and mud in the form of bricks for building construction, the human body, plants and animals to the most recent developments for specialised materials for lightweight vehicles such as cars, planes, rockets and ships. Development of new composites and new applications is now accelerating. The most

visible applications pave our roadways in the form of either steel and aggregate reinforced cement or asphalt concrete. Solid surface, imitation granite and marble sinks and countertops are widely used to enhance our living experiences.

Modern composite materials are usually optimised to achieve a particular balance of properties for a given range of applications. Due to the wide variety of matrix and reinforcement materials available, the design potentials are vast. Composite materials can be classified into three broad categories depending on the type, geometry and orientation of the reinforcing phase, as it is shown in Figure 2.2.

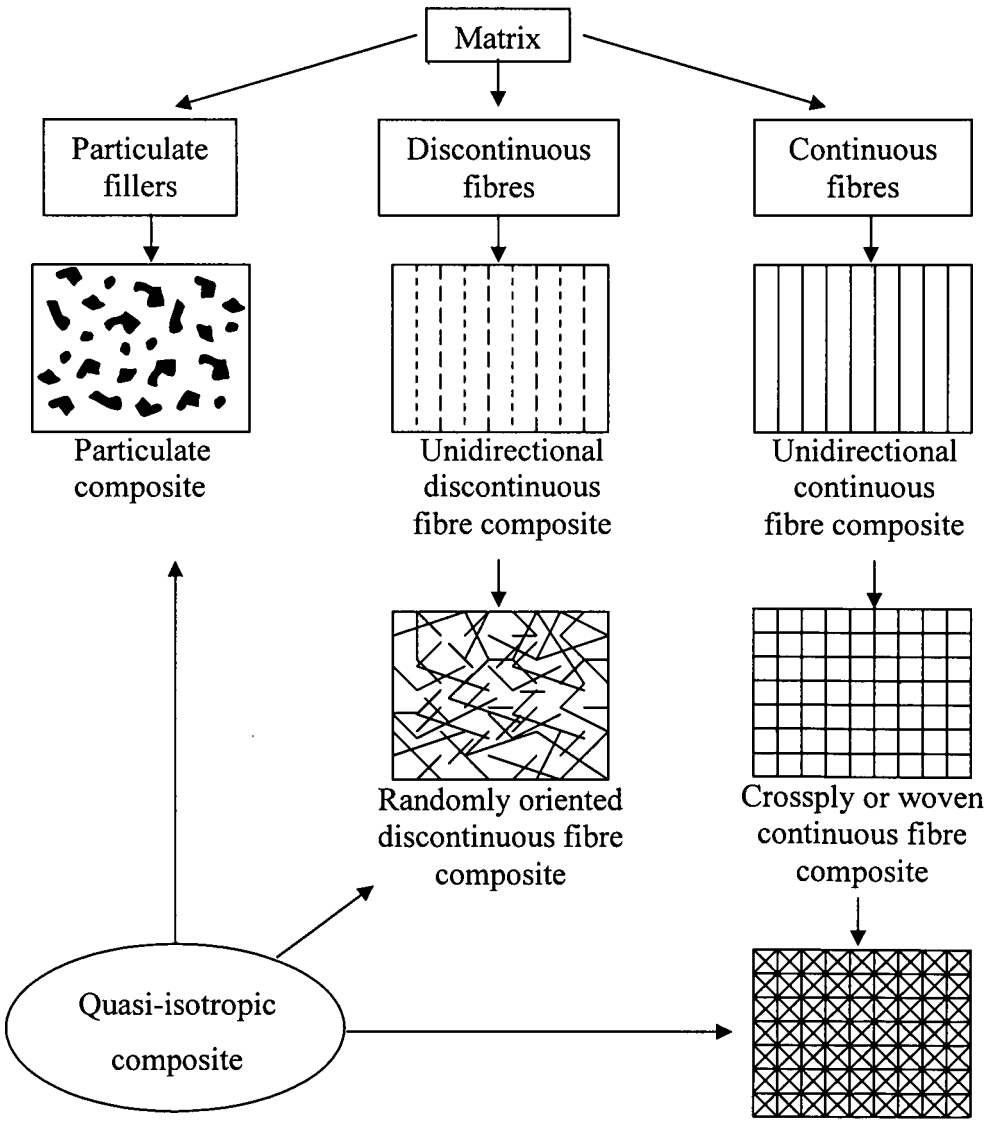

*Figure 2.2. Classification of composite material systems [**14**].*

Composites typically have a fibre or particle phase that is stiffer and stronger than the continuous matrix phase. There are however exception that may still be considered composites, such as rubber-modified polymers, where the discontinuous phase is more compliant and more ductile than the polymer, resulting in improved toughness. Similarly, steel wires have been used to reinforce grey cast iron in truck and lorry break drums [**5,11**].

2.2.1 Manufacturing Processes

There are many processes for manufacturing composites. Each process imposes particular limitations on the structural design and therefore, it is important to understand the advantages, costs, production rate and volume of each of these manufacturing processes. A review of the manufacturing processes used to construct composites is given below [**2,12**].

- ***Hand Lay-up:*** This process involves the manual placement of dry reinforcement onto the mould surface with a subsequent application of the resin. The composite is then rolled to yield a uniform distribution of the resin.
- ***Prepreg lay-up:*** The basic difference of this process from the hand lay-up procedure is that the impregnation of the fibres is undertaken prior to moulding. Prepregs are widely used for manufacturing high performance aerospace components and complex geometries.
- ***Bag moulding:*** The layers are laid up in a mould and a negative pressure is applied with the aid of a flexible diaphragm or bag. There are three basic methods for applying the pressure to the laminate: a pressure bag, a vacuum bag and autoclave processing.
- ***Compression moulding:*** The fibres and resin are placed into a mould and a relatively high pressure and heat is applied using a hydraulic press.
- ***Resin Transfer Moulding (RTM):*** The reinforcing fibres are placed dry in the mould and the liquid resin is pumped into the mould, soaking the fibres and filling the mould cavity. There are several variations of the basic RTM process such as vacuum assisted resin injection moulding, preform moulding, structural reaction injection moulding and flexible resin transfer moulding.

- ***Pultrusion:*** This process involves continuous fibres, which are firstly impregnated with a polymeric resin and subsequently pulled through a heated die.
- ***Filament winding:*** In this process, a continuous reinforcement is wound onto a mandrel until the surface is covered and the required thickness is achieved.

In many composites processing methods, the matrix is added to the fibres at the time of manufacture. Resin transfer moulding and conventional hand lay-up are examples of this. An alternative approach is for the material supplier to bring the resin and fibre together, so that the user has only to lay the material onto a tool and then process it. These materials are called pre-impregnates, almost universally referred to as prepregs, predominantly thermoset based.

Like any other thermosetting composite material, the curing process requires heat and pressure. The requirement with prepregs is to allow them a reasonable shelf-life while ensuring that they are processed at an acceptable temperature. To achieve this, the prepreg will typically be stored in a freezer and then cured at an elevated temperature. A further complication is that the prepreg must have a useful 'out-life', which is the maximum time during which the prepreg can be unprocessed without curing. The earliest prepregs produced in the 1960s necessitated quite high cure temperatures and had very short out-lives. Now it is possible for them to be stored in a freezer, have an out-life of possibly several months and a cure temperature of between 50 and 200 °C. Not surprisingly, the higher temperature cure materials have the longer out-lives. Prepregs tend to be epoxy resins reinforced with carbon, glass or aramid fibres. Other matrix materials are occasionally used, for example, high temperature polymer composites.

2.2.2 Evaluation Techniques

All composites are likely to contain defects of various kinds arising from the manufacturing process or as a consequence of service damage. Sensitive techniques are required for detection of such defects or damage. Brief details of some of the more commonly used non-destructive techniques are described below [**19,20**]:

- ***Optical Inspection:*** In translucent composites, the inspection by transmitted light within a projection of the magnified image can indicate defects in the composite.

In non-translucent composites, surface damage is enhanced by dye-penetrant methods to highlight surface cracking.

- ***Radiographic Methods:*** Radiography can yield high-contrast photographs from low-density materials as a result of their low inherent filtration. Thus, the fibre distribution, quality of weave and the presence of large laminating defects can be easily investigated.
- ***Thermal Imaging:*** This technique involves the application of a heat flux to the composite and the observation of the subsequent temperature distribution within it. This technique is routinely available and is widely used in the aerospace industry.
- ***Ultrasonic Techniques:*** These are probably the most widely non-destructive methods used on composites. The velocity and attenuation of an ultrasonic pulse passing through a composite can provide useful information about its structure and general physical properties. The C-scan procedure is a highly developed technique that is used routinely for inspecting large panels.
- ***Optical Fibre Sensors:*** They are used to reveal any crack in the specimen by detecting changes in the light attenuation level emitted at the end of the fibre.
- ***Microwave Methods:*** Microwave frequencies are applied to the composite and any defect or deterioration of the structure is highlighted by changes in the resonant frequency.
- ***Dynamic Mechanical Analysis:*** The composite structure is subjected to a resonant frequency to obtain the frequency spectrum, which establishes its characteristic "sound". Thus, any damage in the structure will change the characteristic spectrum, which will provide information about damage in the composite.
- ***Acoustic Emission Methods:*** These techniques are based on the detection of acoustic emissions, which result from the dissipation of stored energy as elastic stress waves, due to structural changes within the composite.

2.2.3 Advanced Composite Materials

Organic-matrix composites originated through efforts in the aerospace community during World War II to produce materials with specific strength and stiffness values that were significantly higher than existing structural materials. In addition, existing aerospace structural alloys, such as those based on aluminium, were subject to corrosion and fatigue damage, these composites provided an approach to overcome

these issues. By the end of the war, glass fibre-reinforced plastics had been used successfully in filament-wound rocket motors and demonstrated in various other prototype structural aircraft applications [**21**]. These materials were put into broader use in the 1950s and provided important improvements in structural response and corrosion resistance. Commercial applications in consumer sporting equipment in the 1960s provided a larger market, which improved design and production capabilities, established consumer familiarity and confidence, and lowered costs.

The earliest advanced composites (in prepreg form) were developed for the aerospace industry. They were based on carbon fibre reinforcements and required very high pressures and temperatures to cure them. This drove the users to either autoclaving or hot pressing to achieve the necessary conditions [**22**]. The cost of these processes became very high. Not only was the equipment, such as the expensive autoclave, but also were the materials and the tooling and consumables needed to withstand the processing conditions. For about two decades, prepregs were limited to niche applications in large aerospace structures, generally in non-critical parts. For many and complex reasons, the anticipated move of large civil aircraft aerospace to carbon prepregs in primary structures never really happened, and the materials remained inaccessible to industry, generally because of their high costs and difficult processing. Military aircraft did adopt prepreg materials, to the point that now most of the structure is carbon fibre. Light aviation also adopted composites with enthusiasm. Aircraft such as the Slingsby Firefly (see Figure 2.3) were essentially entirely composite (GFRP) [**23**]. However, these have only recently started to move towards prepregs. In the early 1980s, two factors led to important developments in prepreg technology. The first was that some areas of motorsport, particularly Formula 1, adopted prepreg composites. While this did not significantly change the technology, it did raise the profile. The other was the widespread adoption of carbon fibre composites for racing yachts, particularly in the America's Cup. Along with other applications, the yachts introduced a requirement for prepreg materials on parts that could not be autoclaved. It also meant that the curing temperatures had to be lower as the new customers, often with very large parts (i.e., yacht hulls) would not be able to pay very high 'aerospace' prices for tooling capable of operating at around 200 °C.

Figure 2.3. The first Slingsby model T67B made of composite materials [23].

2.2.3.1 Advantages of Composite Materials

A composite material essentially combines the properties of the reinforcing fibre, which for textile composites may be in the form of woven or a non-crimp fabric, with a high-performance epoxy resin matrix. The main advantages are [**24**]:

- Optimum fibre volume fraction,
- Minimum variability,
- Easy to cut accurately, either by hand methods or machine,
- Controllable tack to allow plies to stay in place during fabrication,
- Plies hold their shape and can be placed accurately,
- Simple vacuum bag processes are available using tooling and processing techniques that are familiar to the industry.

The main disadvantages are that prepregs tend to be more expensive than separate resin and fibre systems, and need to be frozen for long-term storage.

2.2.3.2 Processing of Composites

Almost any polymer matrix composite requires some degree of heat and pressure to complete the cure. The first prepregs were consolidated using a matched die moulding process to achieve the pressure, and an oven to achieve the temperature. Today, many of the prepregs used in some parts of aerospace and related industries still require autoclaves for consolidation and cure at relatively high temperatures of around 200 °C. The autoclave is necessary to achieve the minimum possible level of voids within the structure, giving the highest quality. The high-temperature cure is traditionally

necessary to give useful working temperatures in the finished composite of between 120 and 150 °C [**25**].

When prepregs were developed that could be cured under a vacuum at modest temperatures, they became useful in a much wider range of applications. Prepreg technology became available to many industries where specialist equipment such as the autoclave was not available and temperatures of 200 °C could not be achieved. Some of these prepregs were originally designed as tooling materials where the low weight and high stiffness of composites, particularly those based on carbon fibre, were advantageous, but the parts were often too large for high-temperature autoclave cure. Very large structures, including the hulls and masts of America's Cup yachts, could be produced from prepregs, using vacuum bags and large simple ovens (effectively heated sheds) to cure the composite.

Modern prepreg systems offer extreme flexibility and can be processed under any conditions that can achieve the equivalent pressure to one atmosphere and the cure temperature (typically 50 °C upwards). Far from being restricted to autoclaves, modern processing techniques include:

- Vacuum bagging;
- Pressing;
- Internal pressure bags;
- Diaphragm moulding.

The advantages demonstrated by composites, in addition to high stiffness, high strength, and low density, include corrosion resistance, long fatigue lives, tailorable properties (including thermal expansion, critical to satellite structures), and the ability to form complex shapes. (This advantage was demonstrated in the ability to create "low observable," or stealth, structures for military systems.) An example of recent composite materials application is the next-generation U.S. tactical fighter aircraft, the F-22. Over 24% of the F-22 structure is composite. The B-2 bomber, shown in Figure 2.4 is constructed using an even higher percentage of composites, as are current helicopter and vertical lift designs. The upper-use temperature of polymeric matrix composites has also increased dramatically [**5**]; early epoxies were considered useable

(for extended periods) up to 121 °C. Current generation polymers, such as bismaleimides, have increased that limit to around 204 °C, and the use of polyimide-matrix composites has extended the range to 288 °C.

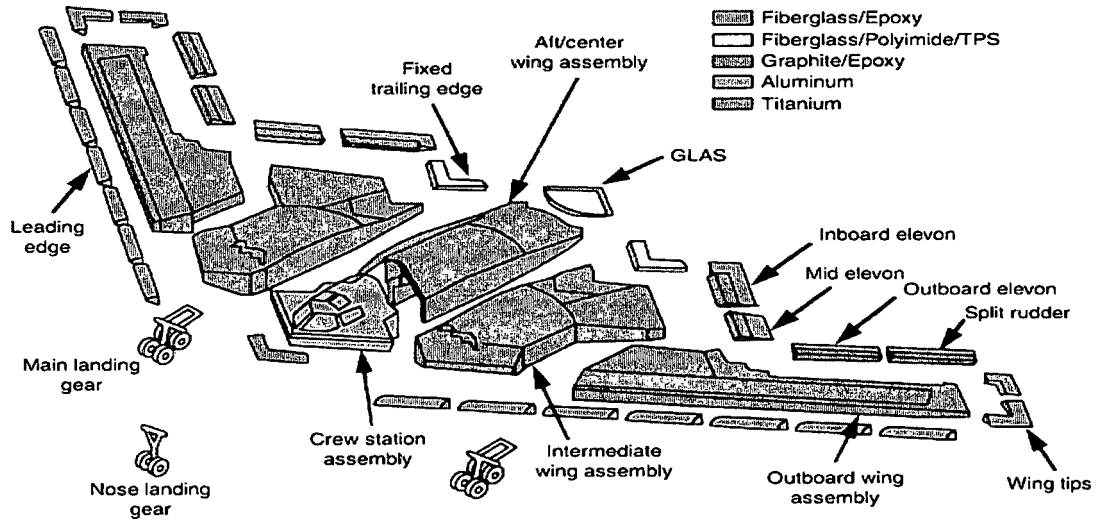

Figure 2.4. All-composite U. S. Air Force B-2 constructed mainly from advanced composite materials [5].

2.2.4 Thermoplastic Composites

Thermoplastic-based composites differ from thermoset-based composites due to the nature of the matrix because the often time-consuming chemical reaction (crosslinking) is not required during the processing of thermoplastics. Harmful chemical emissions are generally reduced during processing. The long shelf-life of thermoplastics is also an advantage because sub-ambient storage is not required. Thermoplastic composites offer increased recyclability and can be post-formed or reprocessed by the application of heat and pressure [**20**]. A large range of tough matrix materials is also available.

The manufacture of components from textile thermoplastic composites requires a heating process, either directly before the final moulding process, where an oven plus a cool tool is used (non-isothermal processing), or in a hot mould (isothermal

processing). This is needed to raise the polymer matrix temperature sufficiently above the melting temperature (T_m) to reduce viscosity for impregnation of the textile structure during the final conversion process.

The application of pressure is necessary to give intimate contact and hence heal adjacent yarns and plies, reducing void content, and complete consolidation followed by cooling, under pressure, to solidify and crystallise the matrix to finish the cycle (see Figure 2.5). Heat transfer thus forms the principal boundary condition governing process cycle times, with a corresponding potential for lower conversion costs. These basic steps define the many processing techniques that can be used to transform different material forms into the final product, where considerable flexibility exists to heat and shape the textile composites.

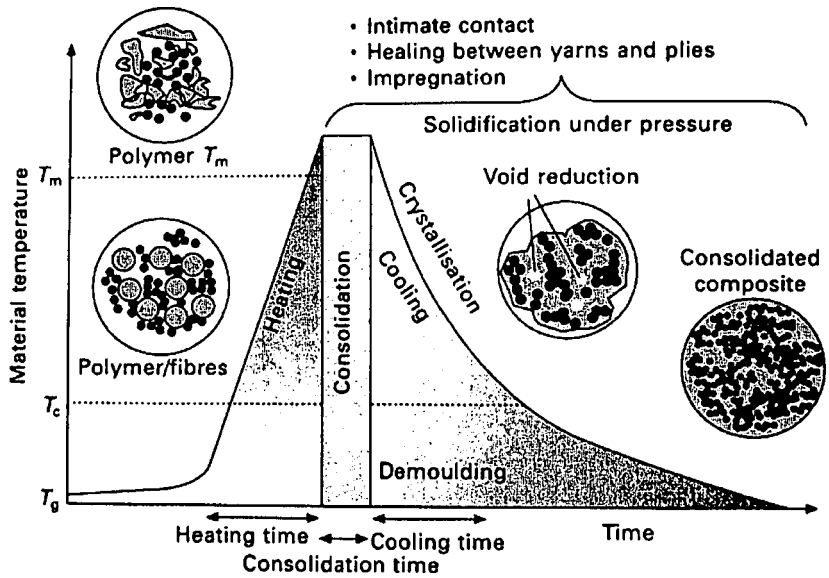

Figure 2.5. Thermal cycle for thermoplastic composite processing. T_m = melt temperature, T_c = crystallisation temperature, T_g = glass transition temperature [20].

Thermoplastic composites evolved from structural polymer composites. While structural polymer composites (i.e., epoxy and polyester thermosetting resins reinforced with continuous fibres) had many beneficial properties such as low density, good mechanical properties combined with good insulation and environmental resistance, they suffered from chemical instability, i.e., the impregnated intermediate or prepreg has a limited shelf life.

Thermoplastic composites do not suffer from this problem as they use a thermoplastic matrix. When heated they soften and can be remoulded without degradation. When they cool, they solidify into the finished shape. This heating/cooling cycle can be repeated many times, thus giving the product an almost indefinite shelf life. They can be shaped using techniques derived from wood and metal working and have increased damage tolerances due to the tough nature of the matrix material. They also lend themselves to recycling, unlike thermoset composites.

2.2.4.1 Engineering Textiles for Composites

Rapid progress in the field of composites has been observed since the introduction of fibres of high specific strength and stiffness. A variety of polymers are available that can serve as a matrix in the fibre-reinforced plastic (FRP) composites. Knowledge of the thermo-mechanical behaviour of unidirectional laminated composites has increased tremendously in recent years. Fibres in textile forms are used in composites to yield advantages such as better dimensional stability, suitable conformability, and deep draw moldability/shapability **[20,26]**.

The variety of manufacturing methods has made textile composites cost-competitive with unidirectional laminated composites. Textile composites are being considered for high intra- and inter-laminar strength and damage resistance. Among the various textile forms, woven fabrics are the most widely used in composites. The 2D orthogonal fundamental weave are plain, twill, and satin as shown in Figure 2.6.

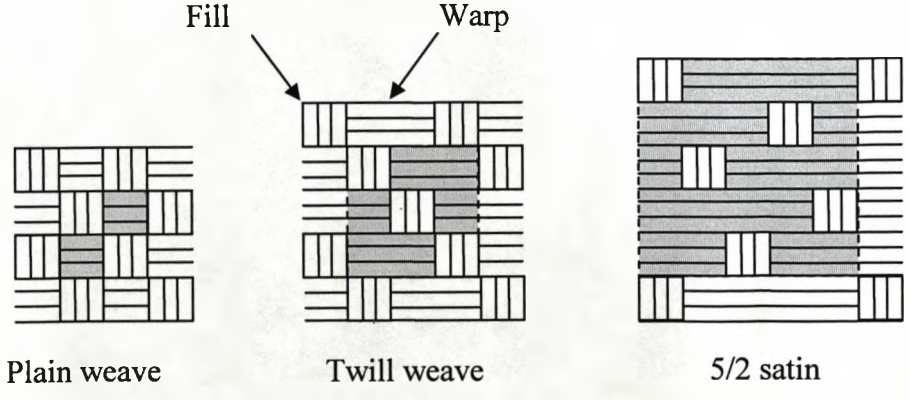

Figure 2.6. Fundamental weave structures [27].

Textiles composites can be formed by weaving, braiding, or knitting the fibre bundles or "tows" to create interlocking fibres that often have orientations slightly or fully in an orientation orthogonal to the primary structural plane. This approach is taken for a variety of reasons, including the ability to have structural, thermal, or electrical properties in the third or "out-of-plane" dimension. Another often cited reason for using these architectures is that the "unwetted" or dry fibre preforms (fibres before any matrix is added) are easier to handle, lower in cost, and conform to highly curved shapes more readily than the highly aligned, continuous fibre form.

In addition to these general categories, it is possible to create fibre architectures that are combinations of two or more of these categories. For example, it is possible to create laminated structures of both knitted fabric and continuous fibre layers. The design flexibility offered by composites is truly infinite [**28**].

Woven fabric composites provide more balance properties in the fabric plane and higher impact resistance than unidirectional composites, and the interlacing of yarns provides higher out-of-plane strength, which can support to secondary loads due to the load path eccentricities, local buckling, etc. It is easier to build thick laminates with woven fabrics than with unidirectional tapes and the handling of woven laminates is easier [**27,29**].

Woven composites offer a number of advantages over unidirectional tapes. Significant cost savings are often achieved during the manufacturing operation since lay-up labour requirements are reduced and complex shapes produced in a single operation.

2.2.4.2 SRPP Composite

Self-reinforced polypropylene is a 100% polypropylene consisting of highly aligned polypropylene fibres embedded in a polypropylene matrix in a woven presentation (Curv® from Propex fabrics). The characteristics and advantages of the SRPP are presented as follow [**30**]:

- ***Weight saving:*** Low density, combined with good mechanical properties, allows the potential for significant weight saving over an equivalent glass reinforced part. Design studies suggest 50% weight savings are possible for the same mechanical stiffness through careful attention to design details.

- ***100% PP:*** Independent life cycle studies demonstrate that 100% polypropylene composites offer significant environmental advantages over alternative fibre-reinforced materials.
- ***Contains no glass:*** The SRPP is gentle on moulds and cutting tools, it is easy to handle in the workplace and causes none of the irritation associated with materials containing glass fibres. Finished surfaces are smooth and hardwearing and products can be used without additional coatings.
- ***Thermoformable:*** SRPP thermoforming characteristics enable parts to be produced using low pressure, low cost tooling at modest temperatures. Significant reductions can be achieved in both capital equipment and energy usage compared to thermoforming alternative fibre-reinforced thermoplastics.
- ***High impact strength:*** The highly aligned fibres combined in a woven structure, results in a good candidate material for impact resistance. All the more remarkable is that the colder it gets (above its glass transition, T_g = -15 °C), the tougher SRPP becomes, providing maximum protection when other materials become easily broken.
- ***Inert:*** SRPP is 100% polypropylene, a material widely recognised as being non-toxic and highly resistant to corrosion. It passes major motor manufacturer's tests for resistance to hydraulic fluids and fuels, washer fluid, etc.
- ***Resistant to abrasion:*** SRPP toughened structure results in a very high level of abrasion resistance which out-performs conventional thermoplastics and fibre-reiforced composites. It is easily cleaned and additional surface protection is not needed.

2.2.5 Application of Composite Materials

Composite materials are being used in an increasing number of applications. The desired mechanical properties can be obtained by carefully selection of the properties of the reinforcements and matrices. Composite materials are ideal for structural applications especially in the aerospace industry where high strength and stiffness to weight ratios are a primary requirement **[3,24]**. In addition, these materials also offer other advantages including a high fatigue resistance and a superior environmental resistance.

Due to the light weight and high toughness, composites have been adopted almost everywhere for the use in the automotive industry. Applications include seat frames, battery trays, bumper beams, load floors, front ends, valve covers, dash panels, fuel tank, fluids containers, under engine covers, etc. (see Figure 2.7). Similarly, thermoplastic composites are used in the construction industry, maritime, aerospace, sport, household appliances and virtually in every moment of our changing life. Even the composite materials designed especially for the aerospace industry such as carbon/epoxy are being used everyday more commonly such as bike frames, tennis rackets, and fashion articles.

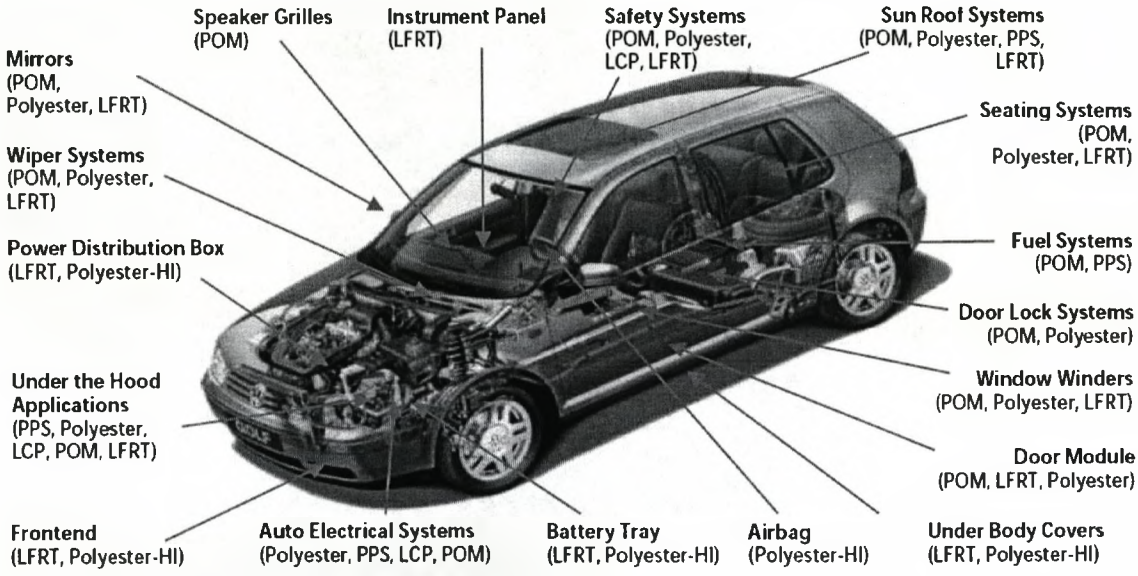

Figure 2.7. An example of the use of composites in a car, VW Golf IV [31].

2.2.6 Advantages and Disadvantages of Composite Materials

All reinforced plastic composites are likely to contain defects of various kinds arising from the process of manufacture. Indeed, composites are noted for the variability of mechanical properties they exhibit unless they have been produced under the most rigorously controlled conditions. The variability of materials produced by hand lay-up methods is more marked than that of composites made by mechanised processes. The specific nature and severity of the defects found in any manufactured product will be also characteristic of the manufacturing process. In addition, any composite consisting of materials of widely different thermal expansion coefficient which is heated during

manufacture may, on cooling, develop residual stresses sufficiently high to crack a brittle matrix. The defects that may be present in manufactured composites highlighted by Harris [**19**], include:

- Incorrect state of resin cure, especially that resulting from variations in local exothermal temperatures in thick or complex sections during autoclaving,
- Incorrect overall fibre volume fraction,
- Misaligned or broken fibres,
- Non-uniform fibre distribution, with resultant matrix-rich regions,
- Gaps, overlaps or other faults in the arrangement of plies,
- Pore or voids in matrix rich regions,
- Disbonded interlaminar regions,
- Resin cracks or transverse ply cracks resulting from thermal mismatch stresses,
- Disbonds in thermoplastic composites resulting from failure of separated flows to re-weld during moulding,
- Mechanical damage around machined holes, and
- Local bond failures in adhesively bonded composite components.

2.3 Metal Alloys

Metal alloys, by virtue of composition, are often grouped into two classes; ferrous and nonferrous. Ferrous alloys, those in which iron is the principal constituent, include steels and cast irons and the nonferrous ones, are all the alloys that are not iron based. Ferrous alloys are widely used as engineering materials in construction structures, since they offer a broad range of mechanical and physical properties and may be fabricated with relative ease and economical procedures. However, they are susceptible to corrosion and have a relatively high density. Therefore, for certain applications such as in the aerospace industry, it is advantageous or even necessary to use other kinds of alloys, such as nonferrous alloys that are not iron based [**32**]. Thus, the aerospace industry has extensively used aluminium alloys as one of its principal constituents in aircraft structures. This is due to its ease of forming, relative low density and high corrosion resistance in some common environments. However, aluminium suffers a decrease in its mechanical properties at relatively high temperatures [**33**]. As a consequence, sometimes it is necessary to consider other

metals for aerospace structures. Titanium alloys appear to be excellent candidates for many high temperature applications.

2.3.1 Ferrous Materials

Steel and other ferrous alloys are consumed in exceedingly large quantities because they have such a wide range of mechanical properties, fabricated with relative ease, and are economical to produce. However, they have some distinct limitations, such as: a relatively high density, a comparatively low electrical conductivity, and an inherent susceptibility to corrosion in some common environments. Thus, for many applications it is advantageous or even necessary to utilise other alloys having more suitable property combinations. Alloy systems are classified either according to the base metal or according to some specific characteristics that a group of alloys share [**34**].

On occasions, a distinction is made between cast and wrought alloys. Alloys that are so brittle that forming or shaping by appreciable deformation is not possible ordinarily, are classified as cast alloys. On the other hand, those that are amenable to mechanical deformation are termed wrought alloys. In addition, the heat treatability of an alloy system is mentioned frequently. ''Heat treatable'' designates an alloy whose mechanical strength is improved by precipitation hardening or a martensitic transformation (normally the former), both of which involve specific heat-treating procedures [**32**].

2.3.2 Aluminium Alloys

Aluminium ore, most commonly known as bauxite, is plentiful in the Earth and occurs mainly in tropical and sub-tropical areas: Africa, West Indies, South America and Australia. There are also some deposits in Europe. Bauxite is refined into aluminium oxide trihydrate (alumina) and then electrolytically reduced into metallic aluminium. Primary aluminium production facilities are located all over the world, often in areas where there are abundant supplies of inexpensive energy, such as hydroelectric power [**35,36**]. Two to three tonnes of bauxite are required to produce one tonne of alumina and two tonnes of alumina are required to produce one tonne of aluminium metal.

Aluminium alloys are widely used in everyday life such as, in aerospace, maritime, automotive and industry in general. This metal is the second most abundant in the earth and also the most popular due to its mechanical and physical properties such as light weight, weather chemical resistant. Aluminium has a density of 2.7 g/cm^3, approximately one third that of steel (7.83 g/cm^3). Many of these alloys are easily formed by virtue of their high ductility; this is evidenced by the thin aluminium foil sheet into which the relatively pure material may be rolled. Since aluminium has an FCC crystal structure (see more properties in Table 2.2), its ductility is retained even at very low temperatures. The limitation of aluminium is its low melting temperature (approximately 660 °C), which restricts the maximum temperature at which it can be used [**37**].

Aluminium alloys, which are usually called light alloys, have been developed in order to increase the strength of the base metal, aluminium. Pure aluminium is soft, ductile, corrosion resistant and has a high electrical conductivity. In consequence it is widely used for foil and conductor cables, but alloying with other elements is necessary to provide the higher strengths needed for other applications [**38**]. During the First World War, aluminium alloys were first employed on a large scale. Since then, aluminium alloys have been widely and successfully used in the aeronautic and industry in general. A consideration of the relative densities shows why this is so; the density (g/m^3) of the magnesium is 1.7, that of the aluminium is 2.7 and that of the titanium is 4.5 compared to iron with 7.9, copper with 8.9 and osmium, the heaviest metal, with 22.6.

Property	Value
Atomic Number	13
Atomic Weight (g/mol)	26.98
Valency	3
Crystal Structure	Face centred cubic
Melting Point (°C)	660
Boiling Point (°C)	2480
Mean Specific Heat (0-100°C) (cal/g.°C)	0.219
Thermal Conductivity (0-100°C) (cal/cms. °C)	0.57
Coefficient of Linear Expansion (0-100 °C) ($x10^{-6}$/°C)	23.5
Electrical Resistivity at 20 °C (μΩcm)	2.69
Density (g/cm^3)	2.6898
Modulus of Elasticity (GPa)	68.3
Poisson's Ratio	0.33

Table 2.2. Typical properties for aluminium [37].

High purity aluminium (> 99%) in the annealed condition has very low yield strength (7-11 MPa), which is too low for most structural applications. Consequently alloying is necessary. The principal elements added to aluminium to enhance strength are manganese, copper, zinc, magnesium and silicon. Figure 2.8 shows the effect of the addition of various elements to aluminium on yield strength. It can be seen from the figure that magnesium is the most effective strengthener on a weight basis because of its relative high solubility. The simple addition of alloying elements to aluminium, which go into solution, does not, however, produce the substantial strengthening required for structural applications. The strength of most alloys can be readily improved by either cold working (strain hardening in case of non-heat-treatable alloys) or by careful heat treatment [**32,39**].

Aluminium alloys are classified as either heat-treatable or non-heat-treatable. Alloys that respond to precipitation hardening are termed heat-treatable and those that do not respond to heat treatment are called non-heat-treatable alloys. Most alloys used in the aerospace industry belong to two systems, both of which are precipitation hardenable; the Al-Zn-Mg-Cu (7000 series) and the Al-Cu-Mg (2000 series) systems.

The chemical composition of the aluminium 2024 (wt %) is; 0.5 (Silicon), 0.5 (Iron), 3.8-4.9 (Copper), 0.3-0.9 (Manganese), 1.2-1.8 (Magnesium), 0.1 (Chromium), 1.7-

2.3 (Nickel), 0.25 (Zinc), 0.15 (Titanium), 0.05-0.15 (others) and aluminium (remainder).

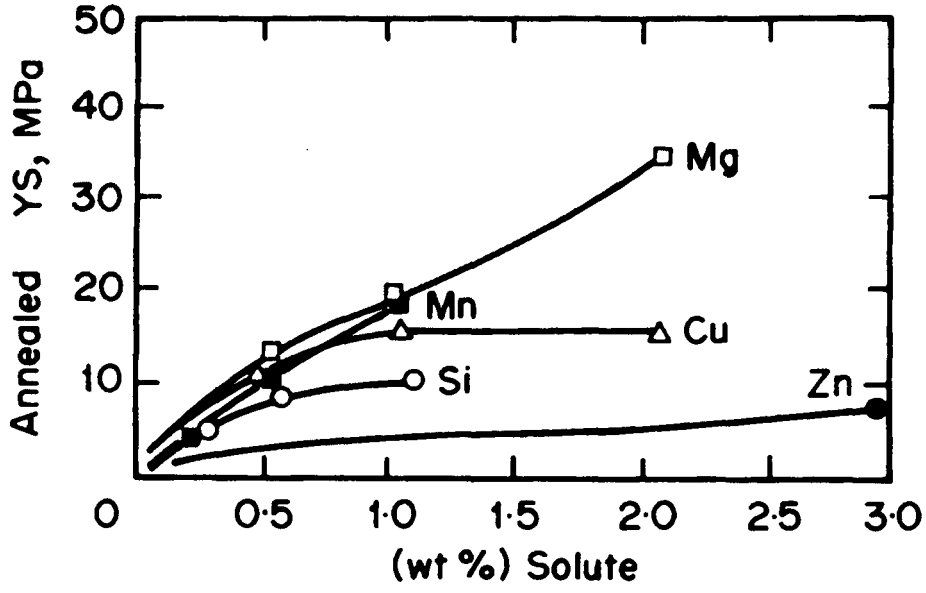

Figure 2.8. The effect of alloying elements on the yield strength of aluminium [33].

Generally, aluminium alloys are classified as either cast or wrought. Composition for both types is designated by a four-digit number (used by the International Alloy Designation System IADS) that indicates the principal impurities, and in some cases, the purity level. For cast alloys, a decimal point is located between the last two digits. After these digits is a hyphen and the basic temper designation; a letter and possibly a one to three digit number, which indicates the mechanical and/or heat treatment to which the alloy has been subjected. For example, F, H, and O represent, respectively, the as-fabricated, strain hardened, and annealed states; T3 means that the alloy was solution heat treated, cold worked, and then naturally aged (age hardened). A solution heat treatment followed by artificial aging is indicated by T6. The compositions, properties, and applications of several wrought and cast alloys are contained in Table 2.3. Some of the more common applications of aluminium alloys include aircraft structural parts, beverage cans, bus bodies, and automotive parts (engine blocks, pistons, and manifolds).

Major Alloying Element	Wrought	Cast
None (99% < Aluminium)	1XXX	1XXX0
Copper	2XXX	2XXX0
Manganese	3XXX	
Silicon	4XXX	4XXX0
Magnesium	5XXX	5XXX0
Magnesium + Silicon	6XXX	6XXX0
Zinc	7XXX	7XXX0
Lithium	8XXX	
Tin		9XXX0

Table 2.3. Aluminium alloy designation system [38].

Special attention has been given to alloys of aluminium and other low-density metals (i.e., Mg and Ti) as engineering materials for transportation, to effect reductions in fuel consumption. An important characteristic of these materials is specific strength, which is defined as the tensile strength–specific gravity ratio. Even though an alloy of one of these metals may have a tensile strength that is inferior to a more dense material (such as steel), but on a weight basis, it will be able to sustain a greater load. A generation of new aluminium-lithium alloys have been developed recently for use by the aircraft and aerospace industries. These materials have relatively low densities (between about 2.5 and 2.6 g/cm^3), high specific modulus, and excellent fatigue and low-temperature toughness properties. Furthermore, some of them may be precipitation hardened. However, these materials are more costly to manufacture than the conventional aluminium alloys because special processing techniques are required as a result of lithium's chemical reactivity.

The 2000, 4000, 6000, 7000 and 8000 series alloys respond as follows; the wide choice of alloy compositions, solution heat treatment temperatures and times, quench rates from temperature, choice of artificial ageing treatment and degree to which the final product has been deformed, permit a wide range of properties to be achieved.

A system of standard designations is used, based upon the letter 'T' followed a number after the alloy designation, to describe the various conditions. These are defined in Table 2.4.

T1	Cooled from an elevated temperature shaping process and naturally aged to a substantially stable condition. This designation applies to products which are not cold worked after cooling from an elevated temperature shaping process, or in which the effect of cold work in flattening or straightening has no effect on mechanical properties
T2	Cooled from an elevated temperature shaping process, cold worked and naturally aged to a substantially stable condition. This designation applies to products which are cold worked to improve strength after cooling from an elevated temperature shaping process, or in which the effect of cold work in flattening or straightening does have an effect on mechanical properties.
T3	Solution heat-treated, cold worked and naturally aged to a substantially stable condition. This designation applies to products which are cold worked to improve strength after solution heat-treatment, or in which the effect of cold work in flattening or straightening does have an effect on mechanical properties.
T4	Solution heat-treated and naturally aged to a substantially stable condition. This designation applies to products which are not cold worked after solution heat-treatment, or in which the effect of cold work in flattening or straightening does not effect mechanical properties.
T5	Cooled from an elevated temperature shaping process and then artificially aged. This designation applies to products which are not cold worked after cooling from an elevated temperature shaping process, or in which the effect of cold work in flattening or straightening does not affect mechanical properties.
T6	Solution heat-treated and then artificially aged. This designation applies to products which are not cold worked after solution heat-treatment, or in which the effect of cold work in flattening or straightening does not affect mechanical properties.
T7	T7 Solution heat-treated and overaged/stabilised. This designation applies to products which are artificially aged after solution heat-treatment to carry them beyond a point of maximum strength to provide control of some significant characteristic other than mechanical properties.

*Table 2.4. Definition of heat treatment designations for aluminium and aluminium alloys [**38**].*

2.4 Fibre-Metal Laminates

Fibre-Metal Laminates (FMLs) are hybrid materials, consisting of alternating layers of thin metal sheets and composite layers. This allows the material to behave much as a simple metal structure, but with considerable specific advantages regarding properties such as metal fatigue, impact, corrosion resistance, fire resistance, weight-savings and specialised strength properties [**40,41**].

These layers are bonded together with the matrix material in the composite layer. FMLs represent a family of new materials: the three main components, the metal alloy, the fibre system and the matrix or resin, are variables which may result in a wide range of different materials. The variety of laminates is further increased by variation of the thickness of the layers, the number of layers in the laminate, and the fibre orientations. For example, Figure 2.9 presents a glass-reinforced laminate, GLARE 2-3/2-0.4 laminate constituents. This commercial laminate is made of the aluminium 2024-T3 alloy, and a unidirectional ply consisting of S-glass fibres in a FM94 epoxy resin with a symmetrical lay-up. In this laminate, each composite layer is made of two unidirectional plies, oriented in the same direction, resulting in a unidirectional laminate [**42**].

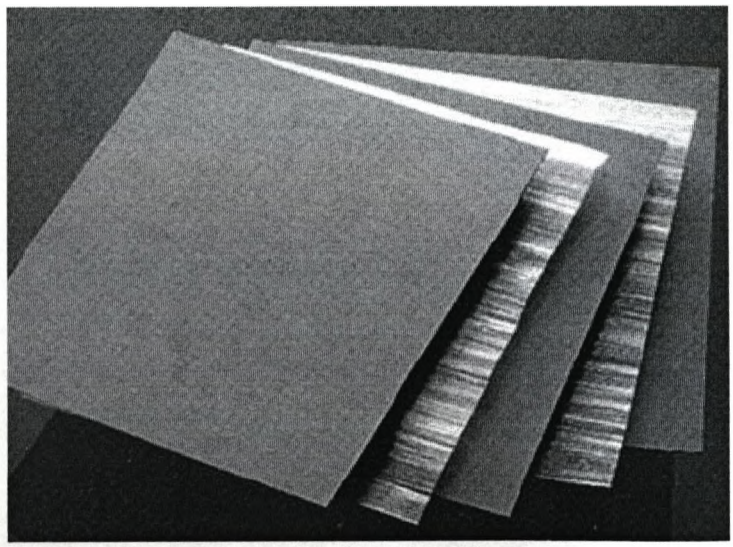

*Figure 2.9. Composition of a GLARE 2-3/2-0.4 laminate [**42**].*

FMLs are relatively novel hybrid materials, which consist of alternating thin metal alloy layers and thin fibre-reiforced polymer matrix composites layers (see Figure 2.10). These hybrid structures are excellent candidates for use in fuselage skin structures in high capacity aircraft not only because of their impressive mechanical properties but also due to the associated reduction in costs and increased damage tolerance [**42-44**].

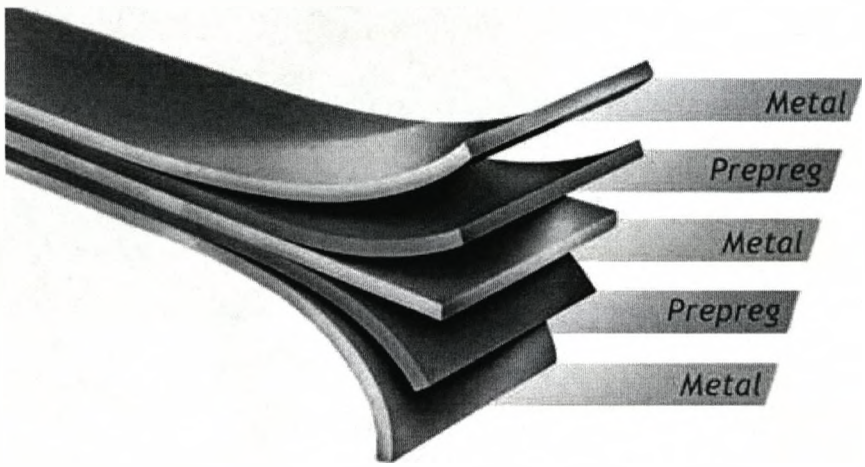

*Figure 2.10. Typical arrangement of a fibre-metal laminate [**41**].*

The aircraft industry is very conservative in the adoption of new designs and technologies. Significant safety issues and low profit margins provide little incentive to change. Even when new aircraft are introduced, they tend to build heavily upon past designs, introducing only incremental updates in technology. Large changes can occur, but the process is very slow.

The history of GLARE can be traced back to early bonded wood and bonded metal aircraft structures. True fibre-metal laminates, comprised of alternating thin layers of aluminium and fibre-reinforced plastic composites, were first developed in the 1970s. The first commercial FML was ARALL, an aramid-aluminium laminate developed at the Delft University of Technology. ARALL was used in a few select aircraft components, but it had structural limitations that prevented wider use. GLARE, a glass-reinforced laminate, was developed in part to overcome these limitations [**22,43**]. The new A380 jumbo jet from Airbus is making extensive use of GLARE in its fuselage.

The idea of the FMLs originates from the 1950s at Fokker in Netherlands, where a bonded laminated structure was found to successfully prevent rapid fatigue crack growth as it can occur in monolithic materials. Milling machines were too expensive for the company that was almost destroyed during the Second World War. Instead of integral machine structures, Fokker chose laminated bonded structures to tailor the local strength. As an added benefit, fatigue cracks in laminated aluminium structures appear to remain mainly in the outer layer. In the late 1970's, the first tests were performed with fibres used to reinforce the bondlines.

In the early 1980's, fibre-metal laminates were developed as an optimised laminated semi-finished sheet [**45,46**]. This was achieved by creating an optimised laminate of thin aluminium layers combined with fibre/epoxy layers. The optimal metal fraction relative to the fibre/epoxy content appeared to be crucial for a satisfactory fatigue performance. From experiments with this new laminate, it became clear that even when large fatigue cracks are present in the aluminium layers, FMLs still show an excellent fatigue performance. The key to this behaviour is the so-called fibre crack bridging mechanism. The stress intensity at the crack tip in the aluminium layers is reduced by effective crack closure stresses in the fibres. The fibres do not fail during crack opening because shear stresses in the adhesive create a controlled delamination under fatigue loading.

The tensile properties of unidirectional FMLs have been described and predicted by using a rule of mixtures approach [**47,48**]. Wu *et al.* [**47**] studied the ultimate tensile strength, yield strength and elastic modulus of FMLs based on a glass fibre-reiforced epoxy. They showed that the tensile strength and tensile modulus are linear functions of the metal volume fraction and that both properties can be predicted using a rule of mixtures approach. Such trends agree with the results obtained by Reyes and Cantwell [**48**] following tensile tests on FMLs based on a glass fibre-reiforced polypropylene.

The initial development of FMLs appears to be a consequence of the limitations in the fatigue properties of the aluminium alloys used in the civil and military aircraft structures. Initially, several thin aluminium layers were bonded together using an adhesive. This new structure, used by the Netherlands Aircraft Factories in a Fokker

F-27, showed a superior fatigue resistance and a higher fracture toughness than its monolithic counterpart [**49**].

The first generation of laminates based on aramid fibres, was called ARALL, and was produced by ALCOA and AKZO. ALCOA was the first industry that could deliver Al 2024-T3 in a thickness of 0.3 mm. These laminates had unidirectional fibre layers and were developed primarily for aircraft wings applications. In 1987 a second generation of laminates was developed with the name GLARE, which was based on high strength glass fibres. Whereas ARALL had unidirectional fibre layers because it was optimised for wing structures, GLARE was developed in a unidirectional variant (GLARE 1 based on Al 7475 and GLARE 2 on Al 2024) as well as biaxial variant (GLARE 3 on Al 2024 with an equal percentage of fibres in the 0° and 90° directions, and GLARE 4 with double the percentage in 0° direction) [**50**].

The subsequent introduction of carbon fibres into the FMLs, resulted in a material known as CARE (carbon-reinforced aluminium laminate). The first CARE laminates were based on T300 carbon fibres, which offered a poor fatigue performance and poorer notch sensitivity than monolithic aluminium alloys [**49**]. The addition of stronger and stiffer carbon fibres with greater failure strains such as TENAX IM-600 and TORAY T-800, lead to improved CARE laminates with higher tensile, compressive and fatigue properties than GLARE. Unfortunately, due to the cathodic nature of carbon fibres, galvanic corrosion occurs in CARE laminates [**51**]. This problem can be solved by isolating the carbon fibres from the aluminium alloy. However, CARE laminates are still under development and are not yet commercialised [**51**]. FMLs for supersonic aircraft applications (such as titanium-CF/PEEK or titanium-GF/PEI) can be used at temperatures up to 250 °C; however, they are still being researched [**52**].

A comparison of the tension and compression stress-strain values of commercial aramid-epoxy, ARALL-1 and aluminium 7075-T6 is shown in Figure 2.11, where it is clear to see that the properties of the FML improves over its constituents.

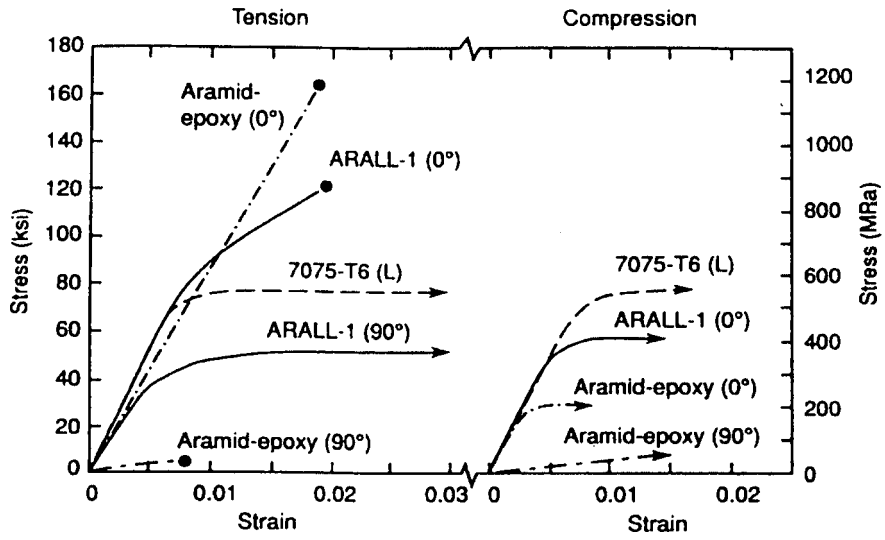

Figure 2.11. Typical stress-strain curves for an ARALL laminate and its constituents at room temperature [53].

2.4.1 Manufacturing Process

The designation system that FMLs use is based on the number of metal and composite plies that form the laminates. A designation 4/3, indicates that the lay-up contains 4 layers of metal and 3 layers of composite, where the thickness of the metal plies vary from 0.2 to 5 mm [**46**]. The consolidation process of the metal sheets and the fibre composite prepreg is achieved using either a press or preferably an autoclave. Generally, the aluminium plies are initially subjected to an etching process to remove the existing oxidised layer. They can subsequently be anodised to create an oxide layer with a uniform morphology. The surface can also be treated with a primer to enhance the durability of the bond [**54**]. This process has resulted in a good bond quality between the aluminium and the prepreg layers. However, several studies have been undertaken in order to characterise and improve metal-matrix adhesion [**55-58**]. It has been shown that chemical and mechanical treatments applied to the metal surface enhance bonding between the metal and the matrix materials. Kinloch [**59**] commented that chemical treatments yield a superior joint durability than mechanical treatments such as the use of wire brushes, sand paper, abrasive pads, grit and sand-blasting. The study showed that a simple abrasion/solvent wipe promoted high interfacial fracture energies. Reyes and Cantwell [**60**] used different mechanical and chemical treatments on aluminium surface to enhance the adhesion between the core

and metal in FML systems, where it was demonstrated that a simple abrasion/solvent wipe enhances the interfacial adhesion.

FMLs can be tailored to suit a variety of applications by varying the fibre-resin system, the alloy type and thickness, stacking sequence, fibre orientation (such as uniaxial and crossply), surface preparation technique, and the degree of postcure stretching or rolling. The number of combinations is many and varied. Nowadays, the number of types of fibre-metal laminate is increasing. The metal used is mostly a high strength aluminium but the composite varies greatly. For example, there are a number of more specialised FMLs such as those based on titanium/PEEK [**61**] and the aluminium/SRPP [**48**], both developed at Liverpool University.

2.4.2 Fracture Mechanisms of FMLs

FMLs were primarily developed for their excellent damage tolerance properties, amongst which the fatigue resistance is the perhaps most important. During fatigue, as with metals, cracks can occur in FMLs when the stress level is sufficiently high. Crack initiation starts at a free surface, i.e., at the outer layer of the laminate, where the crack tends to grow. In metal alloys this crack can grow increasingly up to the failure, but for FMLs there can be a reduced crack growth by the influence of the unbroken fibres in the composite system that transfer and redistribute the stresses [**44**].

The impressive fatigue performance of FMLs has been attributed to a fibre bridging mechanism in the wake of the primary crack, an effect which reduces the stress intensity at the crack tip, restraining crack propagation in the metal layers as highlighted by Sinke [**42**] (see Figure 2.12). It has also been established that fatigue crack growth in the metal layers is accompanied by the growth of a delaminated region around the crack, due to the presence of cyclic shear stresses in the adhesive. This cyclic shear stress behaviour transfers the load from the metal to the fibres, ensuring the re-distribution of strain generated by the crack opening effect and preventing fibre failure. The magnitude of the bridging stress in the fibres is related to the crack opening displacement and the length over which the bridging fibres are elongated [**46**].

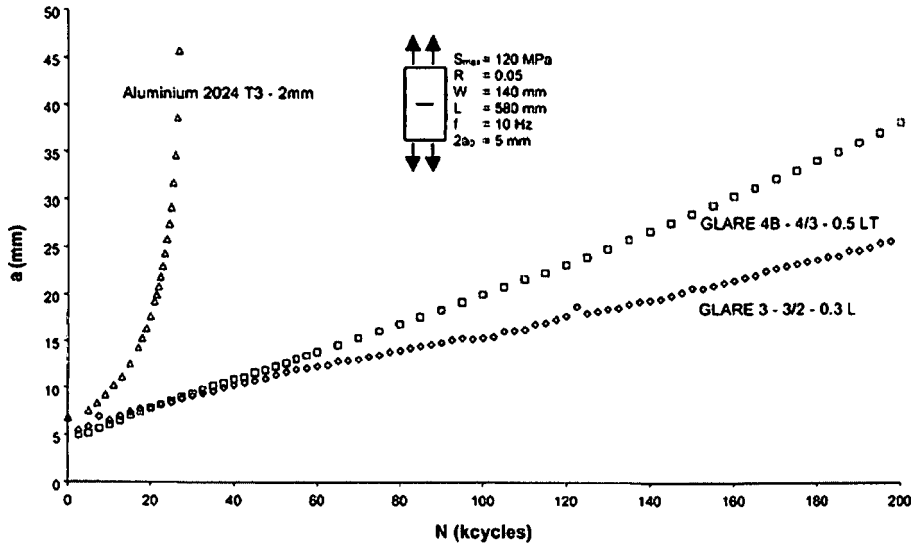

*Figure 2.12. Crack growth curves for Al-2024-T3 and GLARE-3 and -4 [**42**].*

The reduced crack growth is caused by bridging of the fibres (see Figure 2.13). When loaded in fatigue, the crack propagates in the metal layer. The fibre layers however, stay intact reducing the stresses over the crack, thereby reducing the stress intensity factor at the crack tip in the metal layers [**43,49,62**]. Also, metal laminates show some crack bridging but this effect is much smaller than for a FML with fibres in the adhesive layers. Effective fibre bridging is only possible in combination with a correct distribution of the metal and composite layers. This delamination is necessary to give the fibres enough length for elongation. From the crack propagation and delamination growth observed in experiments, it is concluded that both mechanisms are in balance with each other [**63**]. If this delamination was absent, fibre failure would occur, and increasing crack growth would take place. When the debonded region becomes too large, i.e., when the thickness ratio of the metal and composite layers is too large, crack bridging is less effective and the crack growth becomes greater.

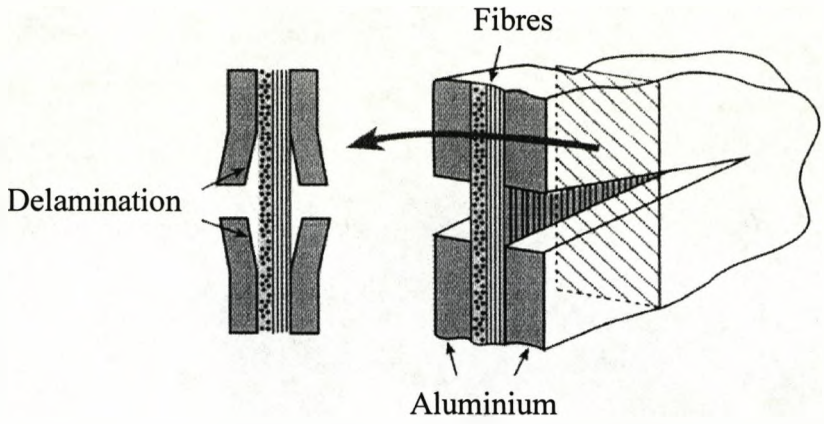

Figure 2.13. Schematic of the fibre bridging mechanism in FMLs [49].

Also the layered nature of the laminate has a large impact on the fatigue life of the FML. As stated previously, crack initiation starts at an outer surface of the FML. Once a crack starts to grow, it takes some time before initiating in the second layer. A through crack in an FML is therefore rare and generally occurs due to some other cause such as damage by a foreign object.

2.4.3 Impact Response of FMLs

One of the major advantages of aluminium alloys over composites is their high resistance to impact loading. Aluminium structures barely suffer any damage from low energy impacts and any minor damage is immediately visible as a dent on the surface of the metal [**64-67**]. On the other hand, fibre-reinforced plastics are highly susceptible to damage, even from relatively low energy impacts, this has been studied widely by Cantwell *et al.* [**68-70**]. Damage from low velocity impact loading is generally internal, taking the form of delamination, that may not be readily detectable, but this can reduce the stiffness of the laminate quite considerably [**51**]. In this respect, the presence of aluminium on the surface of fibre-metal laminates is highly advantageous, in that it can provide a ready mechanism (in the form of an indentation), by means of which impact damage in the laminate can easily be detected.

A number of studies had been carried out in order to evaluate the low velocity impact performance of FMLs [**46,71-73**]. For example, Figure 2.14 shows a comparison of the energy needed to create a through crack under static, low velocity and high

velocity impact loading on aluminium 2024-T3, GLARE 3, GLARE 3I, ARALL and carbon/epoxy for an approximately equal areal density (3.4 kg/m^2). ARALL, CARE and carbon/epoxy have low failure energies [**64**]. The failure energies of GLARE and monolithic aluminium are comparable. The failure energies tend to increase under higher velocity impact. This is related to the strain rate dependent behaviour of the materials and greater dissipation of energy at higher velocities in the form of vibrations.

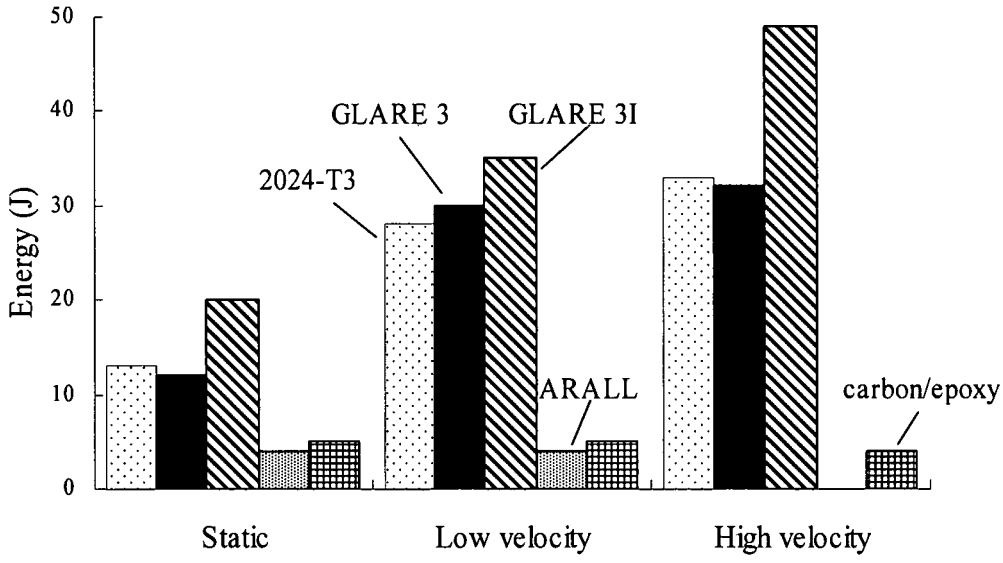

*Figure 2.14. Puncture energies (through crack) for different materials [**64**].*

2.4.4 Applications of FMLs

When considering a material for aircraft applications, an important property is its impact resistance. During operation, an aircraft may encounter many threats such as dropped tools or that associated by flying debris during taking off and landing, hail, thunder, birds, etc. Compared to aluminium alloys and composites, FMLs generally offer superior impact properties. For many types of impact, the metal layers in the laminate absorb significant energy through plastic deformation, while the fibres redistribute the stresses through a membrane effect. Additional advantages include visual dents, which ease inspection for impact damage and the superior residual strength as mentioned earlier.

FMLs were first introduced in the aerospace sector. Today, GLARE is being used in the leading edges of the vertical and horizontal tail plane of the Airbus A380, in addition to the 400 m^2 of GLARE laminate used in the upper fuselage section of this aircraft (see Figure 2.15), representing approximately a weight saving of a ton in the aircraft [**41**]. These days, more active research is being undertaken to extend the use of these systems to more common applications such as those in marine, automotive and industry [**72,74,75**].

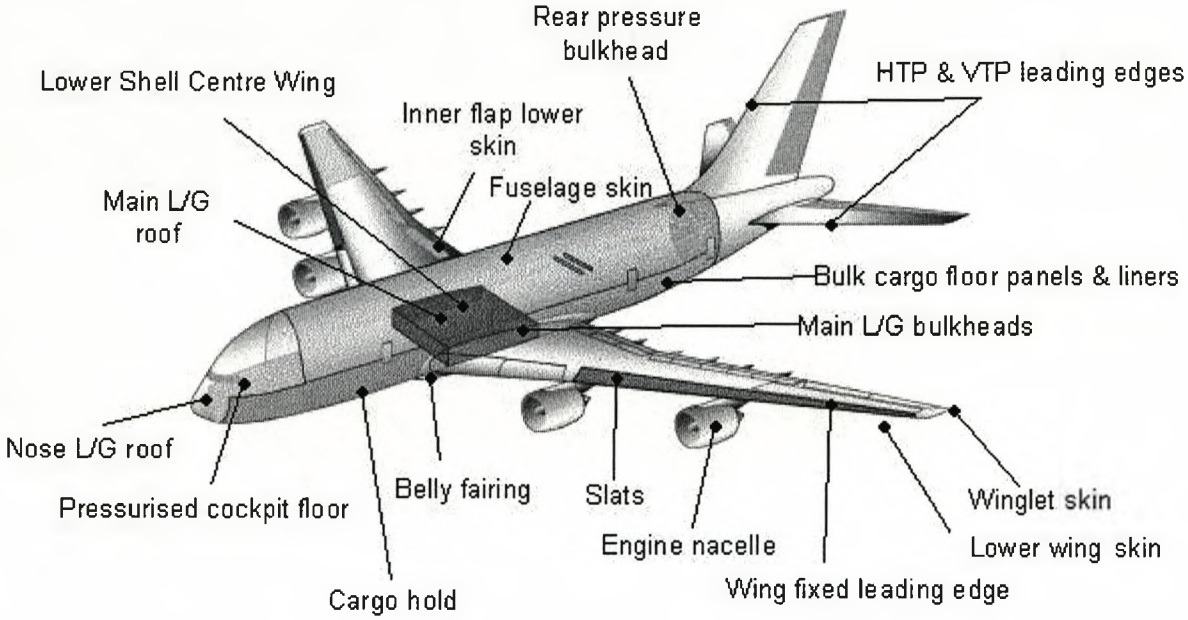

*Figure 2.15. Application of composite materials in a typical civil aircraft [**41**].*

FMLs offer an excellent resistance to blast, where the membrane stresses carry a significant part of the loads and distribute them over a large area. FMLs are currently used in blast-resistant luggage containers for aircraft. FMLs have been also used to produce specialised airline cargo containers, since GLARE is capable of withstanding the effects of an explosion, thus protecting the aircraft in which the container is placed (see Figure 2.16).

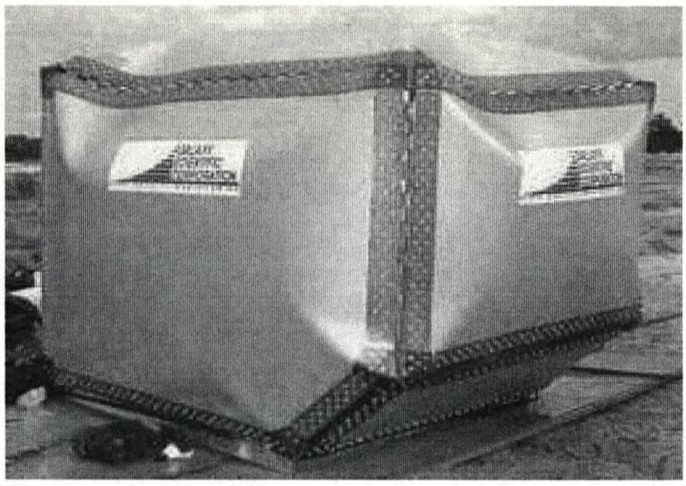

Figure 2.16. A blast-resistant aircraft container based on GLARE laminates [41]

2.4.5 Advantages and Disadvantages of FMLs

The combination of metals and composites in one laminate offers both advantages and disadvantages. The advantages are partly related to damage-tolerant properties. FMLs are, when compared to metals, very damage tolerant in terms of their fatigue, corrosion, impact, and residual strength. When compared to plain composites, damage tolerance enhancement is mainly associated with impact, durability, and fracture toughness [**43,46**].

FMLs offer advantages with respect to manufacturing. For the fabrication of FML skin panels, leading edges and small structural elements, conventional manufacturing processes can be used; these include the same lay-up techniques, some forming processes, as well as the same cutting processes. As a result, the investment costs involved in changing from metal to FML production are small.

One of the disadvantages associated with almost all fibre-metal systems is the relatively long processing cycle required to ensure complete curing of the thermosetting matrix and optimised bonding across the composite-metal interface [**48,76,77**]. In principle, this problem can overcome through the use of thermoplastic-based composites that can be moulded, bonded to metal substrate and shaped in a simply one-shot manufacturing operation. This process clearly offers an attractive option for reducing both the cycle time and the associated manufacturing costs. Other

benefits are likely to include the possibility to reform and reshape components following manufacture, an ease of repair, excellent energy-absorbing characteristics and a high resistance to localised impact loading.

2.5 Review of Scaling Effects

Until about two decades ago, it was generally believed that the size effect in structural failure was of a statistical origin, caused by the randomness of material strength. Accordingly, it was thought that studies of size effects should be left to statisticians, and that size effects should be included in a safety factor. Recently however, it has been shown that important and often dominant size effects can be of purely mechanical and design origin (such as fibre orientation, lay-up distribution, etc.). Such size effects can be caused by the influence of the release of stored elastic energy on the nominal strength of the structure. Many studies, both experimental and theoretical, have considered this type of size effect [**78-83**].

An approximate size effect law, applicable to structures in which fracture is preceded by distributed cracking in a large fracture process zone, has been formulated by Bazant [**84**]. Here, it was concluded that the scaling law follows a power law if, a characteristic dimension is absent. For all the theories in which the failure condition is expressed only in terms of stress or strain, including elasticity with a strength limit, plasticity, and continuum damage mechanics, the nominal strength of the structure is shown to be independent of its size. For linear-elastic fracture mechanics, in which the failure criterion is expressed in terms of an energy per unit area, the scaling law for the nominal strength is shown to be dependent on $(size)^{-1/2}$, provided that cracks in structures of different sizes are geometrically similar [**84**].

The importance of scale model testing has been demonstrated in areas such as aerodynamics and fluid mechanics, where data from scale model tests can be related to full-scale prototypes through well-established laws. However, in structural design and in particular, composite structures, there are no proven laws for predicting the structural response of full-scale components using scale model test data. Earlier research in the area of subscale testing [**85-87**], has indicated that complete similitude between a composite model and the full-scale component cannot be achieved. Factors

such as the fibre diameter, resin rich regions, the fibre/matrix interface, etc., cannot be scaled. Moreover, the laminated nature of a fibre-reinforced composite adds another degree of complexity to the problem of scale model testing, due to the ply constraint, edge effects, the multitude of damage modes, and the method of scaling the stacking sequence.

Weibull [**88**] developed a statistical-based strength theory to successfully model the size strength/relationship in brittle materials such as ceramics. Weibull theory was extended to unidirectional composite materials by Bullock [**89**] to successfully correlate tensile and three-point flexural strengths.

It has been demonstrated that the degree of influence depends on the type of scaling approach used, the stacking sequence and the mode of loading [**83,90,91**]. For example, Lagace *et al.* [**92**], presented results that showed that ply-level scaled $[+15°_n/-15°_n]_s$, $[+15°_n/-15°_n/0°_n]_s$, and $[0°_n/+15°_n/-15°_n]_s$ laminates, exhibited a different tensile strength degradation when the scale '*n*' was increased from 1 to 5 (here, the in-plane dimensions of the scaled specimens were kept constant). The authors attributed the observed scaling effects to interlaminar stress effects. Camponeschi *et al.* [**93**], presented compression data that highlight a strength degradation in sublaminate-level scaled laminates. He showed that the reduction in compressive strength was a through-thickness fixture-induced effect, where the fixture restraint on through-thickness Poisson expansion results in through-thickness fibre misalignment that was significant enough to account for the reduction in measured compression strength.

Most studies on composites have been conducted on aerospace-grade systems using carbon/epoxy laminates and generally use simple Weibull theory to explain any observed size effect [**94-96**]. Bullock described a study of two graphite/epoxy systems [**89**]. A simple Weibull analysis was used to compare the strength of single strand tows, tensile coupons and three point bending specimens. The effect of the difference in volume between similarly stressed tows and coupons was accurately predicted by a Weibull theory that uses both volumes and stresses based on the fibres alone. Similarly, the theory accurately predicts the differences in strength observed between

the tensile and flexural coupons of equal volume, by considering the different stress distributions present [89].

2.5.1 Scaling Study Considerations

The problem of designing, building and testing a scale model structure constructed of advanced fibre-reinforced composite materials is challenging, due to the complexity of the material itself. The problem of scaling a composite component may be examined at different levels. The most elemental approach is to scale the constituent materials (i.e., the fibre and the matrix). This approach is similar to the technique used to fabricate reinforced concrete model structures in which the reinforcing bars and aggregate size are scaled [97]. This, for a fibre-reinforced composite is practically impossible.

The composite laminate represents the next level of complexity to examine. Scaling considerations for the laminate can be simplified if the individual lamina properties are smeared, i.e., the heterogeneous nature of the material is ignored on the microscopic level and the laminate is treated as a homogeneous, orthotropic sheet. This assumption is made when macroscopic structural aspects of the problem are more significant than material considerations for achieving the scale response. For example, to construct a scale model of a stiffened panel, issues like stiffener spacing, aspect ratios, and other construction details may influence the response to a higher degree than minor irregularities in the microstructure of a single ply in the laminated panel. Thus, each level of structural complexity has its own unique set of scaling difficulties and special concerns.

In addition, it is necessary to understand how changes in the material microstructure, including the initiation and growth of damage, accumulate in the material and affect the overall structural response determination at various dimensional scales. Test data obtained in the laboratory on small coupon-type specimens are routinely assumed to be valid for full-scale structures with no regard for possible distortions due to size or scale. The limitations of scale modelling must be identified so that tests on sub-scale composite structures will generate valid data for predicting prototype behaviour. Once

the problems involved in testing scale models are identified and understood, the technique can be utilised as a valuable, cost-effective design tool [**82,98-100**].

Two approaches for scaling composites are available. In ply-level scaling, the baseline, or model, laminate stacking sequence is scaled-up by simply increasing the number of layers for each angular ply orientation [**101-103**]. For example, a baseline $[Al, 0°/90°]_s$ is scaled to twice the baseline thickness by doubling the number of plies at each orientation, $[Al_2, 0°/90°_2]_s$. Ply-level scaled laminates are constitutively similar in that the in-plane and bending stiffness are appropriately scaled.

A second macrostructural technique is called sublaminate-level scaling. In this method the laminate thickness is scaled by repeating the baseline stacking sequence as a sublaminate group [**81,87,102,104**]. For example using the laminate mentioned previously, it scaled-up as $[Al, 0°/90°]_{2s}$ using the sublaminate-level approach.

2.5.2 Factors Influencing Size Effects

2.5.2.1 Material, Microstructure and Lay-ups

The microstructure of the material is important in determining the defects that may give rise to any size effects. It is well established that brittle fibres such as carbon and glass exhibit a size effect due to flaws in their microstructure [**96,105-109**].

A composite has defects within its microstructure in addition to flaws in the fibres and matrix. For example, there are heterogeneities in the packing of the fibres which may give rise to local weaknesses; clusters of closely packed fibres, resin rich regions, fibres debonded from the matrix, voids, broken or misaligned fibres [**110**]. Individual defects may combine together to form higher level effective flaws.

Other defects exist at a ply-level. For example, transverse cracks which arise due to residual stresses generated during curing or which may form at low applied loads, can subsequently lead to delamination. Both the generation and effect of these cracks depend on the ply thickness, creating a kind of size effect, but one that is related to thickness rather than volume. Ply-level fibre waviness may exist, which can be very important in compressive failure [**54,104,111,112**]. Resin-rich regions, voids and

delaminations can also form between plies. There may also be defects associated with the arrangement of the tows of fibres from which composites are normally manufactured [**113-115**].

In a woven material, the geometry of the weave causes crimp in the fibres. This creates an intrinsic fibre waviness in addition to undulations in the whole ply. The weave also creates locations where it is easy for voids to be trapped or for resin cracks to occur.

2.5.2.2 Specimen Finish and Free Edge Effects

Very high interlaminar stresses can arise at the free edge of a laminate with different ply orientations [**21,116,117**]. This phenomenon has been studied extensively in the work of Pipes and Pagano [**118**]. In some laminates this can lead to premature failure at the free edge, and the failure stress will then depend on the ply thickness. For example O'Brien [**119**] showed that in $[+45°_n/-45°_n/0°_n/90°_n]_s$ laminates loaded in tension, the strain at the onset of edge delamination decreased substantially as the scale size was increased from 1 to 3. The effect of free edges on in-plane failure is less well understood, but could be significant for many lay-ups and types of loading.

Free edge stresses may cause effects related to ply thickness, which can be difficult to distinguish from effects due to stressed volume. Consider for example, a series of tests on specimens with the same lay-up where all dimensions are increased together, including the ply thicknesses. If a reduction in strength is observed it could be due to a volumetric size effect, although it may primarily be a lay-up effect due to the increased ply thickness. In this case, there may still be a reduction in strength with increasing specimen length due to the greater probability of finding a larger edge defect, however, the effect is likely to be much smaller than that due to changing the ply thickness [**120,121**]. Specimen width should not affect the strength provided the specimen is wider than the minimum required to develop the full edge stress field.

Another free edge effect arises due to the fact that fibres are broken at the surface when the specimen is cut. This happens even in unidirectional composite because the fibres are not perfectly straight. Splitting and delamination can initiate on the edge from these defects.

O'Brien and Chawan [**110**] studied the influence of polishing on carbon fibre/epoxy and glass fibre/epoxy flexure specimens. He noted that flaws created during cutting the plates do not appear to significantly affect the specimen strength, indeed, when compared with polished samples, a decrease of less than 2% was observed. Moreover, flexure specimens with a polished tension surface, showed a more significant decrease in strength (between 5 to 10%). Hence, instead of increasing the measured strength as a result of removing inherent flaws in the material due to manufacture and handling, polishing appears to be detrimental to specimen strength.

2.5.2.3 Testing Considerations in Scaling

Test specimens should be large compared with any characteristic dimensions associated with the microstructure. For example, with textile composites there is a unit cell size which can, in some cases, be as much as 25 mm or even larger. Where strain gauges are used, it is essential that they are of sufficient size or number that a valid average strain can be obtained. Large errors can occur in measured modulus as well as strain to failure if the gauges are too small [**122**]. Similar errors can arise if measurements are made in areas of non-uniform strain, for example if the specimen gauge length is insufficient or if strain is measured too close to a loading point. This is harder to avoid with composites due to the large distances required to redistribute stresses in highly anisotropic materials.

Differences in test methods can give rise to apparent size effects which may not be real. For example a flexure test may give a higher apparent strength than a tensile test because premature failure due to local loading effects is less likely in the former [**123,124**]. Even if the same test method is used, thicker specimens may give lower strengths than thin samples, because of increased stress concentrations at the gripping area. For example, with side-loaded tension or compression specimens loaded by means of shear in a stiff test fixture, stress concentrations tends to increase with increasing thickness as more load has to be transferred to achieve the same stress. An apparent size effect may be observed which has nothing to do with the volume of material.

Differences in the aspect ratios of specimens can also produce anomalies. For example, a long, slender tensile specimen is much less likely to be affected by bending

and misalignment problems than a short one [**113,125**]. On the other hand, deficiencies in the test method may mask a size effect that is really there. Strictly speaking, only tests that produce gauge length failures should be used to measure strength, but in practice in many test specimens fail near the grips. A reduction in strength with increasing gauge length may not be seen if all the specimens fail prematurely, due to stress concentrations at the ends.

Scaled tests are a more reliable way to investigate size effects. If the complete test arrangement is scaled, then the stress distribution should be the same. Even if there are stress concentrations, they should have the same effect on the different-sized specimens. This requires the full test geometry to be scaled, including any tabs or loading fixtures.

2.5.2.4 Stress Gradient

In many tests, the stress field is not constant. For example in a flexural test there is a stress gradient through the thickness. Higher strengths are often observed under these conditions, where the question arises: is this a volumetric effect due to the smaller amount of material subject to the maximum stress or is it due to the stress gradient itself?

It has been shown theoretically from Weibull theory that the strength in bending should be higher than the strength in tension for a given specimen, and that the same size effect should operate for scaled bending and tensile tests [**126**]. For brittle materials, Weibull theory normally predicts quite well relationships between tension and flexural strength, indicating that the higher strength in bending is indeed a stressed volume effect [**123,124**]. The stress gradient itself is not believed to be responsible for the difference, as shown experimentally for brittle materials by the similar strengths obtained for beams of different heights and width but the same volume [**127**]. However, for composites there are reasons to expect that the stress gradient itself may have an effect over and above that caused by the different volumes.

In tension, for example, the redistribution of load that occurs as fibres progressively fail may produce a higher strength in bending than in pure tension [**123,128**]. The compressive stress at which instability occurs is therefore higher in bending than in

compression, and increases as the thickness decreases. This also explains the tendency of flexural failures to switch from tension to compression as the specimen size increases [**129**], because the constraint due to the stress gradient decreases as the specimen becomes thicker. An effect of stress gradient on compressive failure has also been found experimentally in pin-ended buckling tests on specimens of the same thickness with different ratios of compressive to bending stress [**130**]. The effect of stress gradients on strength is a size effect of a sort, although it is more a structural as opposed to a true material phenomenon. Size effects due to inherent material variability may exist as well, but experimental evidence is currently inconclusive.

One of the difficulties with tensile testing is the stress concentration that arises where the specimens are gripped. These have been shown to have significant effect on tensile strength from both analysis and test results [**131**]. Stress concentrations would be expected to have a greater effect on the thicker laminates than on the single strands, and it could be argued that this might explain some of the differences in strength.

2.5.2.5 Specimen Manufacture and Preparation

Damage caused during specimen preparation can have a significant effect on strength matrix dominated failures [**21,24**]. The strain at which transverse cracking occurs has been shown to increase with edge polishing, and to be closely correlated with the surface roughness [**91**]. Where failures that initiate from machining damage, a size effect based on the machined surface area would be expected. The different ways in which large structures and small test coupons may be produced can give rise to a size effect which is related to the manufacturing process rather than the volume of the material. Even if the same processes are used, there may be differences in the properties of thick and thin composites. For example variations in volume fraction or moisture absorption in the surface region could affect different thickness laminates to different extents.

Thicker sections may also have higher level of voiding and poorer consolidation than thin ones. Another issue is whether the properties are affected by differences in the cure process of thermosettings. As the thickness increases, differences in heat transfer and the effect of exotherms produce non-uniformities of temperature and degree of cure [**26**]. Fibre waviness has an important effect on compressive strength, and may

vary with thickness due to differences in the amount of constraint provided by the tooling in thick and thin laminates.

2.5.3 Methodologies for Studying Scaling

2.5.3.1 Scaling Effects in Tension

There have been several studies of scaled tensile tests on laminates. Results are more difficult to interpret because of the additional effect of ply thickness, and because failure mechanisms often involve interactions between transverse cracking, delamination and fibre failure [**80,81,86,94,95,131,132**]. Jackson *et al.* [**133**] reported scaled tension tests on $[90°_n/0°_n/90°_n/0°_n]_s$ carbon/epoxy laminates. The number of plies blocked together, was varied from $n = 1$ to 4, and the specimen widths, lengths and gripped lengths were changed in the same proportion. Failures were fibre dominated, and a 7% increase in tensile strength was found from the largest to smallest specimens. Similar scaled tests on $[+45°_n/-45°_n/0°_n/90°_n]_s$ laminates showed a much larger size effect. However, the failure modes were more complicated, with considerable delamination that may have influenced final failure.

Johnson *et al.* [**87**] carried out sublaminate-level-scaled tension tests on $[90°/0°/90°/0°]_{ns}$ carbon fibre/epoxy laminates. The number of blocks of plies, '*n*', was varied from 1 to 4, with specimen widths and lengths scaled in proportion. Here, little difference was found in ultimate strengths between the different sized tests. Similar tests on scaled $[+45°/-45°/0°/90°]_{ns}$ laminates actually showed an increase in strength with increasing size, this being attributed to the larger specimens being less susceptible to delamination.

O'Brien and Salpekar [**134**] presented results from transverse tensile tests on AS4/3501-6 laminates of different widths and thicknesses. Specimens were cut from unidirectional plates 4, 8, 16, 32 and 64 plies thick. A few specimens failed at the grips, and the results were not included in the averages. The results are presented graphically in Figure 2.17, plotted on a log-log scale, where a strong trend for the strength to decrease with increasing volume was observed. A straight line fits the data well, indicating that Weibull theory is satisfactory. Local microcracks in the matrix and/or fibre-matrix debonds were suggested as the most likely inherent flaws

responsible for the decrease in strength with volume. It was also suggested that flaws near the edge may be more critical, which was supported by the strengths apparently not varying significantly with width [**134**].

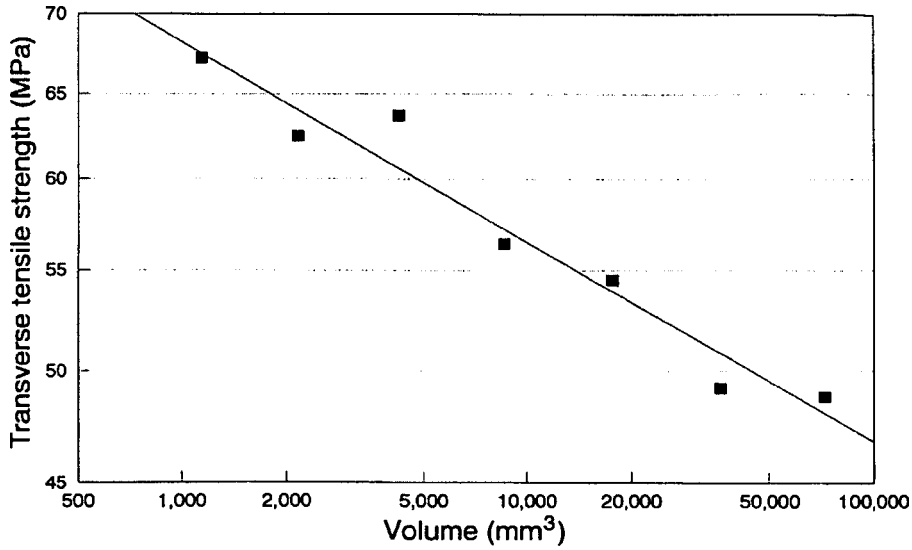

Figure 2.17. Size effects in transverse tensile loading of a carbon/epoxy composite [134].

2.5.3.2 Scaling Effects in Flexure

The flexure test, which is widely used and appears to be very simple, is in fact, complex and often poorly understood due to the complexity introduced by the presence of material non-linearity [**111**]. Several scaling studies in flexure have been carried out in an attempt to clarify the factors affecting the stress/strain performance of composite materials [**90,96,135-138**].

Jackson [**103**] presented results for flexural tests on unidirectional AS4/3502 carbon fibre/epoxy beams from 12 to 48 plies thick. Tests were carried out on the hinged loading fixture shown in Figure 2.18, with all of the dimensions of the specimen and the rig being scaled. Failures occurred due to fibre fracture near the mid-point of the beam in all sizes. The strain at failure was measured by a strain gauge at the centre of each specimen. Table 2.5 shows the tensile strains at failure where a large reduction is apparent with increasing specimen size. A least squares fit of the data gives a Weibull modulus of 12.9.

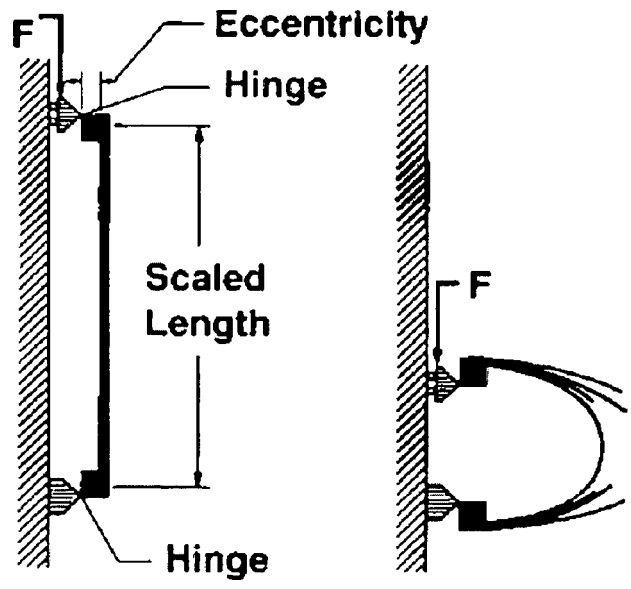

Figure 2.18. Schematic drawing of the flexural test configuration adopted by Jackson [103]

Results from scaled four-point bend tests on unidirectional E-glass/913 specimens based on 16, 32 and 64 plies thick were presented by Wisnom and Atkinson [**139**]. The smallest specimens were 5 mm wide, with distances of 15 and 45 mm between the inner and outer rollers respectively. All dimensions were scaled for the larger tests, including the roller sizes. The maximum strains were measured by strain gauges at the centre of the specimens. Table 2.6 summarises the results, where a clear size effect is evident. The Weibull modulus based on a least squares fit of the data is 24.2.

Nominal size (mm)	Mean strain at failure (%)
1.5x19.0x190	1.72
2.0x25.4x254	1.56
3.0x38.1x381	1.41
4.0x50.8x508	1.35
4.5x57.1x571	1.44
5.0x63.5x635	1.35
6.0x76.2x762	1.13

Table 2.5. Flexural test data for a 0° carbon/epoxy composite [103].

Nominal size (mm)	Mean strain at failure (%)
2x5x45	4.39
4x10x90	4.22
8x20x180	3.71

Table 2.6. Data from flexural tests on 0° glass/epoxy [139].

Wisnom [**129**] observed size effects in a unidirectional carbon/epoxy under four-point bending and in pinned-end buckling tests. A change in failure mode from tensile to compressive was seen with increasing size. He postulated that a greater size effect in compression than in tension caused the larger specimens to have a lower compressive strength than tensile strength. There was a 25% reduction in failure strain between the smallest and largest specimens. Least squares fit give a Weibull modulus of 14.4. Most of the failures initiated at the loading rollers.

A second type of test was undertaken, involving pin-ended buckling similar to that shown in Figure 2.18. Specimens were allowed to buckle, and then failed due to bending at their centre, away from any stress concentration effects of the rollers. This test method eliminated compressive failures for the small specimen sizes, but the large specimens still failed predominantly in compression, showing that the size effect was not caused by the way that the load was applied.

2.5.3.3 Comparison of Scaling Effects in Terms of Tensile and Flexural Strength

Flexural tests subject a smaller volume to the maximum stress than tensile tests, and therefore tend to give higher strengths due to the size effect [**124,140**]. However, there are a number of difficulties in making comparisons between these different types of test, and data must be interpreted with caution. For a valid comparison, the failure modes must be the same. Flexural tests often produce compressive failure at the loading roller. Even if failure occurs in tension, there may be differences which make a direct comparison difficult. For example a flexural specimen may fail progressively through the thickness, whilst in a tensile test, failure may be sudden and catastrophic.

Tensile tests are susceptible to premature failure due to stress concentrations where the specimens are gripped. Such problems do not usually arise in flexural tests since

tensile failure initiates on the opposite surface to the loading rollers, away from localised stress concentrations. Engineer's Theory of Bending is often used to calculate stresses in flexural tests, but this can be inaccurate as a result of large deflections, and for the case of carbon fibre composites, due to material nonlinearity [**123**].

A comparative study in tension and flexure has been carried out by different authors [**86,87,102,103,141,142**]. Here, scaling studies on carbon/epoxy beams were undertaken. Various lay-ups were tested, initially using ply-level scaling, and a size effect was noted for flexural and tensile testing which depended on the lay-up. No size effect was seen in the initial stiffness. Both, Weibull and LEFM theories were applied, the former giving a better and a more variable correlation between theory and experiment. Large variations in the Weibull modulus (m) were observed across the different lay-ups. The fracture mechanics model was thought to be inappropriate due to the complex damage modes exhibited by the composite laminates. Failure mode transitions were noted as the size increased for both tensile and flexural coupons, again, this was dependent on lay-up. In the case of sublaminate-level scaling, a greater scaling effect was observed than in ply-level scaling.

Bullock [**89**] compared strengths from three-point bend tests on 15 ply specimens based on two different carbon fibre/epoxy materials with data form tension tests on 6 ply laminates and impregnated strands. Similar Weibull modulus values were obtained in tension and bending, and the relative strengths were found to agree very well with those derived from Weibull theory. Flexural to tensile strength ratios of 1.35 and 1.49 were measured on the two materials, based on Weibull modulus values of 24 and 18, highlighting a good correlation between the techniques.

Wisnom and Atkinson [**139**] conducted tensile tests on specimens with different gauge lengths and flexural tests on fully-scaled specimens. The samples were made from a unidirectional glass fibre/epoxy. Here, they observed size effects in each case, as was discussed previously. Since the tests were all performed on the same material, the tensile results could also be compared with the flexural data. The strains at maximum load measured in the tension tests were all lower than the maximum strains in the flexural tests. In order to compare the results, an equivalent volume was determined

for each specimen. In the case of the tensile tests, this was simply the volume of the gauge section.

Figure 2.19 shows the results plotted on a log-log scale. The error bars correspond to one standard deviation on either side of the mean values. Weibull theory predicts that all results should lie on one straight line, and this is borne out by the experimental data. The slope of the line gives a Weibull modulus of 29.3. The same set of Weibull parameters is therefore able to reconcile the length effect in the tensile tests, the size effect in the scaled bending tests and the difference between tensile strength in tension and bending.

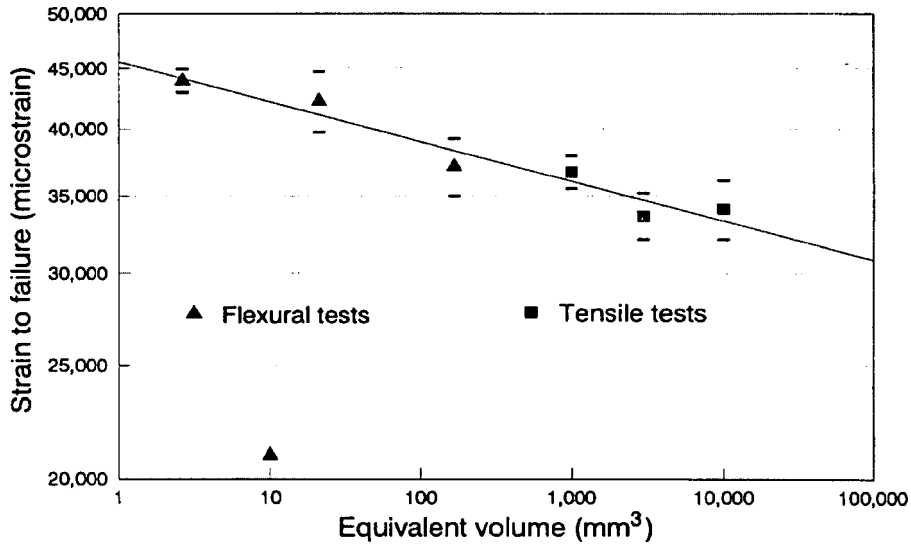

Figure 2.19. Size effects in tension and flexure for a glass/epoxy composite [139].

2.5.3.4 Scaling Effects in Compression

Conducting compression tests on composites is notoriously difficult, and despite the huge amount of research that has been undertaken, there are still many problems obtaining reliable and repeatable data for compressive strength [**100,104,143**]. End-loaded specimens tend to broom or split from the end, and so indirect loading by means of shear is often used. This gives rise to stress concentrations, and failures usually initiate where the specimens are gripped. High shear stresses in this area may also interact with compressive stresses, and this type of test tends to underestimate the intrinsic compressive strength [**144**]. There have been very few systematic studies of size effects in compression, and the problems with testing make it difficult to draw

firm conclusions. Nevertheless there are strong indications that the compressive strength in the fibre direction does decrease with increasing specimen size.

Camponeschi *et al.* investigated the compressive strength of different sized carbon and glass fibre/epoxy specimens [**93**]. Cross-ply laminates with $[0°_2/90°]_{ns}$ lay-ups based on 48, 96 and 192 plies were tested. Most of the cross-ply specimens failed at the start of the gauge section, and the failure modes were all very similar. Table 2.7 summarises the results, showing reductions of 22% and 19% from the smallest to the largest carbon and glass fibre specimens, respectively. It was concluded that this was not a true material size effect, but was due to the misalignment of fibres at the point where the specimen emerges from the constraint of the clamping blocks. A finite element analysis showed that the misalignment angle increased with specimen thickness.

Nominal size (mm)	Material	Mean strength (MPa)	C.V.	No. of specimens
6.35x25.4x31.8	Carbon	1074	6.9	5
12.7x50.8x63.5	Carbon	891	10.7	4
25.4x102x127	Carbon	841	10.4	5
6.35x25.4x31.8	Glass	989	10.9	5
12.7x50.8x63.5	Glass	930	4.5	4
25.4x102x127	Glass	798	5.8	5

Table 2.7. Compressive test data for a $[0°_2/90°]_{ns}$ laminate [93].

Johnson *et al.* [**135**] conducted compressive tests on cross-ply and quasi-isotropic laminates in which all of the dimensions were scaled. An end-loaded, side supported fixture was used, but the specimens showed end crushing, and some failed in the end region, making it difficult to draw conclusions. The $[0°/90°]_{4s}$ specimens gave similar strengths to double sized samples for both ply-level scaled $[0°_2/90°_2]_{4s}$ laminates and sublaminate-scaled $[0°/90°]_{8s}$ laminates. Also, the $[45°/-45°/0°/90°]_{2s}$ specimens appeared to be weaker than larger sized sublaminate-scaled $[45°/-45°/0°/90°]_{4s}$ and $[45°/-45°/0°/90°]_{8s}$ laminates.

There are strong indications from the available experimental data that the compressive strength reduces with increasing specimen size. Misalignment of fibres from the

loading axis is very important, as it may cause shear stresses to develop which can lead to shear strains and hence an increase in the misalignment angle. The initial misalignment angle is a critical parameter, with only a few degrees being sufficient to cause a large reduction in strength [**145**]. Experimental studies have shown considerable fibre misalignment due to variability of the orientation of the individual fibres [**125**] and to a higher level of ply waviness [**93**].

Simple models suggest that failure should initiate from the region of greatest fibre misalignment, which can be considered as a defect. A larger volume of material is likely to contain a greater number of defects, and so a size effect would be expected. However, modelling studies have shown that better aligned fibres can provide support against the collapse of misaligned fibres [**112**]. This highlights the importance of manufacturing quality, and the necessity of testing specimens produced under representative conditions when measuring compressive strength.

2.5.3.5 Scaling Effects in Impact

The increasing use of composite materials in aerospace structures is producing a demand for more competitive designs and a reduction in manufacturing costs. Previously, full-scale components and structures have often been fabricated and tested as part of the design evaluation phase. This is both expensive and time-consuming, and alternative routes are required if composite materials are to compete with developments in advanced metallic alloys [**78,146-149**].

One way forward is to undertake model simulation techniques as a means of predicting the behaviour of large components and structures. However, for composite structures subjected to varying levels of impact damage, the issues are not straightforward. For example, similar structures, except for differences in size, may react quite differently when subjected to similar impact energies due to the complex interaction of the various fracture processes such as indentation, matrix cracking, delamination or fibre fractures. Therefore, initially, a more useful way forward is to combine experimental data with modelling methods [**150-153**].

Morton [**85**] studied scaling effects in the transverse impact response of carbon-fibre composite beams with different fibre lay-ups. He compared the experimental results

with those obtained from a set of non-dimensional parameters applying the Buckingam Pi-theorem. He noted that the impact duration scaled as the scale factor and the impact force as the scale factor squared. He also observed a significant decrease in strength with increasing specimen size. However, he identified difficulties in trying to satisfy the requirements for rate sensitive and notch sensitive materials.

Qian *et al.* **[154,155]** conducted an impact scaling study on specimens based on a carbon/epoxy composite material. An impact pendulum and an airgun were used to test five sizes of plate ranging from 1.07 mm thick to 5.36 mm thick. A ply-level scaling was used along with a $[+/-72°_n/0°_{2n}]_s$ lay-up. They found that the measured structural response agreed well with the predicted scaling behaviour over the range of energies studied. They noted that the strain values were independent of scaling size while time varied linearly with the scale factor (λ) as shown in Figure 2.20, where only three of five scaled sample plots were shown for clarity purposes. They also noted that the level of delamination exhibited a dependence on absolute size while the degree of fibre breakage did not.

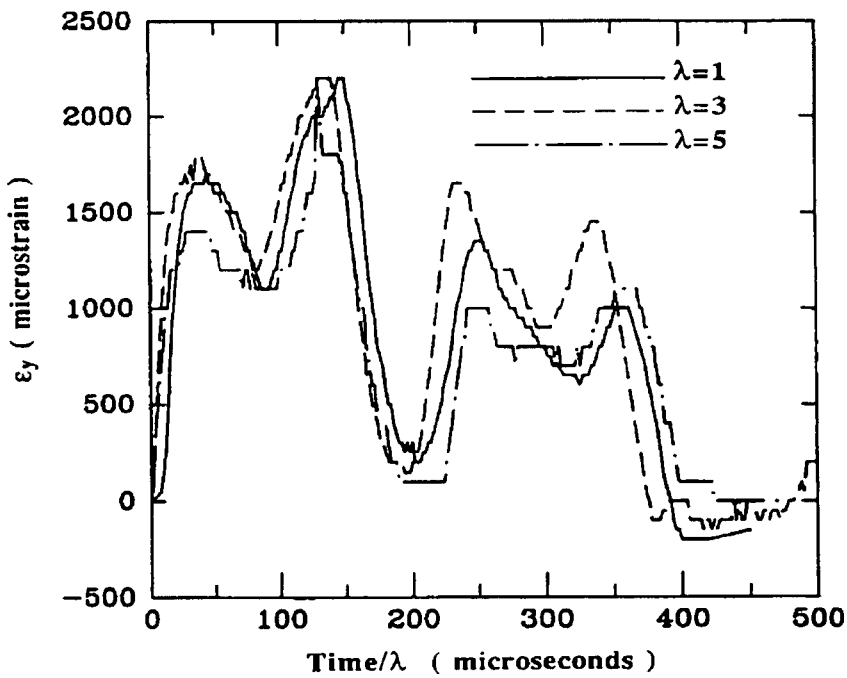

Figure 2.20. Comparison of strain response in impact tests on three different plate sizes, V_0=4.57 m/s ***[154]****.*

More recently, Swanson [**156**] presented a compilation of this work, highlighting the fact that delamination increased more rapidly with specimen size than would be expected if the local stresses controlled the extent of delamination, as would be predicted by fracture mechanics. However, he concluded that specimen size did not have a significant effect on the failure stresses or strains under impact.

2.6 References

1. M M Eisenstadt. *Introduction to Mechanical Properties of Materials*, New York; Macmillan Company, 1971.

2. A W Birley and B Haworth. *Physics of Plastics*, New York; Hanser, 1992.

3. H Kausch and R Legras. *Advanced Thermoplastic Composites Characterisation and Processing*, Hanser, 1993.

4. J Maxwell. *Plastics; The Layman's Guide*, Cambridge; Fakenham Photosetting, 1999.

5. ASM International, *ASM Homepage*. http://www.asminternational.org/, 2006.

6. S R Nutt. *Composites; Constituent Materials*. In: ASM Materials Information, edited by D B Miracle and S L Donaldson, ASM International Handbook, 2001.

7. A Kelly. *Concise Encyclopedia of Composite Materials*, Oxford; Pergamon, 1994.

8. A Kelly and C Zweben. *Comprehensive Composite Materials*, Amsterdam; Elsevier, 2000.

9. J D Muzzy. *Thermoplastic-Properties*. Comprehensive Composite Materials, 2; 57-76, 2002.

10. S L Rosen. *Fundamental Principles of Polymeric Materials*, New York; Wiley, 1993.

11. S Snook. *Engineering Plastics and Elastomers; Design Guide*, London; Institute of Materials, 1994.

12. K Ashbee. *Fundamental Principles of Fiber Reinforced Composites*, Lancaster, USA; Technomic Publishing, 1989.

13. Karian. *Handbook of Polypropylene and Polypropylene Composites*, New York; Marcel Dekker Incorporated, 1999.

14. I M Daniel and O Ishai. *Engineering Mechanics of Composite Materials*, Oxford University Press, 2005.

15. D Gay, V Suong, H Stephen, and W Tsai. *Composite Materials; Design and Applications*, CRC Press, 2005.

16. E J Barbero. *Introduction to Composite Materials*, Taylor and Francis, 1998.

17. T H Courtney. *Mechanical Behaviour of Materials*, Mc Graw-Hill, 2005.

18. E A Muccio. *Plastics Processing Technology*, ASM International, 1994.

19. B Harris. *Engineering Composite Materials*, IOM Comunications, 2005.

20. A C Long. *Design and Manufacture of Textile Composites*, Cambridge; CRC Press, 2005.

21. A Kelly and Y N Rabotnov. *Handbook of Composites; Structures and Design*, North Holland; Elsevier Science, 1989.

22. About, *About Homepage*. http://composite.about.com/, 2007.

23. Pilotfriend, *Slingsby Aviation*. http://www.pilotfriend.com/, 2007.

24. T G Gutowski. *Advanced Composites Manufacturing*, Cambridge, MA; John Wiley and Sons, 1997.

25. P C Powell. *Engineering with Fibre-Polymer Laminates*, Chapman and Hall, 1994.

26. G Lubin. *Handbook of Fiberglass and Advanced Plastics Composites*, New York; SPE; Polymer Technology Series, 1969.

27. N K Naik. *Woven Fabric Composites*, Technomic Publishing Company, 1994.

28. C Zweben. *Composite Materials and Mechanical Design.* In: Mechanical Engineer's Handbook, edited by M Kutz, J. Wiley and Sons, 1998.

29. J A Bailie. *Woven Fabric Aerospace Structures.* In: Handbook of Composites; Structures and Design, edited by C T Herakovich and Y M Tarnopolskii, Netherlands; Elsevier Science Publisher, p. 353-391. 1989.

30. Propex, *Curv Homepage.* http://www.curvonline.com, 2005.

31. *Ticona Composites.* http://www.ticona-media.com, 2007.

32. W D Callister Jr. *Materials Science and Engineering; An Introduction*, John Wiley and Sons, 2005.

33. I J Polmear. *Light Alloys; Metallurgy of the Light Metals*, Chapman and Hall, 1989.

34. R W Hertzberg. *Deformation and Fracture Mechanics of Engineering Materials*, Wiley and Sons, 1996.

35. World-aluminium, *World-Aluminium Homepage.* http://www.world-aluminium.org, 2007.

36. E L Rooy. *Properties and Selection; Nonferrous Alloys and Special-Purpose Materials.* In: ASM Materials Information, edited by M Unterweiser and H Cubberley, ASM International Handbook, 1992.

37. Matweb, *Matweb Homepage.* http://www.matweb.com, 2007.

38. Azom, *Azom Homepage.* http://www.azom.com, 2007.

39. S Chama. *Mechanically Alloyed Aluminium-Magnesium-Lithium Alloys: Structure Property Relations.* University of Liverpool, Ph.D.Thesis, 2001.

40. Wikipedia, *Wikipedia Homepage.* http://en.wikipedia.org, 2007.

41. FMLC, *Fibre Metal Laminates Centre of Competence.* http://www.fmlc.nl, 2007.

42. J Sinke. *Development of Fibre Metal Laminates: Concurrent Multi-Scale Modelling and Testing.* Journal of Materials Science, 41; 6777-6788, 2006.

43. J W Gunnink, A Vlot, T J Vries, and W Hoeven. *Glare Technology Development 1997-2000.* Applied Composite Materials, 9; 201-219, 2002.

44. L B Vogelesang and A Vlot. *Development of Fibre Metal Laminates for Advanced Aerospace Structures.* Journal of Materials Processing Technology, 103; 1-5, 2000.

45. C A J R Vermeeren. *An Historic Overview of the Development of Fibre Metal Laminates.* Applied Composite Materials, 10; 205, 2003.

46. A Vlot and J W Gunnink. *Fibre Metal Laminates*, Kluwer Academic Publisher, 2001.

47. H F Wu, L L Wu, W J Slagter, and J L Verolme. *Use of Rule of Mixtures and Metal Volume Fraction for Mechanical Property Predictions of Fibre-Reinforced Aluminium Laminates.* Journal of Materials Science, 29; 4583-4591, 1994.

48. G Reyes and W J Cantwell. *The Mechanical Properties of Fibre-metal Laminates Based on Glass Fibre Reinforced Polypropylene*. Composites Science and Technology, 60; 1085-1094, 2000.

49. A Asundi and A Y N Choi. *Fiber Metal Laminates: An Advanced Material for Future Aircraft*. Journal of Materials Processing Technology, 63; 384-394, 1997.

50. A Vlot, L B Vogelesang, and T J Vries. *Towards Application of Fibre Metal Laminates in Large Aircraft*. Aircraft Engineering and Aerospace Technology, 71; 558-570, 1999.

51. A Afaghi-Khatibi, L Ye, and Y W Mai. *Polymer Matrix Composites; Hybrid and Sandwidches*. In: Comprehensive Composite Materials, edited by R Talreja and J A Mansoki, Elsevier Science, 2000.

52. P Cortes. *The Mechanical Properties of High Temperature Fibre-Metal Laminates*. University of Liverpool, Ph.D.Thesis, 2005.

53. S Krishnakumar. *Fiber Metal Laminates; The Synthesis of Metals and Composites*. Materials and Manufacturing Processes, 9; 295-354, 1994.

54. J J C Remmers and R de Borst. *Delamination Buckling of Fibre-Metal Laminates*. Composites Science and Technology, 61; 2207-2213, 2001.

55. P Compston, W J Cantwell, and N Jones. *Influence of Loading Rate on the Interfacial Fracture Toughness of a Polyamide-Based Fiber-Metal Laminate*. Journal of Materials Science Letters, 21; 383-386, 2002.

56. P Compston, W J Cantwell, and N Jones. *The Influence of Loading Rate on the Interfacial Fracture Toughness of a Polypropylene-Based Fiber-Metal Laminate*. Journal of Materials Science Letters, 21; 263-266, 2002.

57. P Cortes and W J Cantwell. *Interfacial Fracture Properties of Carbon Fiber Reinforced PEEK/Titanium Fiber-Metal Laminates*. Journal of Materials Science Letters, 21; 1819-1823, 2002.

58. W J Cantwell, R Scudamore, J Ratcliffe, and P Davies. *Interfacial Fracture in Sandwich Laminantes*. Composites Science and Technology, 59; 2079-2085, 1999.

59. A J Kinloch. *Adhesion and Adhesives. Science and Technology*, USA; Chapman and Hall, 1987.

60. G Reyes and W J Cantwell. *The Effect of Strain Rate on the Interfacial Fracture Properties of Carbon Fiber-Metal Laminates*. Journal of Materials Science Letters, 17; 1953-1955, 1998.

61. P Cortes and W J Cantwell. *The Tensile and Fatigue Properties of Carbon Fiber-Reinforced PEEK-Titanium Fiber-Metal Laminates*. Journal of Reinforced Plastics and Composites, 23; 1615-1623, 2004.

62. M Papakyriacou, J Schijve, and E Stanzl-Tschegg. *Fatigue Crack Growth Behaviour of Fibre-metal Laminate Glare-1 and Metal Laminate 7475 with Different Blunt Notches*. Fatigue and Fracture of Engineering Materials and Structures, 20; 1573-1584, 1997.

63. R C Alderliesten, J Schijve, and S Zwaag. *Application of the Energy Release Rate Approach for Delamination Growth in Glare*. Engineering Fracture Mechanics, 73; 697-709, 2005.

64. A Vlot. *Impact Loading of Fibre Metal Laminates*. Journal of Impact Engineering, 18; 291-307, 1996.

65. H M Wen and N Jones. *Semi-Empirical Equations for the Perforation of Plates Struck by a Mass*. In: Structures under Shock and Impact II, edited by P S Bulson, 1992.

66. M V Backman and W Goldsmith. *The Mechanics of Penetration of Projectiles into Targets*. International Journal of Engineering Science, 16; 1-99, 1978.

67. N Levy and W Goldsmith. *Normal Impact and Perforation of Thin Plates by Hemispherically-Tipped Projectiles - II. Experimental Results*. International Journal of Impact Engineering, 2; 299-324, 1984.

68. W J Cantwell, P T Curtis, and J Morton. *Impact and Subsequent Fatigue Damage Growth in Carbon Fibre Laminates*. International Journal of Fatigue, 6; 113-118, 1984.

69. W J Cantwell and J Morton. *Detection of Impact Damage in CFRP Laminates*. Composite Structures, 3; 241-257, 1985.

70. W J Cantwell and J Morton. *Impact Perforation of Carbon Fibre Reinforced Plastic*. Composites Science and Technology, 38; 119-141, 1990.

71. G Reyes and W J Cantwell. *The High Velocity Impact Response of Composite and FML-Reinforced Sandwich Structures*. Composites Science and Technology, 64; 35-54, 2004.

72. M R Abdullah and W J Cantwell. *The Impact Resistance of Polypropylene-Based Fibre-Metal Laminates*. Composites Science and Technology, 66; 1682-1693, 2005.

73. P Compston, W J Cantwell, C Jones, and N Jones. *Impact Perforation Resistance and Fracture Mechanisms of a Thermoplastic Fiber-Metal Laminate*. Journal of Materials Science Letters, 20; 597-599, 2001.

74. J Gresham, W J Cantwell, M J Cardew, and P Compston. *Drawing Behavior of Metal-Composite Sandwich Structures*. Composite Structures, 75; 305-312, 2006.

75. L Mosse, P Compston, W J Cantwell, and M Cardew. *Stamp Forming of Polypropylene Based Fibre-Metal Laminates: The Effect of Process Variables on Formability*. Journal of Materials Processing Technology, 172; 163-168, 2006.

76. M R Abdullah. *The High Velocity Impact Response of Novel Fibre-Metal Laminates*. University of Liverpool, Ph.D.Thesis, 2006.

77. P Cortes and W J Cantwell. *The Prediction of Tensile Failure in Titanium-Based Thermoplastic Fibre-Metal Laminates*. Composites Science and Technology, 66; 2306-2316, 2005.

78. A T Nettles, M J Douglas, and E E Estes. *Scaling Effect on Carbon/Epoxy Laminates under Transverse Quasi-Static Loading*. NASA, TN-1999-209103; 1999.

79. A Tabiei and J Sun. *Analytical Simulation of Strength Size Effect in Composites Materials*. Composites: Part B, 31; 133-139, 2000.

80. A Towse, K Potter, M R Wisnom, and R D Adams. *Specimen Size Effects in the Tensile Failure Strain of an Epoxy Adhesive*. Journal of Materials Science, 33; 4307-4314, 1998.

81. B G Green, M R Wisnom, and S R Hallett. *An Experimental Investigation into the Tensile Strength Scaling of Notched Composites*. Composites Part A, 38; 867-878, 2006.

82. L S Sutherland, R A Shenoi, and S M Lewis. *Size and Scale Effects in Composites: I. Literature Review*. Composites Science and Technology, 59; 209-220, 1999.

83. S R Hallett and M R Wisnom. *Experimental Investigation of Progressive Damage and the Effect of Layup in Notched Tensile Tests*. Journal of Composite Materials, 40; 119-141, 2006.

84. Z P Bazant. *Scaling Laws in Mechanics of Failure*. Journal of Engineering Mechanics, 119; 1828-1844, 1993.

85. J Morton. *Scaling of Impact-Loaded Carbon-Fiber Composites*. American Institute of Aeronautics and Astronautics, 26; 989-994, 1988.

86. S Kellas and J Morton. *Strength Scaling in Fiber Composites*. American Institute of Aeronautics and Astronautics, 30; 1074-1080, 1992.

87. D P Johnson, J Morton, S Kellas, and K Jackson. *Scaling Effects in Sublaminate-Level Scaled Composites Laminates*. American Institute of Aeronautics and Astronautics, 36; 441-447, 1998.

88. W Weibull. *A Statistical Distribution Function of Wide Applicability*. Journal of Applied Mechanics, 18; 293-297, 1951.

89. R E Bullock. *Strength Ratios of Composite Materials in Flexure and in Tension*. Journal of Composite Materials, 8; 200-206, 1974.

90. M R Wisnom, M I Jones, and G F J Hill. *Interlaminar Tensile Strength of Carbon Fibre-Epoxy-Specimen Size, Layup and Manufacturing Effects*. Advanced Composites Letters, 10; 171-177, 2001.

91. A Kitano, K Yoshioka, K Noguchi, and J Matsui. *Edge Finishing Effect on Transverse Cracking of Cross-Ply CFRP Laminates*. ICCM-9, 5; 169-176, 1993.

92. P Lagace, J Brewer, and C Kassapoglou. *The Effect of Thickness on Interlaminar Stresses and Delamination in Straigth-Edged Laminates*. Journal of Composites Technology and Research, 9; 81-87, 1987.

93. E T Camponeschi, J W Gillespie, and D J Wilkins. *Kink-Band Failure Analysis of Thick Composites in Compression*. Journal of Composite Materials, 27; 471-490, 1993.

94. C Hochard, N Lahellec, and C Bordreuil. *A Ply Non-Local Fibre Rupture Criterion for CFRP Woven Ply Laminated Structures*. Composite Structures, Article in Press; 2007.

95. T Okabe and N Takeda. *Size Effect on the Tensile Strength of Unidirectional CFRP Composite-Experiment and Simulation*. Composites Science and Technology, 62; 2053-2064, 2002.

96. J W Hitchon and D C Phillips. *The Effect of Specimen Size on the Strength of CFRP*. Composites, 9; 119-124, 1978.

97. M Maalej and K S Leong. *Effect of Beam Size and FRP Thickness on Interfacial Shear Stress Concentration and Failure Mode of FRP-Strengthened Beams*. Composites Science and Technology, 65; 1148-1158, 2005.

98. K E Jackson. *Scaling Effects in the Static and Dynamic Response of Graphite-Epoxy Beam-Columns*. NASA, TM-102697, 1990.

99. M R Wisnom. *Size Effect in Composites*. Comprehensive Composite Materials, 5; 23-47, 2002.

100. J Lee and C Soutis. *A Study on the Compressive Strength of Thick Carbon Fibre-Epoxy Laminates*. Composites Science and Technology, 2007.

101. D Liu and B Raju. *Size Effect on Impact Response of Composite Laminates*. International Journal of Impact Engineering, 21; 837-854, 1998.

102. D P Johnson, J Morton, S Kellas, and K Jackson. *Size Effects in Scaled Fiber Composites under Four-Point Flexure Loading*. American Institute of Aeronautics and Astronautics, 38; 1047-1054, 2000.

103. K E Jackson. *Scaling Effects in the Flexural Response and Failure of Composite Beams*. American Institute of Aeronautics and Astronautics, 30; 2099-2105, 1992.

104. C Soutis, J Lee, and C Kong. *Size Effect on Compressive Strength of T300/924C Carbon Fibre-Epoxy Laminates*. Plastics, Rubber and Composites, 31; 364-370, 2002.

105. A A Griffith. *The Phenomenon of Rupture and Flow in Solids*. Philosophical Transactions of the Royal Society A, 221; 163-198, 1920.

106. M R Wisnom, T Reynolds, and N Gwilliam. *Reduction in Interlaminar Shear Strength by Discrete and Distributed Voids*. Composites Science and Technology, 56; 93-101, 1995.

107. D L Flaggs and M H Kural. *Experimental Determination of In Situ Transverse Lamina Strength in Graphite/Epoxy Laminates*. Journal of Composite Materials, 16; 103-116, 1982.

108. D Lui and L Hou. *Three-dimensional Size Effects in Composite Pin Joints*. Journal of Experimental Mechanics, 43; 115-123, 2003.

109. L S Sutherland, R A Shenoi, and S M Lewis. *Size and Scale Effects in Composites: II. Unidirectional Laminates*. Composites Science and Technology, 59; 221-233, 1999.

110. T K O'Brien and A D Chawan. *Influence of Specimen Preparation and Specimen Size on Composite Transverse Tensile Strength and Scatter*. NASA, TM-2001-211030; 2001.

111. C Zweben. *The Flexural Strength of Aramid Fiber Composites*. Journal of Composite Materials, 12; 422-430, 1978.

112. M R Wisnom. *Analysis of Shear Instability in Compression due to Fibre Waviness*. Journal of Reinforced Plastics and Composites, 12; 1171-1189, 1993.

113. M R Wisnom. *Size Effects in the Testing of Fibre-Composite Materials*. Composites Science and Technology, 59; 1937-1957, 1999.

114. M Stevanovic, M Gordic, D Sekulic, and I Djordjevic. *The Effect of Edge Interlaminar Stresses on the Strength of Carbon/Epoxy Laminates of Different Stacking Geometry*. Journal of the Serbian Chemical Society, 71; 421-431, 2006.

115. N J Pagano and R B Pipes. *The influence of Stacking Sequence on Laminate Strength*. Journal of Composite Materials, 5; 50-57, 1971.

116. J Lindemann and W Becker. *The Tendency for Free-Edge Delamination in Laminates and its Minimization*. Composites Science and Technology, 62; 233-242, 2002.

117. L Lagunegrand, T Lorriot, R Harry, and H Wargnier. *Initiation of Free-Edge Delamination in Composite Laminates*. Composites Science and Technology, 66; 1315-1327, 2005.

118. R B Pipes and N J Pagano. *Interlaminar Stresses in Composite Laminates under Uniform Axial Tension*. Journal of Composite Materials, 4; 538-548, 1970.

119. T K O'Brien. *Characterisation of Delamination Onset and Growth in a Composite Laminate*. ASTM STP 775, 140-167, 1982.

120. Z P Bazant. *Size Effect on Structural Strength: A Review*. Archive of Applied Mechanics, 69; 703-725, 1999.

121. M R Gurvirch and R B Pipes. *Strength Size Effect on Laminated Composites*. Composites Science and Technology, 55; 93-105, 1995.

122. E J Lang and T W Chou. *The Effect of Strain Gage Size on Measurement Errors in Textile Composites Materials*. ICCM-11, 5; 3483-3490, 1997.

123. M R Wisnom. *The Relationship between Tensile and Flexural Strength of Unidirectional Composites*. Journal of Composite Materials, 26; 1173-1180, 1992.

124. V Laws. *The Relationship between Tensile and Bending Properties of Non-Linear Composite Materials*. Journal of Materials Science, 17; 2919-2924, 1982.

125. S W Yurgartis. *Measurement of Small Angle Fiber Misalignments in Continuous Fiber Composites*. Composites Science and Technology, 30; 279-293, 1987.

126. N A Weil and I M Daniel. *Analysis of the Fracture Probabilities in Non-Uniformly Stress Brittle Materials*. Journal of the American Ceramic Society, 47; 268-274, 1964.

127. I M Daniel and N A Weil. *The Influence of Stress Gradient upon Fracture of Brittle Materials*. ASME Winter Annual Meeting, ASME63-WA-228; 1963.

128. M R Wisnom. *The Effect of Fibre Waviness on the Relationship between Compressive and Flexural Strengths of Unidirectional Composites*. Journal of Composite Materials, 28; 66-76, 1994.

129. M R Wisnom. *The Effect of Specimen Size on the Bending Strength of Unidirectional Carbon Fibre-Epoxy*. Composite Structures, 18; 47-63, 1991.

130. M R Wisnom and J W Atkinson. *Constrained Buckling Tests Show Increasing Compressive Strain to Failure with Increasing Strain Gradient*. Composites Part A, 28A; 959-964, 1997.

131. H F Wu and L L Wu. *A Study of Tension Test Specimens of Laminated Hybrid Composites. Part II. Size and Alignment Effect*. Journal of Materials Science, 29; 5847-5851, 1994.

132. W A Curtin. *Dimensionality and Size Effect on the Strength of Fiber-Reinforced Composites*. Composites Science and Technology, 60; 543-551, 2000.

133. K E Jackson, S Kellas, and J Morton. *Scale Effects in the Response and Failure of Fiber Reinforced Composite Laminates Loaded in Tension and in Flexure*. Journal of Composite Materials, 26; 2674-2705, 1992.

134. T K O'Brien and S A Salpekar. *Scale Effects on the Transverse Tensile Strength of Graphite/Epoxy Composite*. ASTM on Composite Materials, 11; 23-52, 1993.

135. D P Johnson, J H Felts, and M T Ho. *Scaling Effects in Composite Laminates under Tensile, Flexural, and Compressive Loading*. ASME Aerospace Division, 55; 59-66, 199.

136. C Zweben. *The Effect of Stress Nonuniformity and Size on the Strength of Composite Materials*. Composites Technology Review, 3; 23-26, 1981.

137. M F Crowther and M S Starkey. *Use of Weibull Statistics to Quantify Specimen Size Effect in Fatigue of GRP*. Composites Science and Technology, 31; 87-95, 1988.

138. S McKown, W J Cantwell, and N Jones. *Investigation of Scaling Effects in Fiber-Metal Laminates*. Journal of Composite Materials, Article in Press, 2007.

139. M R Wisnom and J A Atkinson. *Reduction in Tensile and Flexural Strength of Unidirectional Glass Fibre-Epoxy with Increasing Specimen Size*. Composite Structures, 38; 405-411, 1997.

140. J A Lavoie, C Soutis, and J Morton. *Apparent Strength Scaling in Continuous Fiber Composite Laminates*. Composites Science and Technology, 60; 283-299, 2000.

141. S Kellas and J Morton. *Scaling Effects in Angle-Ply Laminates*. NASA, CR-4423; 1992.

142. K E Jackson, S Kellas, and J Morton. *Scale Effects in the Response and Failure of Reinforced Composite Laminates*. Journal of Composite Materials, 26; 2674-2705, 1992.

143. H Hamada and Ramakrishna. *Scaling Effects in the Energy Absorption of Carbon-Fiber/PEEK Composite Tubes*. Composites Science and Technology, 55; 211-221, 1995.

144. M R Wisnom. *Effect of Shear Stresses in Indirect Compression Tests of Unidirectional Carbon Fiber/Epoxy.* American Institute of Aeronautics and Astronautics, 29; 1692-1697, 1990.

145. J M Reeder. *Stitching vs. a Toughened Matrix: Compression Strength Effect.* Journal of Composite Materials, 29; 2464-2487, 1995.

146. M S Found, I C Howard, and A P Paran. *Size Effects in Thin CFRP Panels Subjected to Impact.* Composite Structures, 38; 599-607, 1997.

147. K N Shivakumar, W Elber, and W Illg. *Prediction of Impact Force and Duration due to Low-Velocity Impact on Circular Composite Laminates.* Journal of Applied Mechanics, 52; 674-680, 1985.

148. T A Duffey, M C Cheresh, and S H Sutherland. *Experimental Verification of Scaling Laws for Punch-Impact-Loaded Structures.* International Journal of Impact Engineering, 2; 103-117, 1984.

149. L S Sutherland and C G Soares. *Scaling of Impact a Low Fibre-Volume Glass-Polyester Laminates.* Composites Part A, 38; 307-317, 2007.

150. N Jones. *Scaling of Inelastic Structures Loaded Dynamically.* In: Structural Impact and Crashworthiness, edited by G A Davies, Elsevier, p. 45-74. 1984.

151. B V Sankar. *Scaling of Low-Velocity Impact for Symetric Composite Laminates.* Journal of Reinforced Plastics and Composites, 2; 296-309, 1992.

152. E Booth, D Collier, and J Miles. *Impact Scalability of Plated Steel Structures.* In: Structural Crashworthiness, edited by N Jones and T Wierzbicki, Butterworths, p. 136-174. 1983.

153. J E Gibson. *Model Analysis and Similitude Requirements.* In: Small Scale Modelling of Concrete Structures, edited by F A Noor and L F Boswell, Elsevier Applied Science, p. 13-39. 1992.

154. Y Qian, S R Swanson, R J Nuismer, and R B Bucinell. *An Experimental Study of Scaling Rules for Impact Damage in Fibre Composites.* Journal of Composite Materials, 24; 559-570, 1990.

155. Y Qian and S R Swanson. *Experimental Measurements of Impact Response in Carbon/Epoxy Plates.* American Institute of Aeronautics and Astronautics, 28; 1069-1074, 1990.

156. S R Swanson. *Scaling of Impact Damage in Fiber Composites from Laboratory Specimens to Structures.* Composite Structures, 25; 249-255, 1993.

CHAPTER III. EXPERIMENTAL PROCEDURE

This chapter presents a detailed description of the materials used in this research, the manufacturing strategy and the testing conditions employed. Initially, the constituent materials are analysed in order to obtain their properties before they are consolidated to form a FML.

The manufacturing procedure involved consolidating and machining the FMLs, as well as the constituent materials, i.e., the aluminium plies, the thermoplastic composite and the adhesive. Following this, the mechanical tests used to evaluate the materials and their failure modes are discussed.

The second part of the experimental programme involved a study of scaling effects in the properties of the FMLs and their constituents. Here, two techniques were employed, ply-level and sublaminate-level scaling. This investigation was undertaken for a range of specimen sizes (n = ¼, ½, ¾ and full scale size) scaled using a one dimension (1D), two dimension (2D) and three dimension (3D) scaling approach in tension, flexure and under low velocity impact loading.

3.1 Materials Investigated

3.1.1 SRPP Composite

In this study, a self-reinforced polypropylene composite (SRPP) was investigated. This thermoplastic composite consists of a plain woven of high strength fibres which were partially melted and consolidated to yield a flexible laminate.

The term 'self-reinforced' refers to the fact that the composite is based on oriented polypropylene fibres embedded in a polypropylene matrix of the same material. The material originally is in a fabric form (see Figure 3.1), which is consolidated in a high pressure lamination process (40 bars) with a controlled temperature to avoid melting completely the highly align fibres. This process yielded a high strength laminate that is 100% recyclable and offers high reformability. This plain woven has the advantage of having the same mechanical properties in the two main fibre directions (0° and 90°) [1].

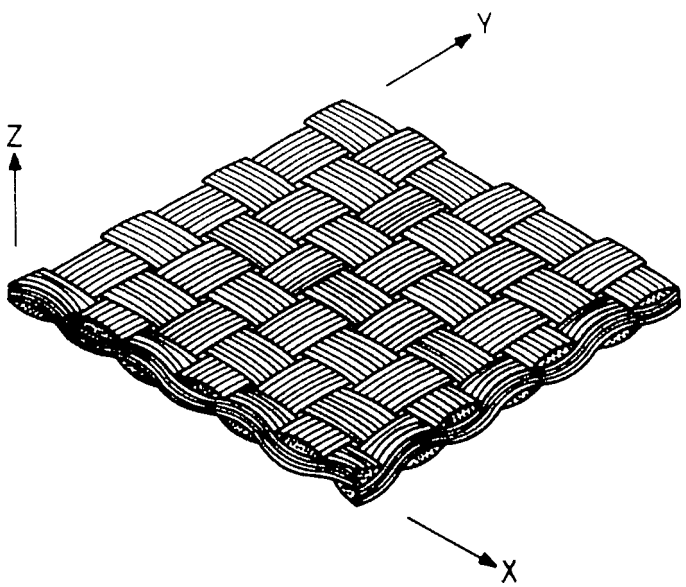

Figure 3.1. Schematic representation of a woven fabric [2].

The SRPP composites that were used to manufacture the different FMLs were supplied by Propex Fabrics under the trade name of Curv® in four different thicknesses: 0.3, 0.6, 0.9 and 1.2 mm. In the case of the 0.3 mm thick laminate, this consist of two layers of woven fabric, the 0.6 mm thick consist of four layers of woven fabric, etc.

The 0°/90° SRPP has a density equal to polypropylene, i.e., 920 kg/m^3, a melting point, T_m = 175 °C, a tensile strength of 135 MPa, a Young's modulus of 5 GPa and a strain to failure of 23% [**1**].

3.1.2 Polypropylene Adhesive Interlayer

A modified polypropylene film with a thickness of approximately 60 microns (Xiro 23.601-40 from Collano) [**3**] was employed as an adhesive to bond the aluminium and the SRPP. The density of this film material is 920 kg/m^3, with a melting point, T_m = 145 °C, a tensile strength of 25 MPa, a Young's modulus of 500 MPa and a strain to failure of 600%.

3.1.3 Aluminium Alloy

The aluminium alloy used in this study was based on a bare aluminium alloy type 2024-0. This aluminium was selected since it is used in secondary structures such as aircraft fittings, gears and shafts, couplings, pistons, etc. It offers good mechanical properties, matching the properties of the composite material studied here. Various suppliers were used for supplying the different thicknesses of aluminium due to difficulties in obtaining small amounts of this specialised alloy for use on a laboratory scale. Table 3.1 summarises the different aluminium alloys used in this study.

Thickness	ALCOA	AMAG	AMAG	KAISER
Inches	0.020	0.040	0.063	0.080
mm	0.5	1	1.6	2

Table 3.1. Thicknesses of the aluminium alloys investigated here.

The general properties of the aluminium 2024-0 reported in the literature [**4**] are, a density of 2780 kg/m^3, a melting point, T_m of approximately 550 °C, a tensile strength of 185 MPa, a Young's modulus of 73.1 GPa and a strain to failure of 20-22%.

3.1.3.1 Indentation Tests

Indentation tests were conducted in order to obtain the indentation resistance of the aluminium plies and to correlate these values with those obtained during the tensile tests.

The Vickers hardness test involves a diamond indenter, in the form of a square-base pyramid, being pressed under load for approximately 10 seconds into the surface of the material under test [**5,6**]. The result is a square-shaped impression as shown in Figure 3.2. After the load is removed, the diagonals (d) of the indentation are measured. The Vickers hardness number (HV) is obtained by dividing force (P) in kgf, by the surface area, in mm^2, of the resulting indentation:

$$HV = \frac{Applied\ force}{Surface\ area\ of\ indentation} \qquad \textbf{3.1}$$

The surface area can be calculated from the mean diagonal, the indentation being assumed to be a right pyramid with a square base and an apex angle θ of 136° with the following equation:

$$Area = \frac{d^2}{2\ sin\ \theta/2} \qquad \textbf{3.2}$$

Thus the Vickers hardness (HV) is given by:

$$HV = \frac{1.854 \cdot P}{d^2} \qquad \textbf{3.3}$$

The Vickers test has the advantage over the Brinell test of the increased accuracy in measuring the diagonals of a square as opposed to the diameter of a circle. The square indentation produced on a particular material depends on the force used, but because the indentation is always the same square shape regardless of how large the force and the surface area is proportional to the force, the hardness value obtained is independent of the size of the force used. Typically, a mass of 30 kg is used for steels and cast irons, 10 kg for copper alloys, 5 kg for pure copper and aluminium alloys, 2.5 kg for pure aluminium and 1 kg for lead, tin and thin alloys [**5**]. Up to a hardness

The hardness test was carried out on a semi-automatic micro-hardness tester model DMH-2 from Matsuzawa Seiki, using a mass of 1 kg applied for 5 seconds. Ten repeat indentations were made for each sample in order to get an average indentation force.

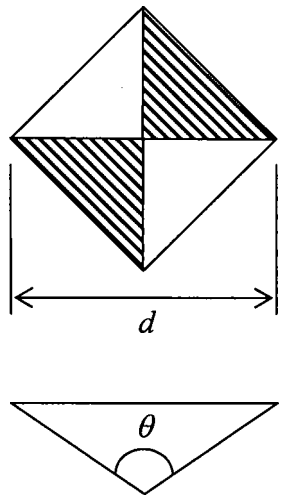

Figure 3.2. Vickers indentation pyramid.

3.2 Manufacturing Process

During the manufacture of a material, it is important to keep all conditions (i.e., time, pressure, temperature, etc.) as similar as possible to minimise variations in the properties of the finished product. Thermoplastic materials, such as SRPP, are very sensitive to changes in pressure and temperature. It is therefore necessary to ensure that all these parameters are identical, especially when scaling effects are being investigated.

The FML laminates were manufactured in a symmetric and balanced manner, based on the previously described constituents. This novel FML, developed at the University of Liverpool [7], combines the stiffness of the aluminium with the high toughness properties of the polypropylene thermoplastic composite. Bonding the layers together in a symmetric and balanced arrangement should yield a material with excellent properties suitable for structural applications.

3.2.1 Manufacture of the Laminates

The constituents of the FMLs play a crucial role in determining its performance. Therefore, prior to manufacturing the multi-layered FML systems, the mechanical properties of the constituents including the SRPP composite, the adhesive interlayer and the aluminium plies, were characterised.

The fibre-metal laminates (FMLs) used in this research were manufactured from an aluminium alloy (type 2024-0) and a 0°/90° plain woven self-reinforced polypropylene (SRPP) composite. A modified polypropylene film with a nominal thickness of 60 microns was used as an adhesive in the FMLs to improve bonding between the aluminium and the SRPP, therefore avoiding the need to surface-treat the aluminium alloy.

A schematic of the basic stacking configuration used in this research programme is shown in Figure 3.3. The FMLs were manufactured by stacking the composite, the interlayer material and the metal plies in a picture-frame mould. The stack was heated to 165 °C under a constant pressure of 7 bars in a Meyer pneumatic press before cooling slowly to room temperature. The processing temperature adopted here was sufficient to melt the polypropylene adhesive (T_m = 145 °C) without degrading the oriented polypropylene fibres in the SRPP. This manufacturing technique yielded high-quality panels exhibiting very little shrinkage in the composite plies. The dimensions of the picture frame mould were 300 by 300 mm.

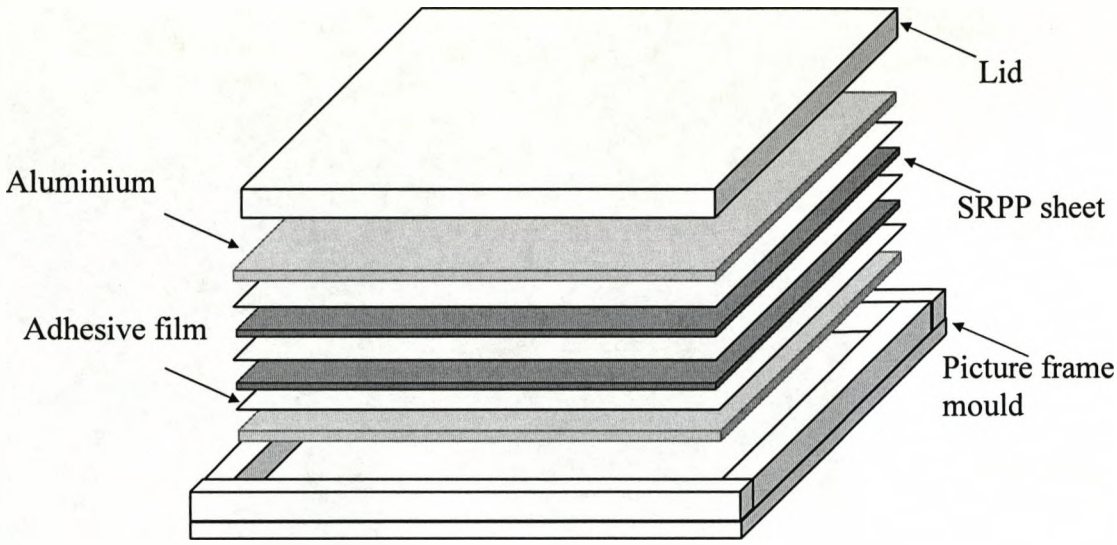

Figure 3.3. Stacking sequence of the FML material.

This technique yielded a symmetric and balanced 2/2 aluminium/composite FML similar to that shown in Figure 3.4, from which specimens for the tensile, flexural as well as impact testing were obtained. The volume fraction of the aluminium in the FML system was 56%.

The two stacking arrangements used in this study were; a [Al, 0°/90°]$_s$ FML configuration, based on the stacking sequence [Al/SRPP/SRPP/Al] with the aluminium rolling direction and the 0° fibres in the composite aligned in the test direction. Similarly, the [Al, +/-45°]$_s$ FML, was based on a stacking sequence of [Al/SRPP/SRPP/Al] with the composite fibres oriented at +/-45° to the test direction as was the aluminium rolling direction.

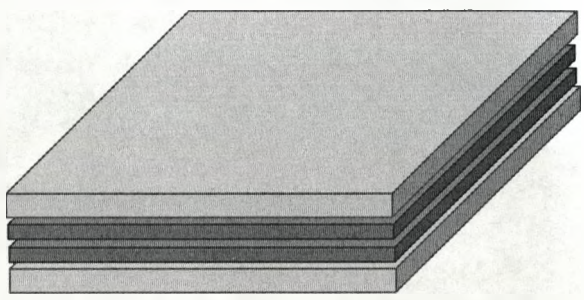

Figure 3.4. Schematic arrangement of a (2/2 aluminium/composite) FML.

In order to characterise the mechanical properties of the adhesive film used to bond the FMLs, 20 layers of polypropylene film were stacked together and processed to create a solid laminate from which tensile test samples were cut and tested following the ASTM D3039 standard [**8**]. During this lamination process, the mould in Figure 3.3 was used. Here, a temperature of 160 °C and a pressure of 1 bar (the latter was selected to avoid squeezing the molten thermoplastic out of the mould) were used prior to cooling the material to room temperature.

A degradation analysis of the SRPP was undertaken during this study. This was carried out in order to detect any degradation in the mechanical properties of the thermoplastic composite. This involved employing the same lamination conditions (i.e., time, pressure and temperature) to which the FML was subjected.

3.2.2 Machining of the Specimens

Individual specimens for tension, flexure and low velocity impact testing were cut from the FML panels using a band saw. Tensile test samples were cut three millimetres wider than required to accommodate the subsequent milling process. The SRPP composites and the laminated polypropylene adhesive were cut by guillotine, again leaving additional width for the finishing process. The milling process involved grouping a number of coupons in a vice mounted on the milling machine and aligning the samples parallel to the milling direction to reduce the width of the samples giving a uniform and smooth finish. The same process was repeated on the other side of the samples, ensuring a high quality finish and parallel faces. The milling tool used here was a 0.5 inch diameter, 4 shanks end-mill suitable for finishing surfaces, rotating at 1300 rpm with a slow longitudinal rate of displacement. This finishing process was adopted for all the specimen sizes since it was not possible to appropriately scale the grinding conditions during the scaling study.

Figure 3.5 shows a schematic of a finished tensile test sample according to the ASTM D3039 standard.

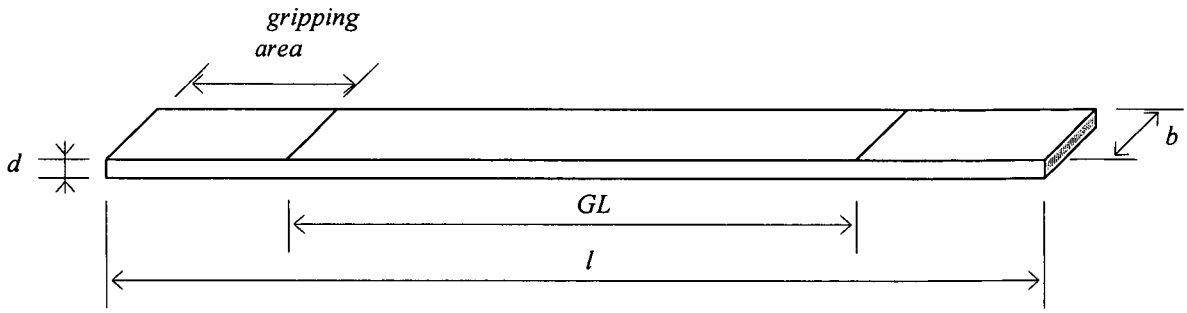

Figure 3.5. Schematic representation of a tensile test sample, 'GL' is the gauge length, 'b' is the width, 'd' is the thickness and 'l' is the total sample length.

The nominal dimensions of the FML samples and their constituents are given in Table 3.2. Here, SRPP samples were prepared with two fibre orientations, these being 0°/90° and +/-45°, the dimensions of the adhesive samples and the aluminium specimens are also given in Table 3.2. Finally, two FML systems were investigated in tension, these being the [Al, 0°/90°]$_s$ FML and the [Al, +/-45°]$_s$ FML. The thickness and width of each specimen was measured at three points along the specimen length using a flat face digital calliper.

Dimensions	SRPP	Adhesive	Aluminium	FMLs
Gauge length (mm)	100	100	100	100
Gripping length (mm)	40	40	40	40
Width (mm)	20	20	20	20
Thickness (mm)	0.6	1.1	1	3.5

Table 3.2. Dimensions of the FML tensile test samples and their constituent materials.

The FML samples used for flexural testing were manufactured using an identical lamination and machining process to the tensile test specimens. Similarly, the aluminium samples for flexural testing were machined to permit comparisons with the tensile test data. Figure 3.6 shows a four point bend sample loaded according to the ASTM D790-80 standard **[9]**. Here, '*L*'' is the inner span, '*L*' the outer span, '*l*' the total length, '*b*' the specimen width and '*d*' the thickness.

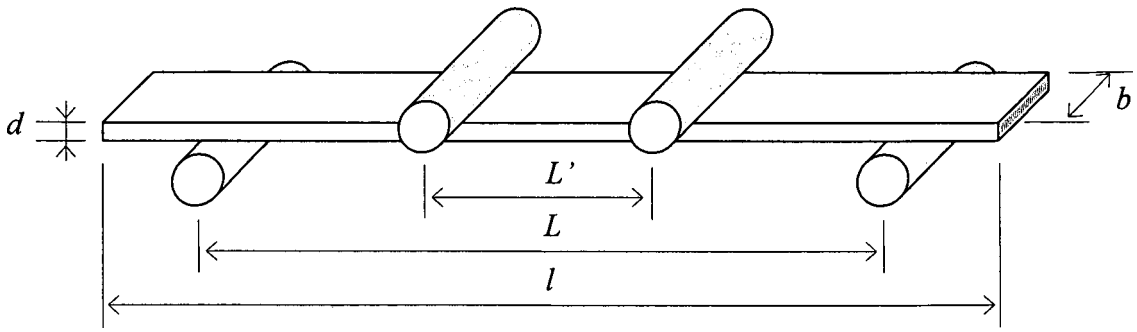

Figure 3.6. Schematic representation of a four point bending test sample.

The dimensions of the aluminium and FML flexural samples are given in Table 3.3. Here, the aluminium rolling direction was along the length of the specimens. The FML specimens were prepared with two fibre orientations; these being the [Al, $0°/90°]_s$ FML and the [Al, $+/-45°]_s$ FML. It was not possible to test the SRPP material in flexure due to its high flexibility.

Dimensions	Aluminium	FML
Width *b* mm	20	20
Thickness *d*. mm	1.0	3.51
Outer span *L* mm	130	130
Inner span *L'* mm	43.3	43.3
Roller supports mm	6.0	6.0

Table 3.3. Dimensions of the aluminium and the FML samples for flexural testing.

As part of the mechanical characterisation, impact samples were prepared following the same procedure described in Section 3.2.1. Here, impact plates with dimensions of 75 x 75 mm were cut from the FML panels using a band-saw and the edges were finished using a milling machine. The mean thickness of the resulting plates was 1.77 mm, where its constituent dimensions were: 0.3 mm SRPP, 0.5 mm aluminium sheet, and 0.5 mm adhesive layer. Subsequently, the samples were weighted on a digital balance in order to determine their areal density, in kg/m^2. A finished plate is shown in Figure 3.7.

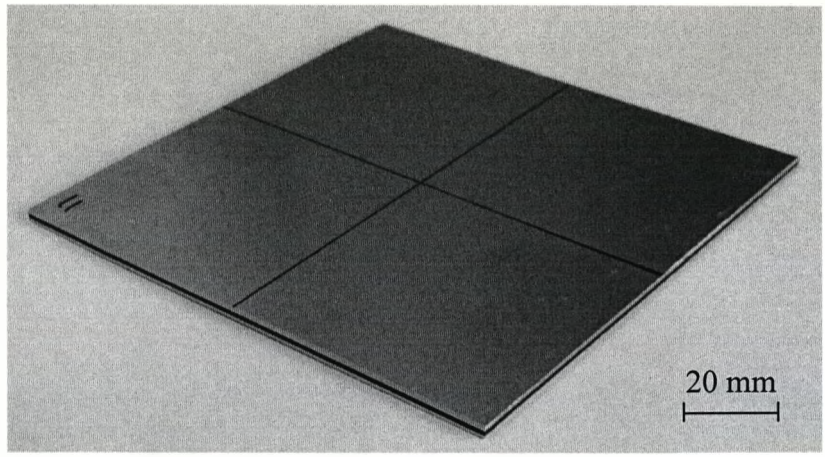

Figure 3.7. Photograph of a plate used for impact testing.

3.2.3 Lamination of the SCB Panels

The single cantilever beam (SCB) technique was employed to investigate the interfacial fracture properties and failure mechanisms occurring within the fibre-metal laminate. This geometry yields mixed-mode loading conditions (tension/shear).

SCB test samples based on aluminium/SRPP bi-material specimens were prepared. Here, a 2 mm thick aluminium plate was bonded to a 0.3 mm SRPP layer using a 60 microns thick PP film as an adhesive; in addition a 3 mm thick GFRP laminate was bonded to the lower surface of the composite to give it increased rigidity, as shown in Figure 3.8. This glass-fibre reinforced plastic (GFRP) stiffener was used since it was not possible to test the SRPP on its own, even when it was consolidated into a thicker laminate.

A folded aluminium foil with a length of 55 mm was incorporated at the interface to act as a starter defect. The materials were placed in a picture frame mould and processed at 165 °C and under a pressure of 7 bars to reproduce the manufacturing conditions experienced by the FML systems. The dimensions of the picture frame mould were 300 by 300 mm.

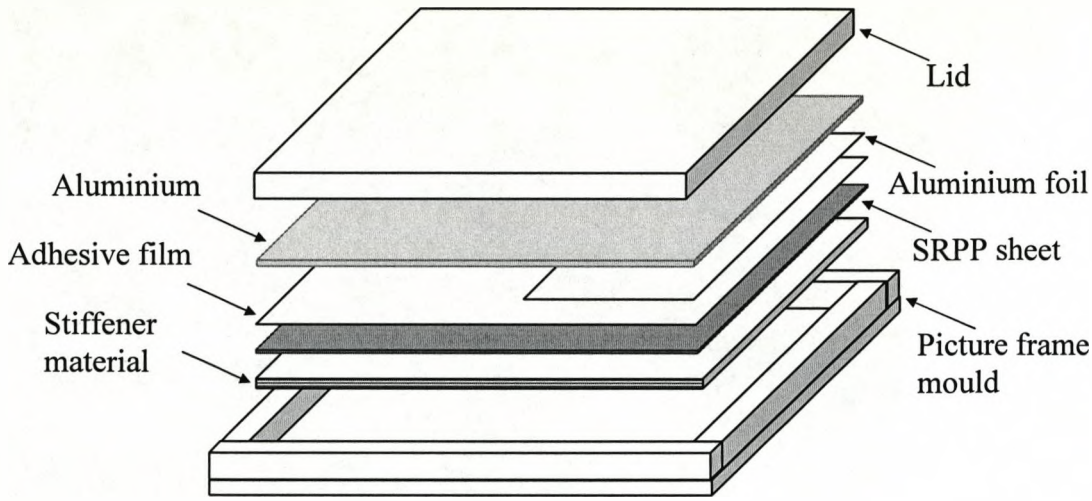

Figure 3.8. Schematic of the stacking configuration for the mixed-mode single cantilever beam (SCB) specimens.

3.2.4 Machining of the SCB Specimens

Once the system was consolidated into a laminated plate, an additional stiffener was added to the SCB panel to increase the stiffness of the aluminium ply; this stiffener consisted of a glass-fibre/epoxy honeycomb bonded to the upper aluminium layer using an Araldite epoxy resin (type 2015 from Huntsman). After manufacture, the panel was cut into samples using a band-saw and subsequently ground to generate a uniform and smooth finish. This specimen is shown in Figure 3.9.

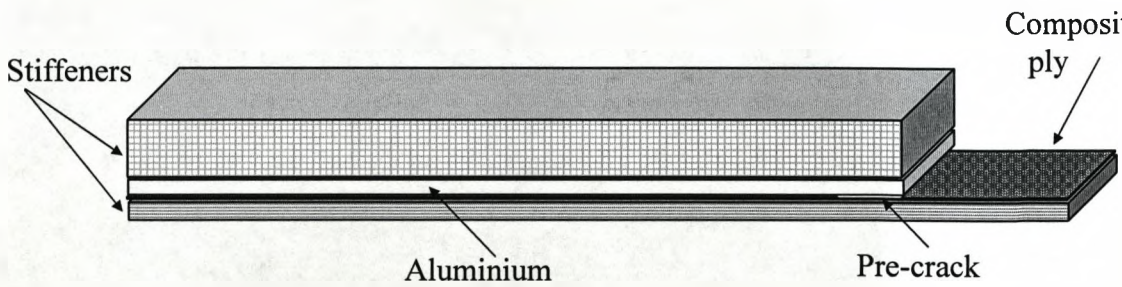

Figure 3.9. Schematic of the mixed-mode single cantilever beam (SCB) specimen.

3.3 Mechanical Properties of the Materials

The tensile properties of the plain aluminium, the SRPP and the fibre-metal laminates were investigated at quasi-static rates of loading in tension and flexure. Additionally, low velocity impact tests were undertaken to highlight the impact energy absorption characteristic of the FML systems. The single cantilever beam (SCB) technique was used to characterise the degree of adhesion between the SRPP composite and the aluminium.

3.3.1 Tensile Tests on the FMLs and their Constituents

Tensile tests were conducted on the FMLs as well as on each constituent to obtain the tensile strength, the strain to failure, the Young's modulus as well as the failure behaviour of each system.

Tensile tests were conducted on the plain aluminium alloy samples, the 0°/90° and the +/-45° SRPP samples, the polypropylene adhesive as well as the [Al, 0°/90°]$_s$ and the [Al, +/-45°]$_s$ FML samples. Tests were conducted on straight-edged rectangular samples in order to avoid the need to machine potentially complex dog-bone geometries as others have done with success [**7,10**]. All tests were conducted at a constant strain rate of 0.04 min^{-1} on an Instron 4204 screw-driven universal mechanical testing machine according to the ASTM D3039 testing standard for tensile testing of composite materials [**8**].

The modulus of elasticity of the samples was measured using a clip-on extensometer with 25 mm gauge length at a crosshead displacement of 0.2 mm/min. The data was collected at an acquisition rate of four points per second and up to 1% strain, after which the samples were unloaded carefully to avoid damage. The samples were subsequently loaded to failure to obtain the stress and strain at break. During the tensile tests, the maximum strain in the samples was measured using an Instron 2603 long-travel extensometer as shown in Figure 3.10. The gauge length over which the strain history was measured was 50 mm. The extensometer was sufficiently versatile to measure the complete strain history of the specimens considered here.

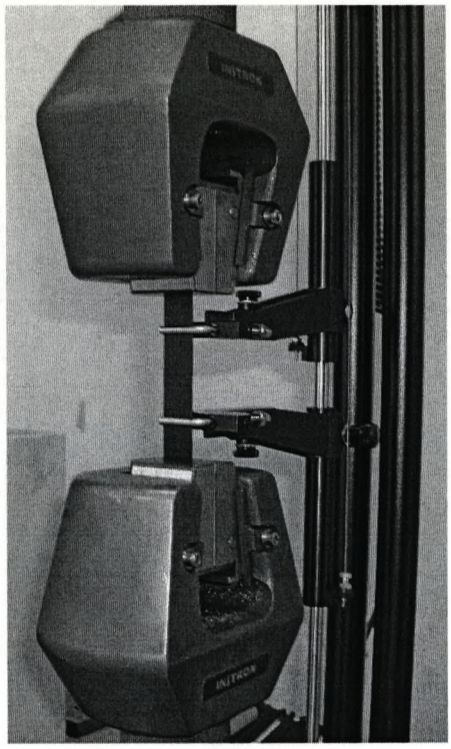

Figure 3.10. Mechanical testing machine showing the long distance extensometer.

After fracture, the specimens were removed from the testing machine for subsequent optical examination in order to highlight the failure modes.
The tensile strength (σ) was calculated using:

$$\sigma = \frac{P}{bd} \qquad \textbf{3.4}$$

where 'P' is the force at fracture and 'bd' is the cross sectional area.

The strain (ε) was calculated directly using the simple formula:

$$\varepsilon = \left(\frac{\Delta l}{l}\right) \cdot 100 \qquad \textbf{3.5}$$

where 'Δl' is the total deformation of the specimen measured by the extensometer and 'l' is the original length, taken in this case as the initial length of the extensometer.

The modulus of elasticity (E) was calculated using:

$$E = \left(\frac{\Delta P}{\Delta l}\right) \cdot \left(\frac{l}{bd}\right) \quad 3.6$$

where $\Delta P/\Delta l$ is the slope of the load vs. deformation curve in the linear region.

Once the properties of the constituents were calculated, it was then possible to predict the tensile strength and the Young's modulus of the FMLs using a simple rule of mixtures approaches as follow:

$$\sigma_{FML} = \sigma_{Al} V_{f_{Al}} + \sigma_{SRPP} V_{f_{SRPP}} + \sigma_{Ad} V_{f_{Ad}} \quad 3.7$$

and

$$E_{FML} = E_{Al} V_{f_{Al}} + E_{SRPP} V_{f_{SRPP}} + E_{Ad} V_{f_{Ad}} \quad 3.8$$

where 'σ' is the measured failure stress of the appropriate constituents (the FML, the aluminium, the SRPP and the adhesive) and the 'V_f' is the volume fraction of the appropriate constituent material. Similarly 'E' represents the Young's modulus of the FML and its constituents.

3.3.2 Flexural Tests on the FMLs and their Constituents

Flexural tests were conducted at a quasi-static loading rate on the plain aluminium alloy samples, the [Al, 0°/90°]$_s$ and the [Al, +/-45°]$_s$ FMLs. The flexural tests were conducted on straight-edged rectangular samples, where the aluminium was oriented along its rolling direction at all the times. All tests were conducted at a constant strain rate of 0.01 min^{-1} on an Instron 4204 screw-driven universal mechanical testing machine according to the ASTM D790-80 testing standard for flexural testing of plastics [**9**]. Strain gauges were situated at the centre of the lower surfaces of at least five specimens.

The flexural properties of the fibre-metal laminates were evaluated at four point bending test as shown in Figure 3.11. Similarly, aluminium specimens were tested.

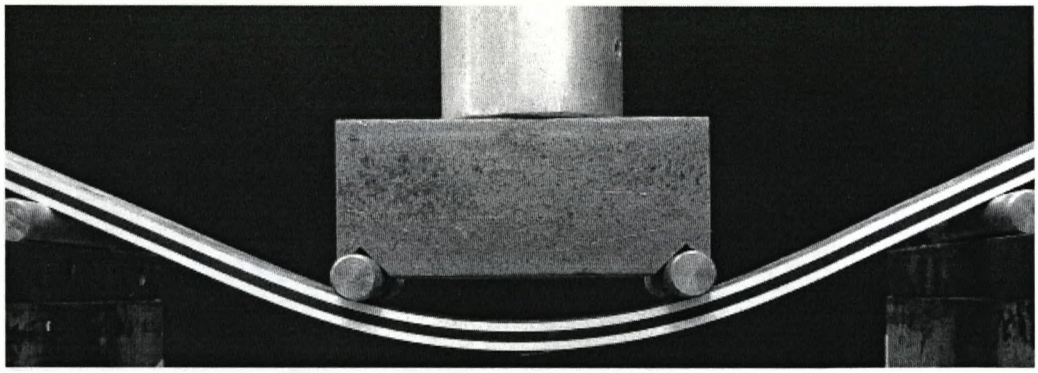

Figure 3.11. Photograph of a four point bending test.

The specimens were mounted on a four point bend fixture, loaded by two rollers and resting on the other two. Each roller was separated by a distance $L/3$, where 'L' was set to 130 mm. The specimen width (b) was 20 mm and the span/thickness (L/d) ratio was 37. The sample was again loaded at a strain rate of 0.01 min^{-1}. The flexural strength (σ_B) was calculated at maximum load using:

$$\sigma_B = \left(P_B L / bd^2\right) \cdot \left[1 + \left(4.7D^2 / L^2\right) - \left(7.04Dd / L^2\right)\right] \quad \textbf{3.9}$$

which corresponds to the case where the span to depth (L/d) ratio is greater than 16. Here, 'P_B' corresponds to the force applied to the sample and 'D' is the maximum deflection of the centre of the beam.

The maximum strain in bending (ε_B) occurs at the midspan and was calculated using:

$$\varepsilon_B = 4.7Dd / L^2 \quad \textbf{3.10}$$

The modulus of elasticity in bending (E_B) was calculated by drawing a tangent to the initial straight linear portion of the load-displacement curve and then by using:

$$E_B = 0.21L^3 m / bd^3 \quad \textbf{3.11}$$

where 'm' is the slope of the tangent to the initial straight linear portion of the load-displacement curve.

During each test, the load-displacement data were recorded and saved on an Excel spreadsheet for further analysis. After the maximum load was reached, the samples were unloaded and then removed from the test machine for subsequent optical examination in order to observe the failure modes. Here, specimens that had not fractured were sectioned using a band-saw and polished to observe the internal damage with the aid of an optical microscope.

3.3.3 Single Cantilever Beam Tests

The single cantilever beam test was used to obtain values of the interfacial fracture energy. The average specimen thickness was 3.5 mm (including the stiffener) and the total specimen length was 200 mm. The distance between the support and the loading point (L) was 110 mm, the length of the starter defect (a) was 40 mm and the width (b) was 20 mm as shown in Figure 3.12. The specimen was supported and clamped in a steel fixture adapted for use on an Instron 4204 screw-driven universal mechanical testing machine with 5 kN load cell. In order to facilitate the observation of the primary crack, the specimen edges were coated with a thin layer of water-soluble typewriter correction fluid starting at the end of the pre-crack.

The support location was marked to enable the initial crack length to be accurately measured from the load point. The specimen was loaded at 2 mm/min in a displacement-control mode, forcing the initial pre-crack to propagate from the tip of the insert. The point on the load displacement plot at which the crack was first observed to grow from the insert was recorded along with the corresponding load and displacement. During the test, the crack length was noted every 5 mm along the bi-material interface, until the crack had propagated approximately 100 mm from the starter defect. The specimen was then unloaded and removed from the test machine. The test was performed at least on five specimens.

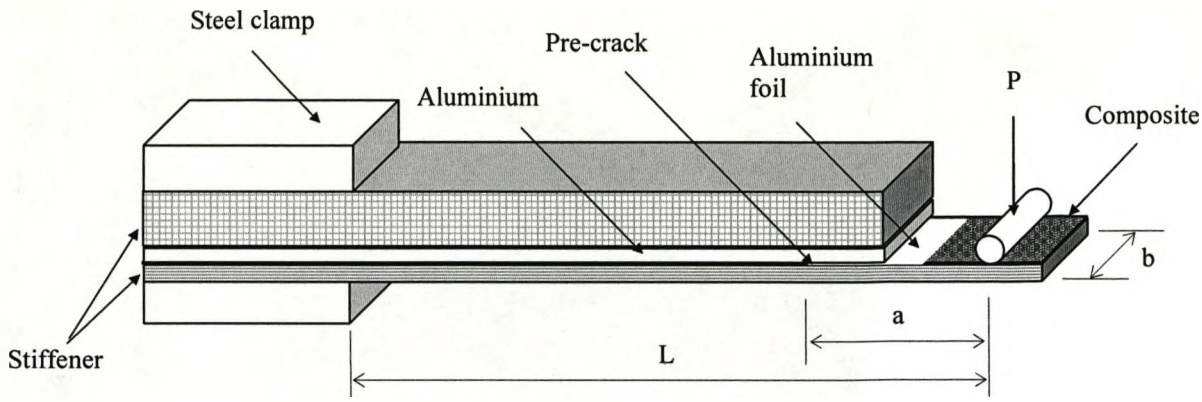

Figure 3.12. Schematic representation of the SCB test.

The mixed-mode interfacial fracture energy was determined using the experimental compliance calibration method. This technique assumes a compliance vs. crack length relationship of the form:

$$C = C_0 + ea^3 \qquad \textbf{3.12}$$

where 'C_0' is the initial compliance taken in this case as zero, and 'e' is an experimentally-determined constant, measured as the slope of the graph of the compliance (C) versus the cube of the crack length (a^3). The mixed-mode interlaminar fracture energy was then determined using:

$$G_{I/IIc} = \frac{3P^2ea^2}{2b} \qquad \textbf{3.13}$$

where 'P' is the load and 'b', the specimen width.

3.3.4 Impact Tests on the FML Specimens

Low velocity impact tests were carried out on samples with areal dimensions of 75 x 75 mm and an average thickness of 1.77 mm, using a falling-weight impact tower. Here, the test specimens were simply supported on a circular ring with internal and external diameters of 50 and 70 mm respectively as shown in Figure 3.13. Here, an

impact carriage attached with a 5 mm diameter hemispherical nose was used for testing the plates for a single strike.

A series of impact tests was conducted in order to characterise the impact response of the FMLs, highlight the failure modes as well as to determine the threshold energies for first damage and target perforation. Here, tests were undertaken by varying the impact mass (values of 0.35, 0.46, 0.54 and 0.6 kg were used corresponding to 4.7, 6.3, 7.3 and 8.1 Joules) whilst maintaining a constant impact velocity of approximately 5.2 m/s. At least four specimens were tested for each impact energy to obtain mean values.

A Kistler 9021A piezo-electric load cell with a 35 kN capacity located just above the impactor was used to measure the force-time history during the impact test as shown in Figure 3.13. The voltage signal from the load-cell was recorded using the Data Flow Plus software package. Prior to testing, a series of weights were placed on the load cell in order to calibrate it. Here, the voltage values were recorded and then plotted against the applied force. The plot yielded a straight line giving a calibration coefficient that was used in subsequent voltage-force conversions.

A laser-Doppler velocimeter was used to measure the velocity of the impactor during the impact event. The signal from the velocimeter was analysed using the BSI Flow software package developed by Dantec Measurement Technology. By combining data from the piezo-electric load cell and the laser-Doppler velocimeter, force-displacement curves were generated following the impact tests.

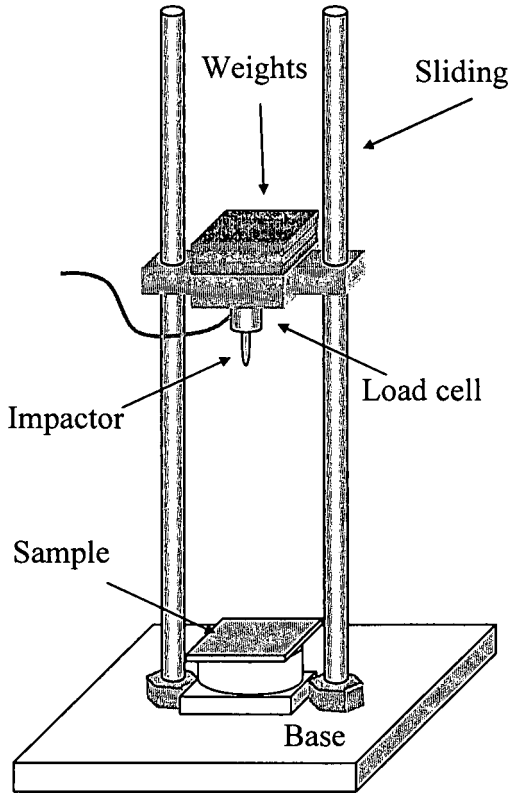

Figure 3.13. Instrumented falling-weight impact tower.

Initially, the preliminary impact energy was determined using:

$$E_{impact} = mgh \qquad \textbf{3.14}$$

where 'm' is the mass of the impactor, 'g' is acceleration due to gravity and 'h' the height from which the impactor was released. The energy absorbed by the specimens (E) was calculated by integrating the area under the load-displacement curve. The percentage of the incident energy absorbed during the impact event was then determined using:

$$E_{abs} = \frac{E}{E_{impact}} \cdot 100 \qquad \textbf{3.15}$$

Once the impact tests were carried out, the data enable the calculation of the impact energy using the following equation:

$$E_{impact} = \frac{1}{2}mv^2 \quad \textbf{3.16}$$

where 'v' is the velocity of the impactor at the point of contact being obtained from the laser Doppler velocimeter.

In addition, the specific perforation energy (SPE) was used to evaluate the low velocity impact performance of the materials investigated in this study; this was determined by dividing the perforation energy by the areal density (ρ_A) of the material:

$$SPE = \frac{E_P}{\rho_A} \quad \textbf{3.17}$$

where

$$\rho_A = \frac{m'}{A} \quad \textbf{3.18}$$

where m' is the mass of the plate and 'A' its planar area.

After testing, the samples were examined optically to identify any damage on the front and distal surfaces of the target. The samples were then cut in half through their centres using a band-saw and polished to highlight the failure modes with the help of a low magnification optical microscope.

3.4 Scaling Study on the Tensile Behaviour of the Materials

This part of the investigation focused on establishing the feasibility of using scaled models to predict the full-scale behaviour of the laminates by monitoring the stiffness, the strength, the strain to failure and the stress/strain response of the FMLs.

The lamination process for the scaling study on the FMLs followed the same conditions as those adopted in the first part of this study discussed in Section 3.2.1 and

shown in Figure 3.3. All of the manufacturing process followed the same conditions, i.e., time, temperature and pressure, to avoid external variations in the different laminates. In the same way, the groups of scaled specimens were ground using a milling machine to yield a smooth finish. Similarly, the FML constituent materials, i.e., the SRPP composite and the aluminium alloys were also scaled. Figure 3.5 shows a schematic representation of the tensile specimen used in this study.

Initially, preliminary tensile tests on the FML constituents were undertaken, from where predictions of the properties of the FMLs were made using the rule of mixtures, this, in order to establish if the maximum values of the scaled dimensions and forces required, were within the range of the testing equipment. Once the scaling dimensions were selected, the FML laminates were made in a 300 x 300 mm picture frame mould using a moulding pressure of 7 bars. The different thickness panels were manufactured with planar dimensions of 300 x 300 mm. Subsequently, the different thickness panels were cut and finished to yield the appropriate scale size. The specimens and test conditions were geometrically scaled as far as possible. Ideally, scaling should include scaling the microstructure which includes the diameter of the composite fibres and the microstructure of the aluminium, but this is clearly impossible.

Scaling effects were investigated by testing four specimen sizes corresponding to ¼, ½, ¾ and 1 as full scale size. Two techniques were employed to investigate stacking sequence effects in scaling the FMLs. In the first method, termed ply-level scaling **[11,12]**, the laminate thickness was increased by scaling the plies in proportion to the scaling factor '*n*', as shown in Figure 3.14. These tests were undertaken on the stacking sequence $[Al_n, 0°/90°_n]_s$, with n = ¼, ½, ¾ and 1 respectively. Here, four aluminium thicknesses (supplied by different manufacturers) were used; these being 0.5, 1.0, 1.6 and 2.0 mm. The properties of these metals are described in Section 3.1.3. As mentioned previously, it was not possible to obtain perfectly-scaled aluminium sheets, particularly for the case of n = ¾, where the thickness of the aluminium was 6.7% greater than the desired value.

Four thicknesses of SRPP composite were used in the construction of the ply-level FMLs, they were supplied from one company with the following thicknesses; 0.3, 0.6,

0.9 and 1.2 mm. The thermoplastic interlayer was also increased in relation to the scaling size by adding layers of the adhesive to maintain the volume fraction of composite and aluminium constant in the FML systems.

The second method, known as sublaminate-level scaling [**13,14**], involved increasing the specimen thickness by repeating the basic sublaminate block 1, 2, 3, or 4 times (n = ¼, ½, ¾ and 1) to achieve the desired scaling size, this procedure yielded laminates with stacking sequences of $[Al, 0°/90°]_{ns}$, with n = ¼, ½, ¾ and 1 respectively, as shown schematically in Figure 3.14. This figure shows the baseline laminate (n = ¼) and also compares the two scaling techniques (for the case where n = 1).

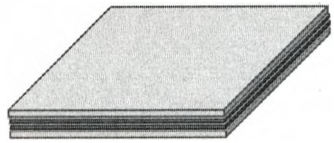

Baseline $[Al, 0°/90°]_s$

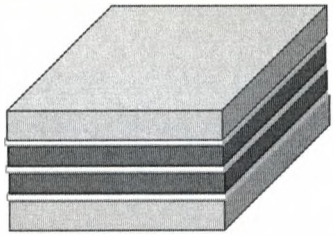

Ply-level
$[Al_n, 0°/90°_n]_s$, n = 1

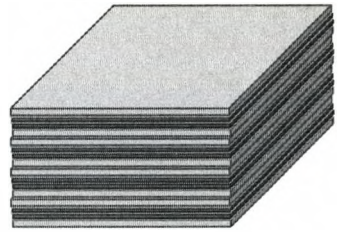

Sublaminate-level
$[Al, 0°/90°]_{ns}$, n = 1

Figure 3.14. Schematic of the two scaling techniques employed in this study, ply-level and sublaminate-level scaling.

Apart from the two scaling techniques (ply-level and sublaminate-level), scaling effects were also studied by varying the dimensions of the specimens, i.e., the thickness, the width and the length. Figure 3.15 summarizes the three scaling configurations used in this work [**11,12**]. A general description of these configurations is as follows; one-dimensional (1D) scaling involves maintaining the in-plane dimensions constant (length and width) and scaling the specimen thickness. In two-dimensional (2D) ply-level scaling, the thickness was maintained constant and the in-

plane dimensions were scaled. Finally, in three-dimensional (3D) scaling, all three dimensions were scaled.

Investigating all of the FML techniques and configurations would be expensive and time-consuming; therefore, representative models were chosen to simplify the analysis. The following configurations were employed in this study: one-dimensional (1D) ply-level scaling with in-plane (length and width) dimensions of 150 and 30 mm, two-dimensional (2D) ply-level and sublaminate-level scaled samples, where the constant thickness was fixed at 3.5 mm. Finally, three-dimensional (3D) ply-level scaling was also studied, where the length, width and thickness dimensions were all scaled appropriately. These three configurations selected for the scaling study are highlighted in Figure 3.15.

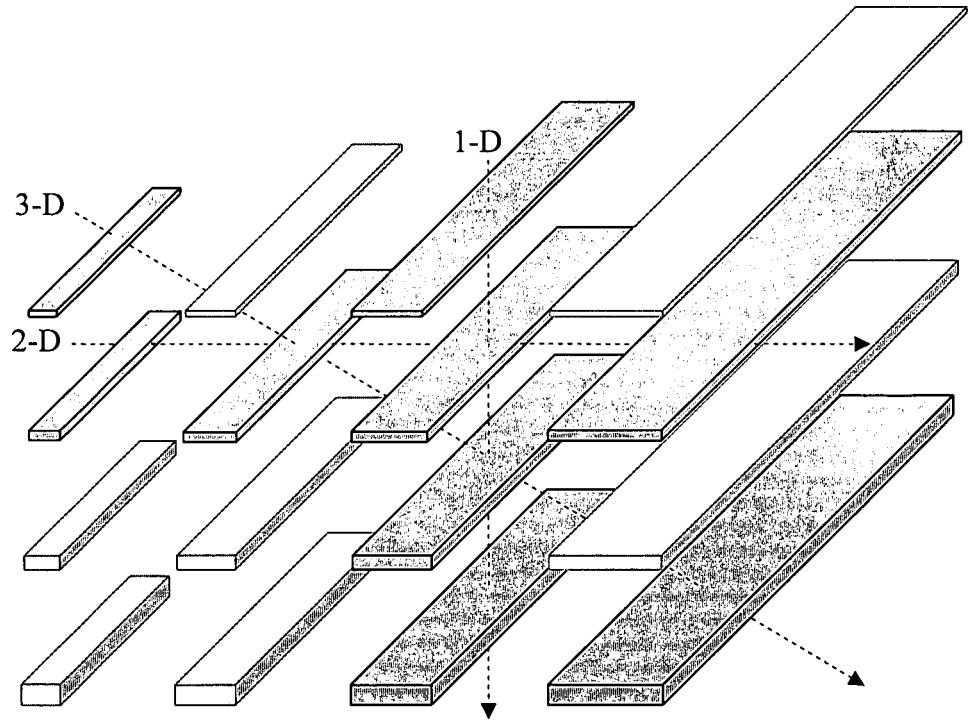

Figure 3.15. Schematic of the different scaling configurations.

During tensile testing, the strain in the samples was monitored using an Instron 2603 long-travel extensometer as shown in Figure 3.10. The gauge length over which the strain history was measured varied depending on the configuration used (1D, 2D or 3D scaling) and on the scaling size. The extensometer was sufficiently versatile to

measure the complete strain history of the specimens considered here. The strain rate was maintained at 0.04 min^{-1} during all tests.

Scaling effects were analysed by using a normalisation procedure in order to make comparable the different techniques and methodologies. This normalisation was also proposed to eliminate any difference between the different aluminium materials.

In order to remove the influence of variations in the tensile properties and thicknesses of the plain aluminium, the data for 1D-scaled samples were presented in a non-dimensional form where the failure stress of the FML, σ_{FML}, was normalised by the fracture properties of the equivalently-scaled aluminium, composite and interlayer materials. Here, the normalised failure stress is given by:

$$\frac{\sigma_{FML}}{\sigma_{Al}V_{f_{Al}} + \sigma_{SRPP}V_{f_{SRPP}} + \sigma_{Ad}V_{f_{Ad}}} \qquad \textbf{3.19}$$

and

$$\frac{E_{FML}}{E_{Al}V_{f_{Al}} + E_{SRPP}V_{f_{SRPP}} + E_{Ad}V_{f_{Ad}}} \qquad \textbf{3.20}$$

where 'E' is the elastic modulus of the appropriate constituent material (the aluminium, the SRPP or the adhesive) at the specific scale size and 'V_f' is the volume fraction of the constituent material.

Many of the explanations for the decrease in strength with increasing specimen size are based on Weibull strength theory **[15]**, from where many authors have found good agreement on their results for linear and non-linear materials **[16-18]**. According to the theory, the probability (P_s) that a specimen containing a distribution of flaws throughout its volume can survive the application of a stress distribution σ (x, y, z) is given by:

$$P_s = exp\left\{-\int_V \left(\frac{\sigma(x,y,z)-\sigma_u}{\sigma_0}\right)^m dxdydz\right\} \qquad \textbf{3.21}$$

where 'σ_0' is the normalised scaled parameter that locates the strength distribution, 'σ_u' is threshold stress below which the material will never fail (usually taken to be zero), 'V' is the volume of the specimen that is being stressed and 'm' is the Weibull modulus or the flaw-density exponent that determines the scatter in the strength of the material.

During tensile testing where the stress is uniform throughout the specimen volume and where $\sigma_u = 0$, Equation 3.21 reduces to:

$$P_t = exp\left[-V_t\left(\frac{\sigma_t}{\sigma_0}\right)^m\right] \qquad \textbf{3.22}$$

where, according to Equation 3.22, the tensile strengths for different volumes of the same material should be related by:

$$\frac{\sigma_1}{\sigma_2} = \left(\frac{V_2}{V_1}\right)^{1/m} \qquad \textbf{3.23}$$

where 'σ_1' and 'V_1' are the values of strength and volume for the model (baseline) and 'σ_2' and 'V_2' are the values for the prototype. The ratio of strengths therefore depends on the relative volumes and the Weibull modulus (m). This is a measure of material variability and is approximately related to the coefficient of variation (CV) of individual specimen strength [**17**] through the relation:

$$m \approx \frac{1.2}{CV} \qquad \textbf{3.24}$$

A highly variable material will have a low value of modulus, and would be expected to exhibit a high degree of scatter in the measured strength and a large size effect. The theory therefore predicts a direct correlation between strength variability and size effects.

Weibull theory satisfactorily explains size effects in brittle materials; however, materials which may be ductile may still exhibit a form of size effect [**19**]. Composites are not completely brittle materials but are sometimes able to sustain quite significant damage before final failure. This type of behaviour would lead to an apparent size effect because the overall stress required to initiate failure would increase with decreasing size due to load redistribution even though the local failure stress remained the same [**20**].

3.4.1 Tensile Tests on 1D Ply-Level Scaled Specimens

Initially, size effects were investigated through a study on the constituents used to manufacture the thermoplastic FMLs. Here, 1D ply-level scaling was carried out by increasing the thickness of the specimens whilst maintaining the in-plane dimensions (width and length) constant as shown in Figure 3.15. The in-plane length and width dimensions were 150 and 30 mm respectively, as outlined in Table 3.4. Associated dimensions, such as thicknesses of the individual SRPP and aluminium sheets, are included in the table as well as the gripping distance used during the tests.

Geometrical effects were investigated by monitoring the stiffness, strength, strain to failure and the stress/strain response of the FMLs and their constituents. In the case of the ¾ scale size FML, it was not possible to obtain the aluminium alloy in the scaled proportion (1.6 mm was used instead of 1.5 mm), being 6.7% thicker than the desired value as shown in Table 3.4. For the scaling study, a number of suppliers were used when purchasing the various thicknesses of aluminium, due to difficulties in obtaining this specialised alloy from one supplier as explained earlier in Section 3.1.3.

Scale size (n)	SRPP thickness (mm)	Aluminium thickness (mm)	FML thickness (mm)	Width (mm)	Gauge length (mm)	Gripping length (mm)
¼	0.3	0.5	1.77	30	150	40
½	0.6	1	3.51	30	150	40
¾	0.9	1.6	5.45	30	150	40
1	1.2	2	7.03	30	150	40

Table 3.4. Dimensions of the four 1D ply-level scaled samples tested in tension.

After testing, the samples were carefully removed from the test machine to highlight the failure modes. Following inspection, representative samples were cut from the damage zone for further microscopic analysis.

3.4.2 Tensile Tests on 2D Scaled Specimens

The 2D scaling study compared the ply-level and the sublaminate-level scaling techniques. Here, identical manufacturing procedures were used for these two techniques to avoid variations in the mechanical properties during the manufacturing process, allowing a direct comparison between them.

3.4.2.1 Tensile Tests on 2D Ply-Level Scaled Specimens

The ply-level (PL) study consisted of scaling the FMLs by increasing the in-plane dimensions of the specimens in proportion to the scaling factor (n) while keeping the thickness constant [**11**]. Here, the stacking sequence used was $[Al_n, 0°/90°_n]_s$ where n = ¼, ½, ¾ and 1 respectively. Tensile tests were undertaken on aluminium and SRPP samples with thicknesses of 1.0 and 0.6 mm respectively. Table 3.5 outlines the dimensions used for these tests. As before, tests were undertaken at a constant strain rate of 0.04 min^{-1}. Geometrical effects were investigated by monitoring the stiffness, strength, strain to failure and the stress/strain response of the FMLs.

Scale size (n)	SRPP thickness (mm)	Aluminium thickness (mm)	PL FML thickness (mm)	Width (mm)	Gauge length (mm)	Gripping length (mm)
¼	0.6	1.0	3.51	10	50	20
½	0.6	1.0	3.51	20	100	30
¾	0.6	1.0	3.51	30	150	40
1	0.6	1.0	3.51	40	200	50

Table 3.5. Dimensions of the four scaled samples used during the tensile tests on the 2D ply-level scaling.

3.4.2.2 Tensile Tests on 2D Sublaminate-Level Scaled Specimens

The second method, known as sublaminate-level (SL) scaling [**13**], involved increasing the specimen thickness by repeating the basic sublaminate block 'n' times,

as shown schematically in Figure 3.14. This procedure yielded laminates with a stacking sequence of $[Al, 0°/90°]_{ns}$, where n = ¼, ½, ¾ and 1 respectively. The dimensions used for this technique are outlined in Table 3.6.

Scale size (n)	SRPP thickness (mm)	Aluminium thickness (mm)	SL FML thickness (mm)	Width (mm)	Gauge length (mm)	Gripping length (mm)
¼	0.3	0.5	3.62	10	50	20
½	0.3	0.5	3.62	20	100	30
¾	0.3	0.5	3.62	30	150	40
1	0.3	0.5	3.62	40	200	50

Table 3.6. Dimensions of the four scaled samples used during the tensile tests on the 2D sublaminate-level scaled samples.

3.4.3 Tensile Tests on 3D Ply-Level Scaled Specimens

A study of scaling effects in 3D ply-level FMLs system was also undertaken. The FML specimens and their constituents were tested under the same conditions outlined in Section 3.3.1. Here, a constant strain rate of 0.04 min^{-1} was employed. The dimensions of the FML and its constituents are given in Table 3.7. In order to satisfy the laws of scaling, all dimensions were scaled in proportion to the scale factor (n), including the number of adhesive layers at each aluminium-composite interface. Symmetric and balanced systems were manufactured based on the following configurations:

$$[Al_n, 0°/90°_n]_s$$

and

$$[Al_n, +/-45°_n]_s.$$

where n = ¼, ½, ¾ and 1 respectively.

The plain aluminium and SRPP materials were also tested in 3D scaling and the dimensions of the samples are shown in Table 3.7. Four thicknesses of SRPP

composite were used in the construction of the ply-level FMLs. These were supplied from a single company.

Scale size (*n*)	SRPP thickness (mm)	Aluminium thickness (mm)	FML thickness (mm)	Width (mm)	Gauge length (mm)	Gripping length (mm)
¼	0.3	0.5	1.77	10	50	20
½	0.6	1	3.51	20	100	30
¾	0.9	1.6	5.45	30	150	40
1	1.2	2	7.03	40	200	50

Table 3.7. Dimensions of the four scaled samples used during the tensile tests on the 3D ply-level scaled samples.

Table 3.8 summarises the thickness of the individual layers adopted for the 3D scaling study. Included in the table are the predicted thicknesses of the laminates (based on the initial thicknesses of the constituent materials) and the resulting measured thicknesses. Differences between these two sets of values are likely to be due to material compression and flow during the manufacturing process, which as can be seen, decreases as the scaling size increase.

Size (*n*)	2 SRPP mm	2 Aluminium mm	3*n* adhesive mm	Theoretical FML thickness	Real FML thickness
¼	0.6	1	0.18	1.78	1.77
½	1.2	2.02	0.36	3.58	3.51
¾	1.8	3.2	0.54	5.54	5.45
1	2.4	4.06	0.72	7.18	7.03

Table 3.8. Summary of thicknesses of the ¼, ½, ¾ and full size specimens for the aluminium alloy, the SRPP and the FML.

Following testing, the specimens were removed from the testing machine for an optical examination to highlight the failure modes. After inspection, samples were cut from the damage zone to further microscopic analysis.

3.5 Scaling Study on the Flexural Properties of the FMLs and their Constituents

3.5.1 Flexural Tests on 3D Ply-Level Scaled Specimens

Scaling tests on four point bending samples were conducted on FML and aluminium samples in the same way as outlined in Section 3.3.2. All tests were conducted on straight-edged rectangular samples with the same dimensions as those used for tensile tests. Tests were conducted on specimens with a stacking sequences of $[Al_n, 0°/90°_n]_s$ and $[Al_n, +/-45°_n]_s$ with n = ¼, ½, ¾ and 1. Similarly, aluminium specimens were tested. However, the flexural properties of the composite material could not be measured since the specimens were very thin and flexible.

Tests were conducted at a constant strain rate of 0.01 min^{-1} on an Instron 4204 screw-driven universal mechanical test machine according to ASTM D790-80. During the tests, the strain was monitored in two ways, using the Instron crosshead deflection and by bonded strain gauges. After testing, the specimens were removed from the test machine for subsequent optical examination.

Four devices were constructed to undertake the four point bending scaling study, as shown in Figure 3.16. The fixtures were constructed in order to ensure that all test conditions were scaled correctly, including the diameter of the roller supports that were maintained constant at 12n mm (i.e., 3, 6, 9 and 12 mm) for the four scaled sizes.

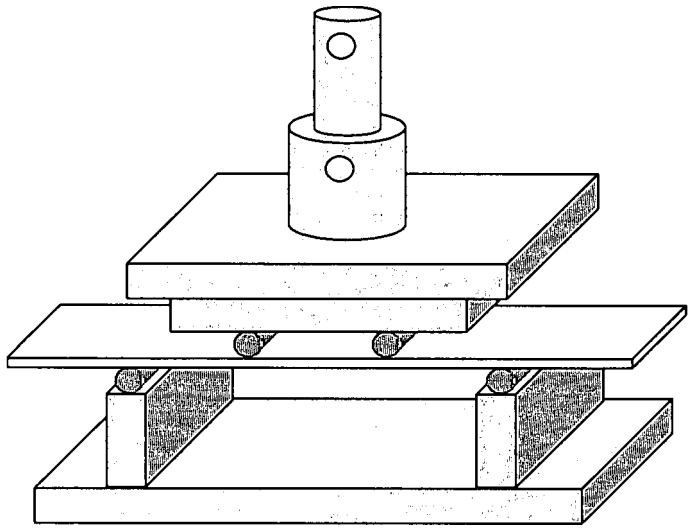

Figure 3.16. Schematic representation of the four point bend test fixture.

The dimensions of the four point bend fixtures and specimens used in this study are given in Table 3.9. Here, the width, the thickness, the outer and inner spans were scaled according to the scaling size, (n). The four point bend devices were adapted to fit on an Instron 4204 screw-driven universal mechanical testing machine.

Dimensions	¼ Size	½ Size	¾ Size	Full-Scale
Width b mm	10	20	30	40
Thickness d. mm	1.77	3.51	5.45	7.03
Outer span L mm	65	130	195	260
Inner span L' mm	21.6	43.3	65	86.6
Roller supports mm	3.0	6.0	9.0	12.0
FML Volume mm^3	1150.5	9126	31882.5	73112
(volume ratio)	(1)	(7.9)	(27.7)	(63.5)

Table 3.9. Summary of the sample dimensions used to investigate scaling effects in the flexural properties of the FMLs and aluminium specimens.

The data obtained from the Instron machine was used to calculate the stress, the strain and the stiffness using an Excel spreadsheet employed equations outlined in Section 3.3.2.

Higher strength is predicted in bending than in tension. This has been explained in terms of Weibull statistical theory **[15]**. Here, the same equation as that used in

tension was employed (Equation 3.23). Strength is assumed to be controlled by critical defects which are statistically distributed. In bending, a much smaller volume of material is subject to the maximum stress than in the case of tension. The chances of encountering a critical defect are therefore lower and so the strength is higher. A direct comparison between tension and flexure responses can be obtained by introducing Equation 3.23 for tension and flexure into Equation 3.21 **[21]**. Yielding the strength ratio:

$$\frac{\sigma_B}{\sigma_T} = [2(m+1)]^{1/m} \qquad \textbf{3.25}$$

3.6 Scaling Study on the Low Velocity Impact of the FMLs

Scaling the low velocity impact response of the FMLs was studied using the ply-level and the sublaminate-level scaling techniques. Symmetric and balanced systems were manufactured based on the two previously-reported stacking techniques (Section 3.4).

The low velocity impact response of FMLs was carried out using the falling-weight impact tower shown in Figure 3.13. Here, an impact carriage with detachable hemispherical noses (5, 10, 15 and 20 mm of diameter) was used for the four scaled sizes of FML. A constant impact velocity of approximately 5.2 m/sec and a release height of 1.5 m were used for all laminates. As explained in Section 3.3.4, a load cell was used to measure the force-time history during the impact test and a laser-Doppler velocimeter to measure the impact velocity. Four differently-sized steel rings were used to scale the test supports with an internal diameter of $200n$ mm (i.e., 50, 100, 150 and 200 mm). The data from the piezo-electric load cell and the laser-Doppler velocimeter were combined to generate force-displacement curves.

In order to predict the full scale impact properties of the FMLs, a range of impact tests from low energies and up to the perforation energy were undertaken on the smallest scale size (n = ¼). By using the same dimensions and test conditions for mechanical characterisation earlier in this chapter, it was possible to introduce the impact conditions from Section 3.3.4 to the scaling study. This group tested earlier (Section 3.3.4) was set as the baseline (n = ¼) and used to predict the forces and impact energies required for the scaled plates (n = ½, ¾ and 1).

The similitude analysis is performed by first recognising and isolating what are believed to be the pertinent input and output parameters of the system, by inspection of their associated physical dimensions. Then using the Buckingham Pi-theorem, a complete set of non-dimensional terms is formed from the isolated physical parameters of the system [**22,23**]. Wen and Jones employed such an approach when investigating the low-velocity impact response of a range of metal plates [**24**]. The input parameters in such an analysis generally include a characteristic geometrical length, L, that defines the physical size of each scale model, and material input parameters that are defined by the density and mechanical properties of the constituent materials. The response parameters include the load, response time, deflections, and the stress-strain response of the model. The physical dimensions of these parameters are reported by McKown *et al.* [**25**] given in Table 3.10 along with the similitude requirement for scale modelling involving a geometrical factor (n), (defined as the ratio of characteristic dimension in the model to the corresponding value in the full-scale model). It is worth noting that in a low velocity impact test, the velocity of the impactor is independent of scale size, whereas the drop-mass scales as the cube of the scale factor.

	Parameter	*Dimension*	*Scale Factor*
	Characteristic length, d	L	n
	Density, ρ	ML^{-3}	1
Input	*Mass, M*	M	n^3
	Velocity, v	LT^{-1}	1
	Material constant, Σ	$MT^{-2}L^{-1}$	1
	Load, F	$MT^{-2}L$	n^2
	Response time, t	T	n
Output	*Strain ε*	-	1
	Stress σ	$MT^{-2}L^{-1}$	1
	Deflection, δ	L	n
	strain rate, $\dot{\varepsilon}$	T^{-1}	n^{-1}

Table 3.10. Similitude parameters and their scale factor relationships.

Since the SRPP composite investigated in this study is based on a polymer fibre in a low modulus polymer matrix, it is likely to exhibit some form of strain-rate sensitivity. Strain-rate effects have been considered in another study [**26**], where it has been shown that the stiffness and strength of this composite increases at strain-rates above 10^{-3} s^{-1}. In contrast, the mechanical properties of aluminium alloy are considered to be strain-rate insensitive [**24**].

The low velocity impact response of these multi-layered plates was further investigated using the non-dimensional approach developed by Wen and Jones [**24**]. Here, it was shown that a plot of the non-dimensional target deflection, (δ), defined as the residual displacement following impact, (Δ), divided by the thickness of the sample, (h), against the non-dimensional impact energy, (χ), should yield a common curve over the range of scale sizes considered. The non-dimensional energy is defined as:

$$\chi = \frac{E}{\sigma_y d^3} \qquad \textbf{3.26}$$

where 'E' is the impact energy, 'σ_y' is the yield stress at scale size (n) and 'd' is a characteristic scale length, chosen in this case to be the indenter diameter.

3.6.1 Low Velocity Impact Tests on 3D Ply-Level Scaled Specimens

Simply supported plates were tested under low velocity impact conditions. Here, the ply-level technique was used where the laminate thickness was increased by scaling the thicknesses of plies in laminates based on the following stacking sequences $[Al_n, 0°/90°_n]_s$, where n = ¼, ½, ¾ and 1. Once the panels were consolidated, square plates with edge dimensions of 300n mm, (i.e., 75, 150, 225 and 300 mm) were removed from the plates.

Table 3.11 summarises the planar dimensions and the thicknesses of the four plates, the inner diameters of the supports, the volumes of the plates relative to the smallest scale size and the diameters of the impactors used in this study. Here, in order to keep

the volume fraction constant, all dimensions were scaled including the number of adhesive layers at each aluminium-composite interface in proportion to the scale factor (n).

Scale size (n)	Edge length of plate (mm)	Ply-level thickness (mm)	Circular support inner diameter (mm)	Sample volume (times)	Impactor diam. (mm)
¼	75	1.77	50	1	5
½	150	3.51	100	7.93	10
¾	225	5.45	150	27.71	15
1	300	7.03	200	63.54	20

Table 3.11. Dimensions of the four different scaled specimens for ply-level samples under low velocity impact testing.

3.6.2 Low Velocity Impact Tests on 3D Sublaminate-Level Scaled Specimens

The impact test response of sublaminate-level scaled samples was investigated in order to compare the scaling effects between this system and the ply-level technique. The basic stacking sequence of the sublaminate-level FMLs was [Al, 0°/90°]$_{ns}$ with n = ¼, ½, ¾ and 1.

The sublaminate-level scaled samples were manufactured by stacking together the required number of baseline laminates as shown in Figure 3.14. The baseline laminate consisted of two 0.5 mm thick aluminium sheets either side of two 0.3 mm thick SRPP core. After manufacture, square plates with edge lengths of 300n mm were removed from the panels.

A summary of the dimensions used for these tests are given in Table 3.12. Here, small differences in thickness of the corresponding ply-level and sublaminate-level scaled samples were observed. This was due to the incorporation of a 60 micron thick layer of polypropylene adhesive between the adjacent aluminium layers in the sublaminate-level scaled samples (note that the aluminium used in this scaling group was the same in all cases).

Scale size (n)	Square plates length (mm)	Sublam.-level thickness (mm)	Circular support inner diameter (mm)	Sample volume (times)	Impactor diam. (mm)
¼	75	1.77	50	1	5
½	150	3.62	100	7.93	10
¾	225	5.44	150	27.71	15
1	300	7.24	200	63.54	20

Table 3.12. Dimensions of the four different sublaminate-level scaled specimens for low velocity impact testing.

After testing, the samples were examined optically to identify any indentation damage on the front and distal surfaces of the targets. The samples were then cut in half through the impact zone using a band saw and polished for further internal examination.

3.7 References

1. Propex, *Curv Homepage*. http://www.curvonline.com, 2005.

2. N K Naik. *Woven Fabric Composites*, Technomic Publishing Company, 1994.

3. Collano, *Xiro Adhesives*. www.collano.com, 2006.

4. L F Mondolfo. *Aluminum Alloys; Structure and Properties*, Butterworth Heinemann, 1995.

5. R B Hilton. *Technology of Engineering Materials*, London; Butterworth Heinemann, 1953.

6. ISO EN 23878. *Hard metals-Vickers Hardness Test*. BSI, 1993.

7. G Reyes and W J Cantwell. *The Mechanical Properties of Fibre-Metal Laminates Based on Glass Fibre Reinforced Polypropylene*. Composites Science and Technology, 60; 1085-1094, 2000.

8. ASTM D3039. *Standard Test Method for Tensile Properties of Polymer Matrix Composite Materials*. Annual Book of ASTM Standards, 2000.

9. ASTM D790-80. *Flexural Properties of Plastics and Electrical Insulating Materials*. Annual Book of ASTM Standards, 1980.

10. H F Wu and L L Wu. *A Study of Tension Test Specimens of Laminated Hybrid Composites. Part II. Size and Alignment Effect*. Journal of Materials Science, 29; 5847-5851, 1994.

11. S Kellas and J Morton. *Scaling Effects in Angle-Ply Laminates*. NASA, CR-4423; 1992.

12. D P Johnson, J Morton, S Kellas, and K Jackson. *Scaling Effects in Sublaminate-Level Scaled Composites Laminates*. American Institute of Aeronautics and Astronautics, 36; 441-447, 1998.

13. H Hamada and Ramakrishna. *Scaling Effects in the Energy Absorption of Carbon-Fiber/PEEK Composite Tubes*. Composites Science and Technology, 55; 211-221, 1995.

14. D P Johnson, J Morton, S Kellas, and K Jackson. *Size Effects in Scaled Fiber Composites under Four-Point Flexure Loading*. American Institute of Aeronautics and Astronautics, 38; 1047-1054, 2000.

15. W Weibull. *A Statistical Distribution Function of Wide Applicability*. Journal of Applied Mechanics, 18; 293-297, 1951.

16. V Laws. *The Relationship between Tensile and Bending Properties of Non-Linear Composite Materials*. Journal of Materials Science, 17; 2919-2924, 1982.

17. J W Hitchon and D C Phillips. *The Effect of Specimen Size on the Strength of CFRP*. Composites, 9; 119-124, 1978.

18. A Tabiei and J Sun. *Analytical Simulation of Strength Size Effect in Composites Materials*. Composites: Part B, 31; 133-139, 2000.

19. A Towse, K Potter, M R Wisnom, and R D Adams. *Specimen Size Effects in the Tensile Failure Strain of an Epoxy Adhesive*. Journal of Materials Science, 33; 4307-4314, 1998.

20. M R Wisnom. *Size Effects in the Testing of Fibre-Composite Materials*. Composites Science and Technology, 59; 1937-1957, 1999.

21. M R Wisnom. *The Relationship between Tensile and Flexural Strength of Unidirectional Composites*. Journal of Composite Materials, 26; 1173-1180, 1992.

22. T A Duffey, M C Cheresh, and S H Sutherland. *Experimental Verification of Scaling Laws for Punch-Impact-Loaded Structures*. International Journal of Impact Engineering, 2; 103-117, 1984.

23. J N Goodier. *Dimensional Analysis*. In: Handbook of Experimental Stress Analysis, edited by M.Hetenyi, John Wiley and Sons, p. 1035-1045. 1950.

24. H M Wen and N Jones. *Experimental Investigation of the Scaling Law for Metal Plates Struck by Large Masses*. International Journal of Impact Engineering, 13; 485-505, 1993.

25. S McKown, W J Cantwell, and N Jones. *Investigation of Scaling Effects in Fiber-Metal Laminates*. Journal of Composite Materials, Article in Press, 2007.

26. M R Abdullah. *The High Velocity Impact Response of Novel Fibre-Metal Laminates*. University of Liverpool, Ph.D.Thesis, 2006.

CHAPTER IV. RESULTS AND DISCUSSIONS

This chapter presents the results obtained from the experimental work conducted in this study. Initially, the results from a comprehensive series of mechanical characterisation tests are presented, including indentation tests, tensile tests, flexural tests, impact tests and SCB tests.

The second part of this chapter investigates scaling effects in the FML materials, where tensile, flexural and impact tests were conducted based on the results of the mechanical characterisation study presented in the first part of this chapter. Here more detailed analyses are given and comparisons are made between the scaling techniques in order to clarify any scaling effects observed with increasing specimen size.

4.1 Mechanical Properties of the FMLs and their Constituents

The results of a series of mechanical tests are presented in this section. Results of indentation, tensile, flexural and low velocity impact tests are presented here. Additionally, interfacial fracture tests were carried out using the single cantilever beam (SCB) technique in order to identify the failure modes occurring at the composite/metal interface.

4.1.1 Indentation Tests on the Plain Aluminium Alloy Specimens

Indentation tests on the aluminium specimens were used in order to determine the hardness values of the various thicknesses of the scaled aluminium investigated here (¼, ½, ¾ and 1 corresponding to thicknesses of 0.5, 1.0, 1.6 and 2 mm respectively). These tests were undertaken in order to explain variations in the mechanical properties of the various aluminium alloys and to assist in any normalisation procedures that may be necessary. The results of these indentation tests are shown in Figure 4.1.

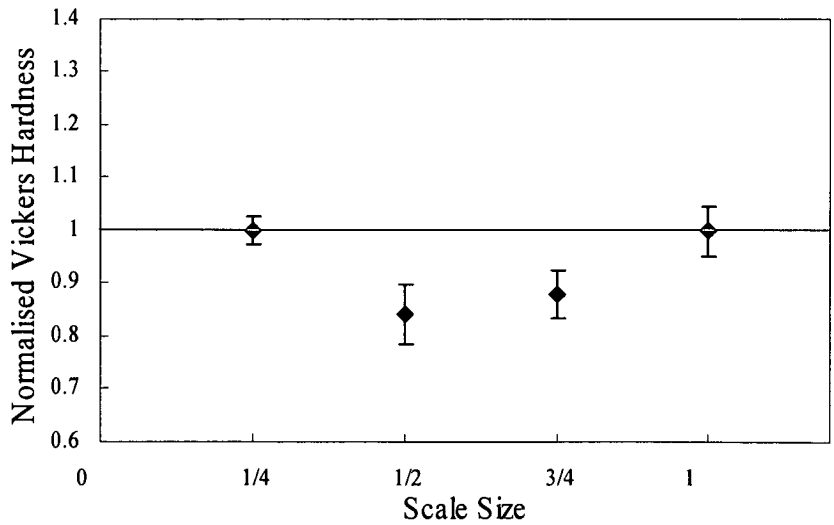

Figure 4.1. Normalised Vickers micro-hardness indentation data following tests on the plain aluminium alloys.

Vickers test results (explained in Section 3.1.3.1), show differences in hardness values relative to the thinnest aluminium sheet, with the indentation resistance for the ½ size being around 18% lower than the baseline, while no difference was observed for the thickest aluminium sheet. Clearly, these differences are quite significant and are likely

to reflect differences in the manufacturing techniques and resulting microstructure. It is believed that there is a direct correlation between the indentation force and tensile strength; therefore it is likely that these results can be related to those presented in the scaling study [**1,2**].

4.1.2 Tensile Test Results on the FMLs and their Constituents

Initially, a study of the constituent materials used to produce the FMLs was carried out to determine their strength, strain to failure and Young's modulus, in order to predict the mechanical properties of the FMLs. The average tensile properties of the aluminium alloy, the plain SRPP composite (in the 0°/90° and +/-45° directions), the polypropylene adhesive, the [Al, 0°/90°]$_s$ FML and the [Al, +/-45°]$_s$ FML are given in Table 4.1. All of these tests were undertaken according to the ASTM D3039 standard as explained in Section 3.3.1.

Material	Tensile Strength (MPa)	Strain to failure (mm/mm)	Tensile Modulus (GPa)
Aluminium	185	0.19	74
SRPP 0°/90°	135	0.22	4.5
SRPP +/- 45°	80	0.38	2.7
PP Adhesive	21	6.00	0.57
[Al, 0°/90°]$_s$	154	0.23	43.6
[Al, +/-45°]$_s$	131	0.27	42.8

Table 4.1. Tensile properties of the aluminium alloy, the SRPP, the PP adhesive and the FML specimens.

Figure 4.2 shows typical stress/strain curves for the plain aluminium alloy and the plain self-reinforced composite based on the same areal dimensions as those associated with the FML. Here, the stress/strain response of the [Al, 0°/90°]$_s$ FML is compared to those of its constituent materials, where it is evident that the response of the FML lies between that of the plain aluminium and the plain SRPP specimens. Clearly, the strain to failure of the FML is similar to that of the plain composite and greater than that of the plain aluminium alloy. This is a result of the high degree of bonding between the components, allowing the aluminium on the FML to deform by up to 25% more than its plain counterpart.

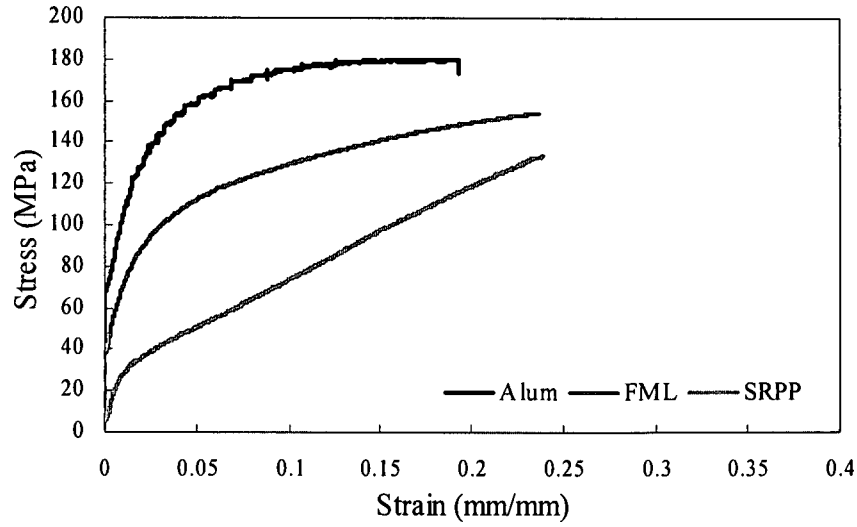

Figure 4.2. Comparison of stress-strain traces following tensile tests on the plain aluminium, the 0°/90° SRPP composite and the [Al, 0°/90°]$_s$ FML specimens.

Figure 4.3 presents the stress-strain curves for the [Al, +/-45°]$_s$ FML and its constituents, where it can be seen that the failure strain of the FML was roughly midway between the failure strains of its constituent materials, exhibiting a strain to failure that is approximately 45% greater than the [Al, 0°/90°]$_s$ FML.

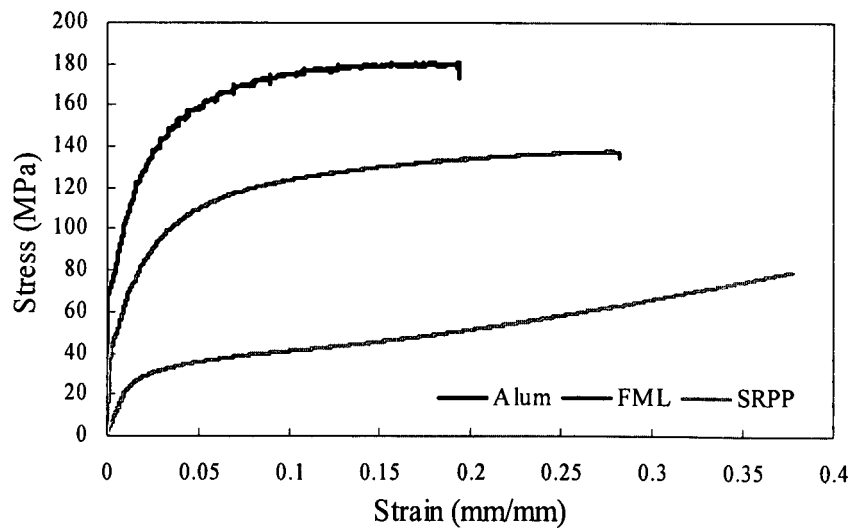

Figure 4.3. Comparison of stress-strain traces following tensile tests on the plain aluminium, the +/-45° SRPP composite and the [Al, +/-45°]$_s$ FML specimens.

It is interesting to note that an optical examination of the specimens during testing indicated that the composite plies in both types of FML failed before the aluminium layers. This is particularly surprising given that the failure strain of the plain +/-45° composite was almost double than that of the aluminium alloy. A comparison of stress-strain responses of the plain composites in Figure 4.3 shows that orienting the fibres at +/-45°, increases the strain to failure of the plain composite, whilst greatly reducing its load-bearing capacity. As a consequence, the [Al, 0°/90°]$_s$ laminate offers a higher strength and a lower strain to failure than the [Al, +/-45°]$_s$ system.

It is possible that the premature failure of the composite plies observed during the tests on the FML specimens resulted from the temperature and pressure excursions that the composite layers encountered during the FML processing cycle. To investigate this further, plain composite panels were subjected to the same processing cycle as that experienced by the FML during manufacture. Specimens were cut from the panels and tested in tension under the same conditions, where a reduction in strain relative to the as-received samples was recorded. This will be investigated further in the next section.

An additional explanation for the premature failure of the composite layers in the FMLs, is the presence of planes of delamination that developed along the edges of the laminates during the tensile test. This delamination process is associated with out-of-plane curving of the outer aluminium layer during the tensile test. This process leads to delamination between the composite plies within the FML, precipitating fibre damage and stress concentrations within the composite layers, mechanisms that may ultimately lead to localised failure of the reinforcing fibres.

4.1.2.1 Thermal Annealing of the SRPP Composite

SRPP specimens with dimensions equivalent to those of the FML specimens were removed from panels that had been subjected to the same lamination conditions as the FMLs. This was undertaken in order to determine if the lamination conditions modified the properties of the as-received composite. Plain, as-received composite specimens and annealed samples were tested in tension under the same test conditions. The data from these tests indicated that whereas the failure stress decreased by only two percent, the strain at failure decreased by 10.8%, suggesting that the FML

processing cycle degrades the performance of the composite plies in these layered materials.

Figure 4.4 shows a comparison of the annealed SRPP and the as-received SRPP composite. Here, two main differences in the stress-strain behaviour of these two materials can be observed. The first, is the reduction in failure strain when the material is annealed, a possible result of the smaller consolidation pressure (7 bars) used here compared to the value used when producing the composite (40 bars). The second difference is a slope reduction after reaching the yield point (see Figure 4.4). This is also, a possible consequence of the reduction in pressure during the consolidation process, which generated a relaxation response in the laminae of the material (each composite laminate sheet received from the supplier consisted of several laminae).

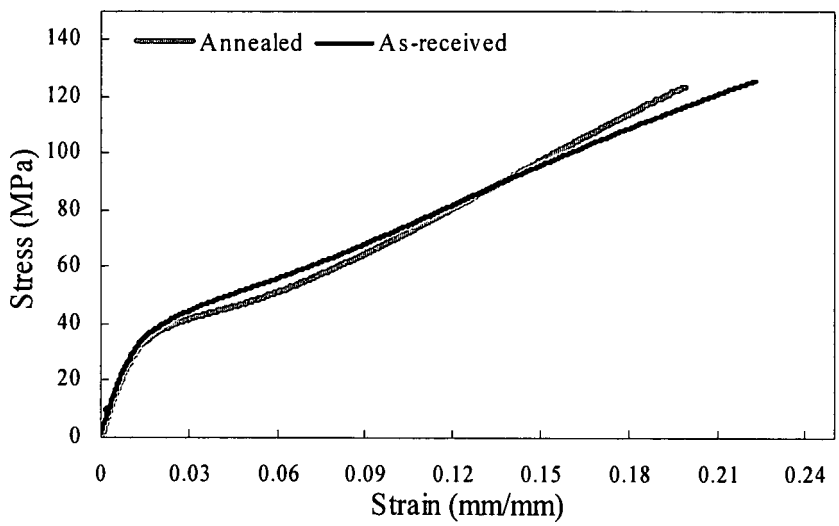

Figure 4.4. Comparison of tensile stress-strain response of the SRPP specimens following annealing and in their as-received condition.

It is possible that the annealing process resulted in relaxation of the highly aligned strands in the composite, reducing the degree of compaction, an effect that is shown in Figure 4.5a, where loose fibre strands are in evidence. This is not the case with the as-received composite shown in Figure 4.5b.

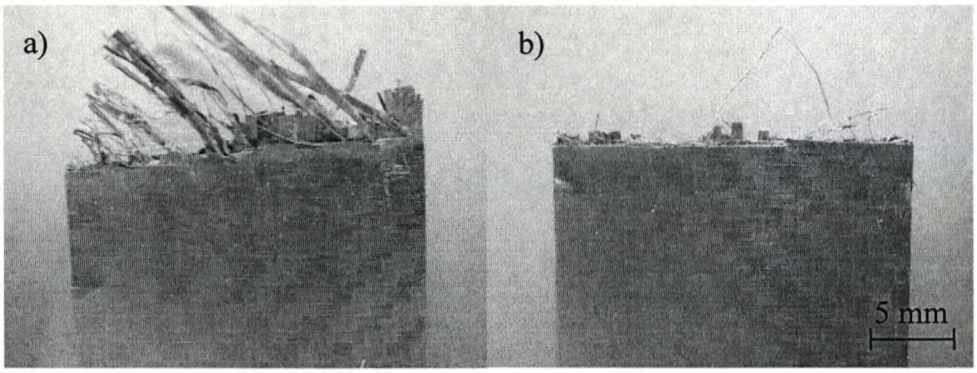

Figure 4.5. Comparison of tensile SRPP specimens a) the annealed sample and b) the as-received sample.

4.1.2.2 Optical Examination of the FMLs and their Constituents

Figure 4.6 shows an aluminium specimen following a tensile test. The rolling direction of the alloy was aligned in the test direction at all times. It is clear that the specimen failed at approximately 65° to the loading direction, being consistent in all of the aluminium specimens. This tendency is related to the way that the aluminium crystals in the microstructure dislocates, which is relative to the slip plane and the slip direction of a single crystal [**3,4**], as explained in Appendix I. It is interesting to note that during the tests, dislocation lines at the same angle of the fracture (left angle) and opposite to the angle (right angle) propagated simultaneously, an effect that was visible by eye.

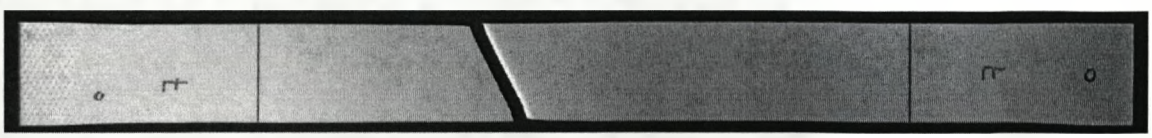

Figure 4.6. Typical failure mode in an aluminium specimen following a tensile test.

Failed 0°/90° and +/-45° SRPP composite specimens tested in tension are shown in Figure 4.7. Clear differences in the failure mode are apparent, with the fracture mode being defined by the fibre orientation. A significant increase in strain was observed in the +/-45° SRPP specimens, with the strain to failure values being approximately 70% greater than that offered by its 0°/90° counterpart. The high deformation associated with the +/-45° sample is clearly evident in Figure 4.7 (lower specimen), where an appreciable reduction in specimen width is evident. This is due to the +/-45° fibres tending to align in the loading direction during the test.

Figure 4.7. Comparison of a 0°/90° SRPP (top) and a +/-45° SRPP (bottom) specimen following tensile testing.

An examination of the failed [Al, 0°/90°]$_s$ and [Al, +/-45°]$_s$ FML specimens in Figure 4.8a highlights the presence of large cracks extending across the aluminium outer layers at approximately 70° and 60° to the applied load respectively, angles that varied due to the influence of the fibre orientation (0°/90° SRPP and +/-45° SRPP respectively). There were also other visible differences in the way that the specimens failed. The [Al, 0°/90°]$_s$ specimens exhibited extensive debonding between the composite plies along the entire length of the specimen (see Figure 4.8ai). In contrast, fracture in the [Al, +/-45°]$_s$ specimens was more localised, showing little debonding or delamination, effects caused by the +/-45° composite fibres tending to align in the loading direction.

Figure 4.8b shows the rear surfaces of both specimens, showing that the [Al, 0°/90°]$_s$ FML (Figure 4.8bi) exhibited a similar fracture angle to that of the front surface (Figure 4.8ai), while for the [Al, +/-45°]$_s$ FML, the aluminium surface did not fail, generating a ridge in the centre of the specimen (Figure 4.8bii) with the edges closing due to the composite tending to contract in the transverse direction, leading to a

reduction in the specimen width during the test, forcing the aluminium to curve along its edges.

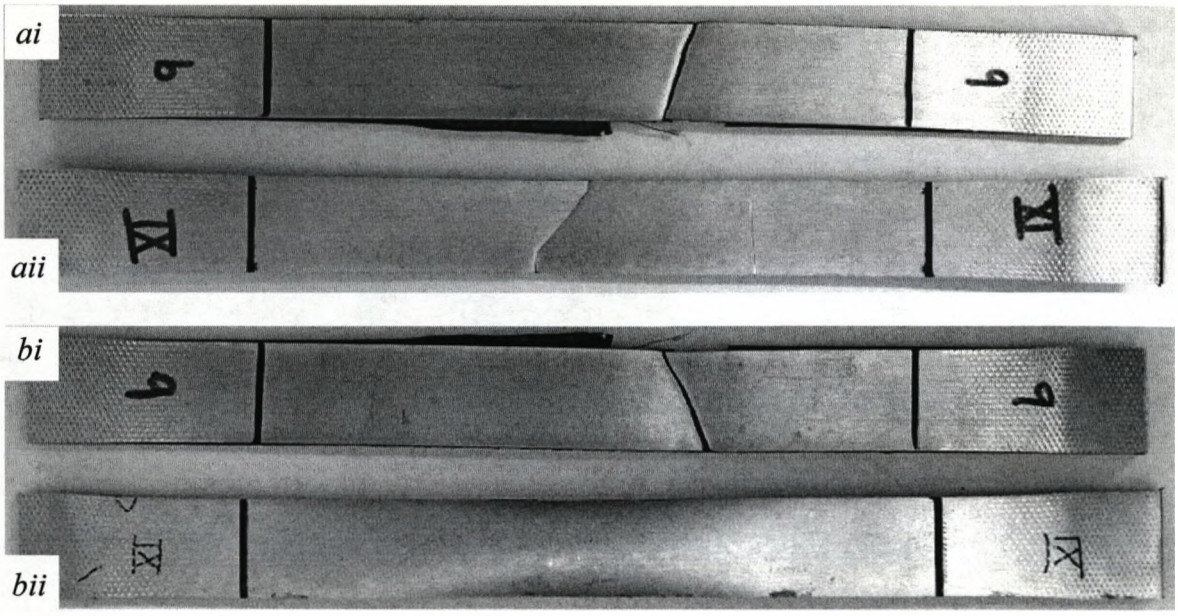

Figure 4.8. Comparison of FML specimens following tensile testing; ai) front surface of the [Al, 0°/90°]$_s$ aii) front surface of the [Al, +/-45°]$_s$ bi) rear surface of the [Al, 0°/90°]$_s$ and bii) rear surface of the [Al, +/-45°]$_s$.

4.1.3 Flexural Test Results

Two stacking sequences were considered in order to investigate the flexural response of FMLs, these being [Al, 0°/90°]$_s$ and [Al, +/-45°]$_s$. In addition, aluminium specimens were also tested; however the composite material could not be tested in flexure, due to its high flexibility. After testing, the specimens were removed from the test machine for subsequent optical and microscopic inspection in order to determine the prevailing failure modes.

4.1.3.1 Flexural Tests on the FML Specimens

Flexural tests on the FML specimens were undertaken based on two stacking sequences, these being [Al, 0°/90°]$_s$ and [Al, +/-45°]$_s$. Figure 4.9 shows typical stress/strain curves following tests on these configurations at a strain rate of 0.01min^{-1}. Details of the specimen dimensions are given in Table 3.3. The figure shows that the

flexural strength for both FML configurations is approximately 160 MPa. It is worth nothing that the tensile strength of the [Al, 0°/90°]$_s$ FML was approximately 150 MPa while for the [Al, +/-45°]$_s$ FML was approximately 130 MPa. Generally, the flexural strength of a material is higher than its tensile strength. This is explained by the fact that during a tensile test, the whole specimen is subjected to a constant stress while in flexure; a relatively small region of the specimen is subjected to the maximum stress, reducing the likelihood of failure in the sample [**5**].

The stress/strain behaviour for both arrangements is very similar, highlighting the strong influence of the aluminium which minimised the fibre orientation effect in bending. The average values of maximum stress and strain for the [Al, 0°/90°]$_s$ FML were 163 MPa and 0.0193 mm/mm respectively. The change in fibre orientation in the FMLs from 0°/90° to +/-45° did not make any significant difference to the mechanical properties; this is in contrast to the observations recorded in the tensile study (see Figures 4.2 and 4.3).

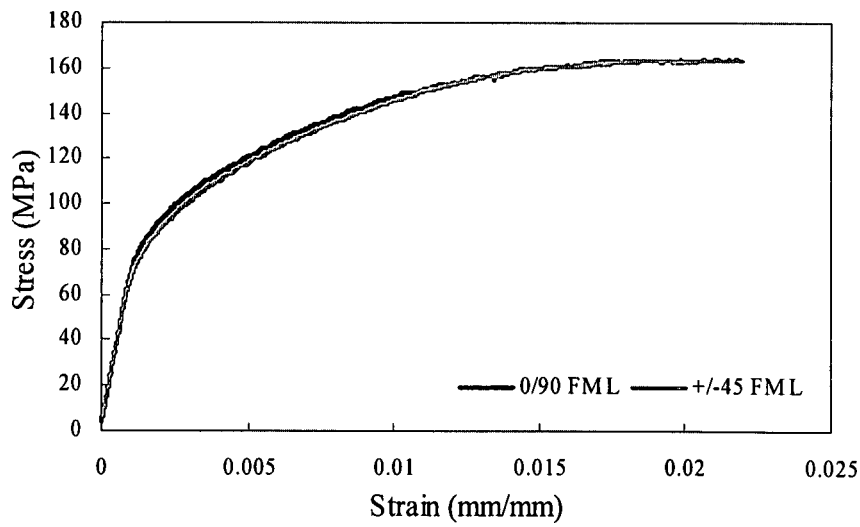

Figure 4.9. Typical stress-strain traces for the [Al, 0°/90°]$_s$ FML and the [Al, +/-45°]$_s$ FML following flexural testing.

For the case of the [Al, +/-45°]$_s$ FML, the average value of the failure stress was 164 MPa and the failure strain was 0.0188 mm/mm. The strain values reported here were obtained from strain gauges bonded to the lower surface of the samples. The values were compared to those obtained from the crosshead displacement of the Instron machine which yielded very similar data. As can be seen in the figure, at approximately 160 MPa the stress reaches a plateau. Following testing, the specimens were then unloaded for a subsequent optical analysis.

4.1.3.2 Optical Examination of the Flexural FML Specimens

Figure 4.10 shows [Al, 0°/90°]$_s$ FML specimens following testing in four point bending. Here, the specimens have not failed after reaching the maximum load. A closer examination shows that the constituents (i.e., the aluminium and the SRPP) remained well bonded.

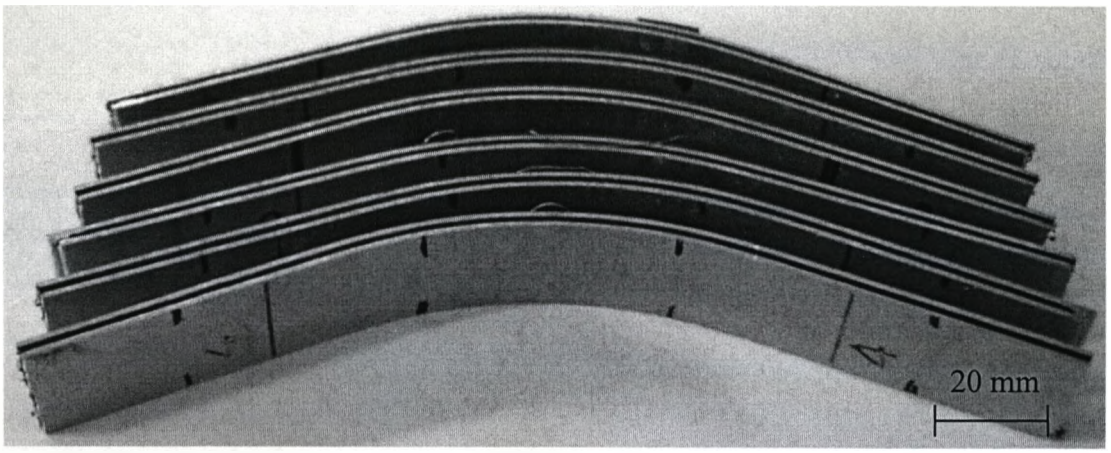

Figure 4.10. Photograph of the [Al, 0°/90°]$_s$ FMLs following flexural testing.

After flexural testing, the [Al, +/-45°]$_s$ FML specimens were examined by eye to identify the deformation and failure modes (see Figure 4.11). Here, none of the specimens exhibited any visible fracture, instead, they showed considerable out-of-plane deformation without apparent damage. This was also the case for the [Al, 0°/90°]$_s$ FML specimens. To investigate this further, a number of specimens were sectioned across their centres and polished in order to undertake a more detailed microscopic observation.

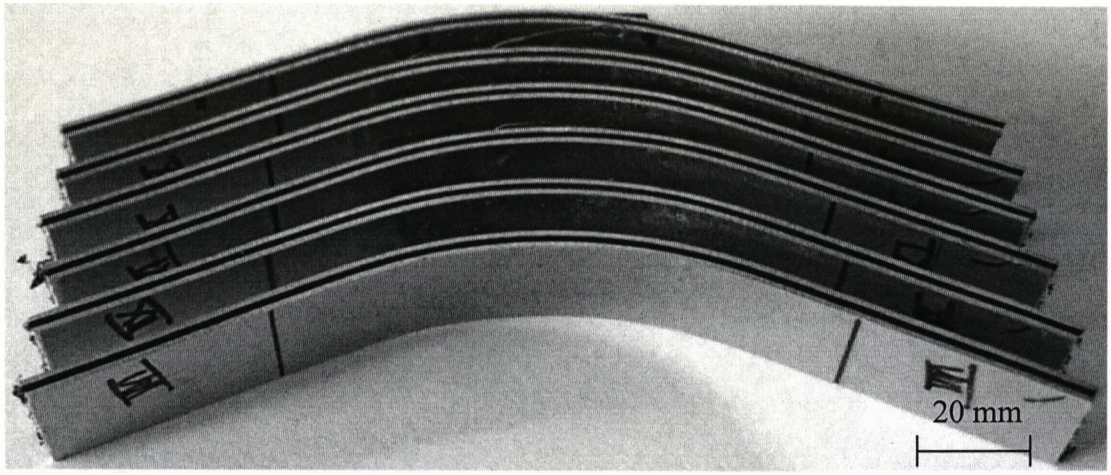

Figure 4.11. Photograph of the [Al, +/-45°]$_s$ FMLs following flexural testing.

Figure 4.12 shows the cross-section of an [Al, 0°/90°]$_s$ FML sample loaded in flexure, where it is evident that the composite laminae are undamaged throughout the volume of the sample. Closer inspection highlights the lack of any delamination at the composite/metal interface, where it is clear that none of the constituents in the FML had failed during testing. Similar observations were made in the [Al, +/-45°]$_s$ FML specimens.

Further studies on this FML have been undertaken by Mosse *et al.* [**6**] and Gresham *et al.* [**7**], where stamp forming was undertaken. These researchers identified the parameters and conditions where the FML can be successfully manufactured, suggesting that this type of material posses superior forming characteristics than monolithic aluminium alloys.

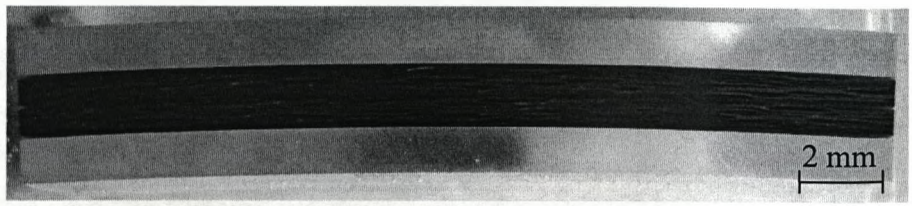

Figure 4.12. Cross-section of an [Al, 0°/90°]$_s$ FML following flexural testing.

4.1.4 SCB Test Results

A series of mixed-mode interlaminar fracture tests were performed using the single cantilever beam technique (SCB) in order to determine the interfacial fracture properties of the fibre-metal laminate. During each test (six in total), the load and displacement were recorded and crack propagation was monitored by eye (see Section 3.3.3).

Figure 4.13 shows a typical load-displacement curve following a SCB test on an aluminium/SRPP specimen tested at 2 mm/min. The initial loading curve exhibits some non-linear response, which may be associated with the elasticity in the composite adherends at the inserted crack tip [**8**]. An examination of the curve highlights a saw-tooth appearance associated with unstable crack propagation. Subsequent unloading of the sample resulted in an appreciable residual displacement in the load-displacement curve, an effect that was probably a consequence of some form of permanent plastic deformation in the composite material [**9**].

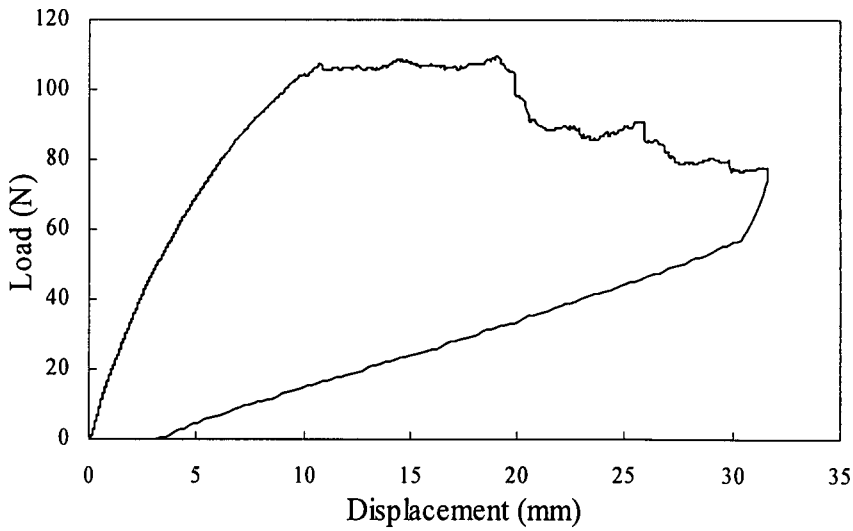

Figure 4.13. Typical load-displacement curve following a SCB test on an aluminium/SRPP specimen at 2 mm/min.

Closer examination of the specimens showed that fracture occurred between the SRPP laminae rather than at the composite/metal interface or the adhesive, suggesting that the latter is tougher than the interface between the laminae within the composite

laminate. This unexpected intralaminar mode of fracture within the composite may be a consequence of the reduction in processing pressure during laminate consolidation, affecting the composite properties and reducing the level of adhesion between the laminae. A lamination pressure of 7 bars was used here whereas the original industrial process involved a pressure of 40 bars. The use of a lower pressure was due to the limitation of the hot press used in this study.

Figure 4.14 shows a typical plot of specimen compliance vs. the cube of crack length for an aluminium/SRPP SCB specimen loaded at 2 mm/min. From the figure, it is apparent that the data lie on a reasonably straight line. A linear fit to the data yields a value for the constant (e) of 0.52. Introducing this constant (e) into Equation 3.13 yields the fracture energy of this system.

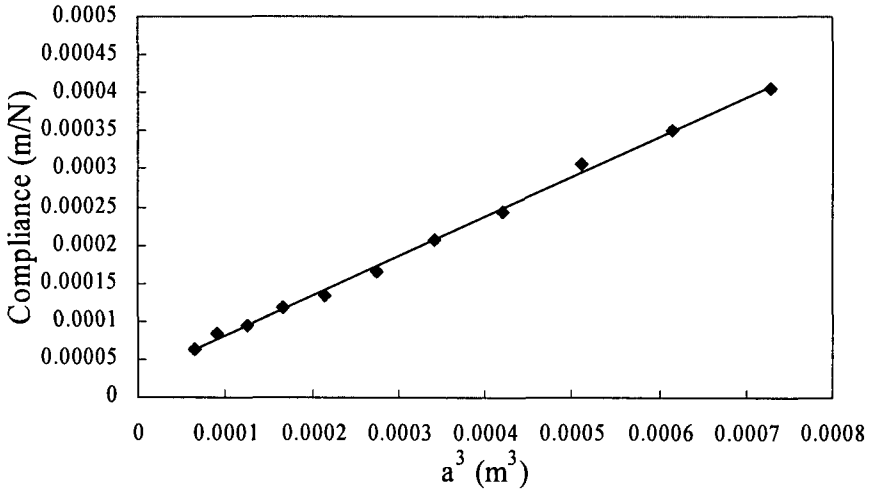

Figure 4.14. Typical plot of compliance versus the cube of crack length (a^3) following a SCB test on an aluminium/SRPP specimen.

The mixed-mode interlaminar fracture energy was then determined using Equation 3.13. Figure 4.15 shows a typical resistance curve for a SCB specimen. From the figure, it can be seen that the fracture energy rises continuously until it reaches a plateau value of approximately 1900 J/m^2. The initial part of the curve is associated with the development of extensive fibre bridging in the wake of the crack.

Specimens prepared with different processing pressures were tested. Following these tests, a direct relationship between the fracture energy and the pressure applied during the lamination process was observed. Specimens with a processing pressure of 9 bars offered a fracture energy of approximately 2200 J/m^2. This highlights the sensitivity of this system to manufacturing pressure suggesting that caution must be exercised during the preparation of FMLs, especially when a scaling study is being undertaken.

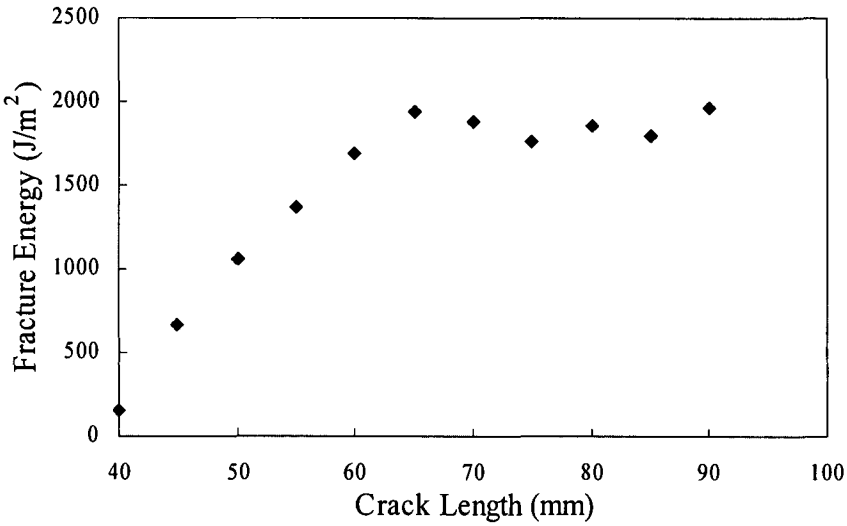

Figure 4.15. Typical resistance plot following a SCB test at 2 mm/min on an aluminium/SRPP specimen.

Figure 4.16 shows an *in-situ* SCB test, from where it is clear that crack propagation occurs between the composite laminae as opposed to the adhesive interlayer, which appears to be tougher than the intralaminar composite. These results can be used to clarify the failure behaviour of the FMLs in tension, flexure and during impact loading.

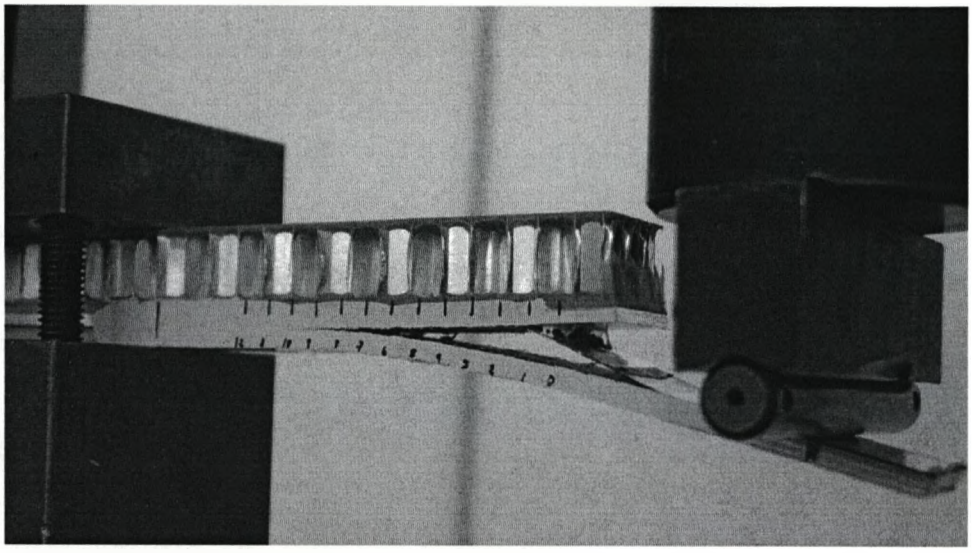

Figure 4.16. Photograph of an aluminium/SRPP SCB test.

4.1.5 Impact Test Results on FML Specimens

Initially, the dynamic properties of the fibre-metal laminates were investigated in order to evaluate the effects of varying impact energy on the development of damage in the hybrid materials.

Figure 4.17 presents a typical force-time history recorded by the piezo-electric load-cell during an impact test in which the target was perforated. Here, the load-cell data exhibits limited ringing following initial contact between the impactor and the test specimen. The impact force subsequently increased until it reached a maximum value of approximately 2.3 kN as can be seen in the figure, at which point damage initiated within the specimen and the load dropped rapidly.

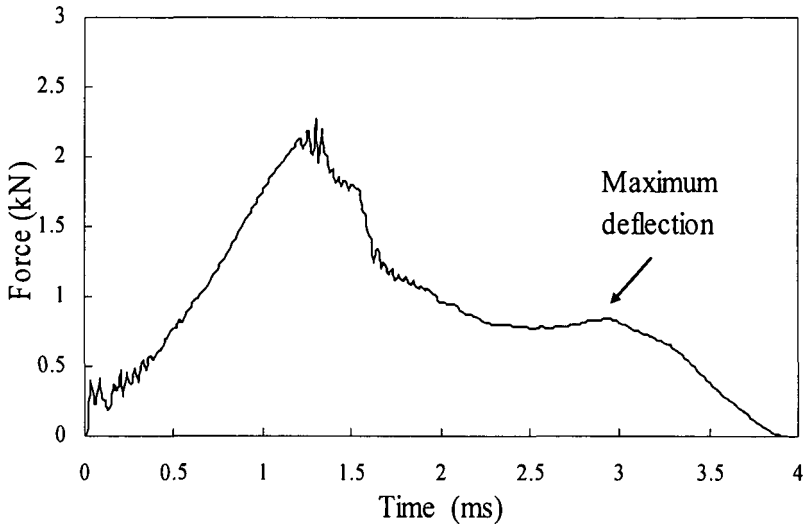

Figure 4.17. Typical load versus time trace following an impact test on a simply supported plate. Here, the impact mass was 0.6 kg. The drop height was 1.5 m giving an impact energy of 8.1 Joules.

The velocity-time trace obtained from the laser-Doppler in Figure 4.18, indicates that the initial velocity of the impactor was approximately 5.2 m/s. Upon initial contact, the velocity of the impactor starts to decrease, reaching a value of approximately 2.5 m/s at the maximum force in the force-time trace (see Figure 4.17). The velocity of the impactor reaches zero after approximately 2.8 ms, corresponding to the maximum deflection of the FML target. Beyond this point, the velocity becomes negative, indicating that the impactor is rebounding.

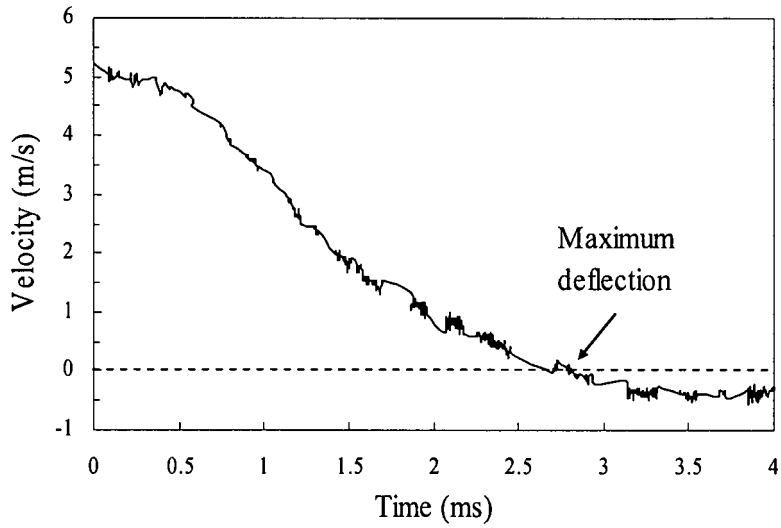

Figure 4.18. Typical velocity versus time trace obtained from the laser-Doppler following impact testing on a simply supported plate at an impact energy of 8.1 Joules.

Combining the data from the load-cell (Figure 4.17) and the laser-Doppler (Figure 4.18), yields force-displacement curve shown in Figure 4.19. Clearly, the force returns to zero at a displacement greater than 6 mm, indicating that the impact event results in considerable plastic deformation in the target.

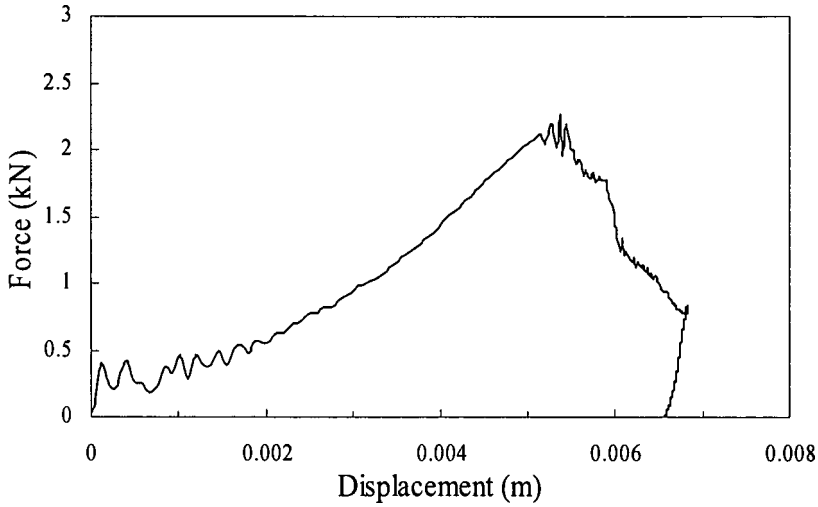

Figure 4.19. Typical load-displacement curve following a low velocity impact test on a FML.

Low magnification optical microscopy was used in order to highlight the failure modes in the fibre-metal laminates subjected to low velocity impact loading. Figure 4.20i shows the polished cross-sectioned of an FML specimen subjected to an impact energy of 4.7 Joules. Here, damage in the specimen subjected to the lowest impact energy takes the form of denting around the point of impact and slight thinning of the aluminium layer immediately under the impact location. No delamination or fracture was apparent in the composite layer in this specimen.

Increasing the impact energy to 6.3 Joules (see Figure 4.20ii) provoked a fracture in the lowest aluminium layer and significant thinning of this metal layer. Here, the composite layer has also fractured whilst the uppermost aluminium layer remains intact. An impact energy of 7.3 Joules (see Figure 4.20iii) resulted in localised fracture through the thickness of the FML. Closer inspection of the cross-sectioned plate indicates that the composite-metal interface has not debonded suggesting that there is a high degree of adhesion across this critical interface. Finally, the laminate was

perforated following an impact energy of 8.1 Joules (Figure 4.20iv), where localised fracture of the metal and composite plies is apparent.

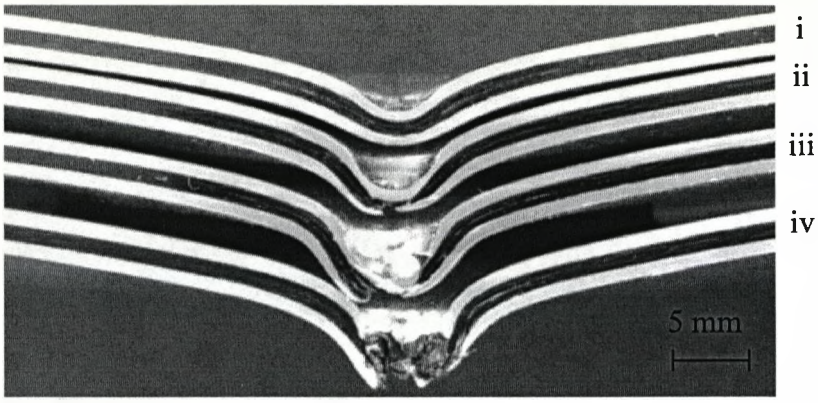

Figure 4.20. Cross-sections of four scaled specimens impacted at energies of 4.7, 6.3, 7.3 and 8.1 Joules (top to bottom).

4.2 Scaling Effects in the Tensile Properties of the FMLs and their Constituents

This part of the investigation focuses on the feasibility of using scale models to predict the full-scale behaviour of laminates based on $[Al_n, 0°/90°_n]_s$ and $[Al_n, +/-45°_n]_s$ stacking configurations with n = ¼, ½, ¾ and 1. Tensile tests were undertaken on laminates that were prepared using three different scaling approaches, these being 1D (scaling the thickness dimension), 2D (scaling the in-plane dimensions) and 3D scaling, where all of the dimensions (thickness, width and length) were scaled appropriately as explained in Section 3.4. The 1D and 2D approaches were applied to the $[Al_n, 0°/90°_n]_s$ configuration, while the 3D approach was applied to laminates with two fibre orientations, these being $[Al_n, 0°/90°_n]_s$ and $[Al_n, +/-45°_n]_s$ configurations. Here, geometrical effects were investigated by monitoring the stiffness, strength, strain to failure and the stress/strain response of the FML configurations.

To date, no attempt has been made to study scaling effects in FMLs, therefore, there is a need to know and understand the factors that are responsible for such effects in this type of material. The majority of scaling studies have focused on composite materials such as carbon/epoxy and glass/epoxy systems [**10,11**], reinforced concrete structures [**12,13**] and metals such as steel and aluminium [**14,15**].

4.2.1 Width/Thickness Ratio of the 1D, 2D and 3D Scaled Specimens

This part of the study investigates the effect of changes in the width and thickness dimensions of the samples, to highlight the influence of these parameters in the 1D, 2D and 3D scaling studies. Figure 4.21 shows a comparison of the three configurations used in this study, where it is clear that the highest w/t ratio is associated with the 2D scaled samples, with values of approximately 300% being recorded in the full-scale sized samples. The w/t should be constant in the 3D scaled samples. However, a slight variation in the ¾ scale is observed in this configuration, due to the fact that it was not possible to scale the aluminium correctly (it was 6.7% greater than the desired value). Therefore, the ¾ scale value of w/t was slightly lower than the ¼ scale size. 1D scaling results in a decrease in the w/t ratio with increasing scale size, with there being a 75% decrease in the value for the full-scale size compared to the baseline (¼ scale size).

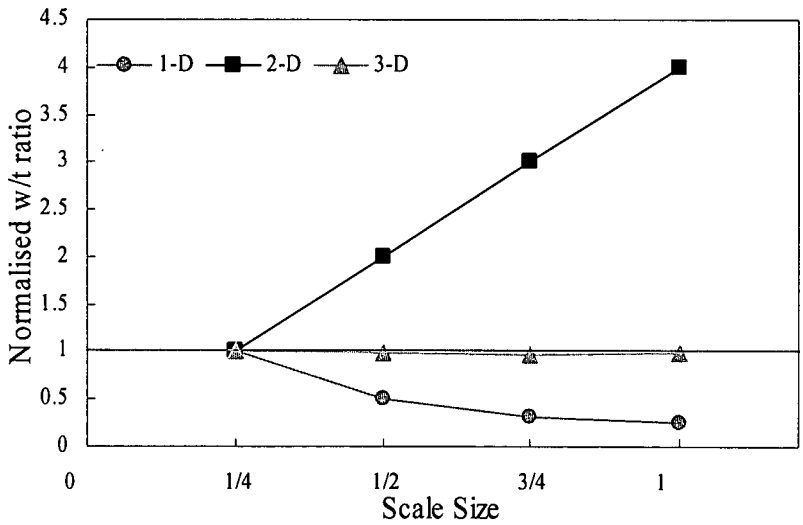

Figure 4.21. Normalise w/t ratio vs. scale size for the three scaling configurations; 1D, 2D and 3D.

A summary of the width and thickness values associated with the ply-level scaled FMLs is presented in Table 4.2. As can be seen, variations in the ¾ scaled specimens (for 1D and 3D scaling), provoked by the aluminium thickness, could not be avoided due to restrictions in the dimensions of sheets available (a thickness of 1.6 mm was used instead of 1.5 mm). Clearly, it was not possible to scale the materials at a microstructural level. Ideally, scaling the composite prototype should include scaling

the microstructure; that is, the fibre diameter should be scaled to keep it in proportion to the weave dimensions and the lamina thickness. Clearly, this is impossible from practical point of view. Even dealing with metallic structures, scaling the microstructure is generally not feasible.

Scale size	1D scaling		2D scaling		3D scaling	
	thickness	width	thickness	width	thickness	Width
¼	1.78	30	3.58	10	1.78	10
½	3.58	30	3.58	20	3.58	20
¾	5.54	30	3.58	30	5.54	30
1	7.18	30	3.58	40	7.18	40

Table 4.2. Summary of dimensions of the 1D, 2D and 3D ply-level scaled specimens.

Composites differ from metals in that they exhibit a number of different damage mechanisms, including fibre fracture, delamination and matrix cracking. All develop at a microscopic scale and eventually interact at a macroscopic laminate level [**16**].

4.2.2 Tensile Tests on 1D Ply-Level Scaled Specimens

Initially, size effects in the FMLs were investigated through a study in which the thickness of the $[Al_n, 0°/90°_n]_s$ laminates was scaled for fixed specimen width and length dimensions of 30 and 150 mm respectively, as shown schematically in Figure 3.15. Figure 4.22 shows the strength data for the four scaled thicknesses of FML. Included in the figure are the corresponding strengths of the four thicknesses of aluminium and plain composite. From the figure, it is clear that the strength of the ¼, ½ and ¾ scaled specimens increases with increasing scale size, before reducing in the largest specimen size. The most significant thickness effect was observed in the plain composite specimens, where the strength of the ¾ specimen was approximately thirty-five percent greater than that of the ¼ scale specimen.

The tensile strength data for the plain aluminium alloy also exhibits some significant variation over the range of scale sizes selected here, with the average tensile strength of the ¾ size specimen being approximately fifteen percent greater than that of the largest specimen. It is believed that these differences are due to variations in the properties of the alloy rather than a true scaling effect. Unfortunately, the aluminium alloys investigated here were supplied by different companies, suggesting that small

differences in manufacturing procedures, and therefore microstructures, may have impacted the mechanical properties of these alloys.

The same scaling effect as that observed in the plain aluminium specimens was apparent in the FMLs as a result of the influence of the aluminium in the FMLs. Here, the tensile strength of the ¾ size was 168 MPa while the strength of the smallest specimens averaged 153 MPa. In order to remove the effect of variations in the properties of the aluminium, it was necessary to present the data in a non-dimensional form. These normalised results are presented in the following section.

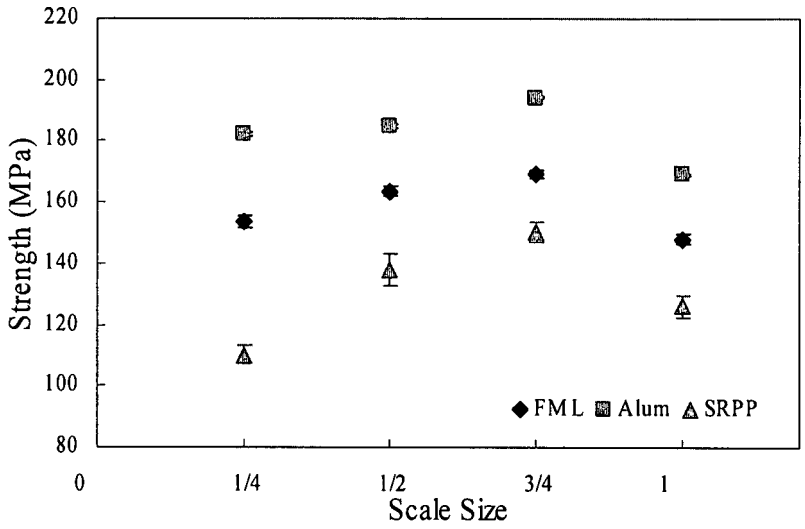

Figure 4.22. Average values of tensile strength for the FMLs and their constituent materials scaled at a 1D ply-level. The data correspond to the 0°/90° SRPP, the plain aluminium alloy and the $[Al_n, 0°/90°_n]_s$ *FML.*

The failure strain data for the 1D scaled SRPP specimens show similar results with increasing scale size, with no clear trend in the strain to failure being in evidence. The average value of strain was approximately 21% in all scaled sizes as shown in Figure 4.23. The strain to failure in the FML and aluminium alloy exhibit a similar response to that exhibited by the composite material.

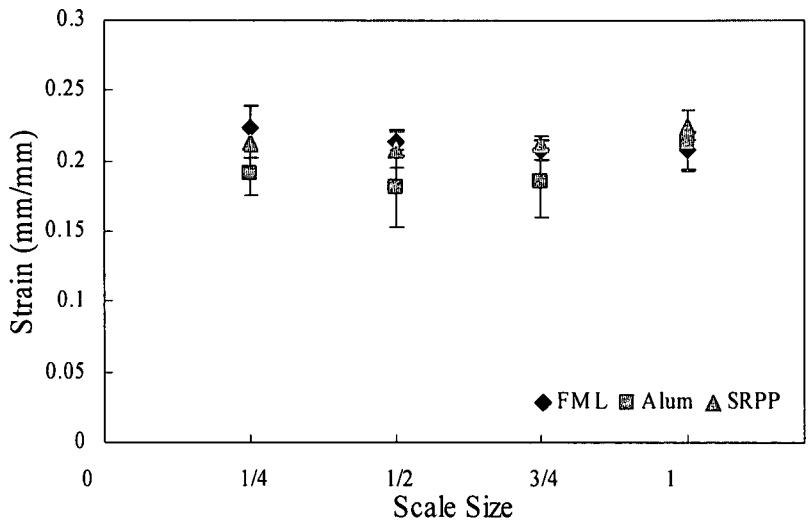

Figure 4.23. Average values of failure strain for the FMLs and their constituent materials scaled at a 1D ply-level. The data correspond to the 0°/90° SRPP, the plain aluminium alloy and the $[Al_n, 0°/90°_n]_s$ FML.

4.2.2.1 Normalisation of 1D Ply-Level Tensile Data

Figure 4.24 shows the normalised strength data for the 1D ply-level scaled FML specimens. Here, normalisation was undertaken using Equation 3.19, from which non-dimensional values were obtained, as follows:

$$\frac{\sigma_{FML}}{\sigma_{Al}V_{f_{Al}} + \sigma_{SRPP}V_{f_{SRPP}} + \sigma_{Ad}V_{f_{Ad}}}$$

The resulting normalised strength data, shown in Figure 4.24, show a tendency to decrease with increasing scale size, a trend that was not clear before the elimination of the differences in the aluminium by the normalisation process (see Figure 4.22).

An inspection of the normalised data indicates that the value corresponding to the full-size specimens is approximately five percent lower than the ¼ scale specimens, variations that can be attributed to small differences in manufacture. Another explanation for the fact that the FMLs show a tendency to fail at lower strength values with increasing the scale size is due to a change in failure mode observed in the different tested samples [**17**].

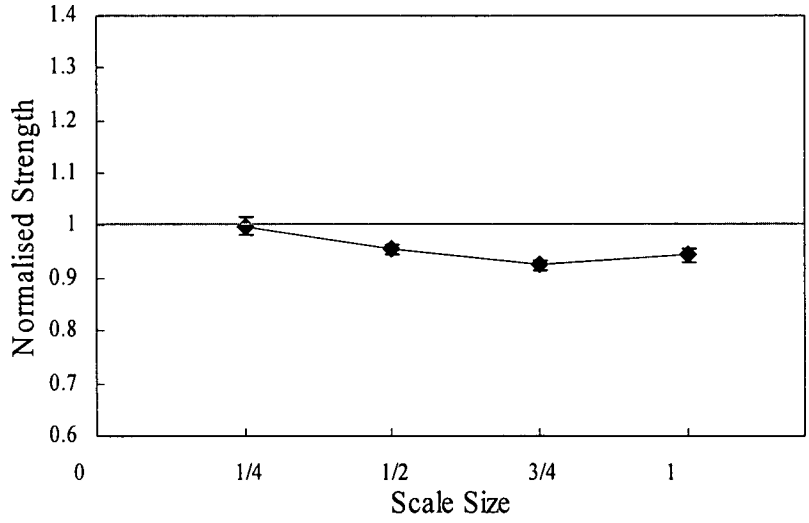

Figure 4.24. Normalised tensile strength for the 1D scaled [Al_n, 0°/90°$_n$]$_s$ FMLs following tensile testing.

Figure 4.25 shows the normalised strain data (normalised with respect to the ¼ value) following 1D scaling tests on the FMLs. It is clear that the strain to failure of these $[Al_n, 0°/90°_n]_s$ FMLs decreases slightly as the scale size increases. The trends are similar to those observed in the normalised strength data, with the failure strain of the full scale size being approximately 6% lower than the baseline value. It is also encouraging to note that there is very little scatter in the experimental data for these 1D-scaled specimens.

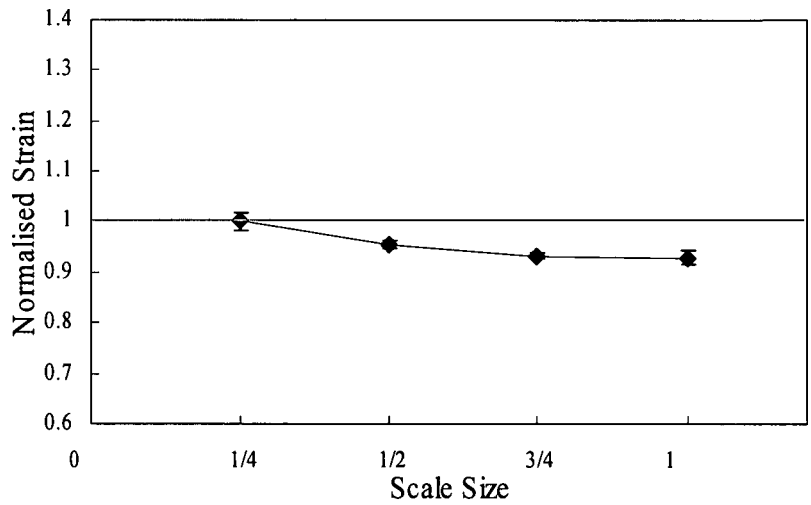

Figure 4.25. Normalised failure strain for the 1D scaled $[Al_n, 0°/90°_n]_s$ FMLs following tensile testing.

Variations in specimen thicknesses (with fixed in-plane dimensions) to those presented in 1-D scaling, show a small tendency to decrease with increasing specimen size as shown in Figures 4.24 and 4.25. This is although for a limited range of scale sizes, with the larger prototype samples being four times thicker than the ¼ scale. A more significant decrease in properties would be expected for even larger specimens as the reduction in strength and strain properties reduce steadily with scale size.

4.2.2.2 Optical Examination of the 1D Ply-Level Tensile Specimens

After failure, the scaled specimens were examined optically in order to elucidate the failure modes following tensile loading. Fracture in all of the plain aluminium alloy samples occurred at an angle of approximately 65° to the loading direction. A closer inspection of the specimens highlighted a distinct textural difference between the four

groups of specimens. The front and rear surfaces of ¼ and ½ scale specimens exhibited a smooth appearance whereas the surfaces of the ¾ and full-scale specimens displayed a more textured appearance associated with a slight surface roughening as shown in Figure 4.26.

It was difficult to determine if this effect was due to the increase in thickness of the scaled specimens or an intrinsic material property associated with the particular microstructure. Indentation tests revealed that the hardness values of the four metals were different (see Figure 4.1), with the ¼ and full-scale sizes offering the same hardness values while the ½ size exhibited a decrease of approximately 18% relative to the baseline (¼ scale) value.

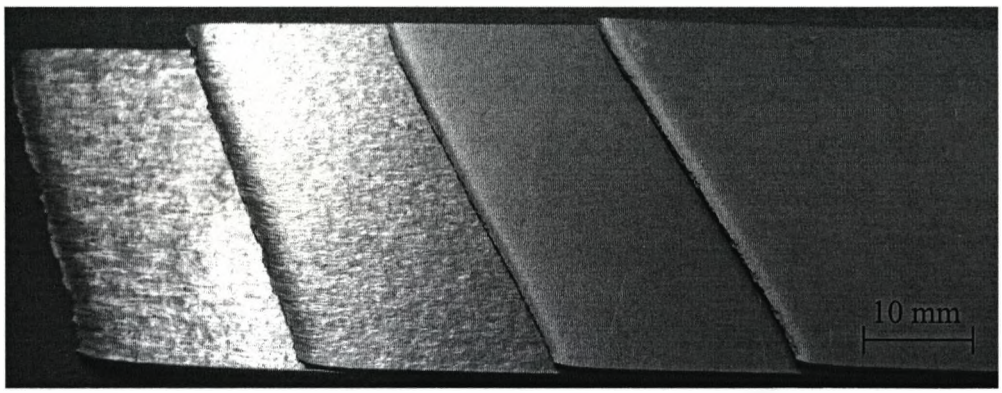

Figure 4.26. Photograph showing the four scaled aluminium coupons following tensile testing. From right to left, thicknesses of 0.5, 1.0, 1.6 and 2 mm.

A similar post-failure examination was undertaken on the four thicknesses of composite material (Figure 4.27). Here, all of the specimens fractured at 90° to the applied loading direction along the fibre direction. A closer inspection of the failed specimens highlighted the presence of a number of transverse secondary cracks in the thinnest specimen that had initiated along the edges of the sample. This suggests that the reduction in thickness makes the specimen more sensitive to the presence of defects, reducing its load-bearing capability as shown in Figure 4.22. Additionally, the thinnest composite specimens who consist of two fabric layers displayed a distinctly wavy appearance along their length, whereas the thicker specimens (eight fabric layers) were generally flat.

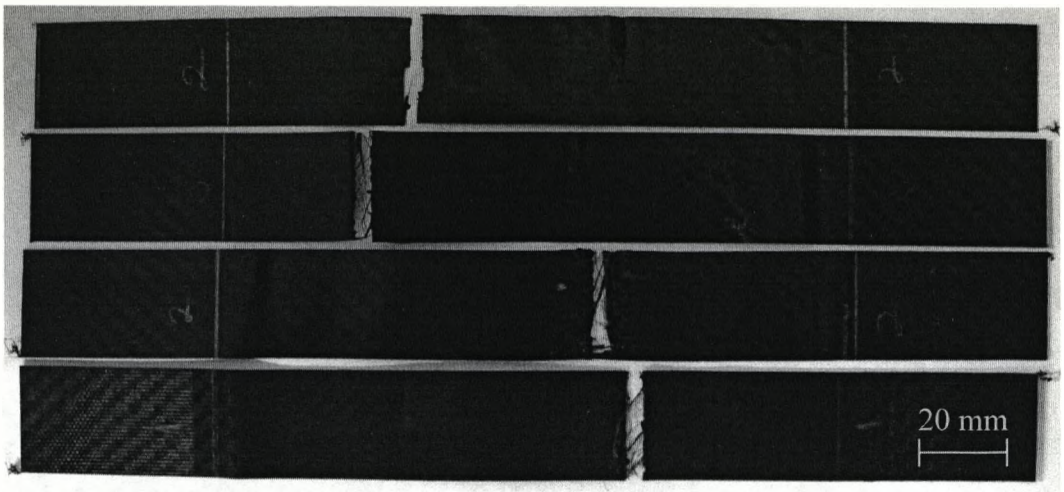

Figure 4.27. Photograph showing the four SRPP coupons scaled at a 1D ply-level following tensile testing.

Pronounced differences were also noted in the appearance of the failed FML specimens. The ¼ scale specimens failed in a transverse mode with a large crack extending through the aluminium and composite plies at 90° to the loading direction, as shown in Figure 4.28.

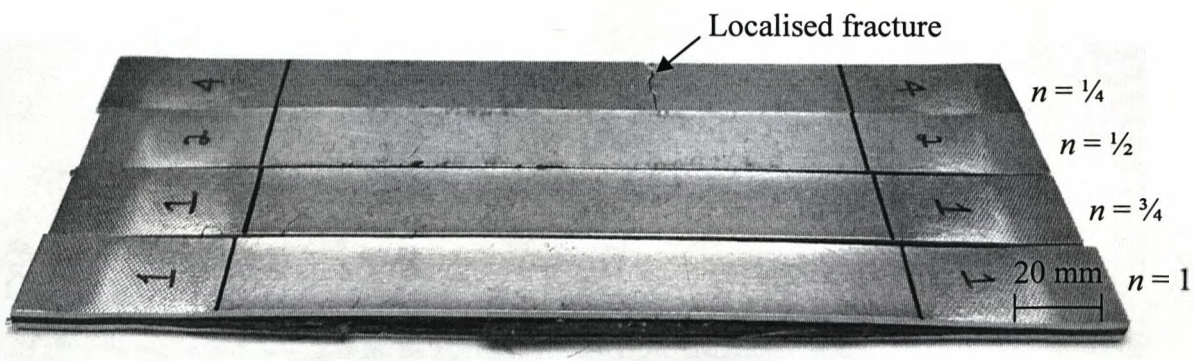

Figure 4.28. Photograph showing the four different FML coupons scaled at a 1D ply-level following tensile testing.

An inspection of the specimen edges indicated that the composite remained well bonded to the aluminium along the entire length of the test specimen (¼ scale) as highlighted in Figure 4.29a. In addition, delamination within the composite plies was limited to a very localised region immediate to the point of fracture. The three remaining FML thicknesses failed in a pronounced delamination mode involving the

propagation of a significant amount of delamination along the entire length of the test specimen (see Figure 4.28). As observed previously for the plain aluminium, the outer surfaces of the aluminium plies in the ¾ and full-scale FML specimens exhibited a textured appearance.

Closer inspection of the edges of the specimens indicated that the aluminium plies exhibited an out-of-plane curvature along the specimen edges, an effect that became more pronounced with increasing specimen size as shown in Figure 4.29b for the full-scale size specimen. This effect is likely to be associated with the three-dimensional stress state present along the edge of the specimens. The presence of these locally high through-thickness normal and shear stresses can initiate delamination-type failure along the edges of the specimen, leading ultimately to an opening of the specimen edge and specimen curving. This evidence suggests that a change in failure mode is responsible for the reductions in the strength and failure strain of the FMLs with increasing specimen size.

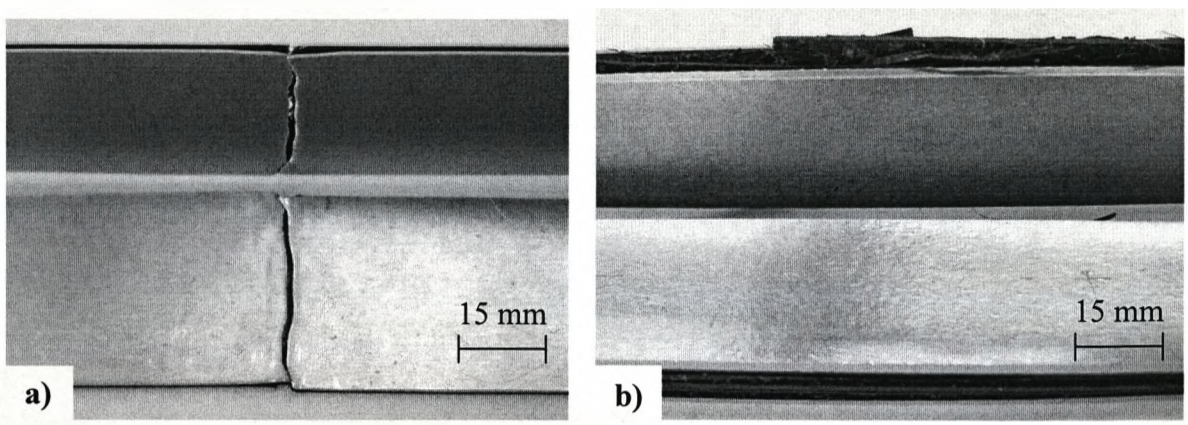

Figure 4.29. Comparison of two scaled tensile specimens following 1D ply-level scaling tests; a) n = ¼ scale size and b) full scale size (n = 1).

4.2.3 Tensile Tests on 2D Scaled Specimens

A 2D comparative scaling study was undertaken in order to highlight the differences between the ply-level and sublaminate-level techniques. These two tests were undertaken following identical processes to ensure that, as far as possible, the same volume fraction and dimensions were similar in all cases (see Section 3.4.2).

4.2.3.1 Tensile Tests on 2D Ply-Level Scaled Specimens

Figure 4.30 summarizes the failure stress data for the ply-level, $[Al_n, 0°/90°_n]_s$ FML, the 0°/90° SRPP composite and the plain aluminium alloy following 2D scaling. Here, the planar dimensions of the specimens were scaled for a fixed specimen thickness (i.e., all of the FML specimens were approximately 3.5 mm thick).

The failure stress of the aluminium alloy remained roughly constant over the four scale sizes considered here. It is important to note that the same aluminium was used in all of the scaled specimens, as only one thickness of alloy was used in this part of study. In contrast, the strength of the FML increases steadily from the ¼ scale specimen to the full-size specimen. This apparent scaling effect in the FML data can be attributed to the fact that the smaller specimens suffer from a higher stress concentration caused by the reduction in the sample width (see Figure 4.21), this, combined with the edge effect of the specimens, increase the likelihood of failure in the smaller FML samples. The strength reduction was such that the FML offered a similar strength to the equivalently-sized composite sample (see Figure 4.30).

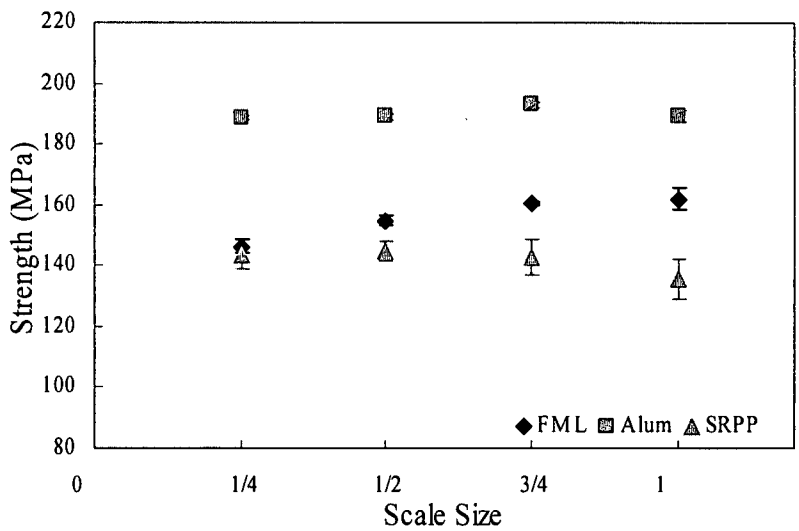

Figure 4.30. Average values of tensile strength for the FMLs and their constituent materials scaled at a 2D ply-level. The data correspond to the 0°/90° SRPP, the plain aluminium alloy and the $[Al_n, 0°/90°_n]_s$ FML.

The SRPP shows a slight tendency to decrease with increasing the areal dimensions, apparently due to the fact that there is a greater likelihood of finding a defect, since a greater number of laminae were used in the manufacture of the thicker composites. In contrast, the strength values of the scaled aluminium specimens remained roughly constant. A comparison of the 2D strength data with the aluminium data from the 1D scaling study (see Figure 4.22), suggests that the variations observed in 1D scaling were due to differences between the properties of the aluminium alloys rather than a true scaling effect.

The tensile strain to failure values for the 2D ply-level scaled FMLs and their constituents are presented in Figure 4.31. Here, constant values of strain to failure were observed in the scaled FML specimens. The ¾ size plain aluminium shows a slight decrease in strain to failure, an effect that is not evident in the FML of equivalent scale size. This small variation could be simply due to scatter, since the full scale size aluminium value was similar to those of the two smaller scale specimens. This is in contrast to the strength of ¾ sized samples (Figure 4.30), where a slight increase in the strength of the aluminium was observed, causing the specimens to fail at a lower strain.

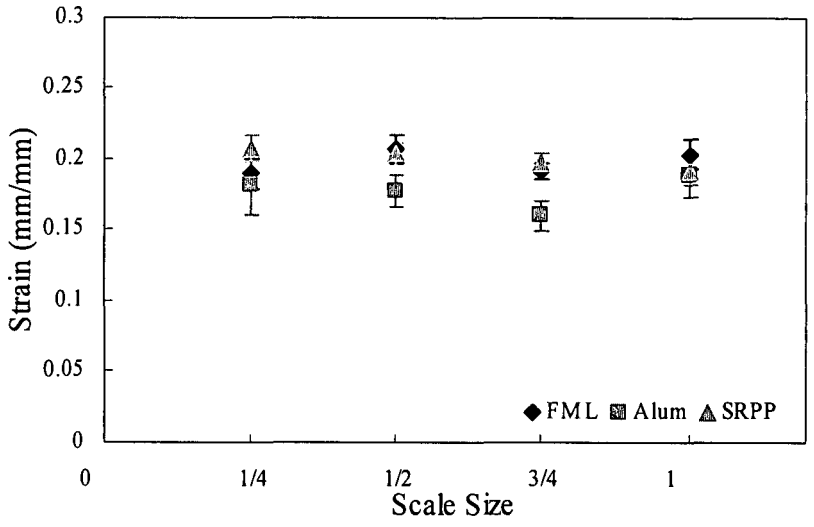

Figure 4.31. Average values of the failure strain for the FMLs and their constituent materials following 2D ply-level scaling. The data correspond to the 0°/90° SRPP, the plain aluminium alloy and the $[Al_n\ 0°/90°_n]_s$ *FML.*

The strain to failure in the scaled FMLs, was approximately 20%. As with the strength data, the strain to failure of the SRPP tended to decrease slightly with increasing the specimen size.

4.2.3.2 Normalisation of the 2D Ply-Level Tensile Data

The strength data for the 2D ply-level scaling specimens were presented in a normalised form using Equation 3.19. As expected from the strength data for the $[Al_n, 0°/90°_n]_s$ FMLs, the non-dimensional strength data also increase with increasing scale size as shown in Figure 4.32. As discussed previously, the apparent increase in strength with increasing scale size in the FMLs is likely to be a consequence of two main factors, the first being the reduction in the width to thickness ratio in the smaller specimens (see Figure 4.21), and the second being the three dimensional stress state along the edges of the specimens. That is, as the distance between the edges of the specimen is reduced (by reducing the width), the normal stress on the edges has a greater relative influence on the specimen. It is well known that edge effects can trigger delamination and provoke premature failure **[18]**.

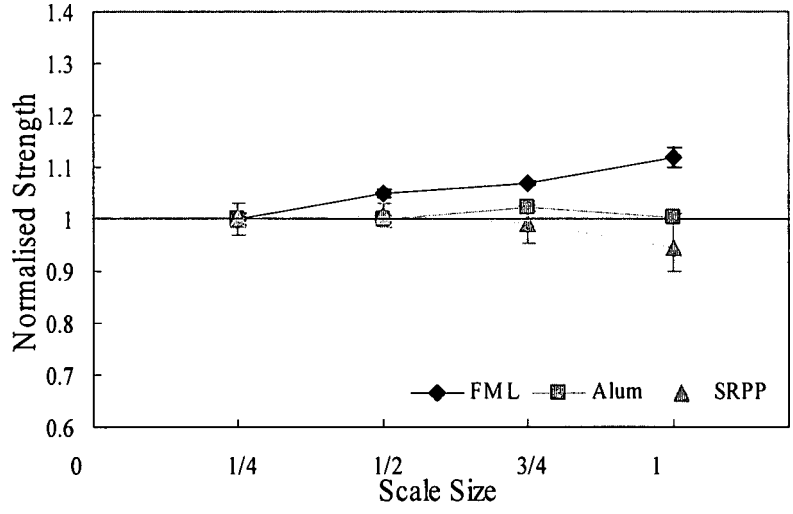

Figure 4.32. Normalised tensile strength for the 2D scaled $[Al_n, 0°/90°_n]_s$ FMLs and their constituents following tensile testing.

An apparent increase in strength of approximately 11% is observed for the full-scale FML when compared to the baseline (from 145 MPa (n = ¼) to 162 MPa (n = 1)).

Included in Figure 4.32 are the data for SRPP and the aluminium specimens, where no significant scaling effect is in evidence.

Figure 4.33 shows the normalised failure strain data for the FMLs and their constituent materials following 2D ply-level scaling. The failure strain in the SRPP composite decreases with increasing scale size whereas the aluminium did not exhibit a clear trend. Here, the FMLs exhibited similar trends to the plain aluminium highlighting the greater influence that the aluminium has on the properties of this FML system. The failure mode in each of the specimen groups was similar, suggesting that no scaling effects are present in the failure strain data with increasing specimen size.

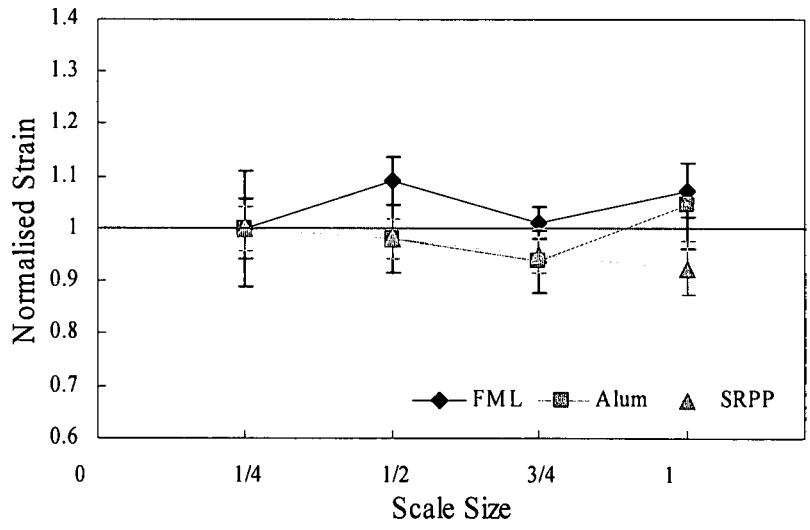

Figure 4.33. Normalised failure strain for the 2D scaled $[Al_n, 0°/90°_n]_s$ FMLs and their constituent materials.

4.2.3.3 Optical Examination of the 2D Ply-Level Tensile Specimens

After failure, the 2D-scaled specimens were examined optically in order to elucidate the failure modes during tensile loading. Fracture in all of the plain aluminium alloys occurred in the same mode as that observed in the 1D scaling study, with the samples failing at 65° to the applied load as shown in Figure 4.34. Here, no difference in surface roughening was observed in the scaled specimens as was noted in 1D scaling (Figure 4.26), this suggests that the surface roughness observed in 1D scaling was

caused by differences in the aluminium alloy rather than a consequence of scaling effects.

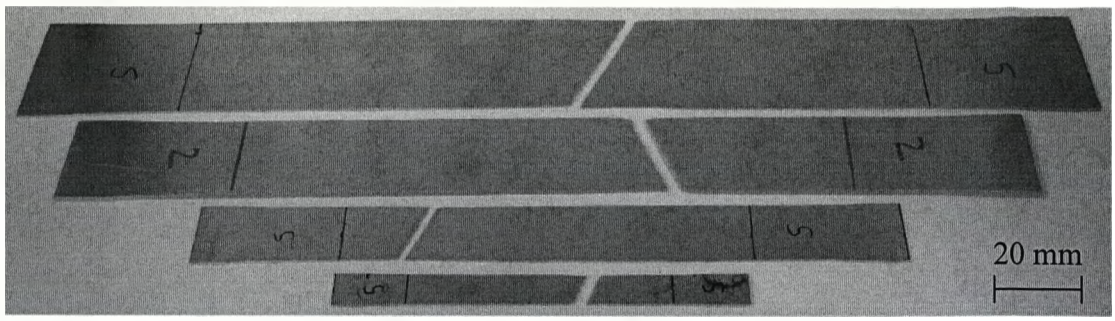

Figure 4.34. Photograph of aluminium specimens at a 2D scaling following tensile testing.

The test results for the 0°/90° SRPP composite specimens following 2D scaling are shown in Figure 4.35. All the composite specimens fractured at 90° to the loading direction generally within the working section of the test specimens. Here, no apparent change in failure mode was observed in the scaled specimens. The trend for the strain to decrease slightly with increasing scale size as shown in Figure 4.33, is likely to be due to the fact that larger composite specimens contain more laminae and offer a larger volume, increasing the probability of finding a defect.

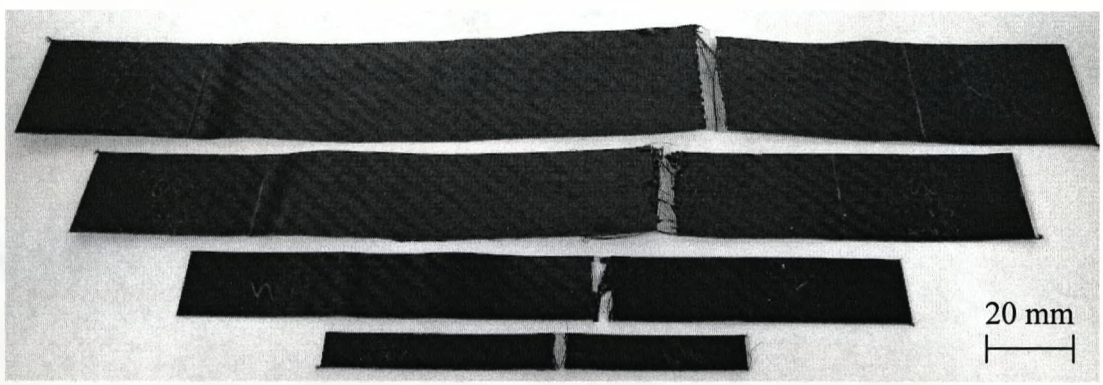

Figure 4.35. Photograph showing fractured 2D SRPP tensile specimens.

An examination of the failed FML specimens indicates that failure occurred at approximately 70° to the loading direction in all scale sizes, with a large crack extending through the aluminium and composite plies as shown in Figure 4.36. Closer inspection of the specimens shows a crack propagating along the specimens extending in the composite plies while the SRPP/metal interface remains intact. This failure

mode is similar to that observed in SCB tests (see Figure 4.16), where it was noted that the aluminium-composite interface was tougher than the interface between the laminae in the composite.

As previously observed in the 1D scaled samples, the aluminium along the edges of the 2D FML specimens exhibited an out-of-plane curvature along the specimen length. However, the width of the edge delamination zone remained roughly constant in all specimen sizes, while the specimen width obviously decreases for the smaller specimens. Clearly, the presence of these regions of ply separation along the edges of the specimens is likely to have a more pronounced effect on the properties of the smaller laminates, since the relative width of this delamination zone was much bigger in the narrower specimens than in their larger counterparts. This is likely to explain the apparent increase in tensile strength with scale size observed in the 2D FMLs.

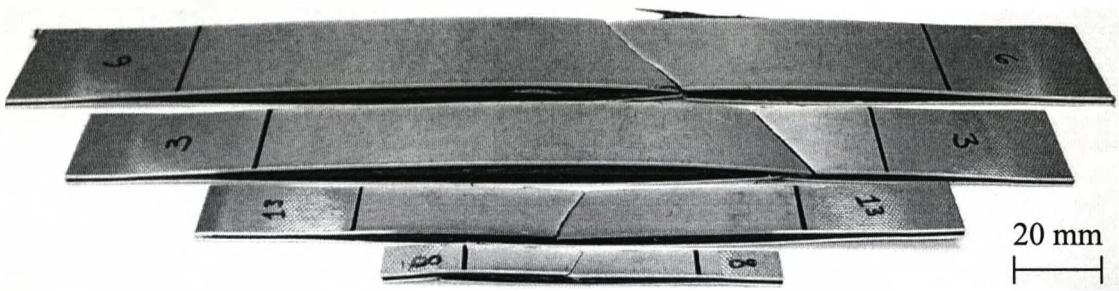

Figure 4.36. Photograph showing the failure modes in the 2D ply-level scaled FMLs following tensile testing.

4.2.3.4 Tensile Tests on 2D Sublaminate-Level Scaled Specimens

Scaled sublaminate-level specimens were manufactured by grouping together the appropriate number of baseline FMLs (in this case, two ¼ FMLs were bonded together), giving a nominal thickness of 3.58 mm. Tensile tests were conducted and the stress-strain response of the laminates was recorded.

Figure 4.37 shows the tensile strength data for the four scaled FML laminates. The strength of the scaled FML specimens shows a slight tendency to decrease with increasing scale size. This FML configuration does not exhibit the size effect that was noted in its ply-level scaled counterpart, particularly in the smaller specimens (see Figure 4.30).

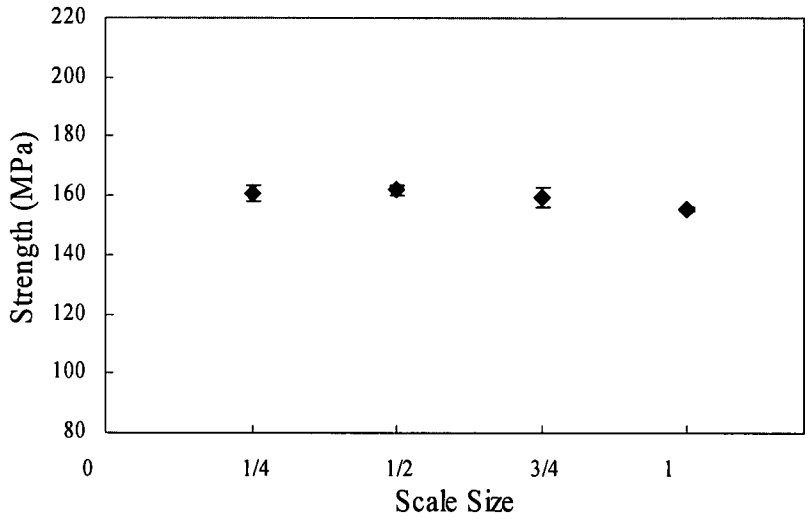

Figure 4.37. Average values of tensile strength for the 2D sublaminate-level scaled [Al, 0°/90°]$_{ns}$ FMLs following tensile testing.

The strain to failure of the FMLs scaled at a sublaminate-level is shown in Figure 4.38. Little variation in the strain to failure of the scaled specimens is apparent, with values of approximately 22% being observed. Here, a higher level of scatter is apparent compared to their counterparts scaled at ply-level. It is clear that higher values of strain to failure were recorded in the sublaminate-level specimens than in the ply-level samples (see Figure 4.31), with values of approximately 20% being recorded.

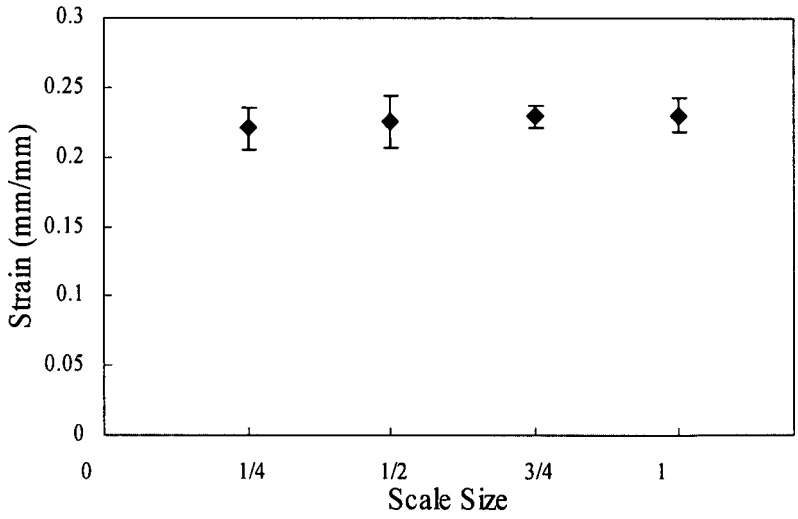

Figure 4.38. Average values of failure strain for the 2D sublaminate-level scaled [Al, 0°/90°]$_{ns}$ FMLs following tensile testing.

4.2.3.5 Normalisation of 2D Sublaminate-Level Tensile Data

Normalised strength data for the 2D sublaminate-level scaled specimens are presented in Figure 4.39. Also included in the figure are the values corresponding to the 2D ply-level specimens.

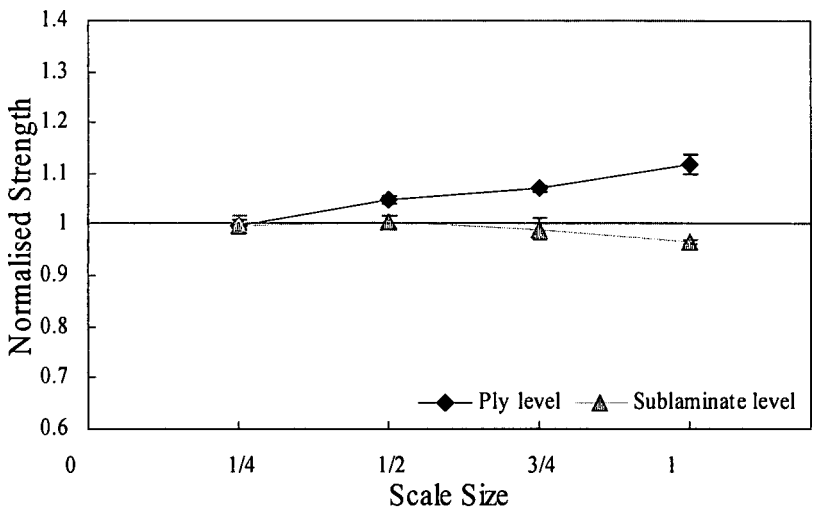

Figure 4.39. Normalised tensile strength for the 2D FMLs scaled at a sublaminate-level and a ply-level following tensile testing.

As shown previously, the ply-level technique shows an apparent scaling effect that was explained in terms of stress concentrations at the specimen edges. This affected most of the smaller specimens, provoking premature failure of the samples. In the sublaminate-scaled samples, this effect was not observed, with the strength remaining constant with increasing specimen size.

A comparison of the two groups of laminates shows that in the case of the sublaminate-level scaled specimens, fifty percent of the aluminium was located in the outermost layers of the FML specimen, with the remaining being in the centre. This distribution of the aluminium through the thickness reduced the out-of-plane forces to which the ply-level samples were subjected, these being responsible for the previously-reported delamination in this system.

Normalised failure strain data for the 2D sublaminate-level scaled FML specimens are shown in Figure 4.40. Additionally, the ply-level scaled data for the FML specimens are included for comparison. Here, it is clear that both techniques show similar trends and no significant scaling effect is apparent.

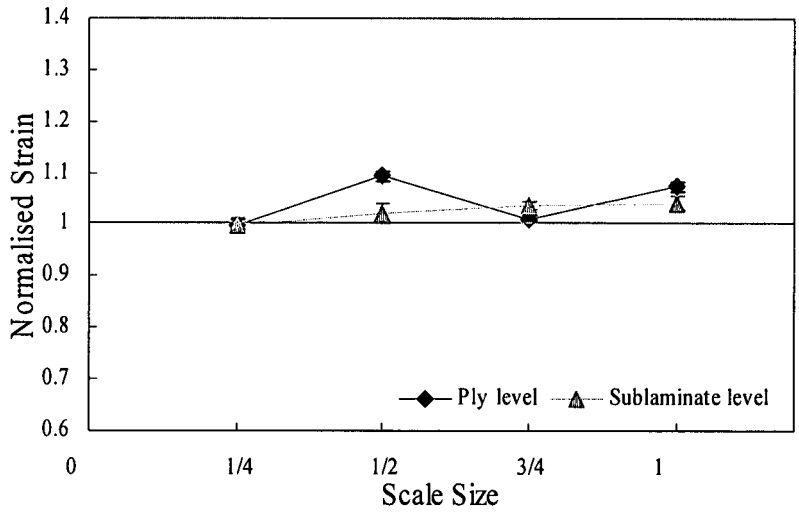

Figure 4.40. Normalised failure strain for the 2D FMLs scaled at a sublaminate-level and a ply-level following tensile testing.

4.2.3.6 Optical Examination of the 2D Sublaminate-Level Tensile Specimens

An inspection of the sublaminate-scaled FMLs shown in Figure 4.41 indicates that the specimens tended to fracture at an angle of 90° to the loading direction. In addition, delamination initiated within the composite plies extending along the length of the specimens. An inspection of the edges of the specimens indicates that the composite remained well bonded to the aluminium along the entire length of the samples. In all of the sublaminate-level specimens, the aluminium plies exhibited less out-of-plane curvature than their 2D ply-level counterparts. This is probably due to the fact that the ply-level scaled specimens had all of their aluminium situated in thick layers at the surfaces of the laminate.

The presence of these thick layers generated significant out-of-plane forces that resulted in their curving away from the plane of the laminate. In contrast, the aluminium layers in the sublaminate-level scaled samples were more evenly distributed through the thickness, with the surface layers being only one half the thickness of the ply-level scaled samples. This reduced thickness resulted in the generation of lower out-of-plane forces and a reduced level of curvature in the aluminium (see Figure 4.41).

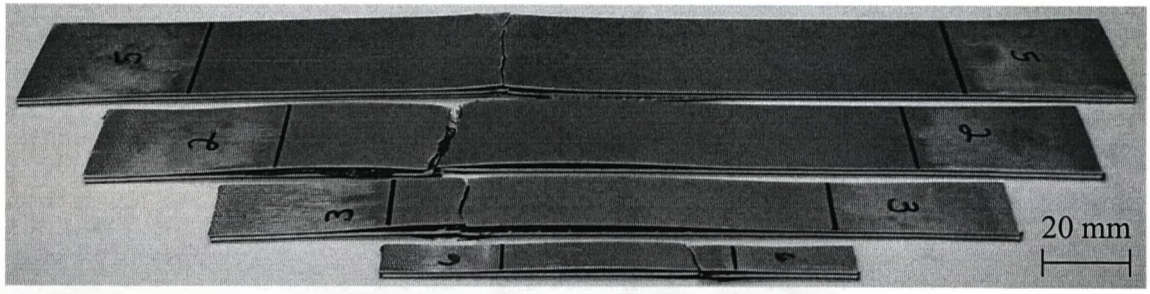

Figure 4.41. Photograph showing the failure modes in the 2D sublaminate-level scaled FMLs following tensile testing.

4.2.4 Tensile Tests on 3D Scaled Specimens

A 3D ply-level scaling study was carried out on the FMLs and their constituent materials. This 3D approach has been widely used for studying scaling effects in carbon/epoxy composites **[5,10,19]**. Here, the 3D scaling behaviour of two

configurations are compared, these being $[Al_n, 0°/90°_n]_s$ and $[Al_n, +/-45°_n]_s$ with n = ¼, ½, ¾ and 1 as full-scale.

4.2.4.1 *Tensile Test Results for the 3D Ply-Level Scaled $[Al_n, 0°/90°_n]_s$ FMLs and their Constituents*

Figure 4.42 summarizes the strength data for the 3D $[Al_n, 0°/90°_n]_s$ FMLs following tensile testing. Included in the figure are the corresponding data for the four scaled sizes of aluminium alloy and plain 0°/90° composite. An examination of the figure indicates that the strength of the four FMLs lies between those of the plain aluminium alloy and the plain composite specimens. The tensile strength data for the plain aluminium alloy exhibits some significant variations over the range of scale sizes selected here, with the average tensile strength of the ¾ size specimen being greater than that of the two smaller specimens. Similarly, the tensile strength of the full-scale aluminium specimens is below than that associated with the other scaled sizes. As mentioned previously in Section 4.2.2, it is believed that these differences are due to variations in the properties of the different alloys rather than a true scaling effect.

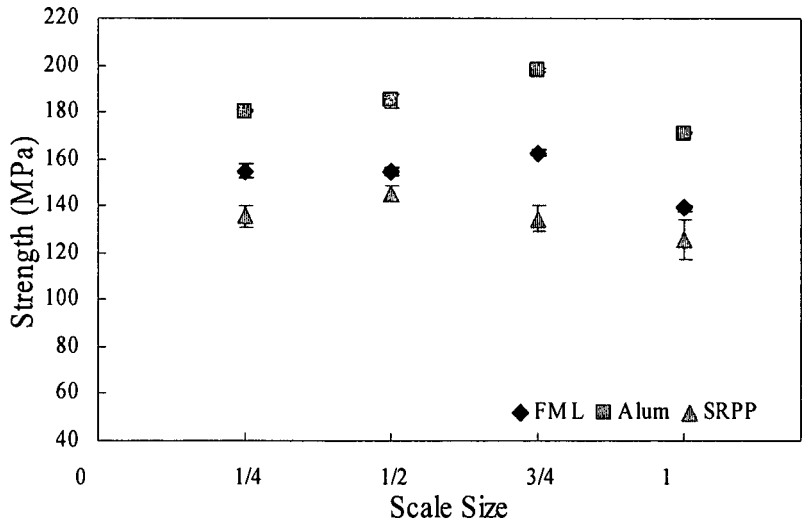

Figure 4.42. Average values of tensile strength for the 3D scaled $[Al_n, 0°/90°_n]_s$ FMLs and their constituents following tensile testing.

The tensile strength data for the FMLs reflect the variations in the properties of the aluminium alloys, with the strength of the ¾ scale specimen being the highest of the four scaled samples and that of the full-scale specimen being the lowest. The

properties of the plain composite appear to be relatively constant over the range of scale sizes considered here, although the strength of the full-scale specimen was slightly lower than that of its three counterparts.

Figure 4.43 shows the yield stress values for the 3D $[Al_n, 0°/90°_n]_s$ FML specimens calculated at a 0.2% offset strain. Here, the samples show a slight tendency to decrease with increasing scale size with the exception of the ½ scale size that shows a sudden increase of approximately 15% relative to the ¼ scale value. It is interesting to note that the ¾ scale size did not exhibit the elevated value noted in the tensile strength data (Figure 4.42).

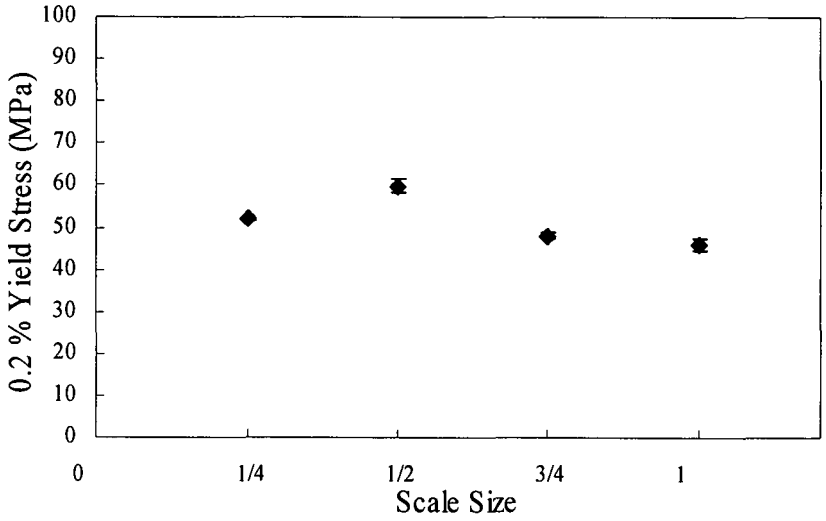

Figure 4.43. Average values of yield stress for the 3D scaled $[Al_n, 0°/90°_n]_s$ FMLs following tensile testing.

Figure 4.44 shows the fracture strain data for the 3D $[Al_n, 0°/90°_n]_s$ FML specimens and their constituents. Here, the FMLs and their constituent materials exhibit what appears to be a constant strain with increasing scale size, with a failure strain of approximately 20% being recorded in all specimens.

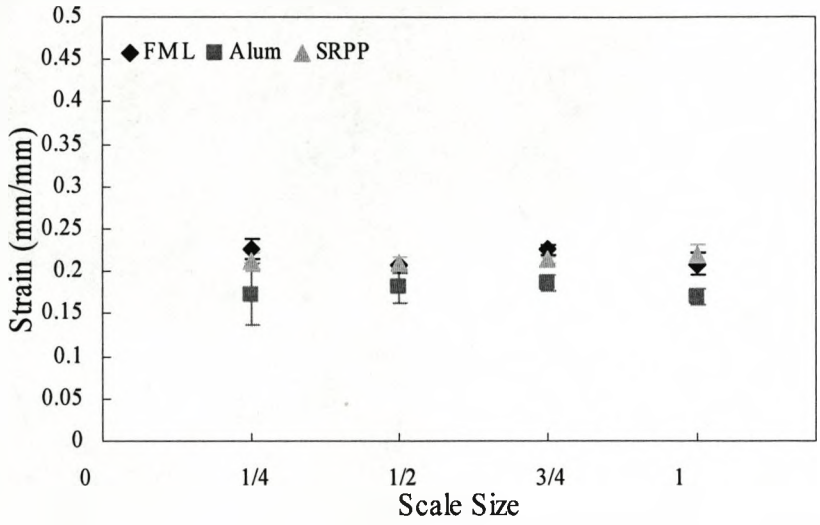

Figure 4.44. Average values of failure strain for the 3D scaled $[Al_n, 0°/90°_n]_s$ FMLs and their constituents following tensile testing.

Young's modulus data for the $[Al_n, 0°/90°_n]_s$ FMLs and their constituents are shown in Figure 4.45. The aluminium data show small variations that are attributed to differences between the individual aluminium alloys. Here, the modulus of the FMLs does not vary with scale size as can be seen in the figure. In the case of the SRPP, only one value of modulus was obtained, this being for the full-scale samples. It was not possible to measure the modulus values for the rest of the scaled composite specimens due to difficulties in fixing the extensometer to the samples, as a result of the reduced thickness and flexibility of the composite specimens. In principle, the Young's modulus should not change with specimen size because this is an intrinsic material property as reported by other authors **[16,19]**.

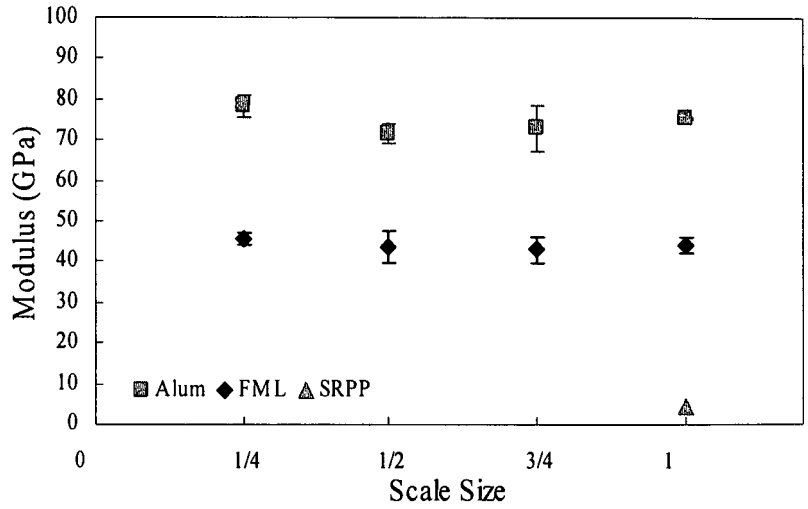

Figure 4.45. Average values of Young's modulus for the 3D [Al_n, 0°/90°$_n$]$_s$ FMLs and their constituent materials following tensile testing.

4.2.4.2 Normalisation of the 3D Ply-Level [Al_n, 0°/90°$_n$]$_s$ FML Data

The strength data for the [Al_n, 0°/90°$_n$]$_s$ FMLs are presented in a normalised form in Figure 4.46 using Equation 3.19. Here, by normalising the strength data, the effects of variations in the properties of the aluminium alloys are eliminated enabling the scaling behaviour to be observed. This technique has been used by others [**20,21**], to normalise their systems. As with the 1D scaling technique, the strength of the FMLs shows a slight tendency to decrease with increasing the scale size, where, it is clear that the strength of this system do not show a significant size effect, at least for the range of sizes studied here, with the strength of the full-scale specimens being approximately four percent lower than that of the ¼ scale specimen.

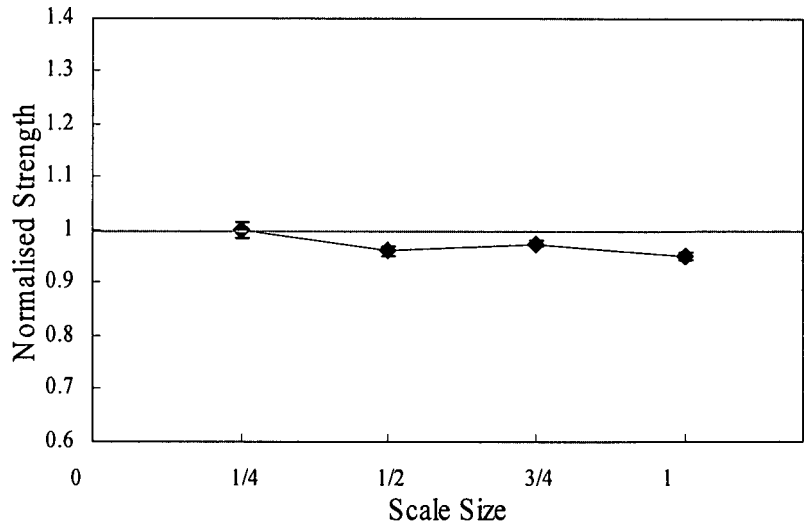

Figure 4.46. Normalised tensile strength for the 3D [Al_n, 0°/90°$_n$]$_s$ FMLs following tensile testing.

Figure 4.47 presents the normalised failure strain data for the 3D [Al_n, 0°/90°$_n$]$_s$ FML specimens. As in other strain results, the data were normalised by dividing the individual values of strain by the ¼ scale values (baseline). Here, no clear size effect was apparent in the strain data of these groups although a slight tendency to decrease was observed with increasing scale size.

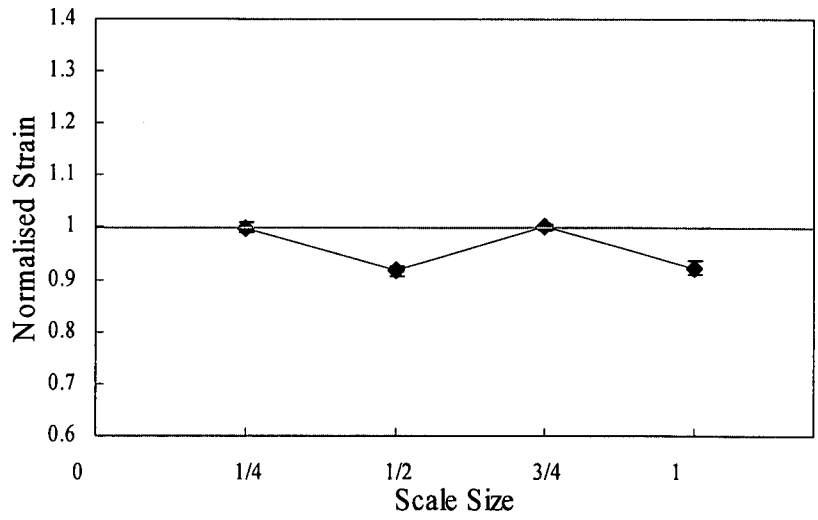

Figure 4.47. Normalised failure strain for the 3D [Al_n, 0°/90°$_n$]$_s$ FMLs following tensile testing.

Many factors can mask a true scaling effect or lead to misconception. These factors can be associated with variations in the lamination process, differences in machining, test conditions, results interpretation, etc. [**16**].

Figure 4.48 shows the normalised Young's modulus data for the 3D scaled $[Al_n, 0°/90°_n]_s$ FML specimens. Here, Equation 3.20 was used to normalise the modulus values, as follows:

$$\frac{E_{FML}}{E_{Al}V_{f_{Al}} + E_{SRPP}V_{f_{SRPP}} + E_{Ad}V_{f_{Ad}}}$$

From the figure, it can be seen that there is not scaling effect in evidence. A tendency for the Young's modulus to remain constant with scale size has been recorded by other authors too [**16,20,22**].

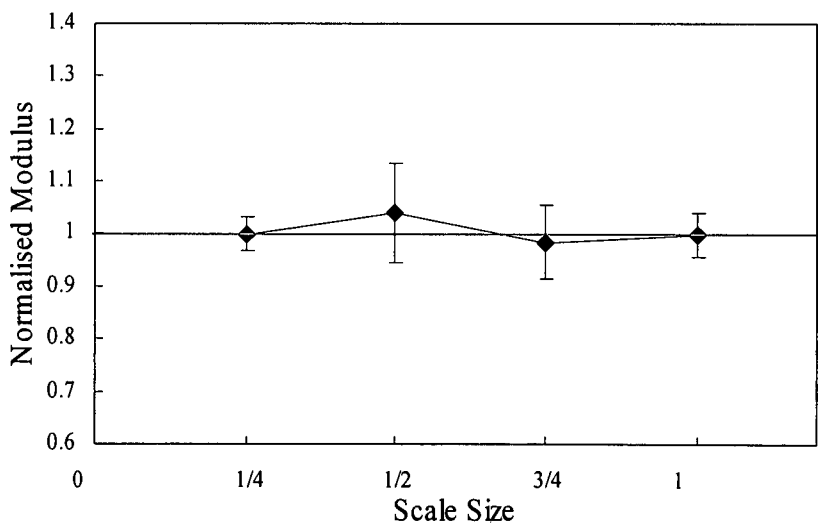

Figure 4.48. Normalised Young's modulus for the 3D $[Al_n, 0°/90°_n]_s$ FMLs following tensile testing.

4.2.4.3 *Optical Examination of the 3D Ply-Level Scaled [Al_n, 0°/90°$_n$]$_s$ FMLs and their Constituents*

Figure 4.49 shows a photograph of fractured 3D scaled plain aluminium specimens following tensile testing. Here, the failed specimens were examined optically in order to identify any differences in the failure mechanisms. Fracture in all of the plain aluminium alloys occurred in the same mode as observed in the 1D and 2D scaling studies, with fracture occurring at approximately 65° to the loading direction. A closer inspection of the specimens highlighted differences in surface roughening similar to that observed following 1D scaling (see Figure 4.26).

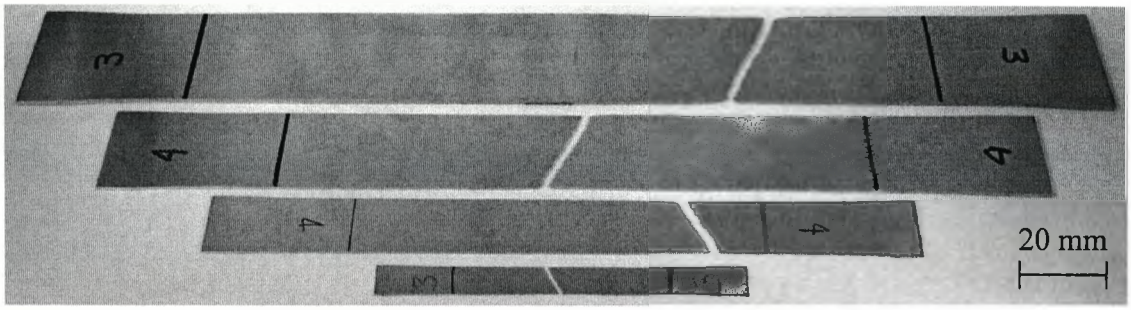

Figure 4.49. Photograph showing four 3D scaled aluminium specimens following tensile testing.

Figure 4.50 highlights the differences in the surface roughness of the four aluminium specimens following tensile testing, where it is evident that there is an increase in roughness with increasing scale size. This effect was observed in the 1D scaling study in which the same aluminium sheets were used. The increased roughening with increasing scale size may be due to the fact that different aluminium suppliers were used in this study, and therefore differences in the production of these metals could be an explanation for these variations. This effect was not observed when aluminium specimens were scaled in 2D scaling (where the same thickness of aluminium was used).

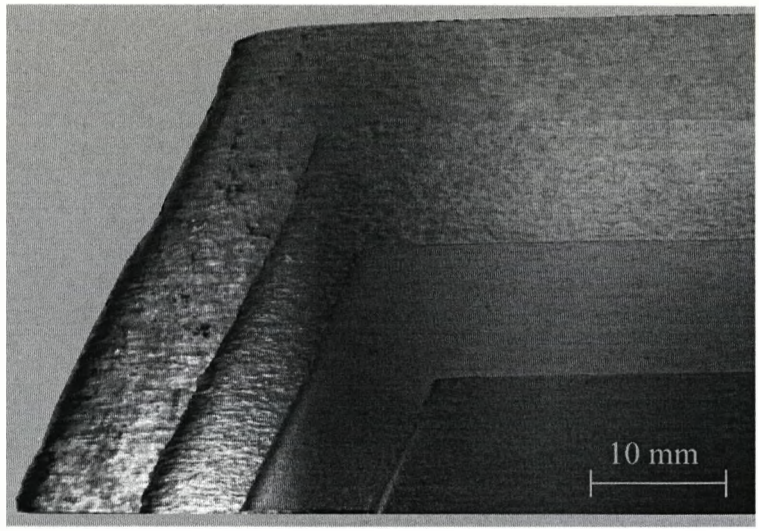

Figure 4.50. Low magnification optical micrograph showing the four 3D scaled aluminium coupons following tensile testing.

Figure 4.51 shows a photograph of the 3D scaled 0°/90° composite specimens following tensile testing. Here, it is clear that all the specimens failed in a similar mode with fracture occurring at 90° to the loading direction. As can be seen in the figure, there is a tendency for the composite strands to split and extend across the fracture zone in the larger specimens, this was not observed in the smallest scale size.

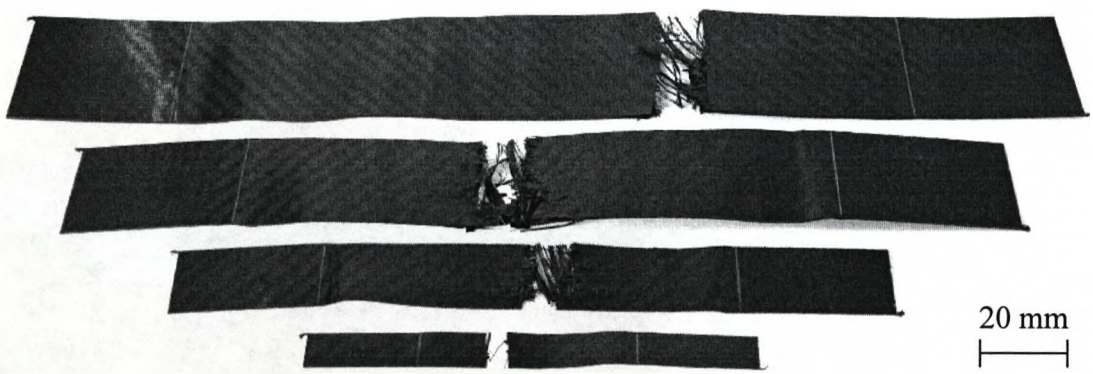

Figure 4.51. Photograph of 3D scaled 0°/90° SRPP specimens highlighting the fracture modes following tensile testing.

This effect can be attributed to the fact that more woven laminae were added to consolidate the thicker laminates. This evidence suggests that the increase in the number of these layers is responsible for the specimens failing earlier as the scale size

increases, since there is more chance to find defects in a larger volume of material (see Figure 4.42), as observed by other authors [**17**]. It is also important to note that during the manufacturing process, the plies were not laid up at an exactly 0°/90° due to small misalignment errors that possibly leading to a reduction in mechanical properties.

Failure in all four scaled sizes of the $[Al_n, 0°/90°_n]_s$ FMLs involved extensive delamination between the composite plies and fracture of the outer aluminium layers as shown in Figure 4.52. The aluminium skins in the ¾ and full-scale specimens exhibited the surface texturing that had been observed during the 1D tests on the two thickest grades of FML. The aluminium layers in all four scale sizes exhibited the previously-discussed curving along the outer edges of the specimens, involving significant pull-out of the fibre tows, an effect that was attributed to the presence of significant normal stresses along the edges of the specimens. A closer examination of the failed $[Al_n, 0°/90°_n]_s$ FML specimens highlighted a similar failure mode with increasing scale size.

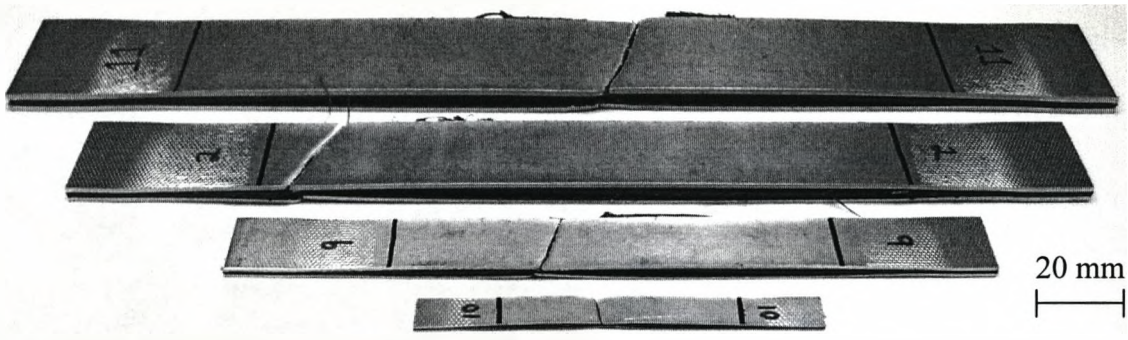

Figure 4.52. Photograph of the 3D scaled $[Al_n, 0°/90°_n]_s$ FMLs following tensile testing.

The edge effect observed in Figure 4.52 is shown schematically in Figure 4.53. Here, the edge delamination is likely to be responsible for the premature failure of the composite. The opening effect observed along the sample edges, provoked regions of intralaminar fracture between the composite edges due to the out-of-plane stress field (stresses acting out-of-plane i.e., σ_z, τ_{xz} and τ_{yz}). This initiated fracture of the SRPP composite at relatively low strains (approximately 12%). This is attributed to the mismatch in the Poisson's ratios of the aluminium and the composite. Here, the

aluminium offered a Poisson's ratio of 0.33 while that for the 0°/90° SRPP was 0.114, this generated a mismatch in strain between the constituents in the transverse direction, forcing the aluminium into compression and the composite into tension. Similar effects were observed by O'Brien [**23**] on edge effect, following tensile tests on $(+45°_n/-45°_n/0°_n/90°_n)_s$ laminates where, the strain at the onset of edge delamination decreased dramatically as the scale size was increased from 1 to 3.

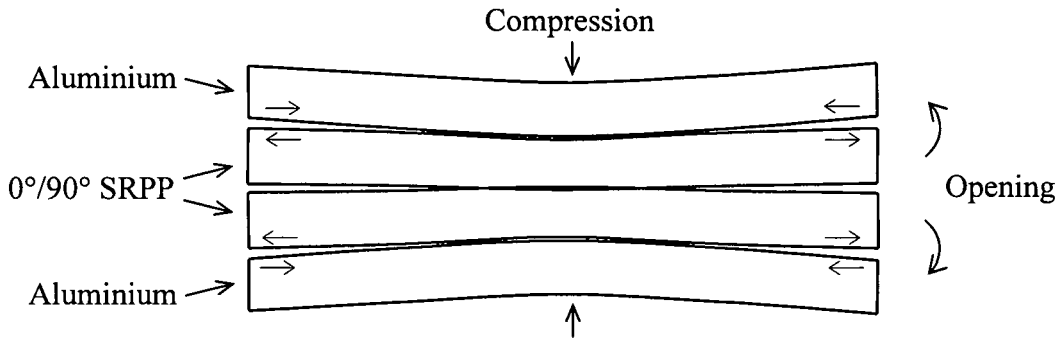

Figure 4.53. Schematic representation of the cross-section of a 3D scaled [Al_n, $0°/90°_n]_s$ FML following tensile testing.

4.2.4.4 Tensile Test Results for the 3D Ply-Level Scaled [Al_n, $+/-45°_n]_s$ FMLs and their Constituents

Figure 4.54 shows the tensile strength data for the 3D $[Al_n, +/-45°_n]_s$ FMLs and their constituents. Here, similar trends are apparent to those observed in the $[Al_n, 0°/90°_n]_s$ FMLs, with the ¾ scale specimens offering the highest tensile strength and the full-scale specimen the lowest. The data show a tendency to decrease with increasing specimen size for the aluminium and FML samples. Interestingly, the tensile strength of the +/-45° plain composite specimens increased continuously with increasing scale size. A comparison of Figures 4.42 and 4.54 highlights the superior strength of the $[Al_n, 0°/90°_n]_s$ FMLs, an effect associated with the greater tensile strength of the 0°/90° composite relative to the +/-45° system. Here, in spite of the fact that the strength of the plain +/-45° SRPP increased with increasing specimen size, the strength of the FML decreases with increasing scaling size, due to the strong influence of the aluminium alloy.

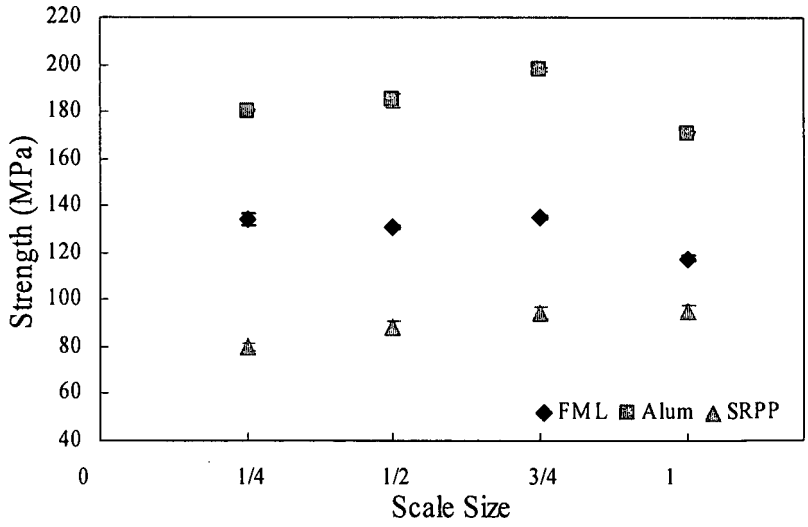

Figure 4.54. Average values of tensile strength for the 3D scaled [Al_n, +/-45°$_n$]$_s$ FMLs and their constituent following tensile testing.

Figure 4.55 shows the yield stress data for the 3D [Al_n, +/-45°$_n$]$_s$ FML specimens calculated at a 0.2% offset strain. Interestingly, the response of these scaled values is very similar to that obtained in their [Al_n, 0°/90°$_n$]$_s$ counterpart (see Figure 4.43), where a slight tendency to decrease with increasing specimen size is observed. Similarly, the yield stress of the ½ scaled specimens for both configurations show the highest values, attributed to differences in the aluminium alloys.

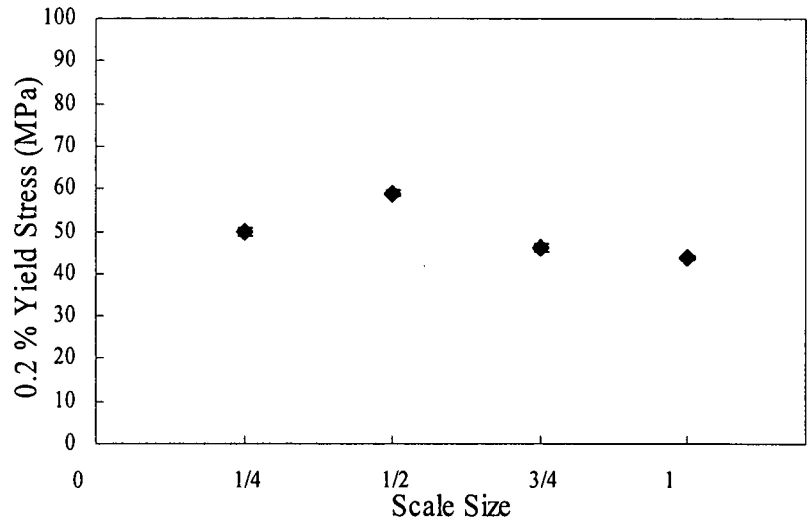

Figure 4.55. Average values of yield stress for the 3D scaled [Al_n, +/-45°$_n$]$_s$ FMLs following tensile testing.

The tensile failure strain data for the $[Al_n, +/-45°_n]_s$ FMLs and their constituents are presented in Figure 4.56. Here, the +/-45° SRPP specimens offered strain values that were approximately 75% higher than those of its 0°/90° counterpart, where the strain of the composite samples did not vary with scale size. The failure strain of the aluminium samples was approximately 17% and this again did not vary with scale size. In the case of the FMLs, no clear scaling effect was observed. Closer inspection highlighted the presence of a larger level of scatter in the smallest specimens, a possible consequence of the increased sensitivity of the extensometer over this small range.

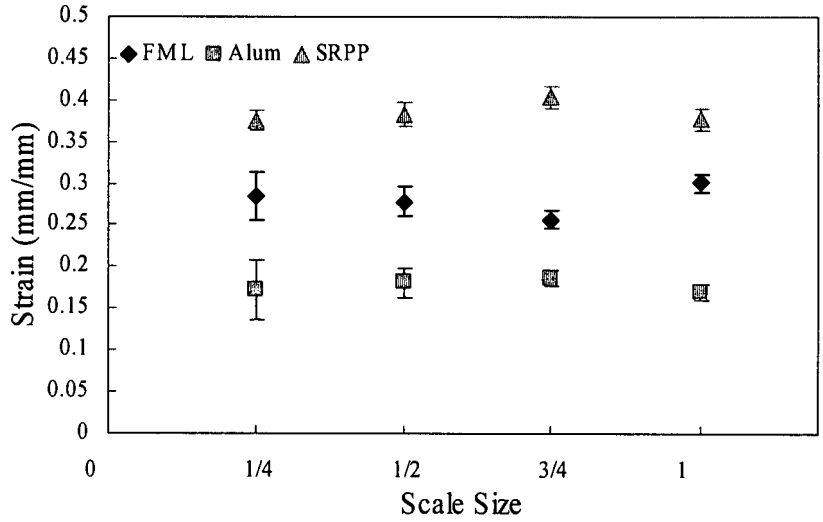

Figure 4.56. Average values of failure strain for the 3D scaled $[Al_n, +/-45°_n]_s$ FMLs and their constituents following tensile testing.

Young modulus data for the $[Al_n, +/-45°_n]_s$ FMLs and their constituent materials are shown in Figure 4.57. As with the $[Al_n, 0°/90°_n]_s$ FMLs, the aluminium data show small variations with scale size, due to small differences between the four aluminium alloys. Here, the modulus of the FMLs does not vary with scale size, with the average value for the scaled specimens being approximately 45 GPa. The Young's modulus of the thickest SRPP specimens was 2.7 GPa.

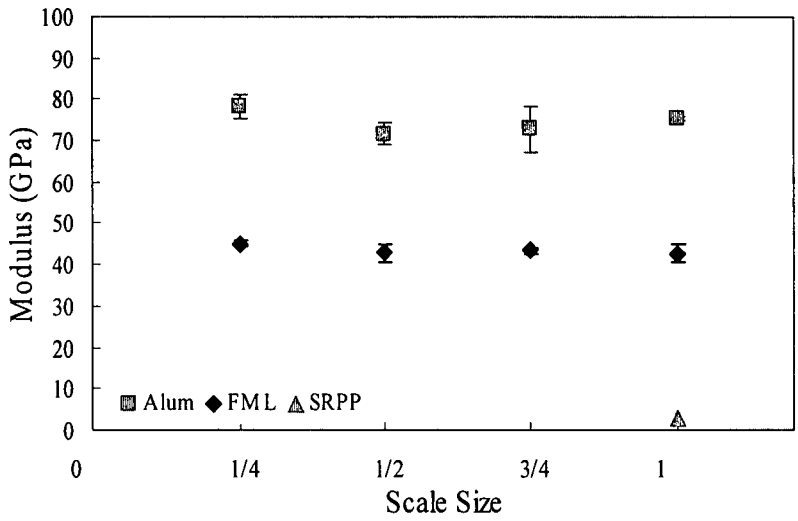

Figure 4.57. Average values of Young's modulus for the 3D scaled $[Al_n, +/-45°_n]_s$ FMLs and their constituents following tensile testing.

4.2.4.5 Normalisation of the 3D Ply-Level $[Al_n, +/-45°_n]_s$ FML Data

Figure 4.58 shows the normalised strength data for the 3D $[Al_n, +/-45°_n]_s$ FMLs. Here, as was the case with the $[Al_n, 0°/90°_n]_s$ FMLs, the strength values were introduced into Equation 3.19 to obtain a non-dimensional strength removing the influence of variations in the properties of the constituents, leaving only variations related to scaling effects. The data exhibit a clear tendency to decrease with increasing size specimen, with the strength of the full scale specimens being approximately 12% lower compared to the baseline. This is in agreement with the findings of Johnson *et al* [**21**], who observed a more significant reduction in properties in specimens based on off-axis fibres rather than a 0°/90° configuration.

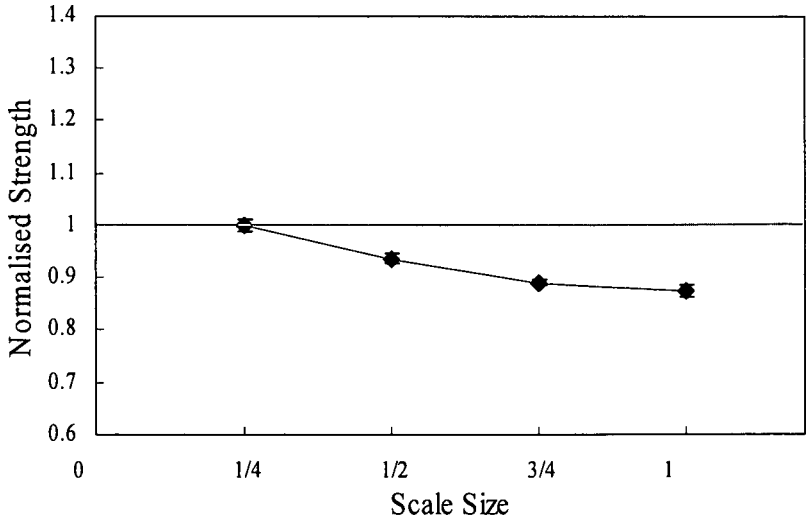

Figure 4.58. Normalised tensile strength for the 3D scaled [Al_n, +/-45°$_n$]$_s$ FMLs following tensile testing.

Normalised failure strain data for the 3D [Al_n, +/-45°$_n$]$_s$ FML specimens are presented in Figure 4.59, where no clear trend is apparent. It is difficult to define whether these trends are related to scaling effects or simply to scatter associated with the different processes involved during the manufacture of the samples.

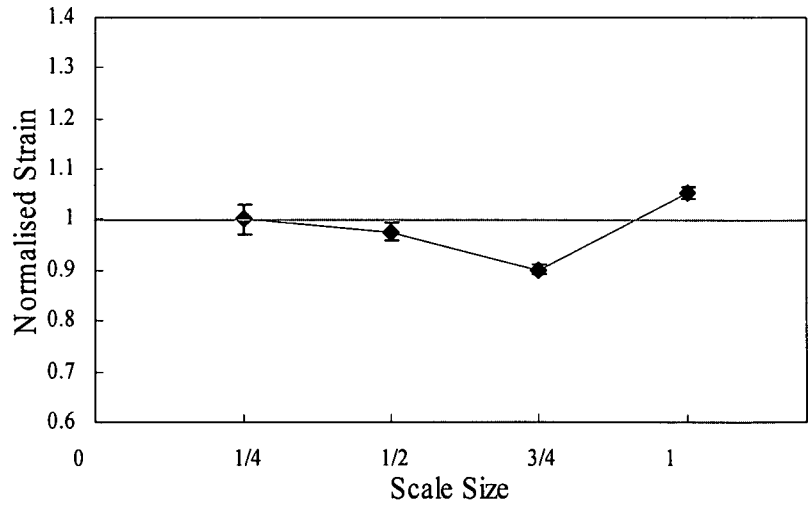

Figure 4.59. Normalised failure strain for the 3D scaled [Al_n, +/-45°$_n$]$_s$ FMLs following tensile testing.

Figure 4.60 shows the normalised Young's modulus data for the 3D $[Al_n, +/-45°_n]_s$ FMLs. Here, as was the case with the $[Al_n, 0°/90°_n]_s$ FMLs, the modulus values show no scaling effect. In principle, this property should not change with scale size since it is an intrinsic property of the material.

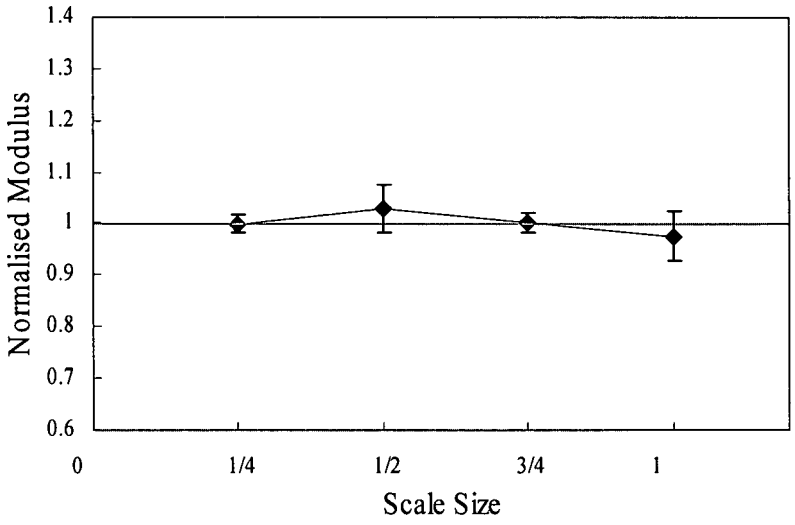

Figure 4.60. Normalised Young's modulus for the 3D scaled $[Al_n, +/-45°_n]_s$ FMLs following tensile testing.

4.2.4.6 Optical Examination of the 3D Ply-Level Scaled $[Al_n, +/-45°_n]_s$ FMLs and their Constituents

Figure 4.61 shows a comparison of the four scaled +/-45° SRPP specimens following tensile testing. Here, a change in the fracture angle from 45° to the loading direction to 90° is observed. This change in angle is associated with an increase in specimen thickness from 0.3 to 1.2 mm. This was achieved through the addition of laminae or plies to increase the thickness of the composite. This increase in the number of layers in the composite increases the likelihood of fibre misalignment, which may in turn lead to the sample failing at 90°. It is then necessary to account for the fact that by increasing the thickness of the SRPP composite, variations in the failure mode may occur when the composite is used in the FML specimen.

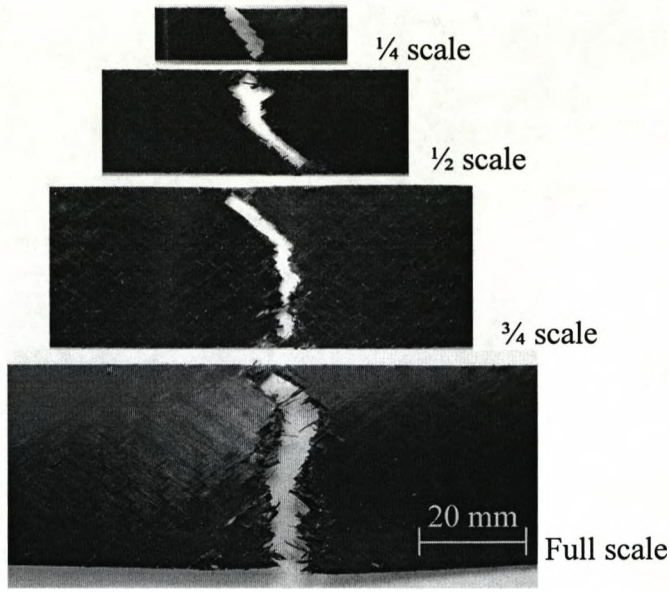

Figure 4.61. Comparison of four 3D scaled +/-45° SRPP specimens, highlighting the fracture modes following tensile testing.

The FML specimens failed as a result of a fracture at approximately 60° that had propagated in only one of the outer aluminium layers as shown in Figure 4.62. Failure in $[Al_n, +/-45°_n]_s$ FMLs involved extensive shearing and re-orientation of the polymer fibres in the loading direction. Longitudinal curving of the specimens was observed in proportion to their scaled size, associated with shearing of the fibres in the angle-ply composite plies. A closer examination of the specimens indicates that the composite remained well bonded to the outer skins along the entire length of the test specimen. In the remainder of the scaled specimens, only one surface remained intact (not visible in the figure).

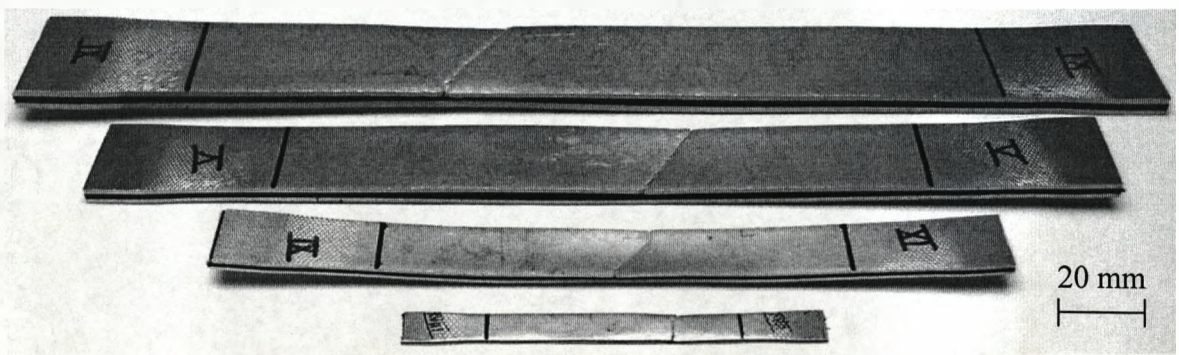

Figure 4.62. Photograph showing the 3D ply-level $[Al_n, +/-45°_n]_s$ FMLs following tensile testing.

The amount of delamination observed in the FMLs increased in proportion to the scaling size over a region close to the point of fracture. The overall length of the $[Al_n, +/-45°_n]_s$ laminates was significantly greater than that observed in the $[Al_n, 0°/90°_n]_s$ coupons, an indication of the greater levels of strain sustained by the FMLs based on angle-ply composite layers.

High interlaminar stresses can arise at the free edge of a laminate with different ply orientations. This phenomenon has been studied extensively by Pipes and Pagano [**24**]. In some laminates, this can lead to premature failure initiating at the free edge, with the failure stress depending on the ply thickness [**16**]. Edge effects are noticeable in the specimens shown in Figure 4.62. Here, the schematic cross-section of a $[Al_n, +/-45°_n]_s$ FML is shown in Figure 4.63. An opposite effect to that observed in the $[Al_n, 0°/90°_n]_s$ FMLs is observed here, with the aluminium edges closing due to the influence of the SRPP generating a ridge in the centre of the aluminium layers.

In contrast to that observed previously in the $[Al_n, 0°/90°_n]_s$ FMLs (see Figure 4.53), the Poisson's ratios of the constituent materials were: 0.33 for the aluminium and 0.44 for the +/-45° SRPP, forcing the aluminium into tension and the composite into compression, generating a mismatch that forced the FML to collapse by the edges.

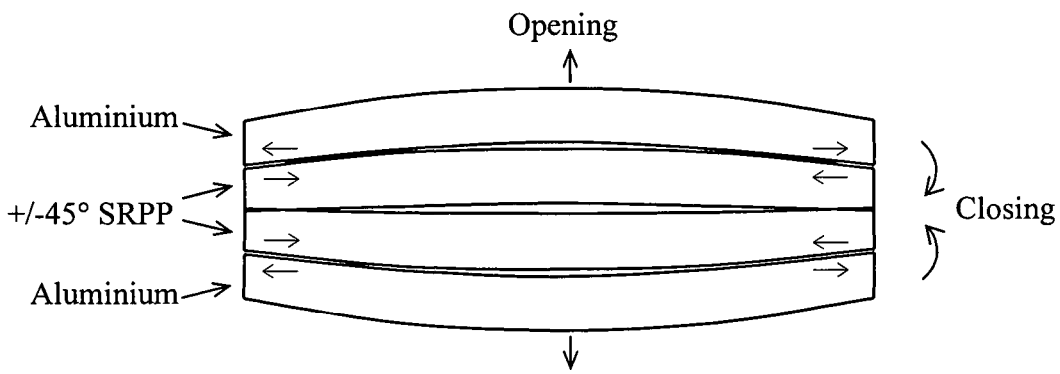

Figure 4.63. Schematic representation of the cross-section of the 3D $[Al_n, +/-45°_n]_s$ FML following tensile testing.

4.2.4.7 *Comparison of Tensile Test Data for the 3D Ply-Level Scaled [Al$_n$, 0°/90°$_n$]$_s$ and [Al$_n$, +/-45°$_n$]$_s$ FMLs*

Weibull predictions are frequently used for materials with a linear response (elastic materials) such as carbon/epoxy, with reported Weibull modulus values of m = 25 [**25**]. Recently, researchers have applied this approach to semi-brittle materials such as glass fibre/epoxy [**10**]. Here, an attempt was made to find if a Weibull approach works for hybrid materials such as thermoplastic FMLs. Figure 4.64 shows a good correlation, obtained when the Weibull equation was applied:

$$\frac{\sigma_1}{\sigma_2} = \left(\frac{V_2}{V_1}\right)^{1/m}$$

The Weibull modulus (m), obtained for the [Al$_n$, 0°/90°$_n$]$_s$ FMLs was 95 while that for the [Al$_n$, +/-45°$_n$]$_s$ FMLs was 35. Indicating that the Weibull modulus number is smaller as greater the scaling effect [**5**].

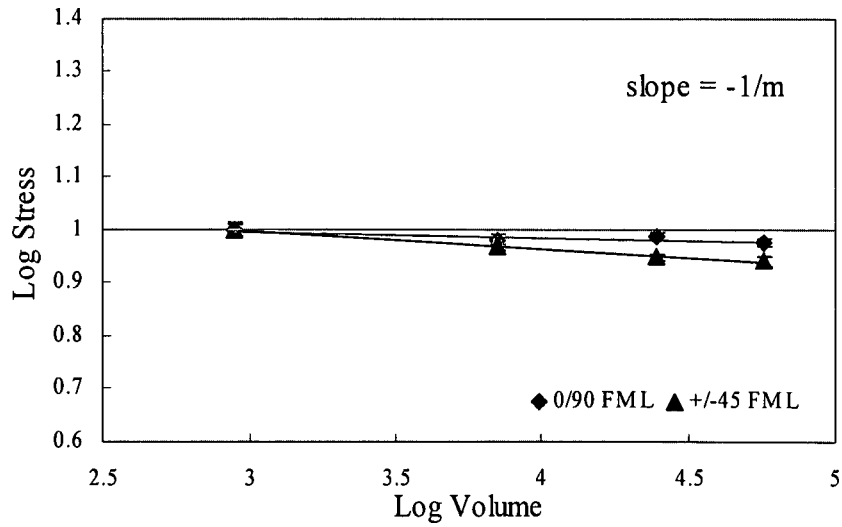

Figure 4.64. Normalised Weibull modulus for the 3D scaled [Al$_n$, 0°/90°$_n$]$_s$ FMLs and the [Al$_n$, +/-45°$_n$]$_s$ FMLs following tensile testing.

4.2.5 Summary of the Tensile Scaling Study

This part of the research study investigated size effects in tensile samples, scaled using 1D, 2D and 3D scaling approaches. Initially, 1D scaling was conducted using the ply-level approach, where a slight decrease in strength and strain to failure was observed for scaled specimens, this representing a 5% reduction in comparison to the baseline value (¼ scale size). 2D scaling was undertaken using two different approaches, ply-level and sublaminate-level. Here, a comparison of the two approaches highlighted differences in the scaling responses. An increase of 10% was observed in the ply-level scaled samples, whereas the sublaminate-level scaled samples did not show any significant variation compared to the baseline value. In terms of the strain to failure, the scaled specimens did not show clear size dependency.

The 3D scaling study was undertaken using a ply-level approach with two fibre orientations, these being $[Al_n, 0°/90°_n]_s$ and $[Al_n, +/-45°_n]_s$. The former exhibited a slight decrease in strength with increasing scale size, whereas the latter exhibited a 12% reduction relative to the baseline value. The strain to failure was similar in all specimen sizes and in both types of laminate, as was the case with the Young's modulus, indicating that this is an inherent material property that does not change with scale size.

4.3 Scaling Effects in the Flexural Properties of the FMLs and their Constituents

A flexural study was carried out using the ply-level scaling technique in which, two configurations were used, $[Al_n, 0°/90°_n]_s$ and $[Al_n, +/-45°_n]_s$, with n = ¼, ½, ¾ and 1. A four point bend fixture was employed for the tests (see Section 3.3.2). Similar studies have been carried out by others on carbon/epoxy [**26-29**] and glass/epoxy systems [**10**].

4.3.1 Flexural Test Data for the 3D Ply-Level Scaled $[Al_n, 0°/90°_n]_s$ FMLs and their Constituents

The maximum flexural stress data for the $[Al_n, 0°/90°_n]_s$ FMLs are shown in Figure 4.65. A tendency for the maximum stress to decrease with increasing specimen size is apparent, especially for the largest specimens, where the maximum stress is 163 MPa for the ½ scale size and 140 MPa for the full scale specimens. A noticeable increase in scatter is observed for the smallest specimens, possibly due to the reduced accuracy of the load cell at these lower loads. Here, the samples did not fracture, instead, the maximum stress value tended to plateau (see Figure 4.9).

A comparison of these results with the tension data reveals differences in the maximum stress values. It is worth nothing that in the $[Al_n, 0°/90°_n]_s$ FMLs tested in tension, the strength was recorded in the ¾ scale size, while here in flexure, the maximum stress was recorded in the ½ scale size.

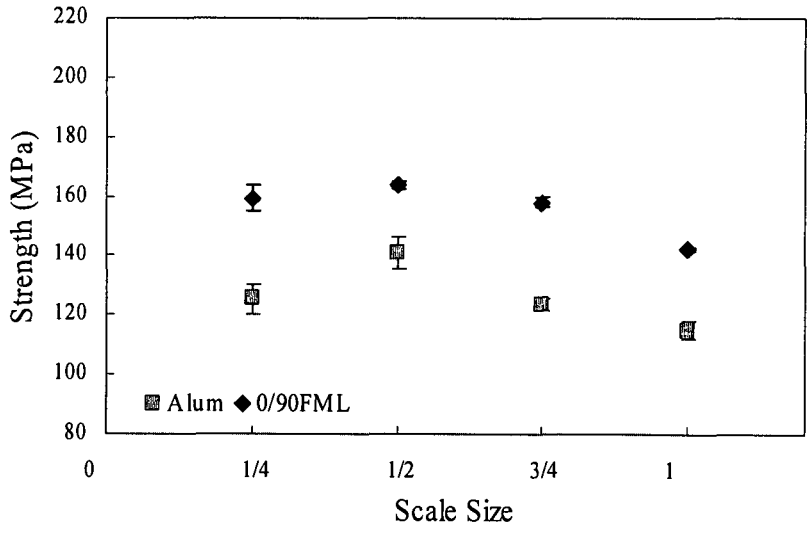

Figure 4.65. Average values of maximum stress for the 3D scaled $[Al_n, 0°/90°_n]_s$ FMLs following flexural testing.

Figure 4.65 also shows the maximum stress values for the aluminium specimens, where it is clear that these values are lower than those of the FMLs presented here and those obtained in tension (see Figure 4.42). This was because two different span/thickness ratios were used here (36.5 for the FMLs and 127 for the aluminium specimens), reducing the relative maximum stress of the aluminium [**30**]. These

aluminium tests were undertaken only with the objective to observe the response of the alloy with scale size, which reinforces the theory that the FMLs response is controlled mostly by the aluminium influence.

A comparison of the $[Al_n, 0°/90°_n]_s$ FMLs with the aluminium samples shows that, the FMLs specimens follow the same trend as the aluminium samples, with the highest value corresponding to the ½ scale samples (163 MPa) and the lowest corresponding to the full scale samples (140 MPa). These variations in data could be then attributed to the different properties of the aluminium alloys as was noted in the tensile study. The plain composite could not be included in this study due to its high flexibility and difficulty in testing it in flexure.

Flexural yield stress data for the $[Al_n, 0°/90°_n]_s$ FML specimens are presented in Figure 4.66. Included in the figure are the corresponding values for the yield stresses of FML specimens tested in tension. Here, a good correlation in the results was observed between the flexural and tensile samples. Higher values of strength are usually observed in flexure than in tension, as reported by other authors [**5,10**].

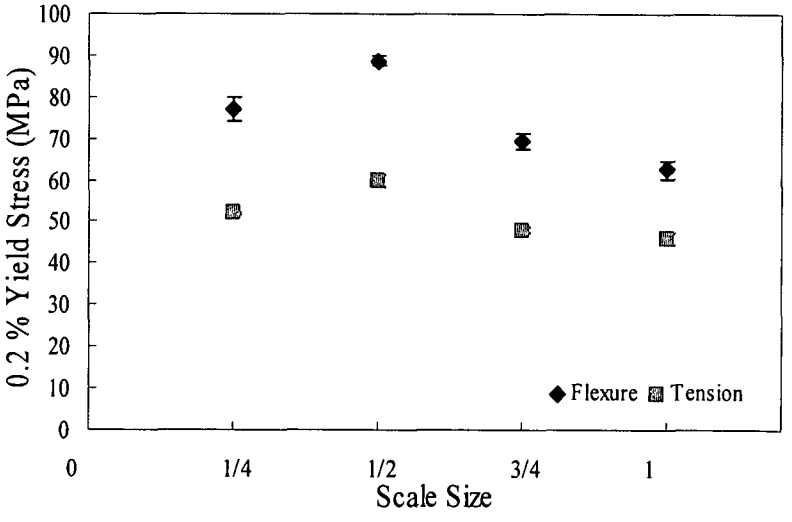

Figure 4.66. Comparison of yield stress data for the 3D scaled $[Al_n, 0°/90°_n]_s$ FML specimens tested in flexure and tension.

As observed previously with the maximum stress in flexure (see Figure 4.65), the yield stress data follow the same trend with scale size, with the highest value being measured on the ½ scale size (89 MPa) and the lower value on the full scale size (61 MPa). It is clear in Figure 4.66, that a tendency to decrease by increasing the scale size is in evidence for the FMLs tested in flexure.

Figure 4.67 shows the strain data at maximum stress for the 3D scaled $[Al_n, 0°/90°_n]_s$ FMLs following flexural testing. Here again, no significant variation with the response of the specimens was observed, with an average flexural strain of approximately 1.9% being recorded in all samples.

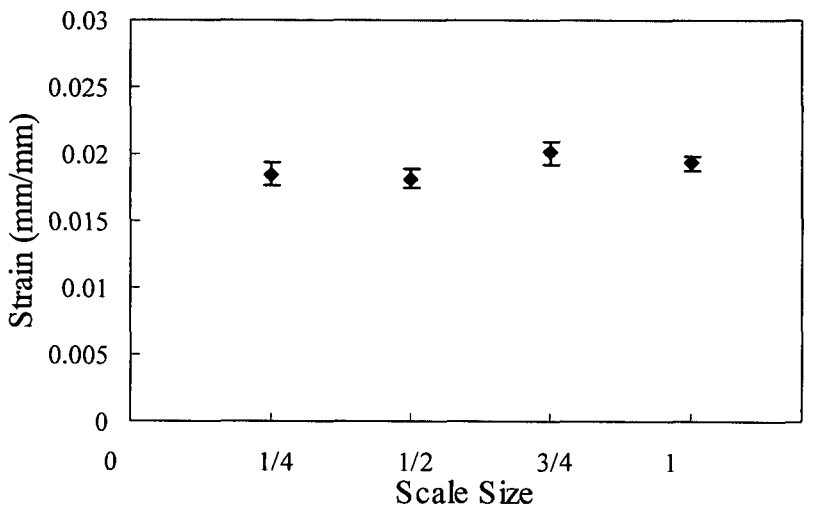

Figure 4.67. Average values of strain to maximum stress data for the 3D scaled $[Al_n, 0°/90°_n]_s$ FMLs following flexural testing.

Figure 4.68 shows the flexural modulus data for the 3D scaled $[Al_n, 0°/90°_n]_s$ FMLs following flexural testing. Here, no significant variation in the stiffness was observed. The flexural modulus should not vary since it is an inherent property of the material. The average flexural modulus for the scaled specimens here is approximately 65 GPa.

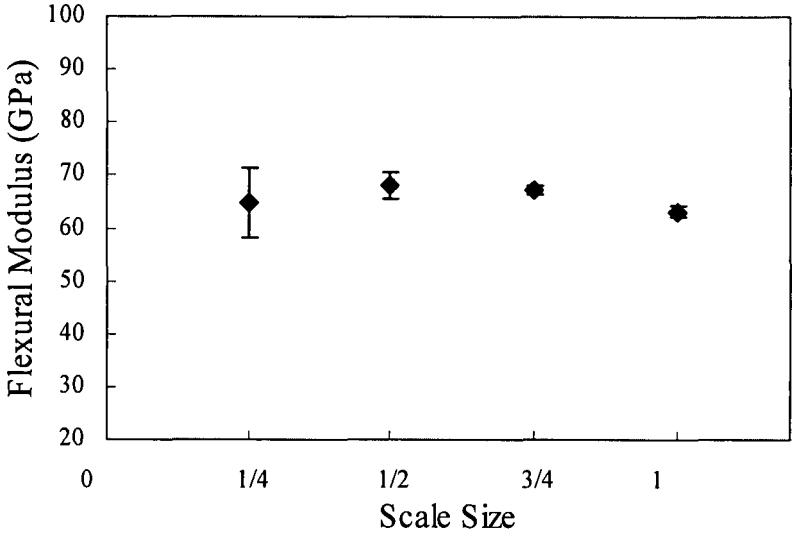

Figure 4.68. Average values of flexural modulus for the 3D scaled $[Al_n, 0°/90°_n]_s$ FMLs following flexural testing.

4.3.1.1 Normalisation of the Yield Stress Data for the 3D Ply-Level Scaled $[Al_n, 0°/90°_n]_s$ FMLs

The normalised values of the yield stress were used here due to the difficulty in defining the exact point of the maximum stress on the curves at which the force reaches a plateau (see Figure 4.9). Instead, the yield stress was chosen to investigate scaling effects as shown in Figure 4.69. Here, a tendency to decrease with increasing the scale size was observed, being only significant for the full scale specimens with approximately nine percent lower the yield stress than the baseline.

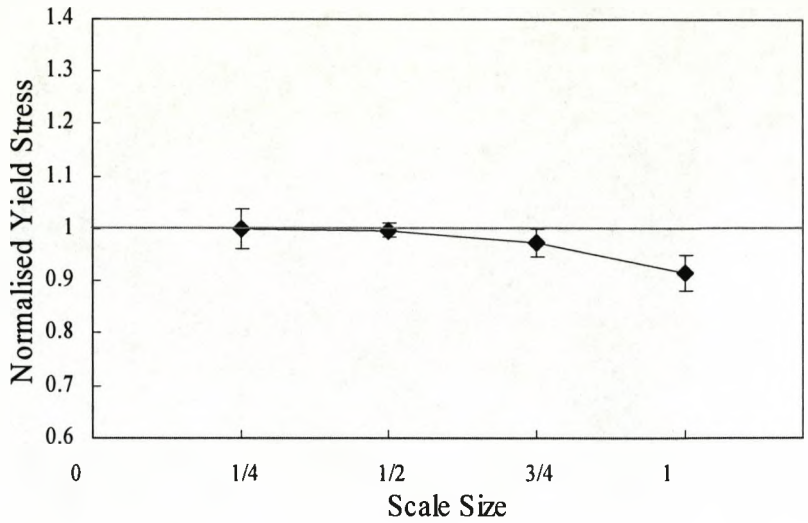

Figure 4.69. Normalised yield stress for the 3D scaled [Al_n, 0°/90°$_n$]$_s$ FMLs following flexural testing.

4.3.1.2 Optical Examination of the 3D Ply-Level Scaled [Al_n, 0°/90°$_n$]$_s$ FMLs

Figure 4.70 shows a photograph of the 3D [Al_n, 0°/90°$_n$]$_s$ FML specimens following flexural testing. As can be seen, none of the constituents in the FMLs show any sign of failure following testing. In order to analyse this further, closer inspection was made by cutting the cross-sections in the middle of representative specimens looking for fracture evidence, where, as shown before in Figure 4.12, no failure was observed.

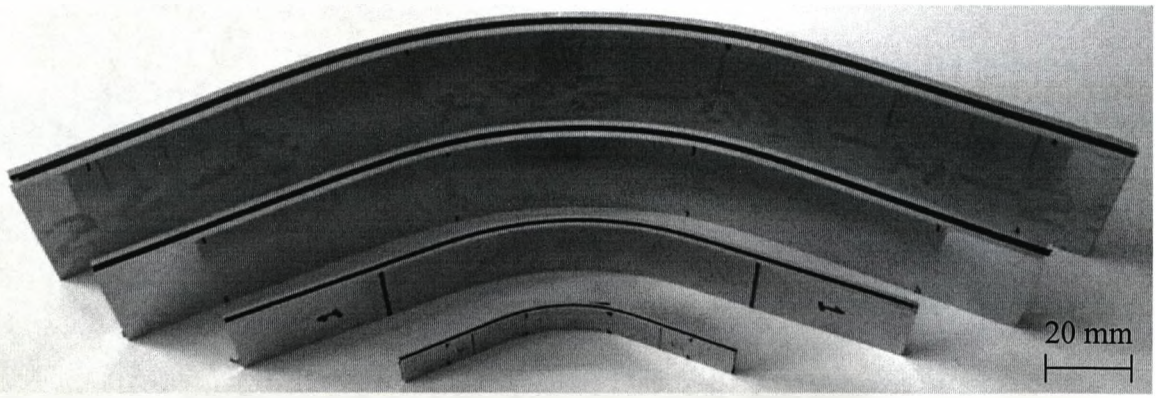

Figure 4.70. Photograph showing the 3D scaled [Al_n, 0°/90°$_n$]$_s$ FMLs following flexural testing.

4.3.2 Flexural Test Data for the 3D Ply-Level Scaled $[Al_n, +/-45°_n]_s$ FMLs and their Constituents

The maximum flexural stress data for the $[Al_n, +/-45°_n]_s$ FML specimens are shown in Figure 4.71. Included in the graph are the values for the scaled aluminium samples for purposes of comparison, where as explained earlier, the aluminium specimens did not have the same span/thickness ratio as the FMLs during the tests (see Section 4.3.1), yielding lower strength values as those observed in tension. As observed previously in Figure 4.65 for the $[Al_n, 0°/90°_n]_s$ FMLs and the aluminium samples, the highest value of stress recorded here was 164 MPa for the ½ scale size and the lowest was 142 MPa for the full scale size. It is important to note that, the maximum stress data were very similar for both, the $[Al_n, 0°/90°_n]_s$ and the $[Al_n, +/-45°_n]_s$ FMLs, with increasing the scale size, highlighting the lack of influence that the SRPP composite had in this study.

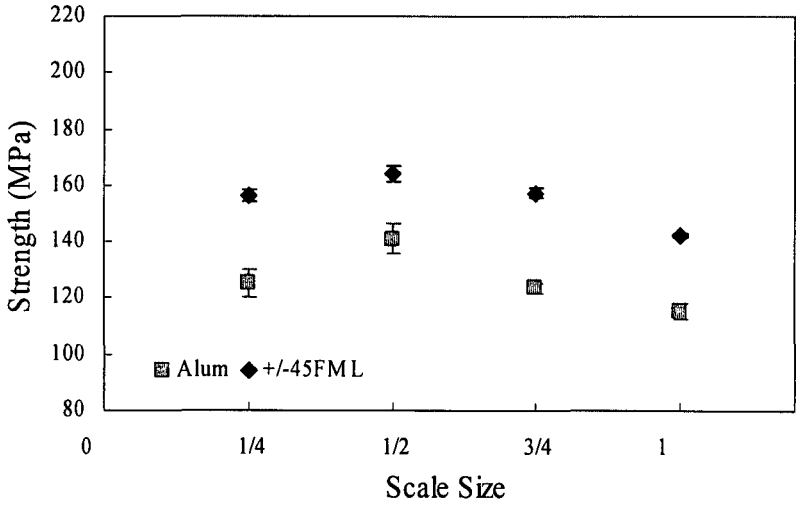

Figure 4.71. Average values of maximum stress for the 3D scaled $[Al_n, +/-45°_n]_s$ FMLs following flexural testing.

Yield stress values for the $[Al_n, +/-45°_n]_s$ FMLs tested in flexure are presented in Figure 4.72. Included in the figure are the tensile yield stress data for the $[Al_n, +/-45°_n]_s$ FMLs. A comparison of both configurations indicates that the data follow similar trends with increasing scale size. This trends in the data for the FMLs, results from the influence of the different aluminium alloys used in this study, as discussed previously (see Figure 4.71). This aluminium influence is removed using the normalisation technique presented later in this chapter.

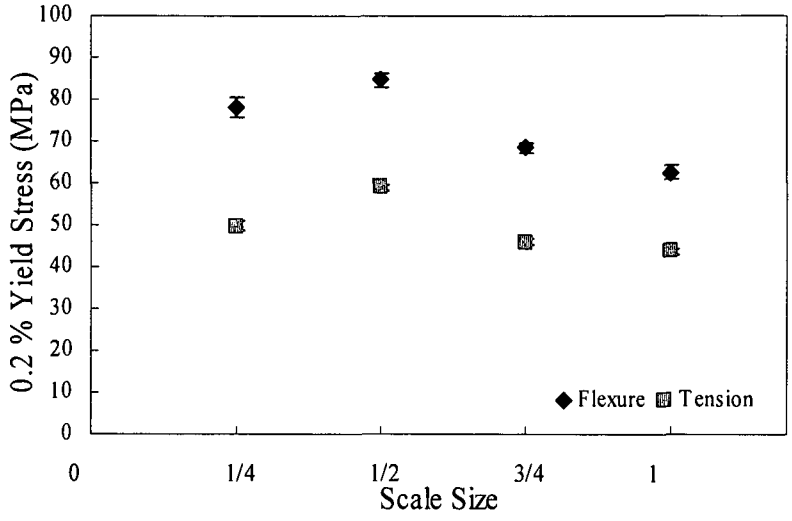

Figure 4.72. Comparison of yield stress data for the 3D scaled $[Al_n, +/-45°_n]_s$ FML specimens tested in flexure and tension.

Figure 4.73 shows the strain data at maximum stress for the 3D scaled $[Al_n, +/-45°_n]_s$ FMLs in flexure. Here, no significant variation in strain is evident, with the average flexural strain for the scaled specimens being approximately 1.9%, this value being very similar to that measured on their $[Al_n, 0°/90°_n]_s$ counterparts (see Figure 4.67). It is clear that this strain value does not change significantly between the two FML configurations under flexural loading conditions.

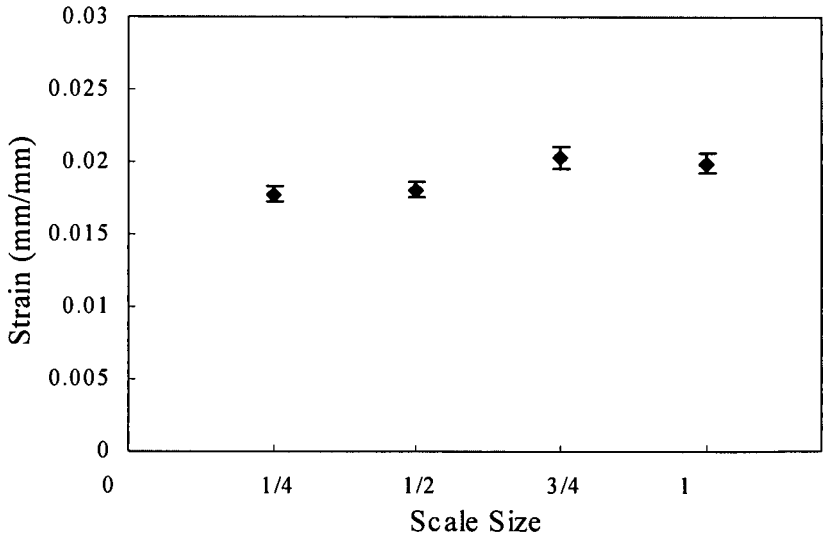

Figure 4.73. Average values of strain to maximum stress for the 3D scaled [Al_n, +/-45°$_n$]$_s$ FMLs following flexural testing.

Figure 4.74 shows the flexural modulus data for the 3D scaled [Al_n, +/-45°$_n$]$_s$ FMLs following flexural testing. The average flexural modulus for the scaled specimens is approximately 65 GPa.

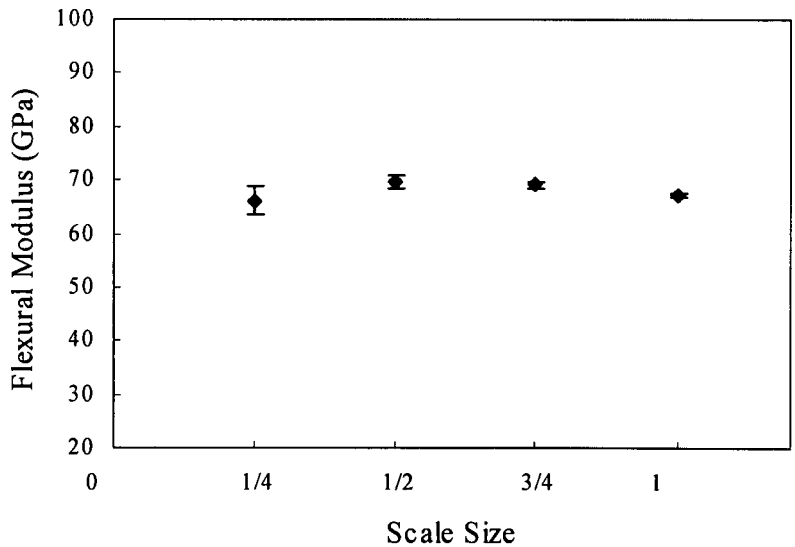

Figure 4.74. Average values of flexural modulus for the 3D scaled [Al_n, +/-45°$_n$]$_s$ FMLs following flexural testing.

This value is similar to that determined on the $[Al_n, 0°/90°_n]_s$ FMLs, where no significant variation in stiffness was observed. This agrees with the findings of other authors who showed that modulus appeared to be independent of specimen size [**19**].

4.3.2.1 Normalisation of the Yield Stress Data for the 3D Ply-Level Scaled $[Al_n, +/-45°_n]_s$ FMLs

Figure 4.75 shows the normalised values of the yield stress for the $[Al_n, +/-45°_n]_s$ FMLs. Here, the normalised yield stress decreases with increasing the scaled specimens, with the full scale samples being approximately 9% lower than the baseline value. It is interesting to note that no significant differences were observed between the two FML configurations studied here (see Figure 4.69). This lack of variation can be attributed to the fact that the outermost layers of the FMLs are based on aluminium which was the same in both configurations. Previous work on a carbon/epoxy system has shown that varying the fibre orientation in samples subjected to bending, significant scaling variations can be observed [**19**].

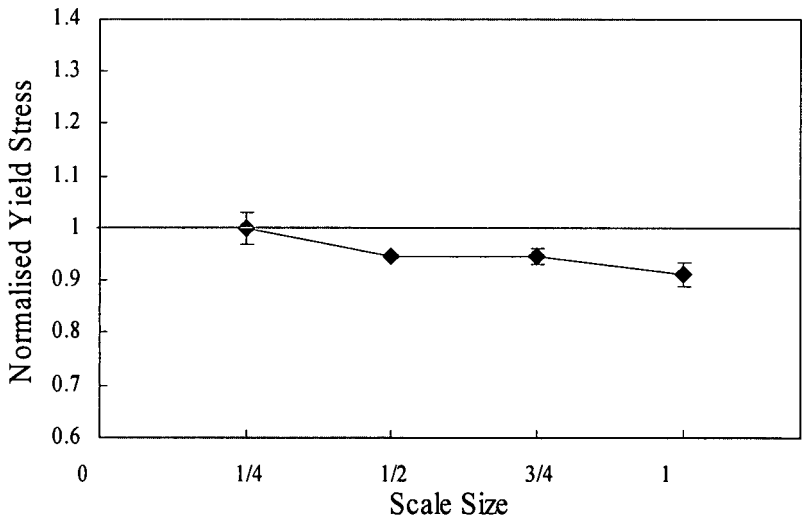

Figure 4.75. Normalised yield stress for the 3D scaled $[Al_n, +/-45°_n]_s$ FMLs following flexural testing.

4.3.2.2 *Optical Examination of the 3D Ply-Level Scaled [Al_n, +/-45°$_n$]$_s$ FMLs*

Figure 4.76 shows a photograph of the [Al_n, +/-45°$_n$]$_s$ FML specimens following flexural testing. As can be seen, none of the constituent materials in the FMLs exhibit any form of failure in this scaling study. Representative tested samples were sectioned transversally to highlight any damage, where no sign of failure was observed, as shown previously in Figure 4.12.

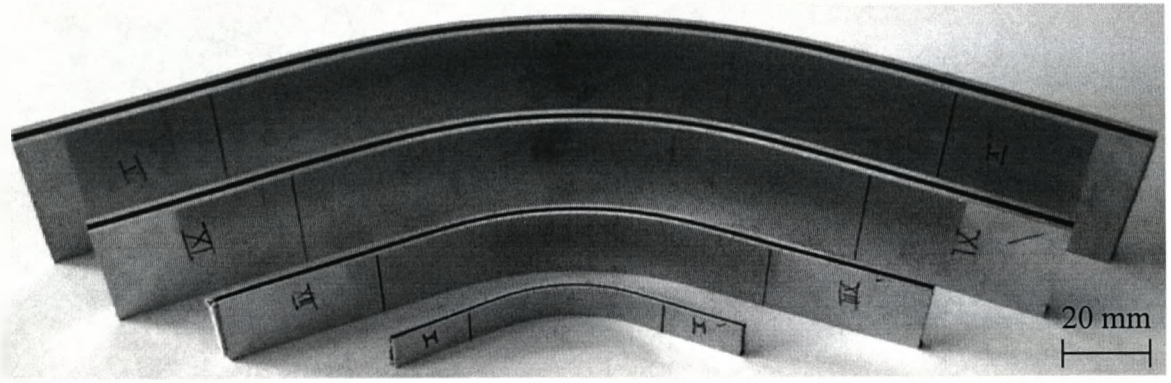

Figure 4.76. Photograph showing the 3D Scaled [Al_n, +/-45°$_n$]$_s$ FMLs following flexural testing.

4.3.3 Summary of the Flexural Scaling Study

This part of the research programme investigated scaling effects in the flexural behaviour of 3D ply-level scaled specimens based on two fibre orientations, these being [Al_n, 0°/90°$_n$]$_s$ and [Al_n, +/-45°$_n$]$_s$. These tests were conducted in order to identify size effects in bending and to directly compare the data to results generated in tension. Here, values of yield stress were used to investigate scaling effects in the four scaled specimens. FML samples with their fibres oriented at (0°/90°) to the loading direction did not show any clear scaling effect with the exception of the full-scale samples which showed a slight decrease relative to the baseline value. In the case of FML samples based on (+45°/-45°) fibres, a more pronounced size effect was observed, with the full-scale samples showing a 9% decrease in strength relative to the baseline value.

4.4 Low Velocity Impact Tests on the Scaled FMLs

The impact responses of the four scale-model sizes of fibre-metal laminates were compared to scaling laws that predict a response based on a simple geometrical relationship of scaled input parameters (see Table 3.10). Simply-supported scaled plates were subjected to low velocity impact loading in order to investigate scaling effects in the process of damage development in the ply-level and the sublaminate-level FML configurations.

The following sections consider the impact response of the FMLs subjected to two scaled impact energies, these being $302n^3$ and $403n^3$ Joules. These two energies were selected since they correspond to energies below and just above those required to initiate external, visible fracture in the FMLs.

4.4.1 Low Velocity Impact Tests on FML Plates Scaled at a 3D Ply-Level

The velocity-time traces obtained from the laser-Doppler velocimeter were converted into displacement-time traces through an integration procedure, and this information was combined with the load-cell data to generate load-displacement traces, similar to those shown in Figure 4.77. Here, a comparison of the four scaled ply-level plates impacted at a constant impact energy of $302n^3$ Joules (equivalent to an impact mass of $22.46n^3$ kg) are presented. From the figure, it is evident that the panels exhibit some recovery at the end of the test, indicative of an elastic response in the aluminium and composite plies. It is worth nothing that none of these specimens showed external damage after the impact test. The residual displacement in the figure is therefore due to plastic deformation in the metal and composite plies. Similar results were observed by McKown *et al.* [**31**] where a 2/1 aluminium/composite FML configuration was investigated. The load-displacement trace for the largest specimen (n = 1) exhibits some initial oscillatory behaviour due to ringing in the load cell, an effect that can be reduced using a damping system [**32**].

Previous work on scaling the low velocity impact response of composites [**33,34**] has shown that the impact force should scale as 'n^2' and the resulting plate deflection as 'n'. Scaling effects in the force-displacement traces were therefore investigated by dividing the impact force by the square of the corresponding scale size, (F/n^2), and the

impact displacement by the scale size, (Δ/n), thereby enabling a direct comparison of the responses of the different scale sizes.

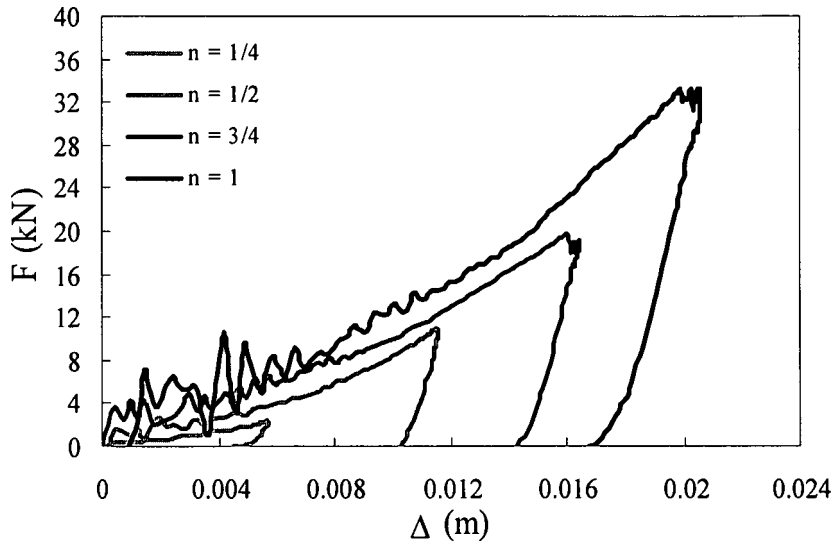

Figure 4.77. Impact force vs. displacement traces for ply-level scaled specimens struck by a hemispherical impactor. Energy = $302n^3$ Joules.

Figure 4.78 shows the resulting normalised force-displacement curves for the ply-level specimens shown previously in Figure 4.77. An examination of the figure indicates that all of the normalised traces are very similar in appearance, collapsing onto what appears to be a single unique trace, suggesting that the FMLs obey a simple scaling law. These findings are similar to those observed by Wen and Jones **[33]** following drop-weight impact tests on steel and aluminium plates, where normalised load-displacement traces from impact tests on four scaled plates were found to exhibit a high level of coincidence.

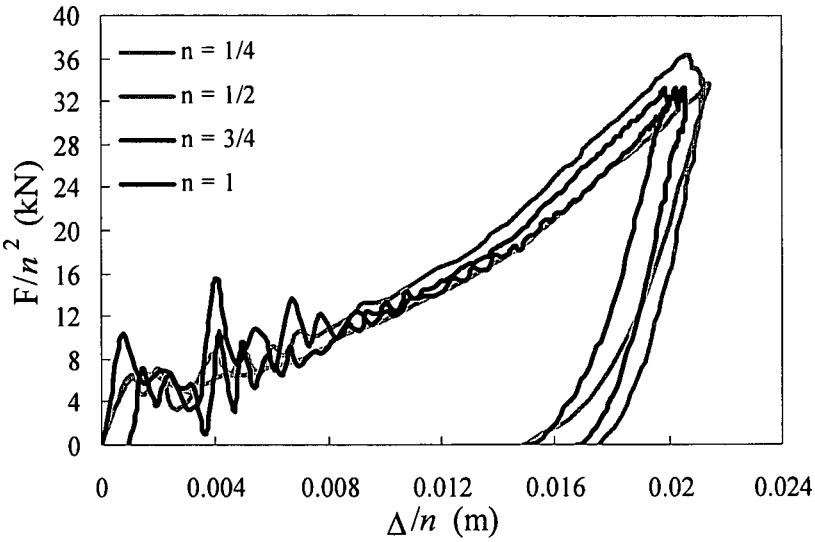

Figure 4.78. Normalised impact force vs. displacement traces. Energy = $302n^3$ Joules.

Table 4.3 presents the average values of the maximum impact force, the maximum displacement and the time duration (see Section 4.1.5) following tests on the scaled plates at an impact energy of $302n^3$ Joules. Included in the table are the predicted values of the plate tests. Following the impact tests, the ply-level scaled plates were examined by eye in order to highlight any external damage.

Scale size ***n***	Force ***F*** (kN)	Predicted force F_P (kN)	Impact displ. Δ (mm)	Predicted displ. Δ_P (mm)	Impact time ***t*** (msec)	Predicted time t_P (msec)
¼	2.2	2.2	4.92	4.92	1.62	1.62
½	9.3	8.8	9.6	9.84	3.07	3.24
¾	17.7	19.8	14.74	14.76	4.57	4.86
1	29.5	35.2	18.53	19.68	5.82	6.48

Table 4.3. Impact data for ply-level scaled plates with an impact energy of $302n^2$ Joules.

Similarly, the resulting data for the scaled plates tested at $403n^2$ Joules are presented in Table 4.4. The force data for the full-scale plate was tested without using the load cell, since it was only capable of measuring loads up to 35 kN.

Scale size n	Force F (kN)	Predicted force F_P (kN)	Impact displ. Δ (mm)	Predicted displ. Δ_P (mm)	Impact time t (msec)	Predicted time t_P (msec)
¼	2.4	2.4	5.52	5.52	1.35	1.35
½	11.37	9.6	10.47	11.04	2.9	2.7
¾	19.66	21.6	14.62	16.56	4.2	4.05
1	--	38.4	20.38	22.08	5.35	5.4

Table 4.4. Impact data for ply-level scaled plates with an impact energy of $403n^2$ Joules.

Figure 4.79 shows a photograph of the scaled plates subjected to an impact energy of $302n^3$ Joules, where damage resulting from the low velocity impact tests can be clearly seen. Here, permanent deformation is in evidence although no external fracture is apparent at any scale size.

Plates tested at $403n^3$ Joules show a similar external appearance to that shown in Figure 4.79. Closer inspection of the plates revealed a region of fracture on the distal side in all specimens. In order to investigate the damage resulting from the impact tests in detail, representative plates were carefully sectioned through the impact area and polished for inspection.

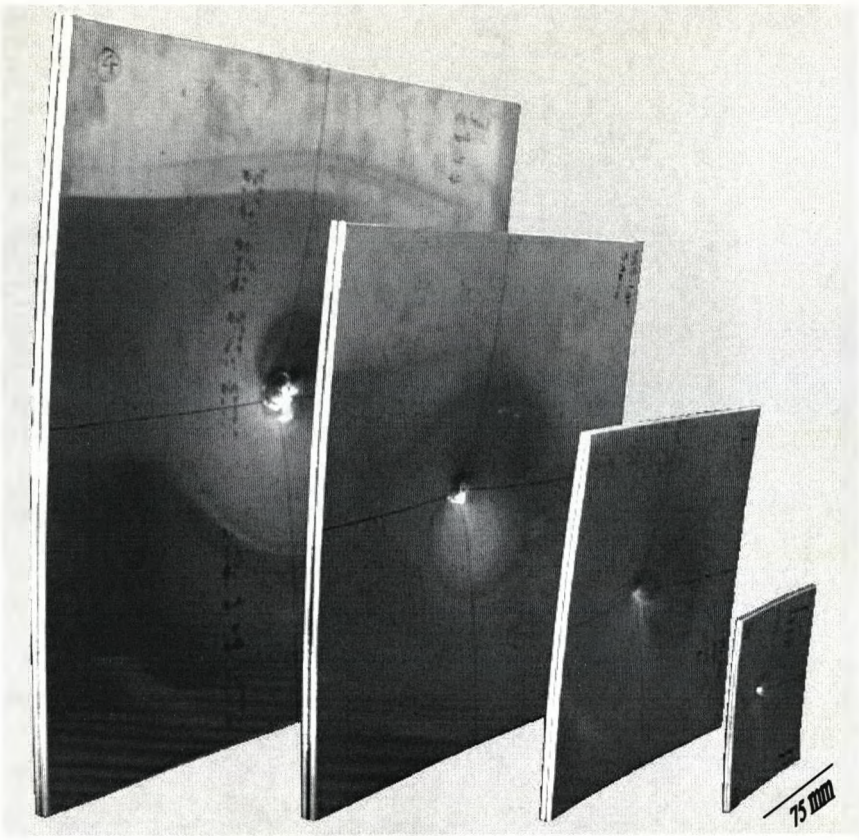

Figure 4.79. FML plates scaled at ply-level following low velocity impact at an energy of $302n^3$ Joules.

A low magnification optical analysis was carried out in order to elucidate the fracture mechanisms during low velocity impact loading. Cross-sections of tested scaled specimens using the ply-level techniques are presented in Figure 4.80. As discussed previously, the impact energy of $302n^3$ Joules did not cause any external visible fracture on the plates. An examination of the scaled specimens indicates that the overall gross plastic deformation in the plates is similar at all four scale sizes. All specimens exhibit localised denting and moderate thinning around the point of impact as well as significant permanent deformation.

The aluminium-composite interface exhibited moderate debonding and delamination in the two largest scaled specimens. In addition, whitening of the interfacial adhesive layer used to bond the composite plies was observed in all specimens at locations away from the point of impact, probably due to shear between the composite layers. In general, damage tended to become more severe as the scale size increased. A closer

examination of the full-scale specimen (see Figure 4.80) indicates that the composite core has failed directly under the point of impact. It is not clear why this localised form of failure has occurred (observed in all plates from the same scale). Clearly, it was not possible to scale the weave structure in the polypropylene composite. As a result, there are a greater number of weave cross-over points in the heavily stressed region under the point of impact in the larger specimens. Given the increase in the number of potential stress-concentrations associated with the weave, there is a greater probability of generating damage in the larger specimens.

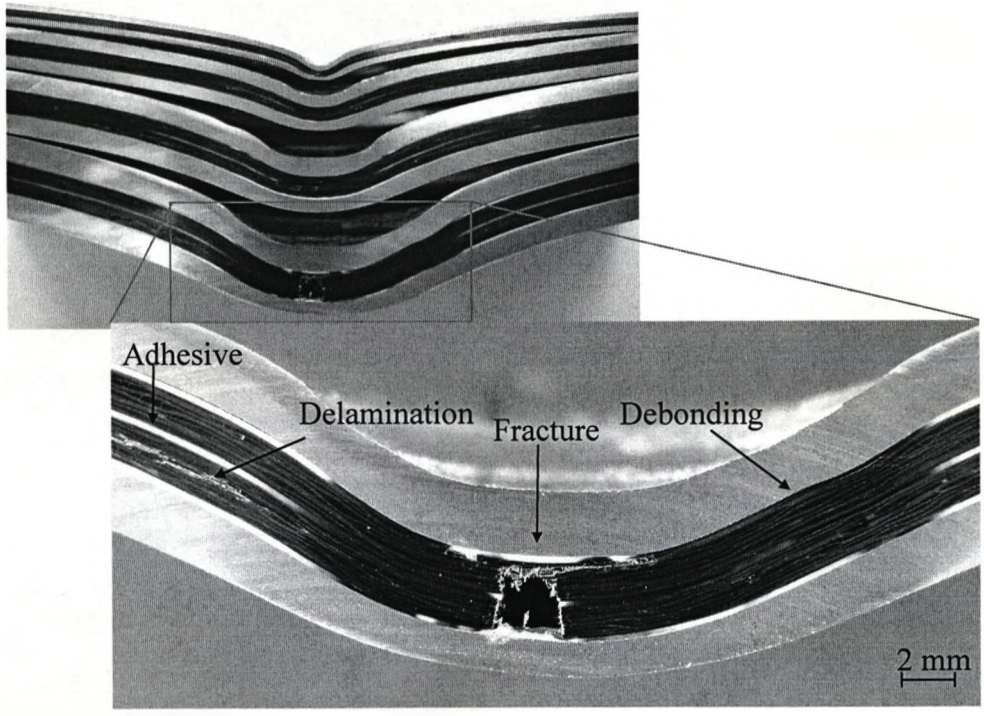

Figure 4.80. Cross-sections of four scaled specimens at ply-level scaling subjected to an impact energy of $302n^3$ Joules.

The cross-sections of specimens subjected to an impact energy of $403n^3$ Joules are presented in Figure 4.81. Here, the incident energy was sufficient to just generate lower surface fracture of the aluminium layer in the FMLs. An examination of the photograph indicates that the level of plastic deformation is similar at all four scale sizes. All specimens exhibit localised denting and thinning around the point of impact and permanent deformation, with fracture in the lowermost aluminium layer. Delamination between the composite plies as well as debonding at the aluminium-composite interface was apparent at all scale sizes. In addition, whitening of the interfacial adhesive layers due to localised shear was observed in all specimens away from the point of impact. Shear failure was observed close to the point of impact, visible in the lowermost aluminium layer, exhibiting a typical 45° fracture [**17**].

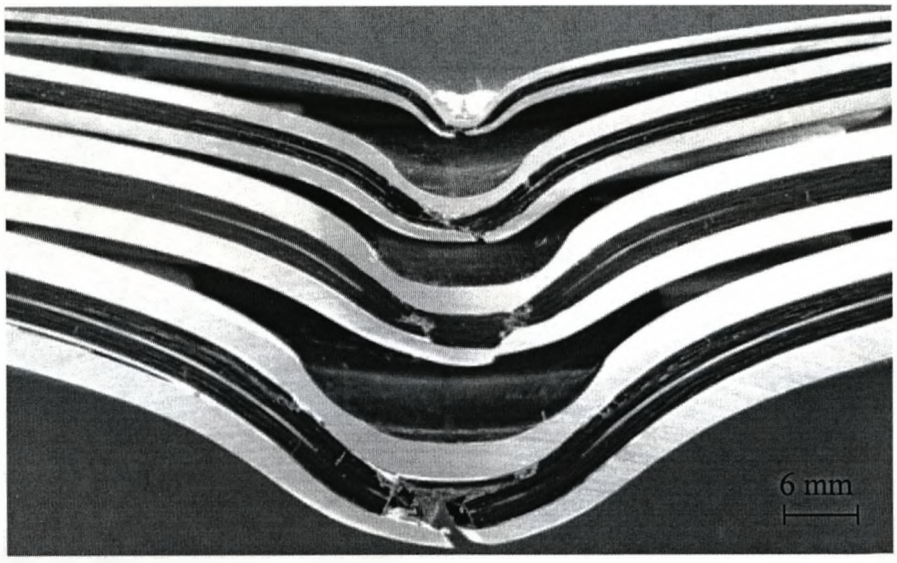

Figure 4.81. Cross-sections of four scaled specimens at ply-level scaling subjected to an impact energy of $403n^3$ Joules.

Figure 4.82 shows a plot of non-dimensional permanent deflection (δ) versus non-dimensional impact energy (χ), using Equation 3.26 for plates scaled at ply-level, as follows:

$$\chi = \frac{E}{\sigma_y d^3}$$

Unfortunately, much of the data in these figures is at higher non-dimensional impact energies, with there being less at lower energy conditions. Nevertheless, an examination of the figures indicates that both sets of data appear to exhibit unique trends with the data collapsing onto straight line. Similar observations were made by Wen and Jones following low velocity impact tests on steel plates [**33**]. It is worth nothing that the intercept of the trendlines occurs at a positive value of displacement. Clearly, this cannot be the case and the curves must deviate from linearity at lower energies. The evidence in Figure 4.82 again supports the conclusion that the FML plates obey a simple scaling law.

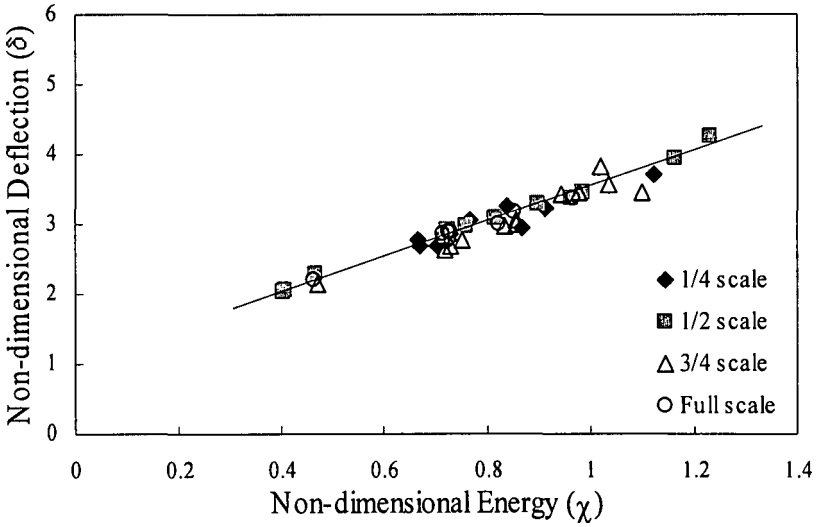

Figure 4.82. Variation of the non-dimensional permanent deflection with non-dimensional impact energy following low velocity impact tests on FMLs scaled at a ply-level.

4.4.2 Low Velocity Impact Tests on FML Plates Scaled at a 3D Sublaminate-Level

Force-displacement traces following impact on plates scaled at a sublaminate-level are shown in Figure 4.83. These traces were obtained following the procedure outlined in Section 4.4.1 for ply-level plates. Here, impact energies of 4.7, 37.7, 127 and 302 Joules corresponding to ¼, ½, ¾ and 1 respectively were used. Similar trends to those observed in ply-level scale samples are apparent. Again, the panels exhibit some recovery at the end of the tests, indicative of an elastic response in the aluminium and composite plies. The plates did not exhibit any external fracture at this impact level. Similitude laws were employed in the force-displacement curves to generate a graph (see Figure 4.84) that enables a direct comparison between the scaled impact tests.

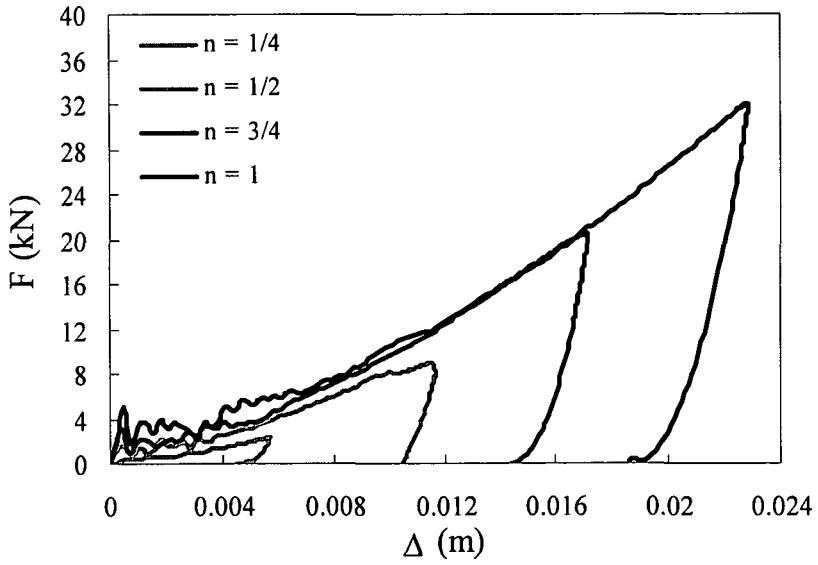

Figure 4.83. Impact force vs. displacement traces for sublaminate-scaled specimens struck by a hemispherical impactor. Energy = $302n^3$ Joules.

Figure 4.84 shows the resulting normalised force-displacement curves for representative sublaminate-level plates. Similarly to the traces associated with ply-level scaling shown in Figure 4.78, these traces appear to follow a similar trend. In all scaled plates, large permanent deformation was observed following testing, a consequence of large level of plasticity occurring during the impact event.

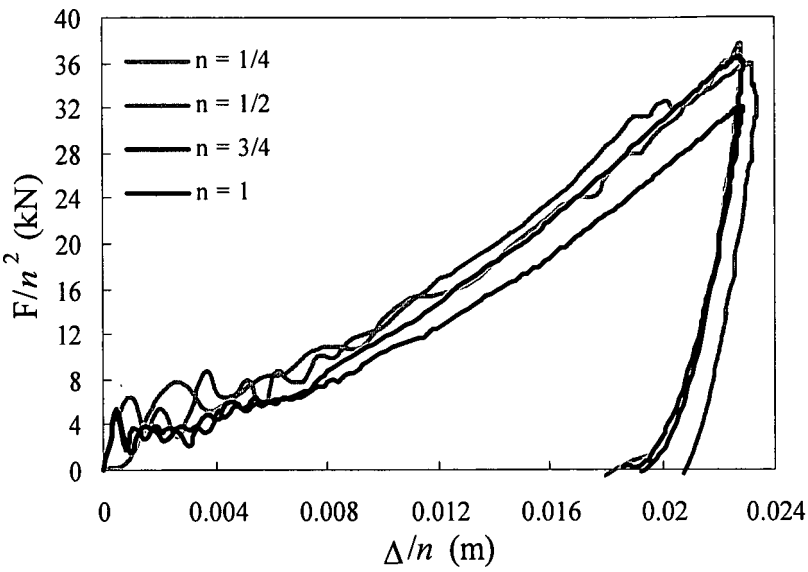

Figure 4.84. Normalised impact force vs. displacement traces for the sublaminate-scaled specimens. Energy = $302n^3$ Joules.

Table 4.5 presents the average values of the maximum impact force, the maximum displacement and the time duration following tests on the scaled sublaminate-plates at an impact energy of $302n^3$ Joules. Included on the table are the predicted values of the sample tests. Following the impact tests, the sublaminate-level scaled plates were examined by eye in order to highlight any external damage.

Scale size n	Force F (kN)	Predicted force F_P (kN)	Impact displ. Δ (mm)	Predicted displ. Δ_P (mm)	Impact time t (msec)	Predicted time t_P (msec)
¼	2.2	2.2	4.92	4.92	1.62	1.62
½	9.7	8.8	9.52	9.84	3.27	3.24
¾	17.9	19.8	14.12	14.76	4.5	4.86
1	31.7	35.2	19.94	19.68	6.6	6.48

Table 4.5. Impact data for the sublaminate-level scaled plates following an impact energy of $302n^2$ Joules.

The corresponding average values for the sublaminate-level plates impacted at $403n^2$ Joules are presented in Table 4.6. Similar to ply-level scaling, the full-scaled plates were tested without the use of the load cell. The load cell limit was 35 kN while predictions suggested that the maximum impact force would be 38.4 kN.

Scale size n	Force F (kN)	Predicted force F_P (kN)	Impact displ. Δ (mm)	Predicted displ. Δ_P (mm)	Impact time t (msec)	Predicted time t_P (msec)
¼	2.4	2.4	5.52	5.52	1.35	1.35
½	10.55	9.6	9.32	11.04	2.7	2.7
¾	19.23	21.6	14.59	16.56	3.9	4.05
1	--	38.4	19.46	22.08	5.4	5.4

Table 4.6. Impact data for the sublaminate-level scaled plates following an impact energy of $403n^2$ Joules.

A photograph of the sublaminate-level-scaled plates subjected to an impact energy of $302n^3$ Joules is shown in Figure 4.85, where the damage resulting can be clearly seen. Similar to the ply-level plates at this energy, no apparent external damage is in evidence. The second group of plates tested at an impact energy of $403n^3$ Joules, shows similar features to those tested at $302n^3$, as shown in Figure 4.85. Damage in $403n^3$ Joules panels took the form of fracture of the aluminium layers on the distal surface of the plates. After impact, the plates subjected to energies of $302n^3$ and $403n^3$ Joules were carefully sectioned through the impact area and polished for inspection.

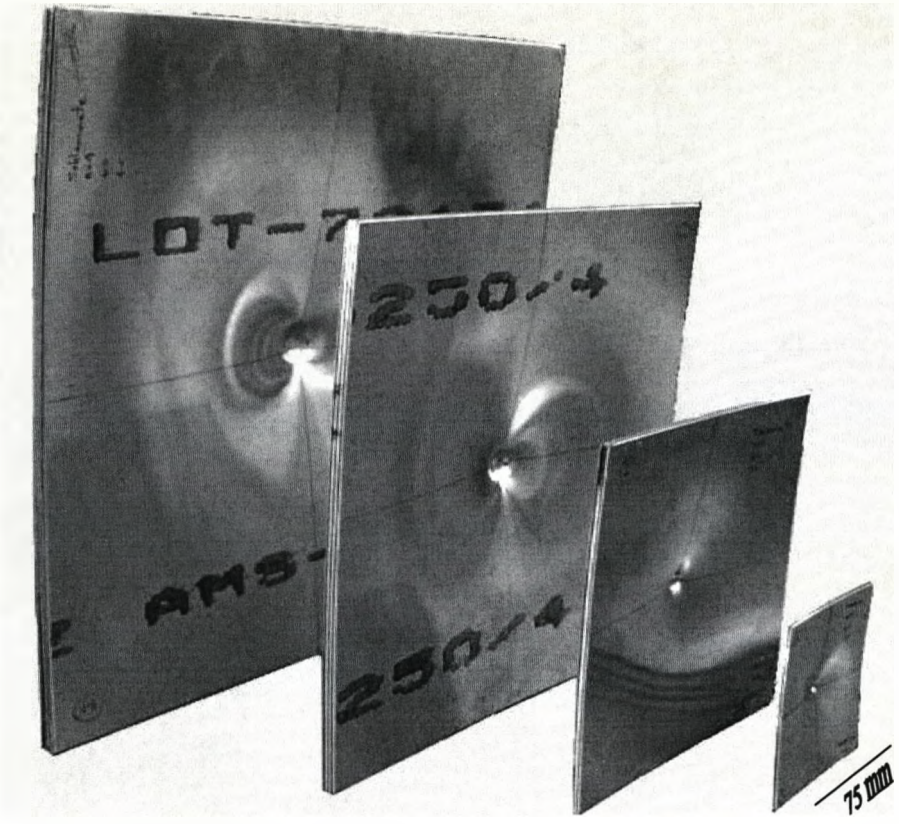

Figure 4.85. FML plates scaled at sublaminate-level following low velocity impact at an energy of $302n^3$ Joules.

Figure 4.86 shows the cross-sections of four sublaminate-level specimens tested under the same impact conditions as the ply-level specimens in Figure 4.80 ($302n^3$ Joules). Once again, the plates exhibit significant plastic deformation without incurring fracture in the outermost aluminium layers. Here, delamination between composite plies was not apparent, although whitening of the interfacial adhesive layers was observed in all specimens around the point of impact. The mean value for the maximum residual displacement was similar in both systems (19.46 mm for the full-scale sublaminate-level plate versus 18.53 mm from its ply-level counterpart). Closer inspection of the full-scale sublaminate specimen shown in Figure 4.86, highlights greater levels of damage to the lowermost composite ply. This observation agrees with that made in the largest ply-level specimen shown in Figure 4.80.

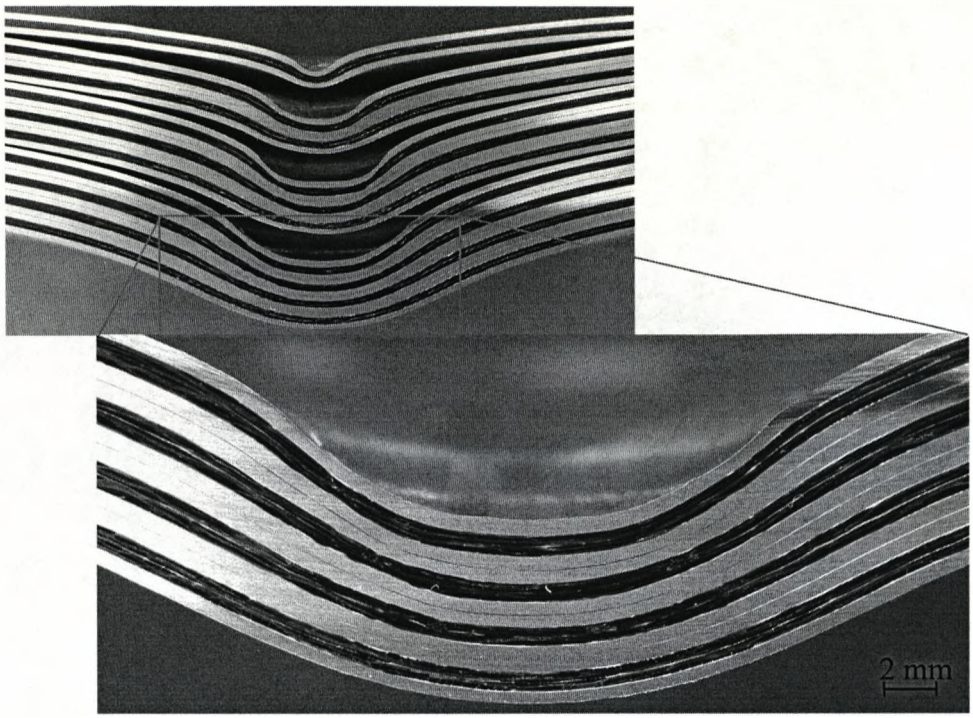

Figure 4.86. Cross-sections of four specimens scaled at a sublaminate-level subjected to an impact energy of $302n^3$ Joules.

Figure 4.87 shows cross-sections of four specimens scaled at a sublaminate-level following impact at $403n^3$ Joules, (these being similar to those tested in Figure 4.81).

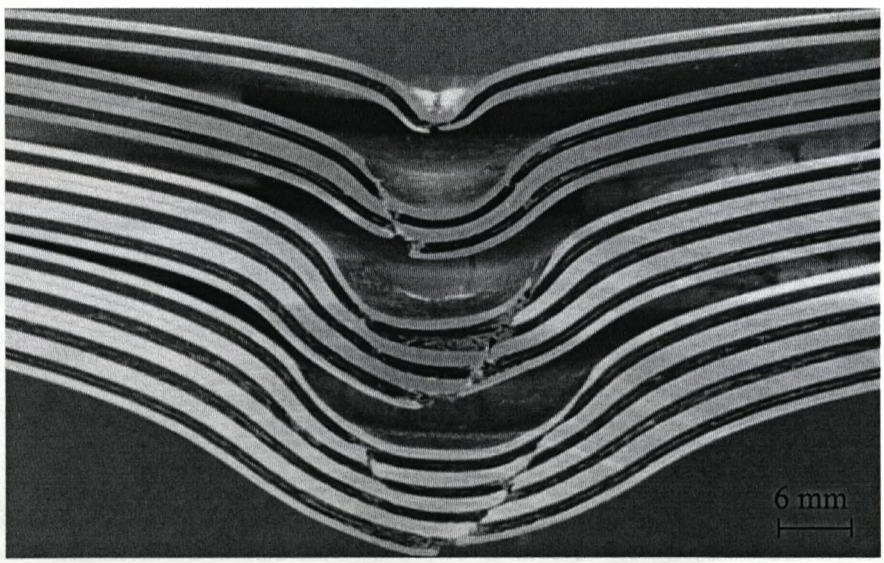

Figure 4.87. Cross-sections of four scaled specimens at a sublaminate-level following an impact energy of $403n^3$ Joules.

An examination of the cross-sections highlights significant plastic deformation as well as fracture in their outermost aluminium layers. Delamination between the composite plies was observed in all four specimen sizes. As with the ply-level scaled specimens, composite fracture was observed in all scale sizes and a distinct zone of shear fracture was evident extending through the thickness of the laminate, close to the point of impact. Closer inspection of the full scale specimens highlights the areas where the adhesive layers failed, generating a debonded region between the composite layers in the impacted zone. Here, a 45° shear fracture similar to that observed in the ply-level specimens is apparent. It is worth nothing in Figure 4.87, that whereas delamination was present between the composite plies, no such interfacial failure was in evidence between the bonded metal layers, suggesting that the degree of adhesion was greater across the adhesive-metal interface than across the composite laminae.

Non-dimensional deflection data versus non-dimensional impact energy are shown in Figure 4.88 for the sublaminate-scaled plates. Here, the data appear to lie on a straight line.

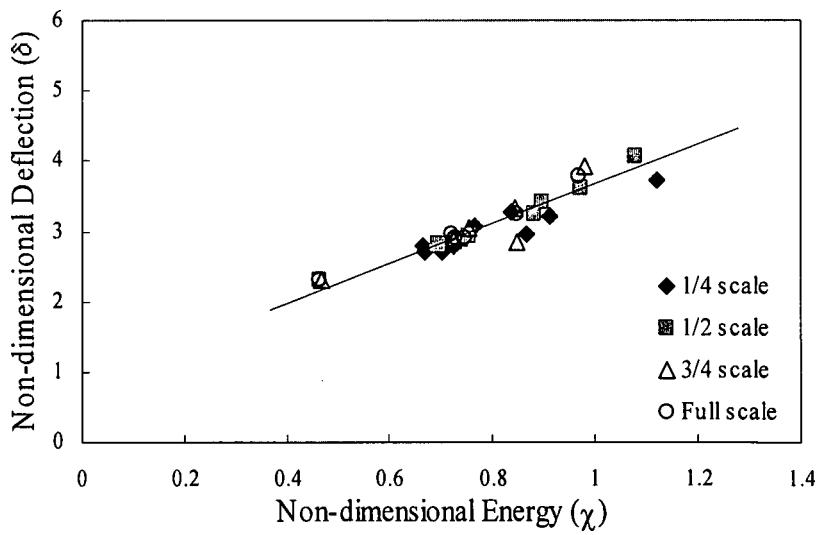

Figure 4.88. The variation of the non-dimensional permanent deflection with non-dimensional impact energy following low velocity impact tests on FMLs scaled at a sublaminate-level.

The specimens were tested at impact energies that generated local indentations up to the perforation threshold of the plate. It is interesting to note that the slope of both the ply-level (see Figure 4.82) and the sublaminate-level traces are almost identical, suggesting that both sets of laminates exhibit a very similar response. Again, as observed previously with the ply-level samples, the intercept of the trendline does not pass through zero. It is believed that at small indentation values, the trendline deviates from linearity due to the elastic response of the FML plates.

4.4.2.1 Comparison of the Normalised Impact Data for the 3D Ply-Level and Sublaminate-Level FML Plates

Figure 4.89 shows the average values of the maximum force for the two types of laminates, plotted in a normalised form relative to the ¼ scale laminate. From the figure, it is apparent that both sets of data exhibit similar trends with the ½ scale values being greater than unity and those for the two largest scale sizes being below the ¼ specimen value (approximately 10%). It is believed that these variations in the impact force are due to scatter in the experimental data rather than any true scaling effect. Interestingly, Wen and Jones [**35**] observed very similar trends to those shown in Figure 4.89 following drop-weight impact testing on scaled steel plates.

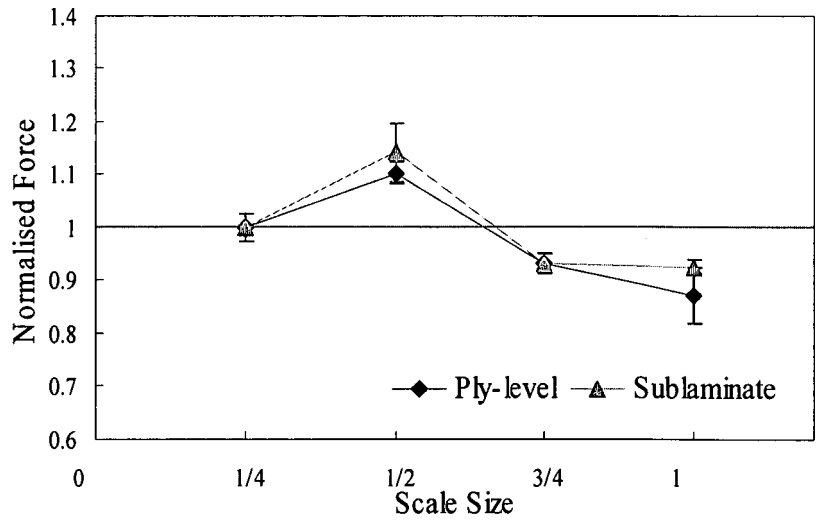

Figure 4.89. The variation of the normalised maximum force versus scale size for the two stacking configurations following impact tests at energies below the damage threshold. Energy = $302n^3$ Joules.

Normalised impact forces at an energy of $403n^2$ Joules are presented in Figure 4.90. The figure shows a comparison of the ½ and ¾ scales relative to the baseline, where it is evident that the plates subjected to this impact energy appears to follow the same trend as those tested at an impact energy of $302n^3$ Joules (corresponding to the specimens tested below the fracture threshold). It was not possible to undertake the tests on the full-scale plates due to the limitations associated with the load cell as discussed earlier.

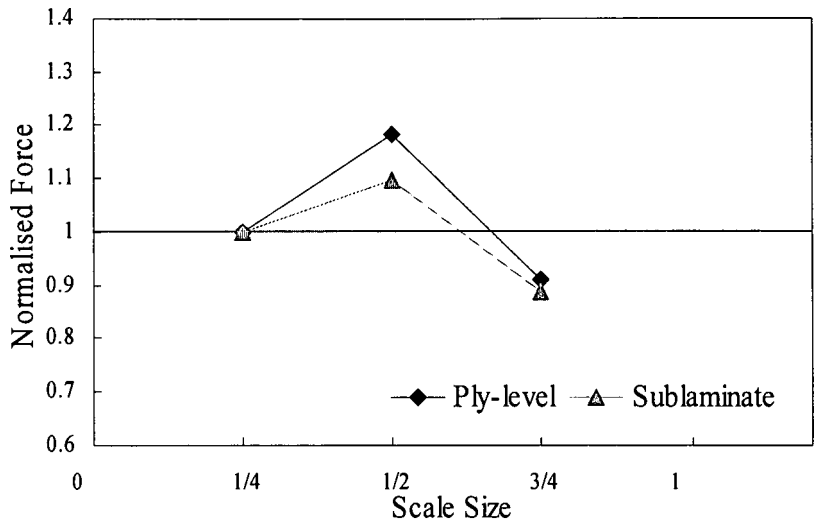

Figure 4.90. The variation of the normalised maximum force versus scale size for the two stacking configurations, following impact tests at the normalised damage threshold energy. Energy = $403n^3$ Joules.

The level of permanent indentation in the impacted plates was measured directly from the force-displacement traces such as those shown in Figures 4.77 and 4.83. Figure 4.91 compares the normalised values of the maximum permanent deflection of both the ply-level and sublaminate-level scaled FMLs following impact tests at an energy of $302n^3$ Joules. Here, the maximum displacement at each scale size (Δ) is divided by the predicted displacement (Δ_p), calculated from the response of the smallest scale specimen. An examination of the figure indicates that neither technique exhibits any significant scaling effect, with the maximum degree of deviation being less than 10% relative to the ¼ scale value.

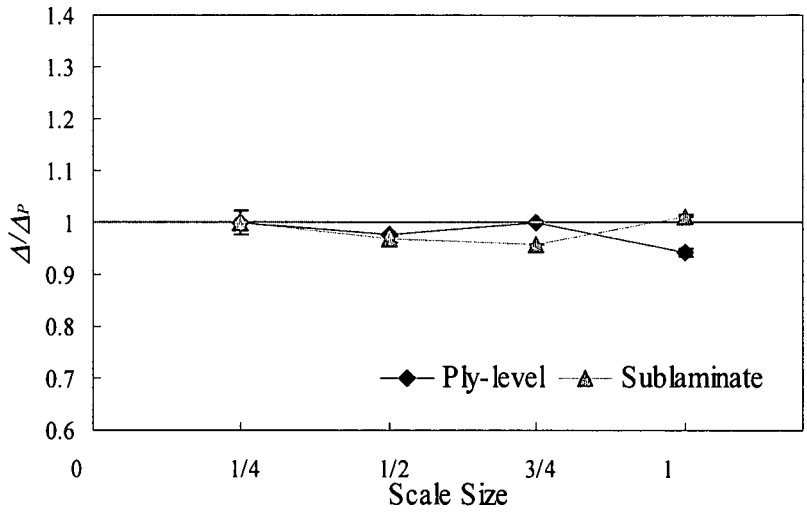

Figure 4.91. Normalised values of the residual displacement versus scale size for ply-level and sublaminate-level scaled specimens following an impact energy of $302n^3$ Joules.

If the impact-loaded FMLs obey a simple scaling law, then impact events should scale with the scale size (n) [**34**]. In this study, the time for the impact force to reach its maximum value was employed to investigate scaling effects in the impact response. Figure 4.92 shows the normalised values of the time to maximum force for both, the ply-level and sublaminate-level scaled specimens. Here, the impact duration (t) is normalised by the predicted impact duration (t_P), calculated from the smallest scale specimens. From the figure, it is evident that the impact duration of the larger ply-level specimens is slightly lower than that predicted from the ¼ scale specimen. However, these differences are relatively small (approximately 10% for the maximum scale size). This evidence again suggests then, that the impact response of the FMLs obeys simple geometric scaling laws. Similar effects have been observed following tests on a carbon fibre/epoxy system [**36**], where no significant scaling effect was observed in the impact duration.

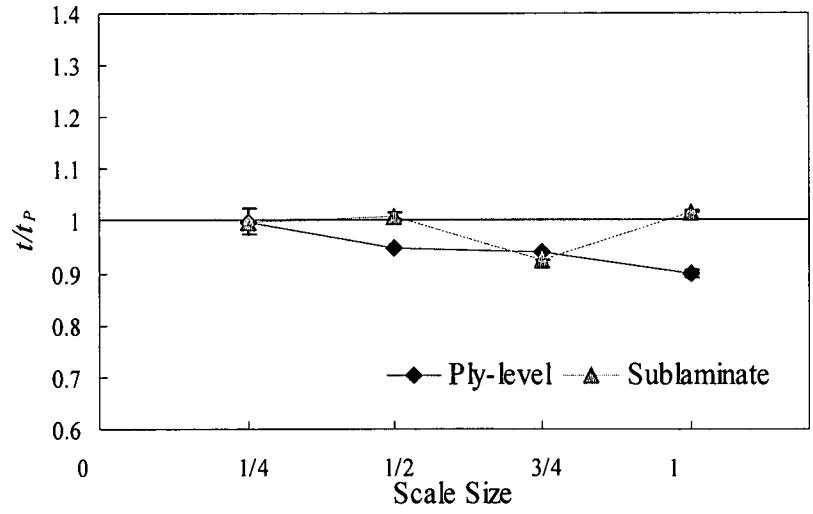

Figure 4.92. Normalised values of time to maximum force versus scale size for ply-level and sublaminate-level scaled specimens following an impact energy of $302n^3$ Joules.

Figure 4.93 compares the normalised values of the deflection at maximum force for both the ply-level and sublaminate-level scaled FMLs following impact at an energy of $403n^3$ Joules. An examination of the figure shows that neither technique exhibits any significant scaling effect. A closer inspection of the figure indicates that the permanent deflection in both sets of data show a tendency to decrease with increasing specimen size, with the largest scale size being approximately 12% lower than the baseline value. However, this effect is not considered to be significant.

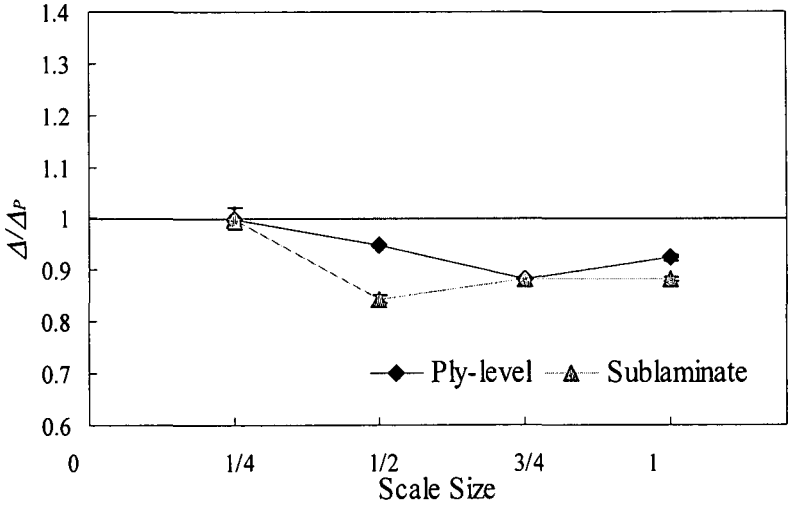

Figure 4.93. Normalised values of the residual displacement versus scale size for ply-level and sublaminate-level scaled specimens following an impact energy of $403n^3$ Joules.

Figure 4.94 shows the normalised values of the time to maximum force for both the ply-level and sublaminate-level scaled specimens using a scaled impact energy of $403n^3$ Joules. Here, the impact duration (t) is normalised by the predicted impact duration (t_P), calculated from the smallest scale specimens. From the figure, it is evident that neither technique exhibits any significant scaling effect, this being similar to the observations made at the lower impact energy ($302n$ Joules).

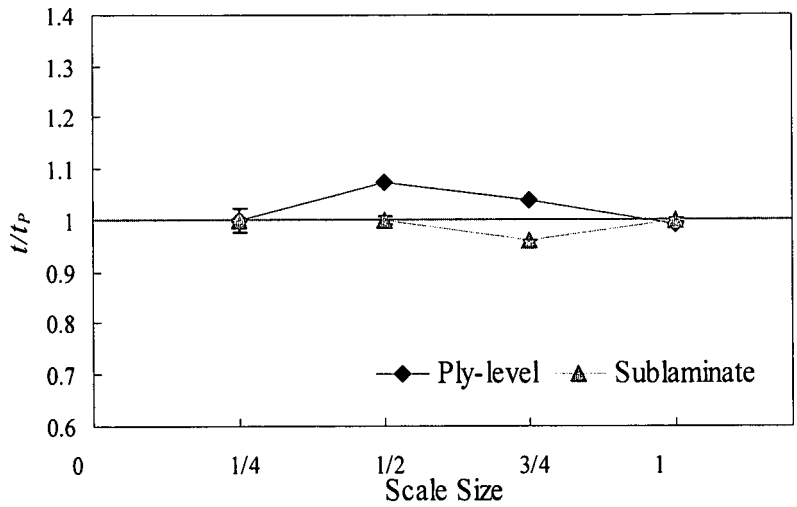

Figure 4.94. Normalised values of time to maximum force versus scale size for ply-level and sublaminate-level scaled specimens following an impact energy of $403n^3$ Joules.

Although the impact energy of $403n^3$ Joules was found to be close to the threshold for rear-surface damage, the incident energy of the projectile was subsequently varied to accurately determine the damage threshold.

Figure 4.95 shows normalised values of impact energy for both the ply-level and the sublaminate-level scaled specimens. Here, the impact energy was varied in order to determine the first damage threshold and identify any scaling effect during the scaling process. Some differences were observed for the ½ scale ply-level specimen (less than 20%) although no significant variation was observed in the two largest specimens. It is interesting to note that the response of the largest specimen is almost identical to that of its smallest counterpart, in spite of the fact that damage to the inner composite core was found to be more severe in the former.

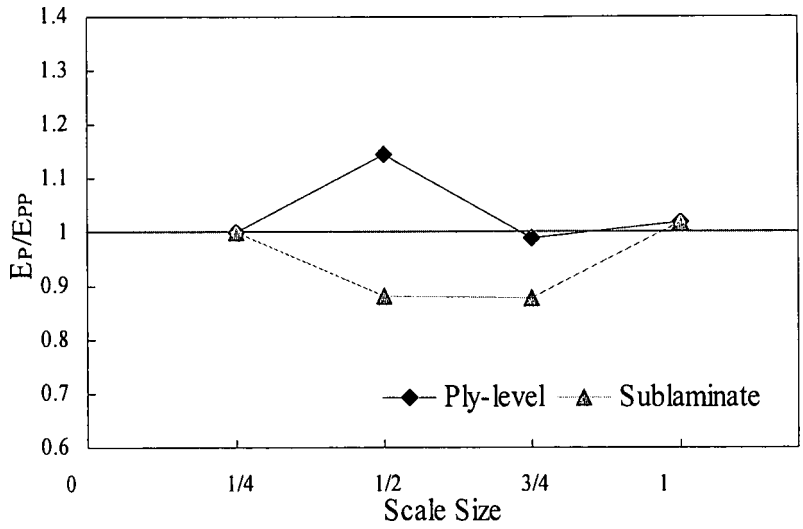

Figure 4.95. Normalised impact energies for damage initiation as a function of scale size.

4.4.3 Summary of Scaling Effects under Low Velocity Impact Loading

This part of the research investigation focused on investigating scaling effects in the impact response of 3D-scaled plates, scaled at both ply-level and sublaminate-level. Here, the impact response of the FMLs was investigated. Polished cross-sections of both types of FML highlighted failure mechanisms such as thinning and fracture of the aluminium alloy, shear fracture through the thickness of the panels as well as fracture of the composite layers. Damage to the composite layers was found to be more severe in the larger scale sizes, an effect that was attributed to difficulties in scaling the dimensions of the weave. The impact energy to initiate fracture in the FMLs did not exhibit any size dependency. Other test parameters, such as the impact

duration were shown to obey the scaling law, where little deviation from the normalised data was observed (less than 10%), suggesting an impact duration of the form (t/*n*).

4.5 References

1. W D Callister Jr. *Materials Science and Engineering; An Introduction*, John Wiley and Sons, 2005.

2. R B Hilton. *Technology of Engineering Materials*, London; Butterworth Heinemann, 1953.

3. M J Sinnott. *The Solid State for Engineers*, John Wiley and Sons, 1963.

4. Van Lancker. *Metallurgy of Aluminium Alloys*, William Clowes and Sons, 1967.

5. M R Wisnom. *The Relationship between Tensile and Flexural Strength of Unidirectional Composites*. Journal of Composite Materials, 26; 1173-1180, 1992.

6. L Mosse, P Compston, W J Cantwell, and M Cardew. *Stamp Forming of Polypropylene Based Fibre-Metal Laminates: The Effect of Process Variables on Formability*. Journal of Materials Processing Technology, 172; 163-168, 2006.

7. J Gresham, W J Cantwell, M J Cardew, and P Compston. *Drawing Behavior of Metal-Composite Sandwich Structures*. Composite Structures, 75; 305-312, 2006.

8. G Reyes. Processing and Characterisation of the Mechanical Properties of Novel Fibre-Metal Laminates. University of Liverpool. *PhD Thesis* , 2001.

9. A J Kinloch and R J Young. *Fracture Behaviour of Polymers*, Applied Science, 1983.

10. M R Wisnom and J A Atkinson. *Reduction in Tensile and Flexural Strength of Unidirectional Glass Fibre-Epoxy with Increasing Specimen Size*. Composite Structures, 38; 405-411, 1997.

11. T K O'Brien and S A Salpekar. *Scale Effects on the Transverse Tensile Strength of Graphite/Epoxy Composite*. ASTM on Composite Materials, 11; 23-52, 1993.

12. M R A Vliet and J G M Mier. *Experimental Investigation of Size Effects in Concrete and Sandstone under Uniaxial Tension*. Engineering Fracture Mechanics, 65; 165-188, 2000.

13. J E Gibson. *Model Analysis and Similitude Requirements*. In: Small Scale Modelling of Concrete Structures, edited by F A Noor and L F Boswell, Elsevier Applied Science, p. 13-39. 1992.

14. N Jones. *Low Velocity Perforation of Metal Plates*. In: Shock and Impact on Structures, edited by C A Brebbia, p. 53-71. 1994.

15. E Booth, D Collier, and J Miles. *Impact Scalability of Plated Steel Structures*. In: Structural Crashworthiness, edited by N Jones and T Wierzbicki, Butterworths, p. 136-174. 1983.

16. M R Wisnom. *Size Effects in the Testing of Fibre-Composite Materials*. Composites Science and Technology, 59; 1937-1957, 1999.

17. A Tabiei and J Sun. *Analytical Simulation of Strength Size Effect in Composites Materials*. Composites: Part B, 31; 133-139, 2000.

18. P C Powell. *Engineering with Fibre-Polymer Laminates*, Chapman and Hall, 1994.

19. K E Jackson, S Kellas, and J Morton. *Scale Effects in the Response and Failure of Reinforced Composite Laminates*. Journal of Composite Materials, 26; 2674-2705, 1992.

20. S Kellas and J Morton. *Strength Scaling in Fiber Composites*. American Institute of Aeronautics and Astronautics, 30; 1074-1080, 1992.

21. D P Johnson, J Morton, S Kellas, and K Jackson. *Scaling Effects in Sublaminate-Level Scaled Composites Laminates*. American Institute of Aeronautics and Astronautics, 36; 441-447, 1998.

22. S Kellas and J Morton. *Scaling Effects in Angle-Ply Laminates*. NASA, CR-4423; 1992.

23. T K O'Brien. *Characterisation of Delamination Onset and Growth in a Composite Laminate*. ASTM STP 775, 140-167, 1982.

24. R B Pipes and N J Pagano. *Interlaminar Stresses in Composite Laminates under Uniform Axial Tension*. Journal of Composite Materials, 4; 538-548, 1970.

25. R E Bullock. *Strength Ratios of Composite Materials in Flexure and in Tension*. Journal of Composite Materials, 8; 200-206, 1974.

26. J A Lavoie, C Soutis, and J Morton. *Apparent Strength Scaling in Continuous Fiber Composite Laminates*. Composites Science and Technology, 60; 283-299, 2000.

27. D P Johnson, J Morton, S Kellas, and K Jackson. *Size Effects in Scaled Fiber Composites under Four-Point Flexure Loading*. American Institute of Aeronautics and Astronautics, 38; 1047-1054, 2000.

28. M R Wisnom. *The Effect of Specimen Size on the Bending Strength of Unidirectional Carbon Fibre-Epoxy*. Composite Structures, 18; 47-63, 1991.

29. M R Wisnom. *Relationship between Strength Variability and Size Effect in Unidirectional Carbon Fibre/Epoxy*. Composites, 22; 47-52, 1991.

30. ASTM D790-80. *Flexural Properties of Plastics and Electrical Insulating Materials*. Annual Book of ASTM Standards, 1980.

31. S McKown, W J Cantwell, and N Jones. *Investigation of Scaling Effects in Fiber-Metal Laminates*. Journal of Composite Materials, Article in Press, 2007.

32. T A Duffey, M C Cheresh, and S H Sutherland. *Experimental Verification of Scaling Laws for Punch-Impact-Loaded Structures*. International Journal of Impact Engineering, 2; 103-117, 1984.

33. H M Wen and N Jones. *Experimental Investigation of the Scaling Law for Metal Plates Struck by Large Masses*. International Journal of Impact Engineering, 13; 485-505, 1993.

34. J Morton. *Scaling of Impact-Loaded Carbon-Fiber Composites*. American Institute of Aeronautics and Astronautics, 26; 989-994, 1988.

35. Z P Bazant. *Size Effect*. International Journal of Solids and Structures, 37; 69-80, 2000.

36. S R Swanson. *Scaling of Impact Damage in Fiber Composites from Laboratory Specimens to Structures*. Composite Structures, 25; 249-255, 1993.

CHAPTER V. CONCLUSIONS

This chapter presents the conclusions from the work undertaken during the course of this research study. The chapter briefly summarises the findings of initial tests undertaken to characterise the tensile, flexural, impact and interfacial properties of the FMLs. The effect of 1D, 2D and 3D scaling on the tensile properties of the FMLs is then presented. Scaling effects in the flexural response of the FMLs are summarised followed by a review of size effects in the low velocity impact response of the FMLs. The chapter closes with suggestions for future work.

5.1 Mechanical Properties of the FML

The FML investigated in this research programme have been shown to offer a range of outstanding mechanical properties that exceed those associated with its constituent materials.

Initially, single cantilever beam tests were conducted on aluminium/SRPP bi-material samples to characterise the degree of adhesion between the composite and metal plies. These samples failed in an intralaminar mode between the plies of the self-reinforced composite, indicating that the composite-metal interface was tougher than the interlaminar fracture toughness of the composite.

Prior to conducting the scaling study, a series of tensile, flexural and impact tests were undertaken in order to characterise the basic properties of the laminates and to identify the relevant failure mechanisms.

A series of tensile tests have shown that the FMLs offer a higher strength than that of the plain thermoplastic composite. Similarly, the strain to failure of the $[Al, +/-45°]_s$ FMLs was much greater than that measured on the plain aluminium alloy. Flexural tests on $[Al, 0°/90°]_s$ and $[Al, +/-45°]_s$ configurations showed that the fibre orientation had only a secondary effect on the properties of the FML, with the maximum stress and the strain at failure being similar in both cases.

Impact tests were undertaken on FML plates to investigate the effect of varying impact energy on the development of damage in these hybrid materials. The impacted plates exhibit a high level of energy absorption, with damage taking the form of thinning in the aluminium plies and fracture in the composite layers. Once again, the PP interface was found to be tougher than the ply interfaces in the composite, this agreeing with the findings of the SCB tests.

5.2 Scaling Study

A normalisation technique has been used to compare the responses of the scaled laminates and this has been shown to be a useful tool for identifying scaling effects that were otherwise concealed by differences in the properties of the individual constituents.

5.2.1 Scaling Results of 1D, 2D and 3D Study in Tension

Scaling effects in the FMLs and their constituents were investigated through a series of 1D, 2D and 3D studies.

The tensile strength and strain to failure of the 1D ply-level scaled specimens decreased by approximately 5% over the range of scale sizes considered here.

Two fundamentally different approaches were used to investigate size effects in the 2D scaling study, these being ply-level and sublaminate-level scaling. The ply-level scaled specimens showed a 10% increase in strength over the range of scale sizes investigated whereas the strain did not show any clear scale size effect. The sublaminate-level scaled specimens did not exhibit any significant variation of strength and strain over the range of specimen sizes studied here.

Two stacking sequences were used to investigate 3D ply-level scaling, these being $[Al_n, 0°/90°_n]_s$ and $[Al_n, +/-45°_n]_s$. The former did not exhibit any clear size effect, whereas the failure stress of the latter decreased by 12% in passing from the baseline sample to the full-scale laminates.

The Young's modulus in all types of laminate was found to remain constant with scale size, reflecting the fact that this is an intrinsic material property.

5.2.2 Scaling Results of Flexural Tests on 3D Specimens

Scaling effects in the flexural properties of the FMLs were investigated through a series of four point bend tests on $[Al_n, 0°/90°_n]_s$ and $[Al_n, +/-45°_n]_s$ FMLs. Here, it was shown that the strength of +/-45° samples decreased with increasing specimen size

whereas no distinct trends were observed in its 0°/90° counterpart. This behaviour was in agreement with the trends observed in tension where it was noted that samples containing off-axis fibres exhibited a greater size effect.

5.2.3 Scaling Results of Low Velocity Impact Tests

Scaling effects in the low velocity impact response of the FMLs were investigated using panels that were scaled at both, a ply-level and a sublaminate-level. Polished cross-sections of both FML approaches, highlighted failure mechanisms such as thinning and fracture of the aluminium alloy, shear fracture through the thickness of the panels as well as fracture of the composite layers. Damage to the composite layers was found to be more severe in the larger scale sizes, an effect that was attributed to difficulties in scaling the dimensions of the weave. The impact energy to initiate fracture in the FMLs did not exhibit any size dependency. Other test parameters, such as the impact duration were shown to obey the scaling law, where little deviation from the normalised data was observed (less than 10%), suggesting an impact duration of the form (t/n).

The evidence presented in this study suggests that for the scaling parameters studied here, simple scaling laws can be used to predict both the static and dynamic response of larger FML structures with some confidence. It is believed that this will lead to a reduction in costs associated with manufacturing and testing full-scale components.

5.3 Future Work

Fibre-metal laminate systems based on a thermoplastic matrix offer considerable potential for use in engineering applications, giving excellent mechanical properties as illustrated through the various tests techniques employed in this study.

The use of scaling approaches in engineering practice is currently attracting considerable interest due to the complex and expensive structural materials used in engineering design. In this study, a scaling analysis has been successfully employed involving simple non-dimensional models, where it can generate an approach to the scaled values of a representative system. In spite of this, greater effort is needed to use

scaling technique as a reliable tool in the wider variety of material systems available on the market.

A natural development of the current study would be to model size effects in the composites and hybrid systems examined here. This should be possible once scaling effects in these systems are better understood. In addition, a wider scaling study is suggested, covering more representative structures, such as stiffened plates, to ensure wider applicability of the proposed scaling techniques.

It would also be interesting to investigate scaling effects in the high velocity impact response of hybrid structures. Under high velocity impact loading, where laminates will exhibit a more localised form of response, size effects may be reduced or may not even exist. Further, scaling effects under more extreme forms of loading, such as that associated with blast, would be of interest for further studies. Although fibre-metal laminates have shown an excellent resistance to blast loading, most testing has been conducted on small square panels, and it is not clear how well this test regime mirrors the response of larger, more realistic structures.

APPENDICES

Appendix I

Slip System of Aluminium

Plastic deformation occurs primarily by sliding along certain planes with one part of a crystal moving relative to another. Since real materials are made from aggregates of single crystals, i.e., Cu, Ag, Au, Ni, etc., dislocations do not move with the same degree of ease on all crystallographic planes of atoms and crystallographic direction. Ordinarily there is a preferred plane, and in that plane there are specific directions along which dislocation motion occurs. This plane is called the *slip plane*, followed by the direction of movement, called the *slip direction*. This combination of the slip plane and the slip direction is termed the *slip system*. The slip system depends on the crystal structure of the metal and is such that the atomic distortion that accompanies the motion of a dislocation is minimum [**1,2**]. Aluminium crystal structure is a face-centred cubic (FCC) which has at least 12 slip systems [**3,4**].

Since the simple force per unit area, (*F/A*), on a single crystal do not correlate because of their orientation differences, it is natural to inquire as to what is the criterion for determining when a single crystal will deform. It will be noted that a given temperature it is always the same set of planes which deform, so it is natural to resolve the applied stress, (*F/A*), onto the area of the slip planes. This is, however, a function of the orientation of the crystal with respect to the loading axis. If the normal to the slip plane makes an angle ϕ with respect to the axis of stressing, see Figure A.1, then the area of the slip plane is (A/cos ϕ) and the stress on this plane is (F cos ϕ /A). It is then, that if the stress is resolved into a component in the direction of the slip, what is obtained is the critical shear stress [**5**].

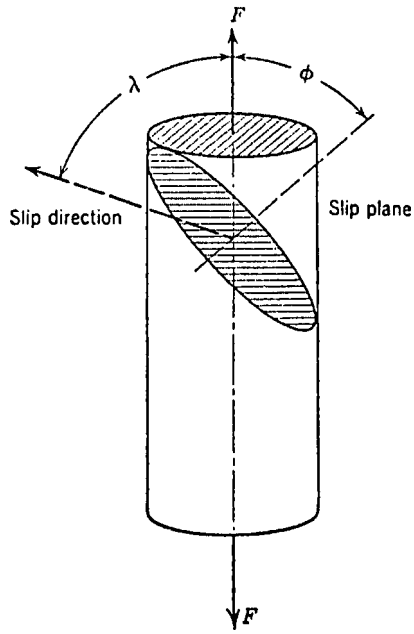

Figure A.1. Diagram showing orientation of slip plane and slip direction in a crystal relative to the loading axis [5].

References

1. W D Callister Jr. *Materials Science and Engineering; An Introduction*, John Wiley and Sons, 2005.

2. T H Courtney. *Mechanical Behaviour of Materials*, Mc Graw-Hill, 2005.

3. R W Hertzberg. *Deformation and Fracture Mechanics of Engineering Materials*, Wiley and Sons, 1996.

4. M M Eisenstadt. *Introduction to Mechanical Properties of Materials*, New York; Macmillan Company, 1971.

5. M J Sinnott. *The Solid State for Engineers*, John Wiley and Sons, 1963.

Appendix II

Some Useful Definitions for this Study

Angle-ply laminate. A laminate formed as result of orienting individual lamina at $+\theta$ and $-\theta$ with respect to a selected reference axis. An angle-ply laminate is often referred to as a bidirectional laminate.

Anisotropic material. Anisotropic materials have properties (i.e., mechanical, etc.) that vary with the orientation, they can be homogeneous but the properties change depending on the orientation along which the property is measured.

Annealing. In plastic, heating to a temperature where the molecules have significant mobility, permitting them to reorient to a configuration having less residual stress.

Balanced laminate. A composite laminate in which all laminate angles other than 0° and 90° occur only in pairs (no necessarily adjacent), and is symmetrical about a centreline.

Compliance. Opposite to stiffness, compliance reflects a material's propensity to deform under load. A measurement of the softness of a material.

Cross-ply laminate. A special case of an angle-ply laminate in which the individual lamina are oriented 0° or 90° to the reference axis.

Fill. Yarn oriented at right angles to the warp in a woven fabric.

Interface. A boundary (or transition) region between constituents (fibre or matrix) or between individual lamina within a laminate.

Isotropic material. Isotropic materials have the same properties in any direction, therefore, an infinite numbers of planes of symmetry, meaning that the properties are independent of the orientation.

Lamina. A single, flat arrangement of unidirectional (or woven) fibres in a matrix material. A lamina is generally assumed to be orthotropic, and its thickness depends on the material from which it is made.

Laminae. Or laminate, is a stack of lamina, oriented in a specific manner to achieve a desired result, normally bonded together by curing procedure or by heat, depending on the material system used.

Lay-up. A process of fabrication involving the assembly of successive layers of resin impregnated material.

Macromechanics. A study of the overall response of a lamina (or laminate) in which the effects of constituent materials are averaged to achieve an apparent response on the macroscopic level.

Micromechanics. A specialised area of composites involving a study of the interaction of constituent materials on the microscopic level. This study is generally conducted by use of a mathematical model describing the response of each constituent material.

Off-axis. Not coincident with the principal material direction.

Orthotropic material. An orthotropic material has three planes of symmetry that coincide with the coordinate planes. A unidirectional fibre-reinforced composite may be considered to be orthotropic.

Plain weave. A weaving pattern where the *warp* and *fill* fibre alternate, where both faces of a plain weave are identical.

Poisson's ratio. Also known as the *lateral strain contraction ratio*, Poisson's ratio relates the change in lateral strain to the longitudinal strain applied directly.

Prepreg. A woven or unidirectional ply or roving impregnated with resin, ready for lay-up or winding. Prepreg is short for preimpregnated.

Rule of mixtures. A linear relationship between volume fractions and constituent material properties used for predicting macromechanical material behaviour.

Strength. Maximum stress or stress at break.

Stress. Force per unit area on a body; *engineering* or *nominal* stress is evaluated according to the *initial* cross-sectional area, whilst *true stress* takes account of the change in area which occurs as deformation progresses.

Strain. Sample extension, expressed as a ratio to its original length.

Stiffness. Resistance to deformation under applied loads, usually expressed as an empirically-derived *elastic modulus*.

Toughness. Resistance to fracture of a material when stressed.

Warp. The longitudinal oriented yarn in a woven fabric; a group of yarns in long lengths and approximately parallel.